University of Sheffield

Novel double-sided microporous layer coated gas diffusion layers for the improved performance of polymer electrolyte membrane fuel cells

By:

Fernando Ruscillo

A thesis submitted in partial fulfilment of the requirements for the degree of Doctor of Engineering

The University of Sheffield
Faculty of Engineering
Department of Mechanical Engineering
Energy 2050

August 2024

Declaration

I, the author, confirm that the Thesis is my own work. I am aware of the University's Guidance on the Use of Unfair Means (www.sheffield.ac.uk/ssid/unfair-means). This work has not been previously been presented for an award at this, or any other, university.

Acknowledgements

Firstly, I would like to extend my thanks to Dr Mohammed Ismail for his unwavering support, mentorship, and supervision throughout my EngD. His expertise in fuel cells has been invaluable, and our numerous discussions and meetings greatly enriched my research experience. I am also grateful to the supervision team at the University of Sheffield: Professor Derek Ingham, Professor Lin Ma, Dr Kevin Hughes, and Professor Mohamed Pourkashanian. The weekly meetings kept my work on track, and your reviews and advice on lab work and research were hugely helpful. I would also like to thank Dr Andy Heeley at TERC for being a great mentor. Working on research projects with him has been a highly educational experience. I also appreciate my friends and colleagues in the fuel cell research group: Florence, Mustafa, Qizhi, Jinbei, and Fatma. It was a privilege to work with you all and I really enjoyed our discussions, particularly the coffee on Tuesdays.

Mohammed Al-Aidroos, deserves a special mention for his support in the lab, ensuring the experimental equipment ran smoothly and maintaining high health and safety standards.

I would also like to thank the CDT team at the University of Nottingham, Professor Robin Irons and Dr Claudia Matz, for their support in the CDT. As well as my friends and colleagues in the CDT: Jack, Jenny and Rahima.

I am grateful to Professor Masamichi Nishihara for the opportunity to conduct my research at the Kyushu University labs. My thanks also go to Dr Kun Zhang at the University of Birmingham for his assistance with fuel cell testing and guidance on fuel cell assembly.

I acknowledge and thank the EPSRC Centre for Doctoral Training for Resilient Decarbonised Fuel Energy Systems and the International Flame Research Foundation for their financial support.

Finally, I would like to thank my parents Dominic and Andrea and my sister Jacinta for their support, along with my partner Elena.

Abstract

Polymer electrolyte membrane fuel cells, known for their high energy density and efficiency, are used in portable devices, stationary power systems, and transportation. However, contact resistance remains a challenge. This issue is particularly pertinent to fuel cells because they comprise different layers made from various materials. The interfaces between these layers can make it difficult for electrons to pass through. The gas diffusion layer and microporous layer are particularly influential. The microporous layer, made of carbon black and polytetrafluoroethylene, is typically applied to the gas diffusion layer facing the catalyst layer, improving electrical contact and expelling excess liquid water.

Applying a double-sided microporous layer to the gas diffusion layer can enhance performance by reducing contact resistance while maintaining efficient mass transport. The microporous layer, coated on both sides of the gas diffusion layer, improves electrical contact between components but increases the thickness, creating a trade-off between electrical contact and mass transport. This thesis investigates these complexities, aiming to balance improved electrical contact with effective gas and liquid management for higher overall fuel cell performance.

The first research chapter examines the performance of double-sided microporous layer coated gas diffusion layers, compared to a conventional single-sided coated gas diffusion layer. Specifically, focusing on using two different conventional carbon blacks that make up the microporous layer. The investigation revealed that double-sided microporous layers are more effective in the fuel cell due to improved water management capabilities and enhanced electrical contact. Of the carbon blacks tested, Vulcan black outperformed Ketjenblack.

Building on these findings, the next study explored integrating novel carbon materials into the microporous layer, to further enhance the double-sided configuration. Graphene, known for its exceptional electrical properties, was introduced to see if it could mitigate the trade-offs associated with increased gas diffusion layer thickness. Vulcan black, graphene and a blend of the two, were used to make the microporous layer. The results showed that the optimal arrangement was found to be with Vulcan black facing the catalyst layer and graphene facing the bipolar plate.

Following this, the research aimed to replicate the beneficial crack structure provided by graphene facing the bipolar plate, by using pore-forming agents. Various quantities and particle sizes of pore formers were tested. These successfully altered the microporous layer's structure, permeability and pore size distribution, while maintaining good electrical conductivity.

Overall, this study concludes that the best gas diffusion layer performance comes from using graphene on the bipolar plate side and Vulcan black on the catalyst layer side, highlighting graphene's unique advantages.

Publications

The work in **Chapter 3** of the thesis has been published and appeared in the Energies Journal as the following:

F. Ruscillo, K. Zhang, M.S. Ismail, K.J. Hughes, D.B. Ingham, L. Ma and M. Pourkashanian, "Characterisation of Novel and High Performing Double-Sided Microporous-Layers-Coated Gas Diffusion Layers for Polymer Electrolyte Membrane Fuel Cells," Energies 2023, Vol. 16, Page 7601, vol. 16, no. 22, p. 7601, Nov. 2023, doi: 10.3390/EN16227601.

The work in **Chapter 4** has been submitted to the International Journal of Hydrogen Energy for publication and is currently under review:

F. Ruscillo, M.S. Ismail, Z.A.R. Gautama, M. Nishihara, K.J. Hughes, D.B. Ingham, L. Ma, M. Pourkashanian, "Characterisation of Double-Sided Graphene Based Microporous Layer Coated Gas Diffusion Layers for the Improved Performance of Polymer Electrolyte Membrane Fuel Cells".

The work in **Chapter 5** of this thesis is under preparation for potential publication:

F. Ruscillo, M.S. Ismail, K. Zhang, K.J. Hughes, D.B. Ingham, L. Ma and M. Pourkashanian, "Characterisation of Double-Sided Microporous Layer Coated Gas Diffusion Layers Treated with Pore Forming Agents for the Improved Performance of Polymer Electrolyte Membrane Fuel Cells".

List of Tables

List of Figures

Nomenclature

Latin Alphabet

A	Cross Sectional Area (m^2)
C	Correction Factor
d	Thickness (m)
D	Gas Free Space Diffusivity (m^2/s)
D_{eff}	Effective Gas Diffusivity (m^2/s)
E	Cell Voltage (V)
E_o	Theoretical Cell Voltage (V)
F	Faraday's Constant (C/mol)
G	Gibbs Free Energy (kJ/mol)
g	Geometrical factor
H	Enthalpy (kJ/mol)
h_{fH2}	Heat of Formation of Hydrogen (kJ/mol)
h_{fH2O}	Heat of Formation of Liquid Water (kJ/mol)
h_{fO2}	Heat of Formation of Oxygen (kJ/mol)
i	Current density, (A/m^2)
I	Current (A)
k	Permeability, (m^2)
K	Thermal Conductivity (W/m·K)
L	Thickness (m)
n	Number of Electrons
P	Pressure (Pa)
P_{H2}	Partial Pressure of Hydrogen (Pa)
P_{H2O}	Partial Pressure of Water (Pa)
P_{O2}	Partial Pressure of Oxygen (Pa)
Q	Flow Rate (m^3/s)
R	Electrical Resistance (Ω)
S	Entropy (J/K)
T	Temperature (K)
t	Thickness (m)
U	Universal Gas Constant, ($Pa·m^3/mol·K$)
V	Voltage (V)
w	Power Density (w/cm^2)
W	Electrical Work (W)
Y_A	Areal Weight (kg)
Z	Frequency Dependent Impedance (Ω)

Greek Alphabet

α	Transfer Coefficient
γ	Surface Tension of Mercury
ε	Porosity of the Porous Medium
η	Efficiency
θ	Angle
μ	Fluid Viscosity (Pa·s)
P	Density (kg/m^3)
ρ	Electrical Resistivity (Ω/m)
σ	Electrical Conductivity (Ωm)
τ	Tortuosity

Abbreviations

AC	Alternating Current
AFC	Alkaline Fuel Cell
BET	Brunauer–Emmett–Teller
BPP	Bipolar Plates
CAES	Compressed Air Energy Storage
CCM	Catalyst Coated Membrane
CCS	Carbon Capture and Storage
CCUS	Carbon Capture, Utilisation, and Storage
CHIC	Clean Hydrogen in European Cities
CHP	Combined Heat and Power
CL	Catalyst Layer
CNT	Carbon Nanotube
DC	Direct Current
DMFC	Direct Methanol Fuel Cell
EIS	Electrochemical Impedance Spectroscopy
GDL	Gas Diffusion Layer
GHG	Greenhouse Gas
HHV	Higher Heating Value
KOH	Potassium Hydroxide
LNG	Liquified Natural Gas
MCFC	Molten Carbonate Fuel Cell
MEA	Membrane Electrode Assembly
MIP	Mercury Intrusion Porosimetry
MPL	Microporous Layer
MPS	Macroporous Substrate
MSP	Method of Standard Porosimetry
MWCNT	Multi-Walled Carbon Nanotube
PAFC	Phosphoric Acid Fuel Cell
PEMFC	Polymer Electrolyte Membrane Fuel Cell
PFPE	Perfluoropolyethers
ppm	Parts per million
PTFE	Polytetrafluoroethylene
PVA	Polyvinyl Alcohol

PVDF	Polyvinylidene Fluoride
R&D	Research and Development
RH	Relative Humidity
SEM	Scanning Electron Microscopy
SLPM	Standard Litres per Minute
SOFC	Solid Oxide Fuel Cell
STP	Standard Temperature and Pressure
UK	United Kingdom
VDP	Van der Pauw
WGS	Water Gas Shift
XCT	X-ray Computed Tomography

Subscripts

A	Area
act	Activation
Cell	Cell
conc	Concentration
fH_2	Formation of Hydrogen
fH_2O	Formation of Liquid Water
fO_2	Formation of Oxygen
Gr	Graphite
H_2	Hydrogen
H_2O	Water
m	Membrane
O_2	Oxygen
ohm	Ohmic
P	Pressure
T	Temperature

Chemical Symbols

CO_2	Carbon dioxide
H_2	Hydrogen
CO	Carbon monoxide
KOH	Potassium hydroxide
Ni	Nickle
Cr	Chromium
Al	Aluminium
K	Potassium
Na	Sodium
e^-	Electron
H^+	Hydrogen ion
H_2O	Water
H_2O_2	Hydrogen Peroxide
Pt	Platinum
Hg	Mercury

Contents

Chapter 1: Introduction

Energy is fundamental to civilisation, it facilitates the development of society and technology which in turn increases living standards. Currently, most of the world's energy is supplied using fossil fuels: coal, oil and gas [1]. As society grows, the energy demand also increases. This has led to an increasing usage of fossil fuels. As a result, more greenhouse gas (GHG) emissions are released into the atmosphere [2]. One of the main GHG emissions is CO_2, significant increases in anthropogenically derived CO_2 are suggested to be one of the largest contributors to climate change [2]. The CO_2 in the atmosphere has increased rapidly (Figure 1-1), from 278 ppm to over 400 ppm, since the Industrial Revolution [3]. As a result of increasing GHG emissions, the potential of more frequent extreme weather patterns and irreversible change to the earth's climate has increased [4].

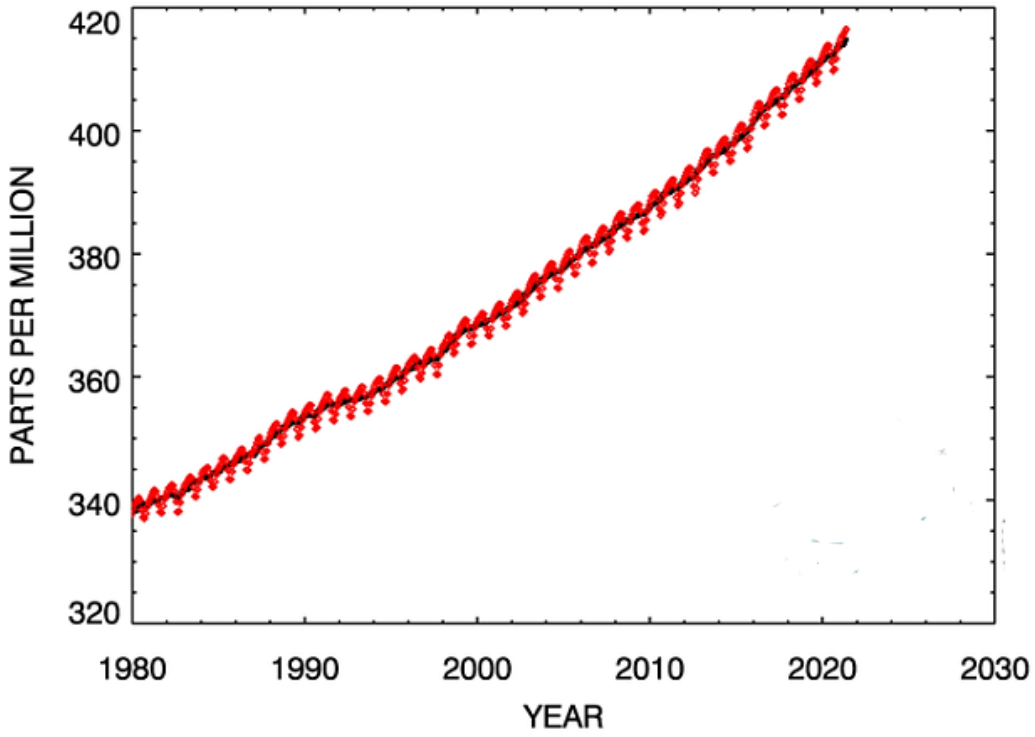

Figure 1-1 Global monthly mean of CO_2 (ppm) since 1980 [5].

1.1 Net Zero

In 2019, the UK government passed legislation requiring a 100% reduction of UK net GHG emissions by 2050 relative to 1990 levels [6]. This net-zero ambition is consistent with the Paris Agreement which aims to keep the global average temperature rise below 2°C above preindustrial levels [7]. The security of the supply of energy, energy affordability and climate change are the major challenges concerning countries with regard to the future energy mix. The intention is to find the best way to reduce GHG emissions whilst securing energy affordably and reliably, in order to meet the future demands required to sustain and develop economies [8].

Net zero can be achieved, in part by the reduction of the dependence on fossil fuel energy sources. To achieve this, countries around the world are developing and adopting sustainable and cleaner energy technologies [9].

Despite this, fossil fuels still account for the largest proportion of energy consumption. One way to decrease our dependence on fossil fuels is by employing renewable energy technologies. Renewable technologies, such as wind and solar are becoming more widespread and affordable. Even so, these technologies are afflicted with the same limitation, they are dependent on the weather and, therefore are intermittent. Part of the initiative to mitigate this is the enabling of the hydrogen economy [10]. Storing excess energy produced at peak times in the form of hydrogen, for later energy usage will be critical to enabling efficient usage of renewable energy sources. Fuel cells will constitute an important part of the energy mix in the future and be a key component of the hydrogen economy.

1.2 Hydrogen Economy

In the quest for adopting renewable energy technologies, many countries aim to electrify various processes by using clean energy sources. However, the challenges in decarbonising certain sectors persist, primarily due to the diverse applications of fossil fuels.

One promising alternative to fossil fuels is "green" hydrogen, produced through the process of water electrolysis. This method utilises an electric current to split water into its fundamental elements: hydrogen and oxygen. This process emits no greenhouse gases if the electricity provided comes entirely from renewable sources. Hydrogen offers other advantages, such as high mass-energy density, lightweight and ease of electrochemical conversion [11]. These attributes make it a suitable option for transporting energy over long distances, either through pipelines, compressed gas, liquid fuels, or as ammonia transported on freighters.

1.2.1 Hydrogen Production

Obtaining hydrogen in its elemental form, despite its abundance, presents a complex and labour-intensive challenge. Hydrogen is not naturally found in an isolated state in sufficient quantities for practical use; instead, it predominantly exists in chemical compounds, often combined with other elements, such as carbon and oxygen [12]. This necessitates specific extraction methods, as outlined in Table 1-1.

Table 1-1 Summary of hydrogen production techniques [13].

Source	Hydrogen Production Technique
Natural Gas	• Steam reforming • Pyrolysis
Coal, Oil	• Gasification • Partial oxidation
Biomass	• Fermentation • Gasification • Pyrolysis
Solar Energy	• Electrolysis of water • Photolytic splitting of water • Thermal splitting of water
Wind, Hydro, Wave	• Electrolysis of water
Nuclear Fission	• Electrolysis of water • Thermal splitting of water

In practical industrial applications, the primary techniques for hydrogen generation involve gasification and reforming to produce synthesis gas (syngas), primarily composed of H_2 and CO. Syngas is a valuable gaseous mixture that serves as a raw material for synthesising various hydrocarbons. In this case, the syngas is used in the water-gas shift (WGS) reaction, where carbon monoxide (CO) reacts with water vapour (H_2O) to produce carbon dioxide (CO_2) and hydrogen (H_2) [13]. The carbon dioxide can then subsequently be removed. While gasification of coal, biomass, and oil offers potential pathways for syngas production, the prevailing industrial practice overwhelmingly relies on natural gas steam reforming. This preference is driven by the high H_2/CO ratio in the resulting syngas [13].

The production of green hydrogen from electrolysis using water has been increasing in recent years. The research into fuel cell technology could assist with technological advancements in electrolysis and vice versa, given that they share identical electrochemical reactions, albeit functioning in opposite directions.

1.2.2 Hydrogen in Industry

Hydrogen already has an established global marketplace. Traditionally, hydrogen has played a pivotal role as an intermediate component in a range of chemical processes. Its most significant and prevalent application can be found in the field of crude oil refining. Additionally, hydrogen is extensively used in the Fischer-Tropsch Gas-to-Liquid process, for example, ammonia production.

Looking to the future, hydrogen is expected to assume novel roles in various industries. These emerging roles encompass iron and steel manufacturing, chemical production, transportation, and integration into the gas grid, among other potential applications. The versatility of hydrogen positions it as a key player in multiple sectors as industries seek cleaner and more efficient solutions [13].

1.2.3 Hydrogen for Energy

As renewable energy gains wider adoption as a key pathway to a low-carbon future, understanding its unique characteristics and impact on the power grids becomes critical. Specifically, the significant variability of solar and wind energy, compared to the steady supply from traditional fossil fuels, poses major challenges for the current grid systems, which were engineered for more stable energy inputs.

In response to this challenge, there has been a growing emphasis on the development of grid energy storage technologies aimed at effectively managing the intermittent nature of renewable energy generation. A range of technologies has been explored for this purpose, including pumped hydro, compressed air energy storage (CAES), lithium-ion batteries, and hydrogen [14].

Currently, electricity is difficult to store in large amounts [11]. This is due to the low capacities of current technologies and their relatively high cost per kilowatt of storage (e.g. batteries) [15]. Hydrogen has an advantage over electricity as it can be stored for an indefinite amount of time. The stored hydrogen can then be easily converted into energy with the use of fuel cells [[16], [17]]. Figure 1-2, displays the different types of energy storage systems, comparing the power storage capacity and the amount of time that the power can be stored. It can be seen that there are a range of different storage technology options depending on the requirements (e.g. long vs short storage, low power vs high power requirements). Hydrogen occupies a large and key area in Figure 1-2. It is a flexible storage option that can store energy from hours to weeks and can provide power when required.

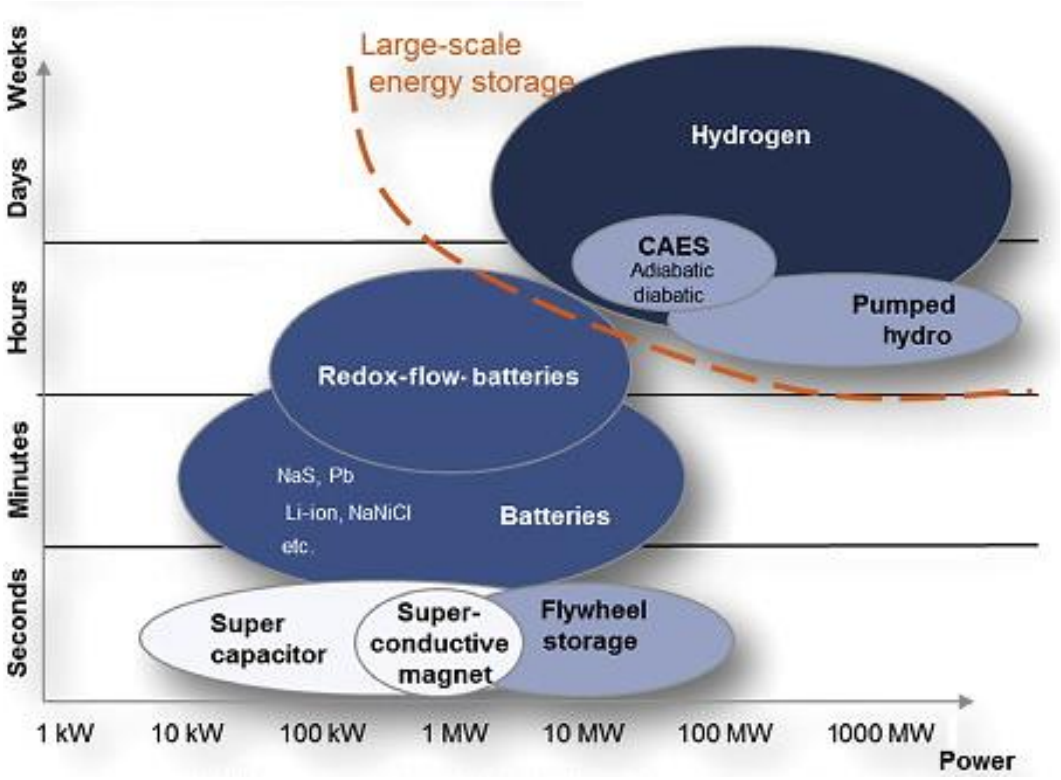

Figure 1-2 Comparison of different energy storage technologies [18].

This elegant concept of using hydrogen as an energy carrier emerges as a highly promising choice for large-scale grid storage. With its impressive gravimetric energy content of around 143 MJ/kg, hydrogen can be effectively employed in conjunction with fuel cells for reliable backup power generation. Notably, the use of hydrogen is linked to zero CO_2 emissions, and any surplus hydrogen produced can be securely stored for future use within a hydrogen-based energy system.

Furthermore, when evaluating the entire life cycle of hydrogen technology, it compares favourably to the primary alternative in energy storage, namely lithium-ion batteries. This is primarily due to the non-toxic nature of hydrogen, which stands in contrast to the typical acidic chemistries associated with lithium-ion batteries [19].

On the other hand, it's important to highlight that hydrogen possesses a low density when in its gaseous state and the energy-consuming process of converting it into a liquid or a compressed gas, presents a notable drawback when contemplating its use as a fuel. Table 1-2 displays the comparison of hydrogen and conventional fuels, comparing both the energy per mass and energy per volume. It is apparent that hydrogen has the highest energy per unit mass, but has a lower energy per unit volume.

Table 1-2 Comparison of volumetric and gravimetric energy densities of common fuels [12].

Material	**Energy per Mass (MJ/kg)**	**Energy per Volume (MJ/L)**
Hydrogen (ambient)	143	0.0107
Hydrogen (liquid)	143	10.1
Hydrogen (700 bar)	143	5.6
Methane (ambient)	55.6	0.0378
Natural gas	53.6	0.0364
Petrol	46.4	34.2
Diesel	45.4	34.6

Despite it being in its early stages and currently associated with significant costs, technological advancements are progressively making the hydrogen-based energy economy more feasible. Hydrogen has a high potential, particularly where a clean and reliable power supply is crucial, along with substantial energy storage needs. It not only acts as a storage medium for intermittent renewable electricity but also serves as an energy carrier.

Within this context, hydrogen can be described as an “energy vector", much like electricity. An energy vector is a substance rich in energy that facilitates the transportation and/or storage of energy. Hydrogen holds the potential to establish novel connections between centralised and decentralised energy supply and demand points, thereby enhancing the overall flexibility of the energy system [13]. In the future hydrogen economy, hydrogen will play two important key roles: as a chemical feedstock and a fuel (Figure 1-3).

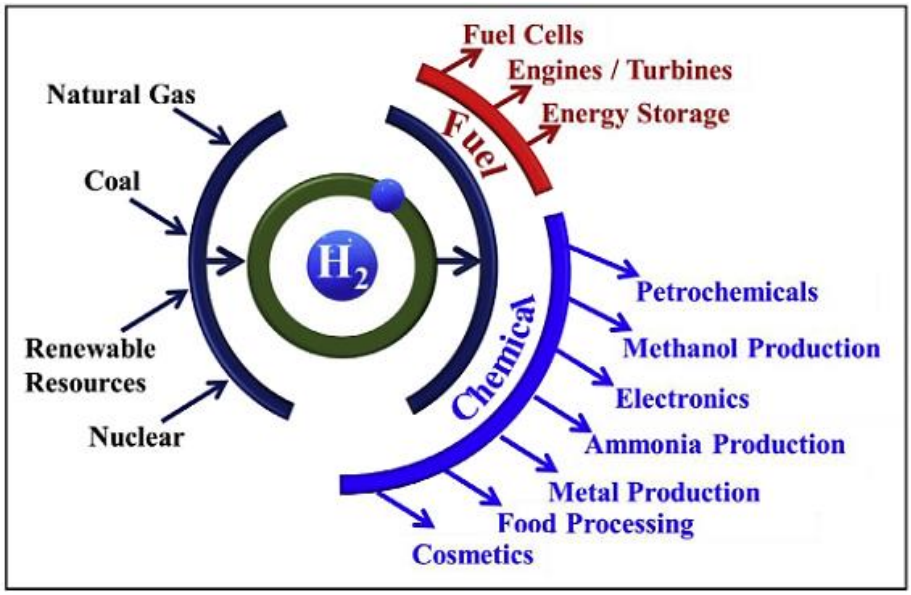

Figure 1-3 Hydrogen production and use case pathways featuring fuel cells [16].

Hydrogen's versatility extends across various sectors, serving as a chemical feedstock, a heat source when combusted, a reagent for synthetic fuel production and even as a convertible source of electricity through fuel cells. Furthermore, hydrogen's ability to store energy for the long term, in tanks or underground reservoirs positions it as one of the few sustainable technologies capable of storing energy throughout different seasons [20].

Hydrogen as an energy vector offers a solution to problems such as energy security, fossil fuel availability, and environmental sustainability [21]. Hydrogen potentially has an unlimited supply, as the main sustainable feedstock would be water. It also has the potential to be carbon-free, assuming it is produced by water electrolysis via sustainably sourced electricity.

The hydrogen economy is not just a distant concept, it is already expanding to meet future energy demands. For example, in the near future, hydrogen will play a pivotal role in the decarbonisation of the transportation sector. This includes the adoption of heavy-duty and long-range fuel cell vehicles. Moreover, hydrogen's potential extends to the heating and building sector, where it can be blended with natural gas and transported through pipelines for heating purposes.

Fuel cells will be a core technology of a future hydrogen economy as highlighted in Figure 1-3. In particular, it offers a cleaner, more efficient way to convert energy, particularly when considering internal combustion engines, gas turbines, coal-fired boilers and steam turbines [[22], [23]].

1.2.4 The UK Hydrogen Strategy

The energy landscape in the UK has been changing rapidly and the need for a hydrogen strategy will be crucial to the future UK energy mix. In 1982, the UK energy industries' contribution to the economy peaked at 10.4% but then dropped to 3.6% in 2022 [24]. Initially a net energy importer in the 1970s, the UK shifted to a net exporter in 1981 after developing North Sea oil and gas, though it returned to being an importer in 2004. By 2022, the UK was a net importer of all main fuels but became a net electricity exporter for the first time in over four decades, mainly to France. Figure 1-4, shows the energy supply of the UK from 1970-2022.

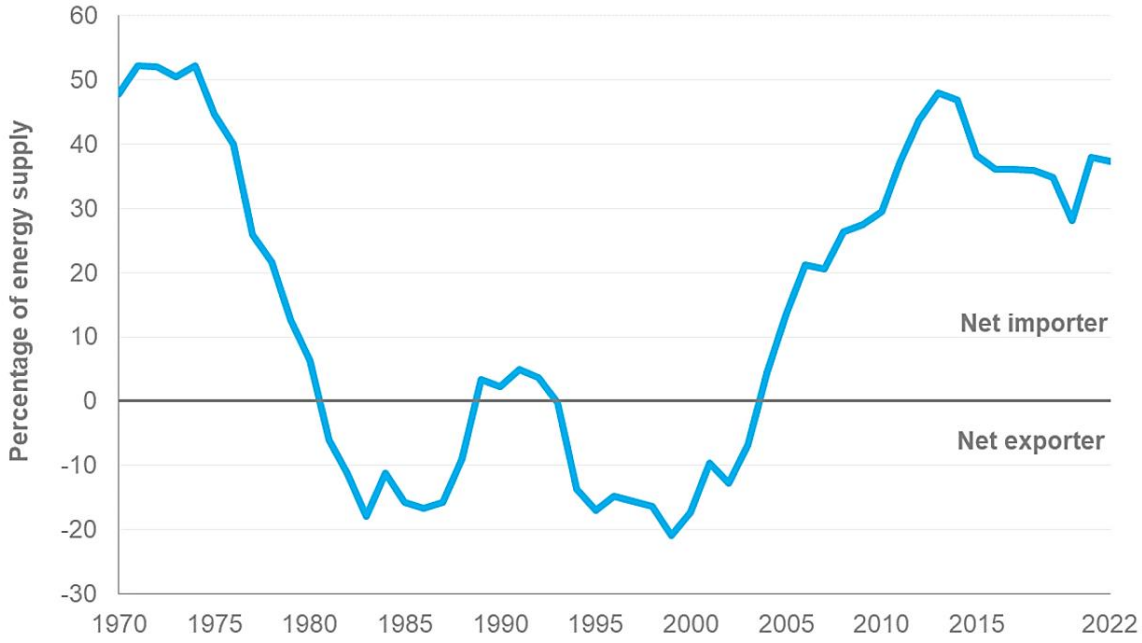

Figure 1-4 UK energy supply [24].

It can be observed that UK energy production peaked in 1999. Also, there has been a significant increase in UK fuel imports, which doubled and reached their highest in 2013. Although imports surpassed domestic production in 2010, the UK's continued large export volume kept net imports below production levels until 2021. This shift occurred as the UK increased its fuel imports to satisfy the heightened demand following the Covid-19 pandemic. The trend continued into 2022, with the UK leveraging its extensive Liquefied Natural Gas (LNG) regasification capabilities to import and then re-export energy to mainland Europe. This also helped to decrease reliance on Russian gas, which was a critical energy security issue, due to the invasion of Ukraine. In 2022, there was an 11% increase in imports across coal, primary oil, petroleum products, and gas, despite a decline in the imports of bioenergy, waste, and electricity.

The UK has an interest in energy security and tackling rising energy imports by decreasing its reliance on fossil fuels and turning more to renewable sources. In 2022, the UK sourced 20.7% of its primary energy from low-carbon alternatives (34% from bioenergy, 30% from nuclear power, and 20% from wind energy) [24]. Historically, the UK's energy landscape has continuously evolved. Figure 1-5 highlights that since 1990, there has been a notable decline in coal usage, an increase in gas, and a surge in renewables. Particularly, wind and solar power have seen substantial growth from 2000 to 2022. This growth is evidenced by record generation figures in 2022, with wind generating 80.3 terawatt-hours and solar producing 13.3 terawatt-hours, even though wind speeds were below the decade's average [24].

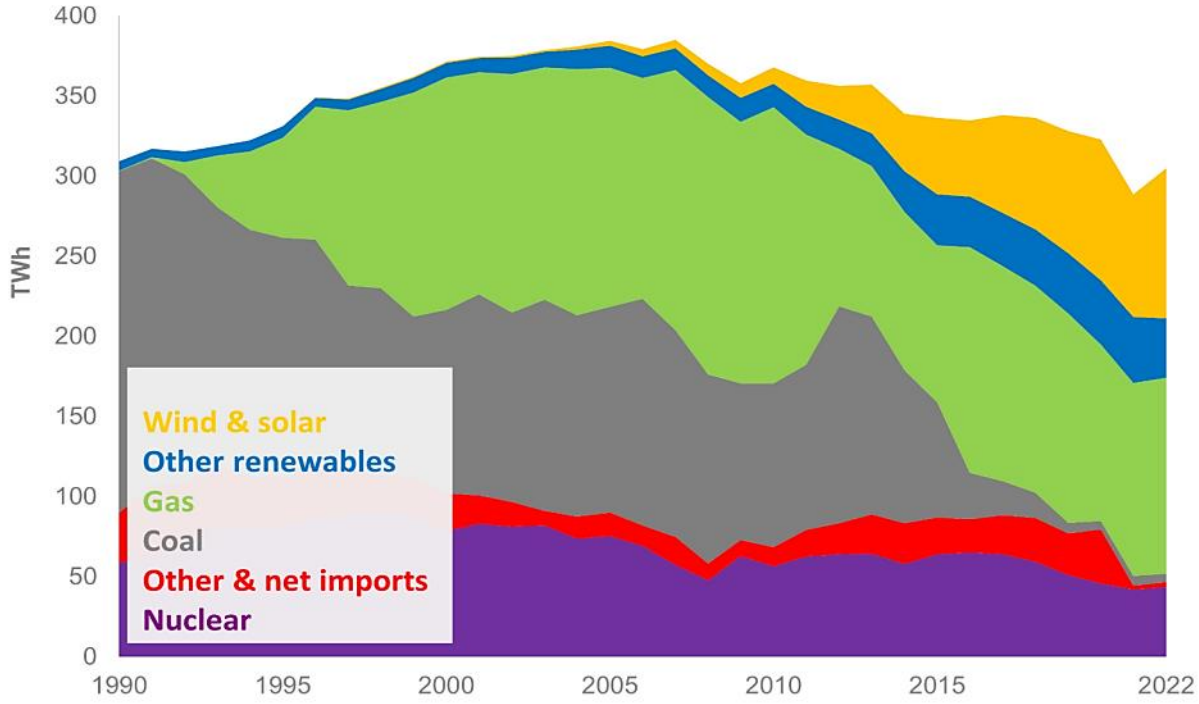

Figure 1-5 The UK energy mix since 1990 [24].

By 2050, electricity demand in the UK is expected to increase by 30% to 100%, driven by a growing reliance on renewables, nuclear energy, and fossil fuel stations equipped with carbon capture and storage (CCS) technology [25]. This diversification aims not only to increase energy security but also to meet stringent national carbon emission reduction targets. The Climate Change Act seeks to reduce the UK greenhouse gas emissions by at least 100% relative to 1990 levels [6].

Hydrogen will play a key role in underpinning the UK's ambitions to achieve energy security, reliability, affordability and sustainability. As previously discussed, renewable energy technologies face issues with intermittency. Hydrogen and fuel cell technology will play a key role in tackling this issue.

Furthermore, transportation in the UK could potentially be one of the first use cases for hydrogen and fuel cell technology. Transportation is the primary source of GHG emissions in the UK, with energy generation following closely behind [26]. In efforts to mitigate these emissions, the UK has been incorporating electric buses and more recently, hydrogen-powered buses, into its public transport system. Electric buses are currently more popular than their hydrogen counterparts because the recharging infrastructure is more easily available and can be found in most major UK cities. These buses, unlike conventionally fuelled buses, do not emit pollutants directly during operation. Instead, any emissions associated with them occur upstream during the production of the fuel or electricity used. Studies have shown that battery electric buses are most efficient for short-range journeys whereas hydrogen fuel cell buses are best suited for long distances [26].

Looking ahead, the UK plans to ban the sale of conventional fuel vehicles, including vans and hybrid vehicles, by 2035 [27]. This move is expected to significantly increase the presence of electric and hydrogen fuel cell-powered vehicles in the transport network, further aligning with

the country's environmental goals by potentially reducing both direct and indirect emissions from the transport sector [27].

Low-carbon hydrogen is crucial for the UK to meet its net zero emission targets by 2050 and the mid-2030s goals outlined in Carbon Budget Six. Hydrogen is vital for the deep decarbonisation of hard-to-electrify sectors of the UK economy, providing a sustainable alternative for energy across power, heat, and transport. The UK's unique geographic and geological attributes, along with its robust infrastructure and expertise, position it as a potential global leader in the hydrogen sector, with opportunities to generate economic benefits.

The UK government has committed to establishing long-term policy frameworks to promote low-carbon technologies, aiming for a hydrogen production capacity of 5GW by 2030 [28]. This target is intended as a foundation to scale up efforts, to achieve future carbon budgets and the ultimate goal of net zero emissions by 2050.

Introducing hydrogen into the UK's energy mix brings in diverse new feedstocks, thus improving security in the energy system. To fully exploit hydrogen’s benefits, comprehensive policy reforms are necessary to modify and improve the energy infrastructure and to secure long-term investments.

Furthermore, a detailed hydrogen roadmap is crucial, outlining the most effective production methods for the short, medium, and long term. This strategy should account for the availability of feedstocks, fluctuations and future trends in global feedstock prices, the impacts of environmental regulations (for example, carbon pricing), and changes in fuel import and export patterns, as well as the technological readiness levels. Such strategic initiatives are essential for hydrogen and fuel cell technologies to significantly enhance the resilience and security of the UK's energy system.

1.3 Fuel Cells

Fuel cells are electrochemical devices that convert chemical energy directly into direct current (DC) electricity [29]. The principle of the fuel cell was first discovered in 1839 by Sir William Grove. Grove carried out experiments with electrolysis and the Voltaic pile. He hypothesised that if electricity could decompose water into hydrogen and oxygen, then combining these gases should produce electricity and water. To test his theory, Grove developed what he called a "gaseous voltaic battery." When hydrogen and oxygen were reacted together, electricity was generated, and water was produced as a byproduct. Grove recognised the elegant symmetry of the electrolysis processes by the recombination of reactant gases and created the fuel cell process [11].

Although his invention did not immediately lead to widespread applications, Grove's concept of the fuel cell was revolutionary. It demonstrated the foundational principles for converting chemical energy directly into electricity through an electrochemical process.

Unlike a battery, which will run out of charge once the chemical constituents are fully converted. Fuel cells can undergo continuous operation if a steady supply of fuel is provided. Furthermore, as a fuel cell is not combusting fuels, it is not limited by the Carnot cycle efficiency. The Carnot cycle is the theoretically most efficient heat engine to operate between a temperature difference [23]. Fuel cell efficiency will be discussed in more detail in Section 1.3.3.1.1.

1.3.1 Types of Fuel Cells

Fuel cells are usually classified by the type of electrolyte used. There are five main categories of fuel cells [30]:

- Phosphoric acid fuel cells
- Alkaline fuel cells
- Molten carbonate fuel cells
- Solid oxide fuel cells
- Polymer electrolyte fuel cells

Polymer electrolyte fuel cells can further be classified depending on the fuel used. When methanol is used, this is a direct methanol fuel cell (DMFC). When hydrogen is used, it is a polymer electrolyte membrane fuel cell (PEMFC). Below, these different types of fuel cells are discussed in more detail.

1.3.1.1 Phosphoric Acid Fuel Cells

Phosphoric acid fuel cells (PAFCs) use phosphoric acid as an electrolyte. They also employ porous carbon electrodes with a platinum catalyst. Hydrogen is fed to the negative electrode and oxygen to the positive electrode.

Operating temperatures are typically in the range of 175°C – 200°C. The platinum catalyst can be susceptible to CO poisoning, so the hydrogen fuel supplied must have a very high purity [31]. PAFCs were the first fuel cells to be commercialised and are primarily used for stationary power generation. PAFCs can achieve overall efficiencies of around 37 – 42%. They can achieve higher efficiencies of around 85% when used in electricity and heat co-generation systems [31].

PAFCs tend to be larger and heavier than other fuel cells for the equivalent power output. This makes them more expensive to make as they require much more platinum for the catalyst.

1.3.1.2 Alkaline Fuel Cells

Alkaline fuel cells (AFCs) typically use concentrated potassium hydroxide (KOH) as the electrolyte. They can operate between 20°C – 200°C. They have found widespread use in the space industry for onboard power generation, this is due to their good performance and reliability [32].

AFCs can achieve high efficiencies of around 60%. However, they are very vulnerable to poisoning by small amounts of carbon dioxide [32]. This means that AFCs need a pure oxygen supply to operate as they can be susceptible to poisoning if using air.

1.3.1.3 Molten Carbonate Fuel Cells

Molten carbonate fuel cells (MCFCs) are a high-temperature fuel cell. Operating temperatures range between 600°C – 700°C. MCFCs are constructed from a solid electrolyte matrix made from LiK or Li-Na compounds supported within a porous aluminate. Electrode materials typically use Ni with Cr or Al additive to provide additional structural strength. Due to the high operating temperatures, they do not require a precious metal catalyst [31].

MCFCs, unlike other fuel cells, use carbonate ions to carry the ionic charge through the electrolyte. MCFCs can achieve efficiencies of up to 60% and up to 90% if used in cogeneration [31].

MCFCs are used mainly in stationary power generation applications. It is thought that if used together in combined heat and power (CHP) systems, CO_2 emissions from fossil fuel power plants could be used as an input and thus help reduce GHG emissions and improve efficiency [[33], [34]].

1.3.1.4 Solid Oxide Fuel Cells

Solid oxide fuel cells (SOFC) are high-temperature fuel cells. They operate between 800°C – 1000°C and the high temperatures mean that precious metal catalysts and external reformers are not necessary. SOFCs use a non-porous ceramic-based, zirconia compound as the electrolyte. The electrolyte conducts oxygen ions formed at the positive electrode. High temperatures enable the high ionic conductivity of the electrolyte. However, this also increases the degradation of the materials used. SOFCs do not require a catalyst, but they do need large effective surface areas [31].

SOFC have a high efficiency of around 70%. In cogeneration applications, efficiencies can be up to 80 – 85%. However, due to the high temperatures involved, SOFCs have long start-up times [31].

SOFCs have the potential to use CO as fuel. They are best used in stationary power generation applications. R&D targets are aiming to allow them to be fuelled by coal-derived gas [[34], [35]].

1.3.1.5 Direct Methanol Fuel Cells

Direct methanol fuel cells (DMFCs), use methanol rather than hydrogen as a fuel. DMFCs were developed because methanol has a higher energy density per unit of volume than hydrogen. This gives methanol an advantage as it can easily be transported and stored. Furthermore, methanol is a low-cost chemical that can be readily produced. This could allow DMFCs to be a promising option for portable applications. Such as replacing batteries in phones and laptops [36].

DMFCs work in a very similar way to PEMFCs. The difference is that liquid methanol fuel is supplied to the anode rather than hydrogen. It is then oxidised in the presence of water and this generates CO_2, hydrogen ions and electrons.

DMFCs have an efficiency of around 15 – 20%. This is quite low and is due to the methanol cross-over from the anode to the cathode. Crossover can also cause the methanol to poison the catalyst [31]. Platinum catalyst loading in a DMFC is much higher than in a PEMFC, by at least one order of magnitude [30].

1.3.1.6 Polymer Electrolyte Membrane Fuel Cells

Polymer electrolyte membrane fuel cells (PEMFCs), use a solid polymer membrane for the electrolyte. They also have porous carbon electrodes with a platinum catalyst. They operate at relatively low temperatures of between 50°C – 100°C. PEMFCs have the advantage of quick start-up times. However, the platinum catalyst is costly and sensitive to CO poisoning [31].

Due to their quick start-up time, relatively lightweight and low operating temperatures. PEMFCs are thought to be the most versatile fuel cell technology, in terms of the number of applications they can be used for. PEMFCs will be discussed in more detail in the following sections as this will be the fuel cell technology investigated in this thesis.

1.3.2 Fuel Cell Applications

Fuel cell applications can be divided into three main categories: portable, stationary and transportation.

1.3.2.1 Portable

Portable applications include mobile phones, laptops, cameras, portable power generators etc. In the technology market, there is an ever-increasing demand for high-quality and long-lasting power supplies, as more powerful devices are developed that require a steady supply of reliable electricity. Fuel cells are well placed to cater for the portable market. This is because they have good energy density, durability and modularity [37].

1.3.2.2 Stationary

Stationary applications are mainly used as power generation sources. They can be used as a primary power source, in place of the electric grid, or used to supplement power in hybrid systems. A particularly successful application is its use in residential CHP systems. CHP is a promising application to be used in conjunction with fuel cells. Systems can be fuelled by natural gas or hydrogen. The CHP unit will be able to produce grid-synchronised alternating current (AC) power alongside low-grade heat for space heating and domestic hot water [37].

Japan is a global leader in fuel cell technology, in particular CHP. According to Japan's road map for hydrogen and fuel cells, 5.3 million units of residential CHP systems will be installed by 2030 [38]. The CHP units typically have capacities of 0.7 – 0.75 kW for electricity and hot water generation [39].

1.3.2.3 Transportation

Transportation is one of the biggest potential uses for fuel cells. The world's total energy consumption is highly dominated by the transport industry [40]. Batteries currently dominate electrical vehicle technology. However, fuel cells are becoming more popular due to better energy density and quicker refuelling time. Affordable, fuel cell vehicles using PEMFC technology are available on the market, led by the Toyota Mirai, Hyundai ix35 and Honda Clarity.

Over recent years, fuel cell vehicles for use in public transport have been gaining more attention. The Clean Hydrogen in European Cities (CHIC) initiative was launched with the aim of building up a fleet of hydrogen fuel cell buses in Europe [41]. Fuel cell buses show great promise as they meet sustainable performance criteria if using hydrogen from green sources. Also, the commercial viability of fuel cell buses is projected to achieve economic parity with their fossil fuel counterparts by the end of their given lifetimes [42].

There are still major barriers that must be overcome such as hydrogen generation, hydrogen storage, hydrogen delivery infrastructure and governmental policy change before fuel cell technology can be deployed with impact [43].

1.3.3 Fuel Cell Working Principles

A fuel cell is a device that facilitates the conversion of chemical energy to electrical. It does this by a series of oxidation and reduction reactions. The oxidation and reduction reactions take place on the surface of the catalyst, which is situated between the electrodes and the membrane [44].

As illustrated in Figure 1-6, the process begins when humidified hydrogen enters the anode side, hydrogen molecules are then ionised at the catalyst layer, resulting in the creation of two H^+ ions. The electrons generated from the ionised hydrogen molecules are then directed into an external circuit, producing useful DC electricity. The oxygen supply at the cathode moves through the porous gas diffusion layer towards the catalyst layer. Here, the oxygen atoms react with the H^+ ions and two electrons from the external circuit, to form the waste product, water.

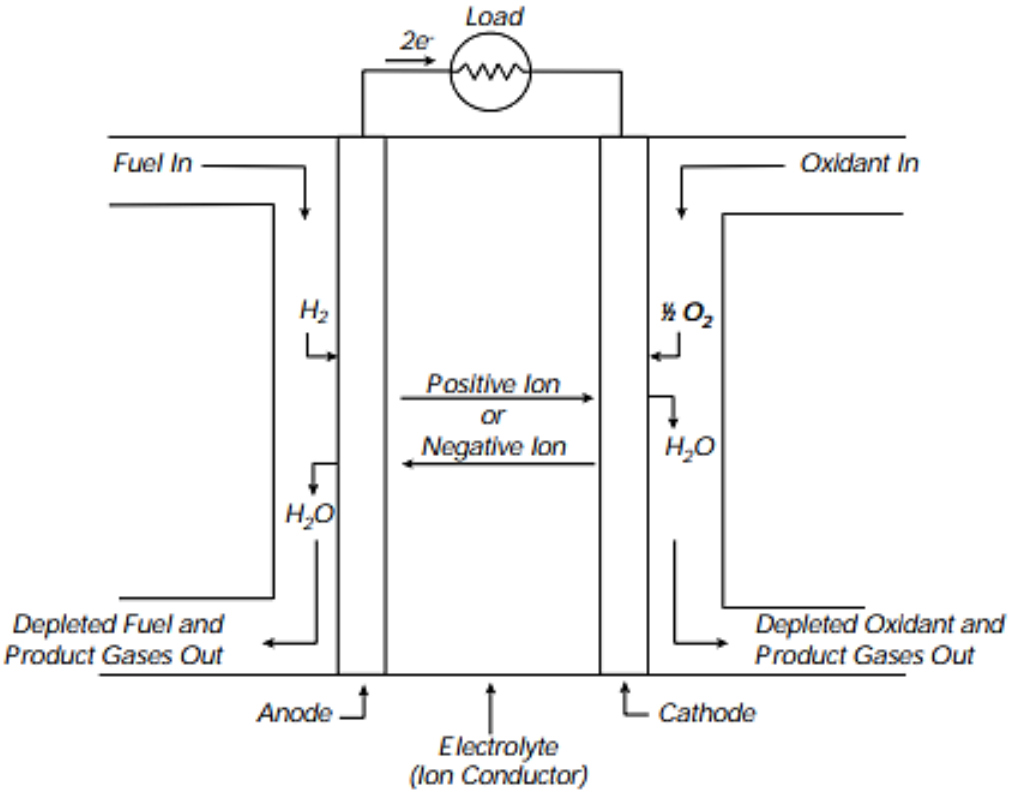

Figure 1-6 Diagram of an operating fuel cell [45].

At the anode side, an oxidation reaction takes place. Hydrogen is oxidised and dissociates into hydrogen ions and electrons.

Anode reaction:

$$H_2 \rightarrow 2H^+ + 2e^- \tag{1.1}$$

The hydrogen ions travel through the membrane, which is only conductive to ions. Electrons travel through electrodes and an external circuit to produce useful electrical work in the form of a direct current.

At the cathode, oxygen is reduced and is then combined with the hydrogen ions and the electrons to form water. The water by-product created in the electrochemical process is then expelled from the fuel cell along with excess oxygen.

Cathode reaction:

$$\frac{1}{2}O_2 + 2H^+ + 2e^- \rightarrow H_2O \tag{1.2}$$

The overall reaction for the fuel cell is the combined anode and cathode reaction as follows:

$$H_2 + \frac{1}{2}O_2 \rightarrow H_2O \tag{1.3}$$

1.3.3.1 Thermodynamics of PEMFCs

The overall fuel cell electrochemical reaction is exothermic, as can be seen in equation 1.6. The heat produced from this reaction can be expressed as follows [29]:

$$\Delta H = h_{f_{H_2O}} - h_{f_{H_2}} - \frac{1}{2}\left(h_{f_{O_2}}\right) \tag{1.4}$$

Where the change in enthalpy is (ΔH) and heat of formation of each chemical species is (h_f).

The heat of formation of liquid water is -286 kJ/mol at 25°C. The heat of formation of the elements is zero. Therefore, by substituting in the values, the enthalpy can be found as follows:

$$\Delta H = -286 - 0 - 0 \tag{1.5}$$

$$\Delta H = -286\ kJ/mol \tag{1.6}$$

Electrochemical reactions involve a transfer of electrons and a change in the Gibbs free energy. The Gibbs free energy is the maximum amount of electrical energy that can be generated in a fuel cell. It is related to the maximum conversion of chemical to electrical energy for a given reaction. The Gibbs free energy also shows if the reaction will spontaneously occur, it is defined as follows [29]:

$$\Delta G = \Delta H - T\Delta S \tag{1.7}$$

Where the Gibbs free energy (ΔG) equals the change in enthalpy minus temperature multiplied by the change in entropy (ΔS). At 25°C, from the 286.02 kJ/mol of available energy, 48.68 kJ/mol is lost as heat and 237.34 kJ/mol can be converted into electricity [23].

Electrical work must now be considered. Electrical work is defined as follows:

$$W = nFE \tag{1.8}$$

Where the number of electrons released in the reaction (n), Faraday's constant (F) and voltage (E).

Electrical work can be equated to the Gibbs free energy.

$$W = -\Delta G \tag{1.9}$$

After combining equations 1.8 and 1.9, the theoretical cell potential of a fuel cell can be expressed as follows:

$$E = \frac{-\Delta G}{nF} \tag{1.10}$$

The theoretical reversible potential of the fuel cell is calculated as follows:

$$E = \frac{-(-237.34)}{2 \times 96485} = 1.23\ V \tag{1.11}$$

In this case, E is the reversible voltage of the fuel cell. This means that it is the maximum possible voltage that the fuel cell can obtain without any irreversible polarisation losses [46].

1.3.3.1.1 Theoretical Efficiency

The theoretical efficiency of a fuel cell is the ratio of useful energy output and energy input. With regards to a fuel cell, this would correspond to the electrical energy produced being the output, in the form of Gibbs free energy. Assuming all potential chemical energy for a reaction is transformed into electrical energy, the enthalpy of hydrogen would be the input. In this case, the higher heating value (HHV) of hydrogen is used. The HHV is the amount of heat that can be generated from the complete combustion of 1 mol of hydrogen and 0.5 mol of oxygen. If this mixture is fully combusted and allowed to cool down to 25°C at atmospheric pressure, only liquid water will remain. This process will release 286.02 kJ of heat [23].

The fuel cell efficiency is defined as follows:

$$\eta = \frac{\Delta G}{\Delta H} \tag{1.12}$$

Substituting in the Gibbs free energy and the hydrogen HHV, the efficiency of a fuel cell is:

$$\eta = \frac{237.34}{286.02} = 83\% \tag{1.13}$$

The Nernst equation is an expression of the maximum possible open-circuit voltage as a function of temperature and pressure. It is used to calculate the change in the Gibbs free energy in nonstandard operating conditions. The Nernst Equation is as follows [46]:

$$E = E_0 + \frac{UT}{nF} \ln\left(\frac{P_{H_2} P_{O_2}^{0.5}}{P_{H_2O}}\right) \tag{1.14}$$

Where, E_0 is the theoretical voltage and U is the universal gas constant. The Nernst equation shows that the higher the partial pressure of reactants, the higher the cell potential.

1.3.3.2 Polarisation Curve

Performance losses in a fuel cell can be characterised by a polarisation curve. A polarisation curve represents cell voltage as a function of the current density, as shown in Figure 1-7.

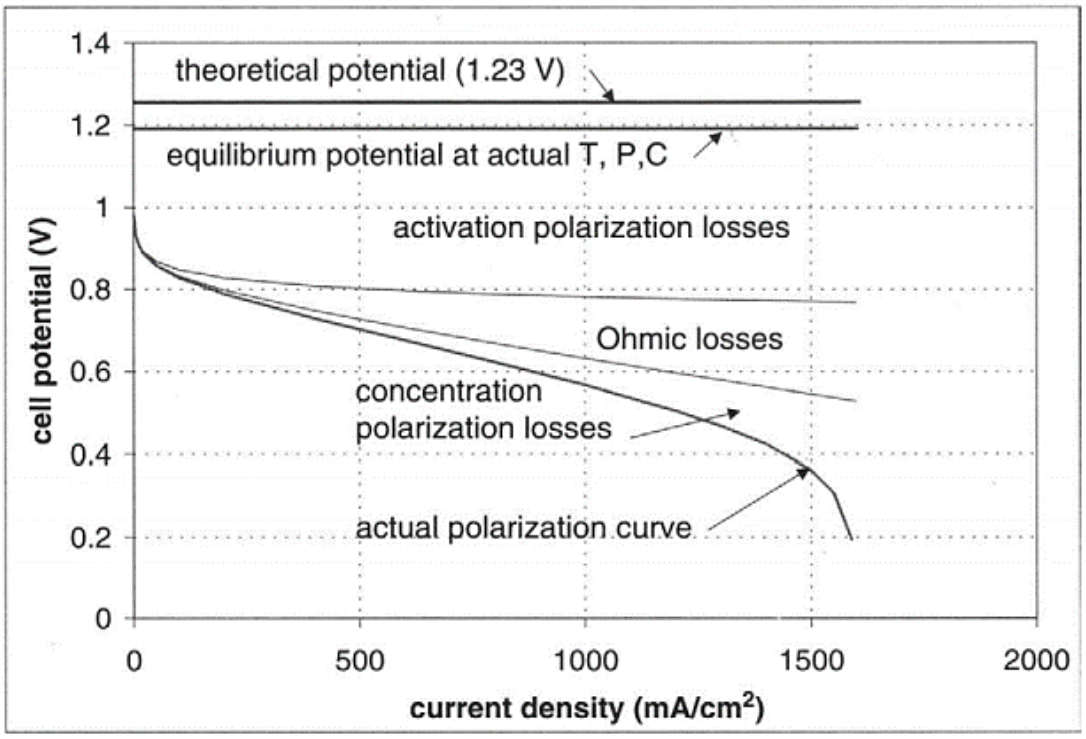

Figure 1-7 Fuel cell polarisation curve [29].

The losses in a fuel cell can be categorised by the following:

- Activation losses
- Ohmic losses
- Concentration losses

It is important to note that the regions of the performance losses are not discrete and that all modes of loss contribute throughout the entire current range of the polarisation curve. However, in the regions highlighted, they are dominated by a particular loss. Thus, each region shown on the polarisation curve is not unique, all losses contribute throughout the operating current regime.

1.3.3.2.1 Activation Losses

Activation losses dominate at low current densities. It is the voltage overpotential required to overcome the activation energy of the electrochemical reaction on the catalytic surface. Activation polarisation losses are dependent on the electrode reaction kinetics. These losses occur at both the anode and cathode. However, oxygen reduction requires much higher overpotentials, thus losses are larger at the cathode. Activation losses at the anode are assumed to be negligible as they are very small in comparison with the cathode. Activation polarisation can be expressed using the Butler-Volmer equation [29]:

$$\eta_{act} = \frac{UT}{\alpha F} ln\left(\frac{i}{i_O}\right) \quad (1.15)$$

Where, U is the universal gas constant, T is the temperature, α is the transfer coefficient, F is the Faraday constant, i is the current density and i_O is the reference exchange current density.

1.3.3.2.2 Ohmic Losses

Ohmic losses occur because of electrical resistance from the cell components and ionic resistance in the electrolyte. Resistance from components in the PEMFC is due to the inherent resistivity properties of the materials facilitating the flow of electrons. The resistance of hydrogen ions flowing through the membrane causes the resistance in the electrolyte. Ohmic losses can be expressed as follows [29]:

$$\eta_{ohm} = iR \quad (1.16)$$

Where i is the current density and R is the total cell internal resistance.

1.3.3.2.3 Concentration Losses

Concentration losses occur when there is a lack of reactant gases as the current increases. This takes place when reactant gases are consumed rapidly at the electrodes. This decreases reactant gas partial pressure. Which in turn, reduces the voltage in the Nernst equation and the current density from the Butler-Volmer equation. The surface concentration of reactants can eventually reach zero if the reactant gas is consumed faster than it can diffuse to the surface. The current density at which this occurs is called the limiting current density. Concentration polarisation can be expressed as follows [29]:

$$\eta_{conc} = \frac{UT}{nF} ln\left(\frac{i_L}{i_L - i}\right) \quad (1.17)$$

Where, nF is the charge transferred.

Overall, an approximation of the PEMFC polarisation curve can be shown from the following equation, considering all the losses discussed [29]:

$$E_{Cell} = E_{r,T,P} - \eta_{act} - \eta_{ohm} - \eta_{conc} \quad (1.18)$$

1.3.3.2.4 Other Losses

Fuel cells also exhibit some other minor losses, which can cause a “current leak”, these can be classified as fuel crossover and electrical short circuit.

1.3.3.2.4.1 Fuel Crossover

Fuel crossover losses are caused when un-oxidised hydrogen fuel crosses through the polymer membrane, it then reacts with oxygen at the cathode. This produces an unwanted hydrogen peroxide by-product and creates an overall drop in fuel cell efficiency [44]. The crossover of reactants in a fuel cell can also be a major issue in fuel cell degradation and efficiency. Crossover can cause the Nernst potential to be decreased slightly by affecting the surface concentrations of reactants at the catalyst surface, but this effect is usually negligible.

1.3.3.2.4.2 Electrical Short Circuit

Electrical short circuits can occur when the electrolyte does not fully insulate electron flow. This is not so much of an issue for low-temperature fuel cells such as PEMFC but is more common in high-temperature fuel cells such as SOFC [44].

Both of the above losses cause a small amount of internal current to be generated, which is known as a "current leak". However, these losses are insignificant in overall fuel cell operation because the rate of hydrogen permeation or electron crossover is several orders of magnitude lower than the hydrogen consumption rate and the total useful electrical current generated [44].

1.3.3.3 Power Density

The power density of a fuel cell is an important parameter used in conjunction with the polarisation curve to help understand fuel cell operation. It also gives insights into the potential optimum point of fuel cell operation. Power density is given by:

$$w = i \cdot V \tag{1.19}$$

Where w is the power density (W/cm^2), i is the current density (A/cm^2) and V is the voltage of the cell (V). Figure 1-8 shows an example of a fuel cell polarisation curve and the resulting power density curve.

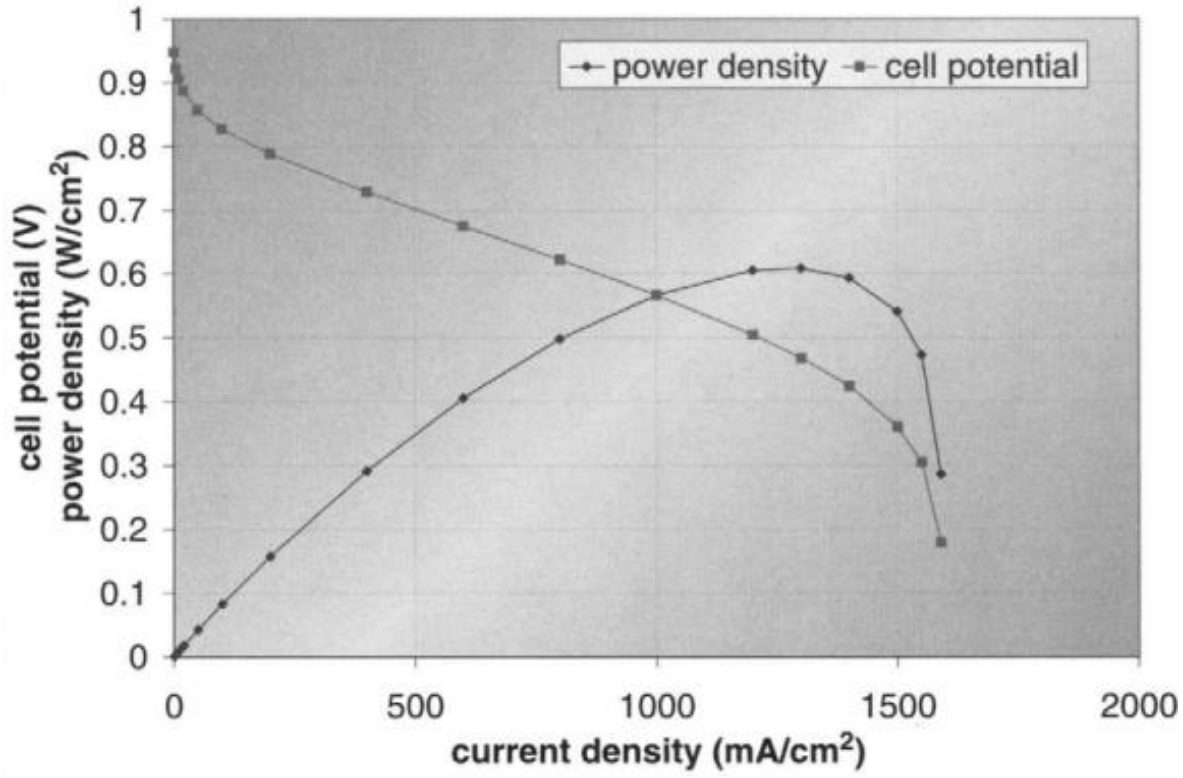

Figure 1-8 An example of a fuel cell polarisation curve and corresponding power curve [23].

The power density of the fuel cell increases as the current density increases. It then reaches a maximum, peak power density. After this maximum, the power then starts to decrease as the limiting current density is reached. The power density curve in conjunction with the polarisation curve can be a good indication for the optimum operating point of a fuel cell. A current density and a voltage close to the peak of the power density will give the highest power output of the fuel cell. The trade-off of operating at this point is that the fuel cell operating

efficiency isn't at its optimum due to thermal losses. Therefore, in practical applications, a fuel cell is usually in operation below the peak power density to achieve higher efficiencies. When considering fuel cell design and engineering, there is always a trade-off between operating efficiencies and power density output.

1.3.3.4 Electrochemical Impedance Spectroscopy (EIS)

A technique to measure voltage losses in a fuel cell is by using electrochemical impedance spectroscopy (EIS). This is a commonly used in-situ method of analysing the losses in a fuel cell and it can be useful in determining which losses predominate. It has been used in experiments when considering the contact resistance of a double-sided MPL coated GDL [[47], [48]].

EIS assesses the impedance response in an electrochemical system when subjected to an AC signal over various frequencies. This method involves introducing a small AC and measuring the resulting voltage and current responses using a frequency response analyser. EIS applies the AC version of Ohm's Law:

$$R = \frac{V}{I} \tag{1.20}$$

This takes into account the frequency dependency of impedance, as outlined in equation 1.21 [49].

$$Z(\omega) = \frac{V\,(t)}{I\,(t)} \tag{1.21}$$

Where $Z(\omega)$ is the frequency-dependent impedance (Ω), $V(t)$ is the voltage (V) and $I(t)$ is the current (A).

In PEMFC, EIS is conducted within a limited current range to address the non-linearity of the polarisation curve and maintain near-linear conditions. The technique is especially adept at independently analysing the distinct fuel cell loss processes (activation, ohmic, and concentration losses) each occurring at different rates. EIS allows for the separate examination of these losses at specific frequencies.

EIS data can be modelled using equivalent circuits. A simplified model for a membrane electrode assembly features each catalyst layer as a resistor and capacitor in parallel, linked by another resistor symbolising the membrane. This setup helps represent the charge transfer resistances at the catalyst layer and the electrochemical double-layer at the electrode-electrolyte interface, as depicted in Figure 1-9.

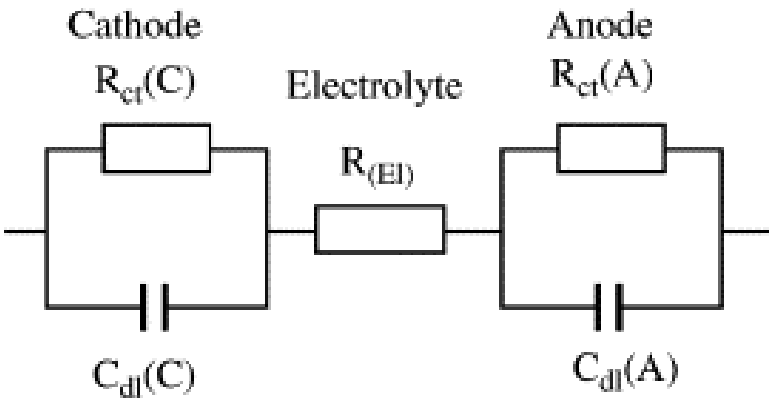

Figure 1-9 Equivalent circuit for a fuel cell [50].

In EIS measurements, impedance is analysed as real (Z_{re}) and imaginary (Z_{im}) components, represented through Bode phase, Bode magnitude, and Nyquist plots. The Nyquist plot, which displays these components along the x-axis and y-axis respectively, typically features arc-shaped curves that reflect the system's distinct time constants. For example, a circuit with two time constants will show two arcs on the Nyquist plot. Bode plots, on the other hand, plot frequency against phase and impedance magnitude.

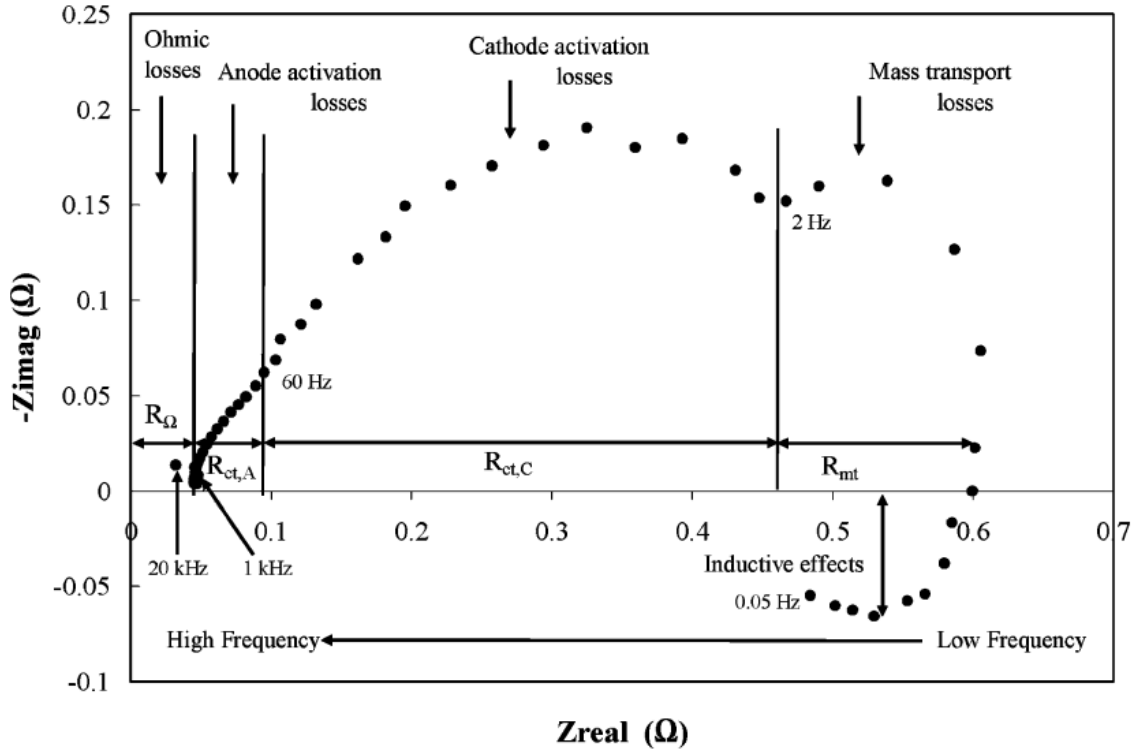

Figure 1-10 Typical Nyquist plot [51].

In Nyquist plots specific to PEMFC EIS measurements, three regions can be distinguished: the high-frequency intercept on the real impedance axis indicates internal resistances or high-frequency resistance, the first small arc reflects anode-related losses, and the second larger arc represents cathode-related losses. The high-frequency resistance, often simplified as membrane resistance, actually includes various resistive elements like charge transfer and internal resistances. Anode kinetics, being rapid, often results in a smaller, sometimes indiscernible arc, with the width of each arc correlating to the charge transfer resistances within the cell.

Asghari et al. [52] employed EIS to evaluate PEMFC performance across varying operational parameters, including clamping torque, assembly pressure, temperature, and current density. Key findings indicate that optimal clamping torque minimises ohmic and mass transport resistances. Non-uniform assembly pressure increases ohmic resistance and introduces transport limitations, which are mitigated by uniform tightening. Higher operating temperatures enhanced fuel cell performance by speeding up the oxygen reduction reaction and improving membrane hydration. EIS effectively monitored the fuel cell's break-in process, showing reductions in ohmic and charge transfer resistances. Additionally, increased current density reduces charge transfer resistance and slightly lowers ohmic resistance due to better membrane hydration.

Brunetto et al. [53] used EIS for PEM fuel cell testing and modelling, emphasising the use of real-time diagnostics. They developed software that enabled efficient EIS analysis suitable for constrained environments such as vehicles and residential systems. The study includes a software module that models electrical circuits and diffusion phenomena, aiding in optimising fuel cell operations by adjusting parameters like water content and reactant flow. EIS is also vital for ongoing performance monitoring, particularly for water management, ensuring stable operation and preventing failures through tailored impedance measurements.

EIS has proven effective in analysing how fuel cell resistances can change due to changes in fuel cell layer materials, dimensions and compositions and also how it can be used to make overall performance changes in the fuel cell itself.

1.3.4 PEM Fuel Cell Components

This next section will explore the individual components that make up a PEMFC, with a particular emphasis on the gas diffusion layer, as this is the principal component explored in this thesis. Figure 1-11 displays the different components that constitute a fuel cell and the sequence in which they are layered.

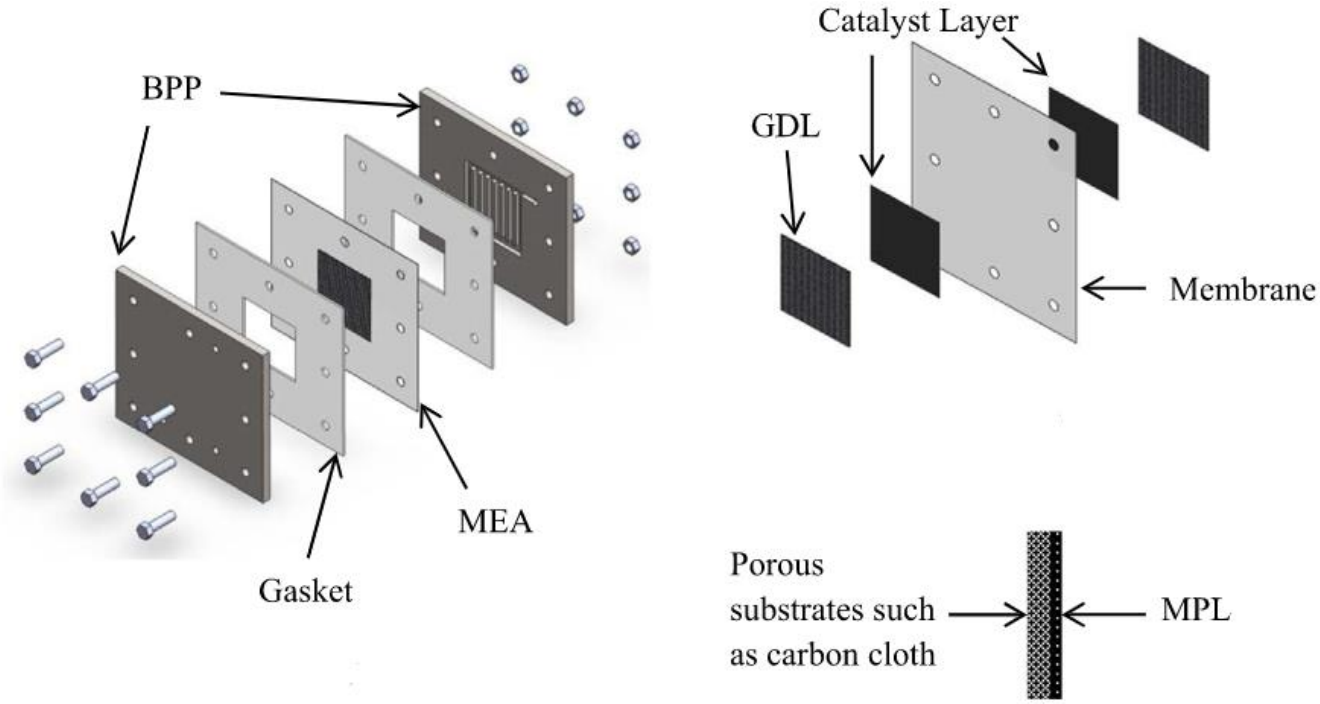

Figure 1-11 Components of a polymer electrolyte membrane fuel cell (PEMFC) [54].

1.3.4.1 Bipolar plates

Bipolar plates (BPP) are also known as flow field plates. They allow for a uniform distribution of reactant gases in the fuel cell. They also act as current collectors in the fuel cell. In a PEMFC stack, they interconnect the anode and cathode of adjacent sides as each opposing side of the BPP will be the anode and cathode current collector. Further to this, BPPs also give the PEMFC structural support. Graphite and coated metals are typical materials used for BPPs, as they provide good electrical conductivity and structural support. They are also able to dissipate waste heat away from the PEMFC stack [55]. BPPs account for 80% of the fuel cell stack weight and 40% of the fuel cell stack cost [45]. In addition, the materials used when fabricating BPP should have the following qualities [45]:

- Structural integrity
- Excellent electrical conductivity
- Low gas permeability
- Resilience against corrosion
- Good machineability

Graphite and graphite composites are typically used for BPP, this is because they satisfy most of the above points. However, graphite can be brittle and have poor machinability and gas permeability. Metals such as steel, nickel and aluminium have also been used as BPP materials to try and mitigate the shortcomings of graphite [56]. Metal BPP offer advantages such as reduced stack volume and better machinability [57].

BPPs are also responsible for the uniform distribution of gases into the PEMFC. As a result, BPPs must house the flow field channels, which help distribute the gases uniformly. There are 5 main flow field channel configurations (Figure 1-12): serpentine, parallel, interdigitated mesh, and spiral [55].

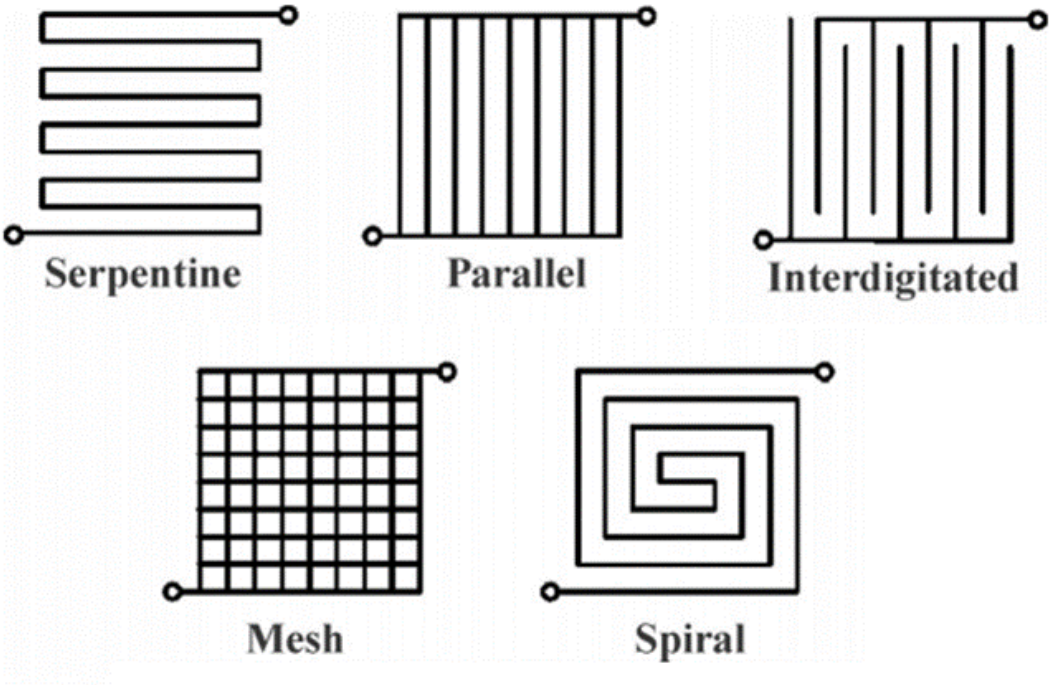

Figure 1-12 Bipolar plate (BPP) flow field configurations [44].

1.3.4.2 Catalyst Layer

The catalyst layer (CL) in the PEMFC is composed of a finely distributed layer of a platinum and carbon black mixture, over the surface of the Nafion membrane. It is characterised by its thinness and porosity. This layer is critical for ensuring both high electrical and ionic conductivities. Due to its strong ability for oxygen reduction, platinum is the chosen catalyst for PEMFCs [37] Platinum, facilitates the key electrochemical processes by offering a site for the reactions of the gases hydrogen and oxygen. It is applied in nanoparticle form onto conductive carbon black to increase the effective surface area of platinum, thereby enhancing its utilisation [58]. The thickness of the catalyst layer and the platinum loading per electrode in a PEMFC typically ranges from 0.2 to 0.4 mg/cm^2 [[55], [59]].

This layer is pivotal for electrochemical reactions, which involve the interplay of gases, electrons, and protons. These reactions are possible in regions where all three components can access the catalyst. Electrons traverse conductive materials, including the catalyst, which must maintain electrical connectivity with the base material. Protons pass through the ionomer, which means there must be good contact between it and the catalyst. The porosity of the electrode is important as it allows for gases to reach the reactive sites and facilitates the removal of water produced in these reactions. This assists in preventing flooding in the fuel cell, which would potentially block the flow of reactant gases.

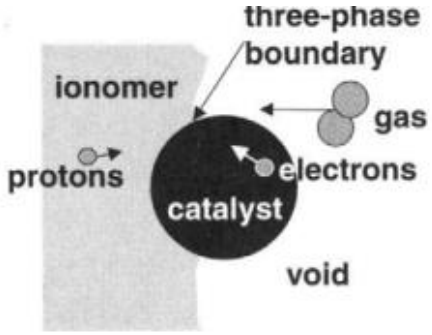

Figure 1-13 Catalyst reaction sites [23].

Figure 1-13, illustrates these processes that take place at a three-phase boundary. Comprising of, ionomer, solid, and void phases. Practically, the reaction area is expanded beyond this boundary because gases can permeate through the ionomer, thus increasing the size of the reaction zone.

1.3.4.3 Membrane Electrolyte

In PEMFCs, the membrane is a thin layer of solid polymer electrolyte, between 10 – 100 μm [60]. Its main purpose is to conduct hydrogen ions from the anode to the cathode. To do this membrane materials must have the following properties: high ionic conductivity, prevent electron transport, low fuel crossover and chemical stability.

Nafion is widely used as a membrane in PEMFC technology and it was first developed in the 1960s by DuPont. Most modern Nafion membranes are made from perfluorinated ionomers, incorporating sulphonic acid groups that are covalently bonded to the chemically resistant and inert base of polytetrafluoroethylene (PTFE). This design (Figure 1-14) results in a membrane that exhibits a dual sub-structure: a hydrophilic, ion-conducting structure, stemming from the sulphonic acid groups that can absorb water, and a hydrophobic, non-ion-conducting polymer

backbone that, while not involved in ion transport, contributes to the membrane's overall chemical stability and durability [60].

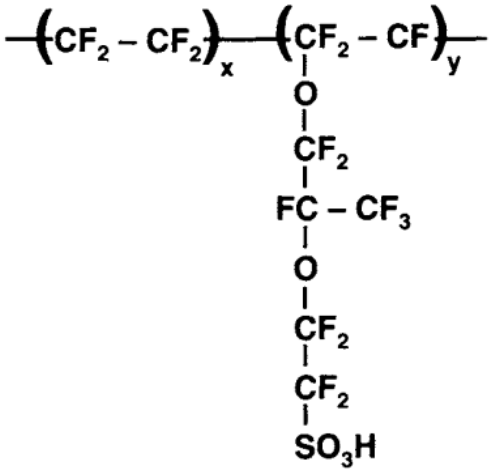

Figure 1-14 An example of the structure of a Nafion membrane

Hydration of the membrane is very important as it enables the transportation of hydrogen ions. Water molecules generally move from the cathode to the anode through back diffusion, and from the anode to the cathode via electroosmotic drag. However, too much water can cause flooding which inhibits the performance of the PEMFC by preventing mass transport from taking place [42].

When considering membrane thickness, there is a trade-off between effective water management and minimising electrical resistance. Thicker membranes are better at preventing hydrogen crossover from the anode to the cathode, which as discussed earlier, can lead to fuel cell voltage drops. A thicker membrane, however, lengthens the ionic conduction path, which in turn, increases the membrane's ohmic resistance. Moreover, the likelihood of the membrane drying out is higher with increased thickness, which can further elevate resistance due to reduced proton transport efficiency from the anode to the cathode [61].

1.3.4.4 Gas Diffusion Layer

Gas diffusion layers (GDLs) are situated between the CL and BPP. They are typically made from a porous carbon-based material. The GDL plays a critical role in a PEMFC. It distributes the reactant gases to the CLs, conducts electrons to the BPP, keeps the membrane hydrated, transports excess liquid water away from the membrane and provides structural support to the membrane electrode assembly (MEA).

1.3.5 Gas Diffusion Layer

The GDL consists of two main parts (Figure 1-15): the macroporous substrate (MPS) and the microporous layer (MPL).

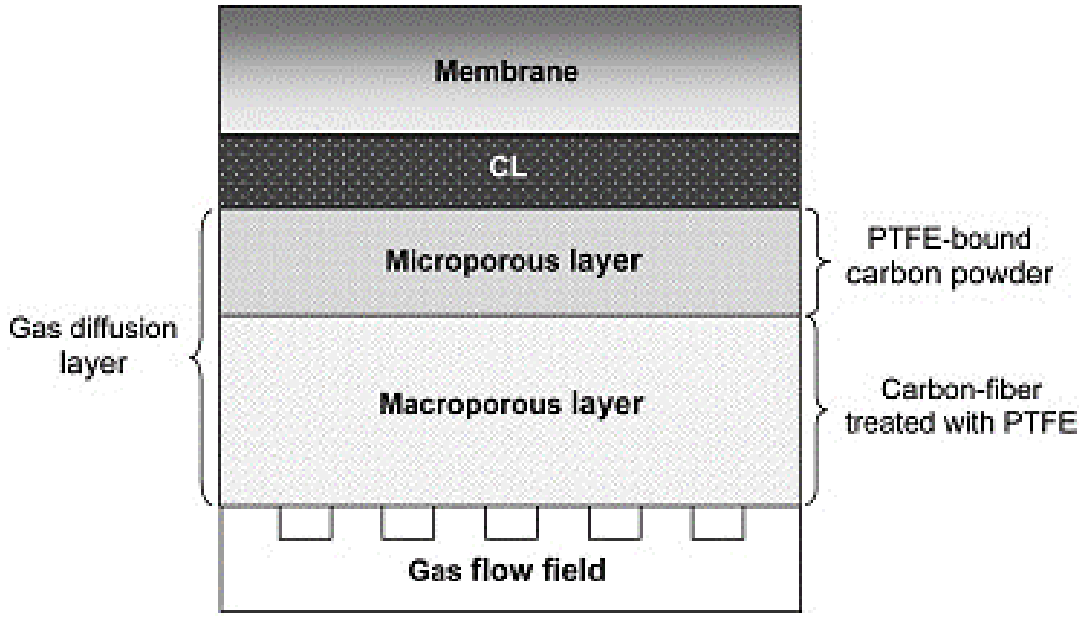

Figure 1-15 Diagram of gas diffusion layer (GDL) and corresponding layers [62].

The GDL must carry out the following important functions in a PEMFC [29]:

- Provide a pathway for reactant gases to travel effectively from the BPPs to the CL.
- Allow excess liquid water formed at the CL to leave the PEMFC via the channels in the BPPs.
- To be electrically conductive, carrying electrons from the CL to the BPP and the external circuit.
- Conduct and expel the heat generated in the electrochemical reaction from the CL to the BPP.
- Provide mechanical support for the MEA.

The GDL's material and structural properties need to satisfy the requirements of the various functions listed above. Firstly, the GDL must be porous to allow reactant gases to flow in and for water to be expelled. It must also be made from a material that is electrically and thermally conductive to allow the flow of electrons and the dissipation of unwanted heat. Finally, it must be a rigid material to give support to the MEA but also flexible so that it can maintain good electrical contacts.

When considering GDL properties, one of the main trade-offs is between good electrical conductivity and optimum mass transport processes. Gas transport requires a porous structure for it to be effective. On the other hand, electrical conductivity is facilitated through the solid structure. Thus, these properties should be optimised in a GDL to allow for efficient mass transport and electrical conductivity.

The capability of the GDL for mass, heat, and electron transport is represented by its transport properties: diffusion coefficient, permeability, surface wettability, thermal conductivity, and electrical conductivity.

Carbon fibre has been found to be the best material to accommodate these requirements and is discussed further in the following section.

1.3.5.1 Macroporous Substrate

The MPS is the primary component of a GDL and is typically made from carbon fibres (Figure 1-16). This is because carbon fibre fulfils the requirements of high electrical conductivity, structural integrity and high gas permeability. The most common configurations of carbon fibre used are carbon paper and carbon cloth. Carbon fibre sheets can be woven together to form a cloth or compressed and bound together with resin to form a paper. The individual carbon fibres typically have diameters between 5 – 10 μm [63] and overall MPS thickness can vary between 100 – 500 μm [64]. Carbon cloth and paper can have porosities of over 70% [65].

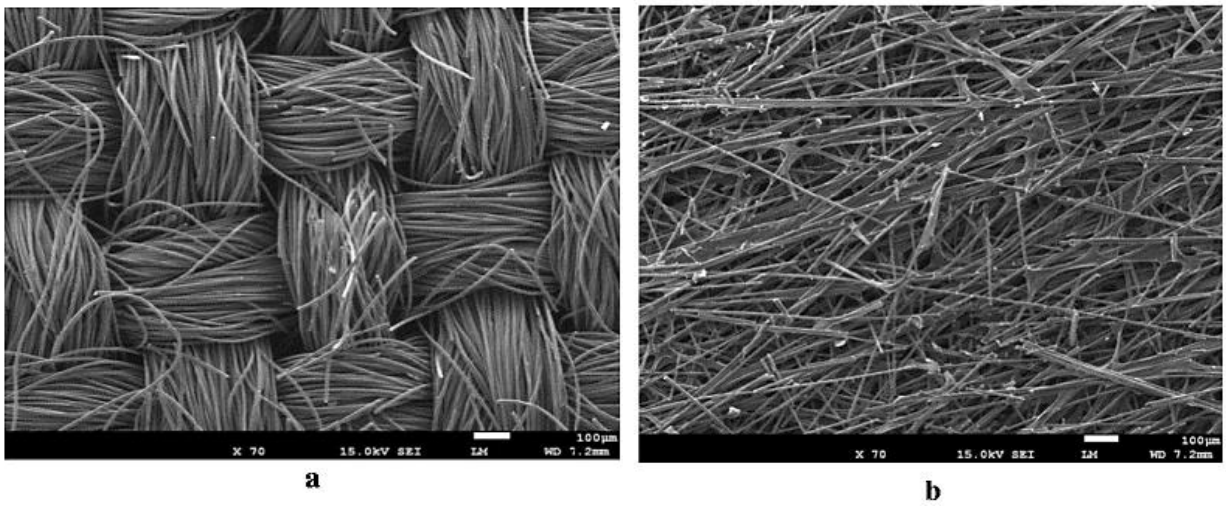

Figure 1-16 (a) Image of carbon cloth and (b) carbon paper [64].

1.3.5.2 Microporous Layer

The MPL is usually applied as a layer on top of the MPS facing the catalyst layer [66]. The MPL is usually comprised of a composite mixture of carbon powder and PTFE. The MPL offers several benefits to the GDL, these include [67]:

- Homogenous distribution of gases to the catalyst.
- Increase of capillary pressure thus reducing liquid water saturation.
- Improved catalyst utilisation by preventing Pt particles from migrating into the GDL.
- Improved interfacial interactions between the GDL and CL, in particular decreasing electrical contact resistance.

The MPL thickness can be in the range of between 10 and 100 μm when applied to the surface of the GDL [63]. It should be noted that although the MPL is initially applied as a separate layer, once applied there is no clear interface between the MPS and MPL. This is because the structure of the MPL is composed of very small particles that can be several orders of magnitude smaller than the pores of the MPS. This allows them to penetrate the MPS creating an ambiguous border between the two substances [63].

The application of an MPL significantly influences the morphological and transport properties of the GDL. This can be due to the type of carbon particle used, carbon loading and PTFE loading [63].

For example, the thickness of an MPL can potentially have a negative effect on the oxygen diffusion and delivery of gas to the CL, by increasing the mass transport limitations and hence reducing the overall fuel cell performance. Therefore, an optimal design and thickness should be considered to achieve the best PEMFC performance based on the specific operating conditions [68].

Between low and medium load conditions, fuel cells with and without MPL have similar performances. However, under high current densities, the addition of an MPL shows better performance than an uncoated GDL.

MPLs have also been shown to improve the diffusion of reactant gas supply and facilitate the removal of liquid water. A thin MPL has very small pores and low gas permeability this then limits the gas supply and increases the mass transport resistance. A thick MPL has a higher electrical resistance because of the increased amount of PTFE [68].

When applying an MPL to the GDL, there are always engineering trade-offs that need to be considered and optimised.

1.4 Thesis Overview

The research in this thesis aims to improve the overall performance of PEMFCs. This will be investigated by focusing on the impact of modifying the conventional MPL structure. The main modification will be employing the novel double-sided MPL coated GDL. The double-sided MPL coated GDL will be modified further by investigating the use of novel materials such as graphene and the introduction of pore-forming agents to change the microstructure. These modifications aim to help reduce contact resistances in the fuel cell and increase the overall PEMFC performance. In-depth characterisations will be carried out, both ex-situ and in-situ for the modifications made.

Chapter 2 will explore relevant literature concerning recent research developments on the GDL, MPL and contact resistances. It will examine the theoretical background to GDL characteristics and consider PEMFC contact resistances and the efforts made to reduce them. Particular attention will be given to MPL modifications, especially the double-sided MPL coated GDL.

Chapter 3 experimentally investigates the application of a double-sided MPL coated GDL. This includes the experimental methodology for the fabrication and the characterisation of the double-sided MPL coated GDL. Two different carbon blacks for the MPL are explored: Vulcan black and Ketjenblack. These are compared to determine which carbon black is the optimum choice in the double-sided MPL coated GDL configuration.

Chapter 4 builds on this further and investigates the use of novel materials, in this case graphene, in the double-sided MPL coated GDL configuration. The experimental investigations will determine if using a novel material can further enhance the performance of the double-sided MPL coated GDL.

Chapter 5 explores the use of pore-forming agents in the double-sided MPL coated GDL, specifically with the MPL facing the BPP. This is to examine the effects of water management in the double-sided MPL coated GDL and to analyse if further improvements can be made to this configuration by modifying the microstructure of the MPL.

Finally, **Chapter 6** summarises the findings of this research and the impact on the development of the MPL design. It will also suggest future work that could be undertaken on the MPL to further enhance the fuel cell performance.

Chapter 2: Theoretical and Experimental Background

Characterisation of the GDL is an important process for analysing, understanding, and quantifying its performance within a fuel cell system. There are two main types of characteristics that must be considered: structural properties and transport properties. Structural properties concern the physical structure of the substrate, while transport properties deal with mass, electrical and thermal transport through the GDL.

This chapter comprises a comprehensive literature review which will examine GDL characteristics, MPL materials, contact resistance and novel MPL modifications.

2.1 Structural Properties

2.1.1 Anisotropy

Anisotropy refers to the characteristics of certain materials that demonstrate varied physical or chemical properties when measured along different directions. This phenomenon is especially relevant in the context of the GDL, as they are composed of numerous individual carbon fibres. These fibres, due to their intrinsic material properties and the way they are assembled, can be oriented in multiple directions within the GDL layer. Consequently, this orientation affects how the GDL behaves and interacts with other fuel cell components, depending on the direction in which it is assessed.

For instance, the anisotropic nature of GDLs can influence the material's electrical conductivity, mechanical strength, and gas permeability. When electrical conductivity is measured along the plane of the fibres, it might show a higher value compared to measurements taken perpendicular to the fibres. This is because the electrical current can flow more easily along the aligned fibres than it can across them [69].

Gas permeability is another critical property affected by anisotropy. The flow of gases such as oxygen and hydrogen, essential for the fuel cell's operation, can be more efficient in one direction compared to another, based on how the fibres are oriented. This anisotropy can impact the overall performance of the fuel cell, influencing factors such as the uniformity of gas distribution and the removal of water produced in the cell's operation [69].

A study conducted by Ahmed et al. [70] used a comprehensive numerical analysis to explore the influence of varying GDL permeabilities, both isotropic and anisotropic, in PEMFCs featuring a single straight channel geometry. The findings reveal that cell performance is significantly impacted by the permeability characteristics of the GDL, with a notable effect observed when permeability is low in either or both in-plane and through-plane directions. It was discovered that changes in GDL permeability had a more pronounced effect on ohmic losses rather than cathode overpotential. This is attributed to the critical role of water and thermal management in determining ohmic losses. A key observation was that effective water and thermal management could be achieved in systems where at least one direction (in-plane or through-plane) exhibited high permeability. Conversely, systems characterised by low permeability in both directions suffered from inadequate water and thermal management, markedly impairing water removal from the GDL to the cathode channel and significantly hindering the heat removal process. This, in turn, led to elevated cell temperatures, particularly at higher operating current densities.

The study concludes that relying on models that assume isotropic permeability conditions could lead to overestimations of cell performance and misrepresentations of water and thermal management efficiencies in PEMFCs. The insights underscored the importance of considering anisotropic permeabilities in GDLs for a more accurate prediction and understanding of PEMFC performance.

Moreover, it was shown by Li et al. [71] that assuming an isotropic structure for the GDL can lead to an over-prediction of fuel cell performance compared to an anisotropic model by 10% when the fuel cell operating voltage is at 0.3 V.

Another case exploring the effects of anisotropy was carried out by Todd et al. [72], they experimentally investigated anisotropic electrical resistance in a fuel cell as a function of cyclical compression strain. It was found that the greatest changes in resistances were observed after the first compression. Continuity in the through-plane improved but diminished for the in-plane [72]. Recent studies of anisotropy have included X-ray computed tomography characterisation. These have provided good visualisations of the fibrous structures of the GDL. This, in turn, gives strong insights into the inherent anisotropic nature of the GDL [73].

Understanding and controlling the anisotropic properties of GDLs are crucial for optimising fuel cell performance. Engineers and researchers work to manipulate the orientation of carbon fibres within the GDL to achieve the desired balance of properties, ensuring efficient operation, durability, and reliability of the fuel cell. Additionally, as new GDL substrates are explored for use in PEMFCs, the study of anisotropy will be crucial to engineering designs.

2.1.2 Porosity

The porosity of the GDL allows the reactant gases from the BPP to reach the CL. Porosity also enables the removal of the liquid water produced. This is important as a build-up of liquid water can inhibit the electrochemical reaction, as reactant gases are prevented from reaching the catalyst, thus causing concentration polarisation losses [64]. GDLs typically have porosities that range between 30 – 90% depending on the type of materials used [64].

Porosity (ε) of a GDL can be calculated from its areal weight (Y_A), thickness (d) and density of the solid phase (P). The bulk porosity of a GDL can be expressed as follows [23]:

$$\varepsilon = 1 - \frac{Y_A}{Pd} \tag{2.1}$$

The main experimental method used to measure the porosity of a GDL is mercury intrusion porosimetry (MIP). In this process, a mercury pore analyser is used to measure mercury intrusion into the pores of the GDL [73]. In the MIP method, mercury can only penetrate the pore spaces upon the application of pressure. When mercury is first introduced into the sample, no pressure is applied, therefore, no pore volume is penetrated. Following this, a small amount of pressure is applied which forces mercury into the largest pores. Incremental increases of pressure are then applied, with each increment forcing mercury into smaller pores until the sample is filled. This technique was used by Malik et al. [73] when they carried out characterisations of pore structures in a PEMFC.

Another well-used technique to estimate porosity is X-ray computed tomography. Wargo et al. [74] investigated the porosity of the GDL using this technique. The aim was to obtain an estimation of the MPL-coated GDL bulk porosity. It was found that the MPL had a significant

impact on the transport properties of the GDL. The porosity fraction of the GDL decreased from 0.85 to 0.5 with an addition of MPL. However, the automated segmentation method used wasn't precise enough when defining a value. They then furthered this investigation by using a combination of MIP with X-ray computed tomography, which managed to accurately evaluate the pore structure of the catalyst layer [73].

It should be noted that porosity through a GDL is heterogeneous rather than homogenous, this is important to consider when modelling a GDL, as a homogenous assumption will incorrectly represent the characterisation of the GDL [74].

2.1.3 Pore Size Distribution

As discussed concerning porosity, the GDL contains pores of various sizes. These fall into three main categories based on the pore size: a pore radius less than 50 nm are micropores, a pore radius between 50 – 7000 nm are mesopores, and pores that have a radius larger than 7000 nm are designated as macropores [63].

The assortment of these different pore sizes throughout the material is known as the pore size distribution. The varying range of pore sizes, coupled with their distribution and accessibility, plays a crucial role in defining the properties and performance of the GDL. Figure 2-1 displays an example of the pore size distribution for the MPS and MPS+MPL. The graph is divided into the three main pore size categories described above.

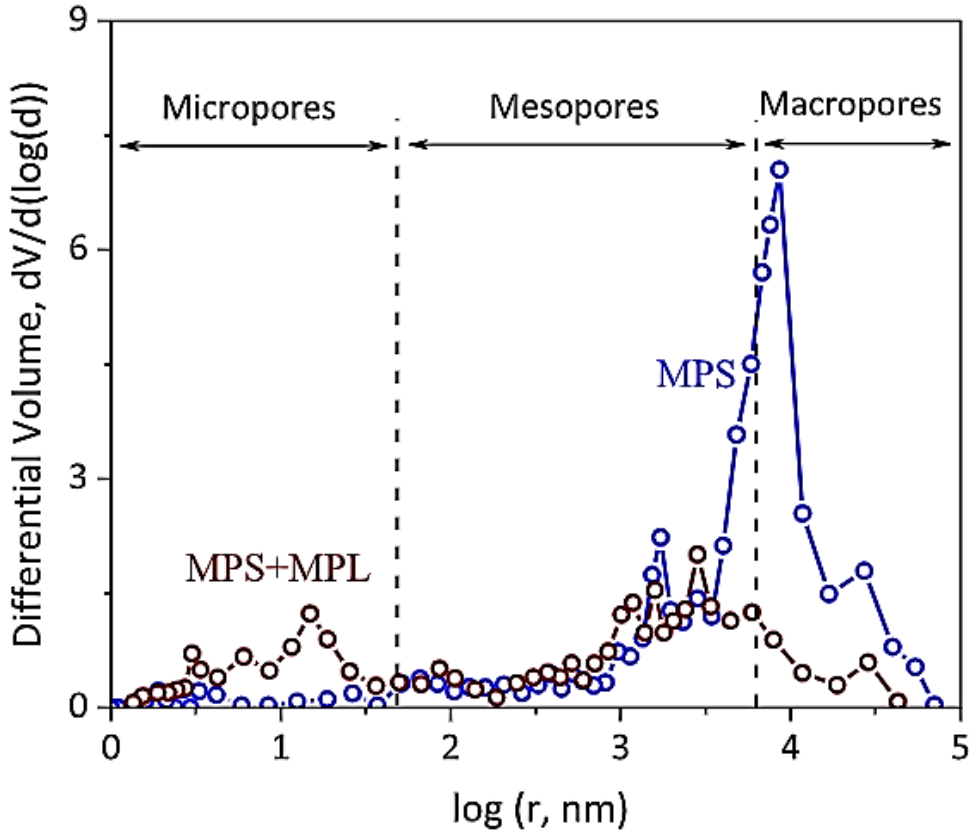

Figure 2-1 Different pore sizes and their distribution through the GDL [63].

It can be seen in Figure 2-1 that the addition of MPL onto the MPS will affect the overall pore size distribution of the GDL. The MPL creates more pores in the micropore and mesopore range. It should also be noted that different MPL carbon blacks will have different influences on pore size distribution [75].

Pore size distribution influences the way a gas molecule will diffuse through the substrate. In general, macropores facilitate the diffusion of gases, whereas micropores allow for the removal of liquid water. At standard temperature and pressure, the mean free path (distance travelled by the molecule) of air is approximately 70 nm [76]. When the pore diameter is larger than one hundred times the mean free path (7 μm), then bulk diffusion dominates. If the pore diameter is smaller than a tenth of the mean free path (0.007 μm), then Knudsen diffusion will dominate. A pore size in between these two limits will see both bulk and Knudsen diffusion taking place [76].

According to research [[77], [78]], water transport can occur simultaneously through micropores and macropores. The GDL mainly consists of macropores [79] as also seen in Figure 2-1. The addition of an MPL influences the pore size distribution by increasing the amount of micropores and mesopores. A detailed characterisation of pore size distribution is an important GDL design prerequisite [79].

Knowledge of the pore size distribution of the GDL is very important when considering water and gas transport in a porous media. Experimental methods include MIP and the method of standard porosimetry (MSP). MSP differs from MIP as it uses a different working fluid rather than mercury, the most common being octane and decane [77]. It works by measuring the dependence of the working fluid volume in the test sample as a function of the working fluid volume in the reference sample [77].

MIP is a widely utilised method for determining the pore size distribution materials. It leverages the high surface tension of mercury (Hg). The mercury is not easily absorbed into the pores at low pressures due to its high surface tension. As the pressure increases, mercury penetrates from larger to smaller pores, as described earlier. The pore size distribution is determined by measuring the intrusion pressure and volume, where the necessary pressure to intrude mercury into the pores is inversely proportional to the size of the pores. This relationship is governed by the Washburn equation [80], which establishes an equilibrium between the intrusion pressure (P) and the resisting force. The equation states that smaller pores require higher pressures for the mercury to penetrate due to their smaller openings as follows:

$$D = -4\gamma \cos\theta / P \tag{2.2}$$

The surface tension of mercury (γ), the diameter of the pores (D), and the contact angle of mercury with the material (θ) are crucial parameters. The Washburn equation uses these factors to describe how mercury penetrates the pores under varying pressures [80].

MIP is highly regarded for its reliability and accuracy, especially in the characterisation of GDLs. Additionally, the rigid structure of carbon-paper GDLs supports the assumption of cylindrical pores, with the presence of closed pores being rare in carbon paper. Thus, making MIP a suitable and effective technique for studying their pore structure [80].

Chun et al. [81] investigated the change in pore size distribution by using pore-forming agents in the MPL. Characterisations using MIP and single-cell in-situ tests were carried out. The in-

situ fuel cell tests found that the optimum pore size distribution depends on how humidified the operating conditions were. GDLs which had formed more micropores, were better at removing liquid water in high humidity and in improved single-cell performance. A GDL which contained numerous macropores improved cell performance under low humidification conditions. It is beneficial to the mass transport processes to obtain the best ratio of pore size distribution within the GDL.

An experiment by Kong et al. [77] used MIP and showed that increasing the macropores by using a pore-forming agent helps to reduce the mass transport limitations caused by water flooding since the reactant gases had more macropores to diffuse through. However, if the macropore volume is too large, the electric conductivity can decrease [77]. Therefore, it was found that the performance improvement of a GDL is attributed to the appropriate ratio of pore size distribution rather than increasing the overall porosity [77]. Nevertheless, the use of MIP to measure pore size distribution does have its limitations, the main one being the "necking effect". This occurs when a void behind a neck is incorrectly classified as a pore.

Gostick et al. [82] used a combination of MIP and MSP in their study to mitigate the necking effect. The study compared pore size distribution measurements, using this technique, with the manufacturers in house values, in which they found consensus. Moreover, it was highlighted that MSP can distinguish between hydrophilic and hydrophobic pores, whereas MIP could not. Therefore, MSP has greater potential for analysing the effect of hydrophobic/hydrophilic pores on liquid water and gaseous transport.

Porosity and pore size distribution are two of the most important characteristics of GDL that affect mass transport processes. A change in the GDL porosity can affect the overall permeability. Whereas a change in pore size distribution can cause different mass transport processes of water and gas. Therefore, both porosity and pore size distribution must be understood comprehensively for effective GDL design. Furthermore, there is a wide range of carbon substrates and carbon particles that can be used in various combinations for fabricating the GDL and MPL. When designing a GDL, it is crucial to understand the porosity and pore size distribution of these materials. The choice of carbon particles and substrates significantly impacts the pore size distribution and overall porosity when they are combined. Therefore, knowing how different combinations of these materials affect the GDL's structure and performance is essential for optimising the fuel cell efficiency. This is an ongoing and important topic of study when it comes to GDL/MPL design and optimisation.

2.1.4 Tortuosity

Tortuosity is used to describe gas diffusion through a porous structure. It is the ratio of the actual mean path divided by the thickness of the porous structure in the direction of the diffusing gas [83]. The more tortuous the path, the longer the effective path length is through the porous substrate, as shown in Figure 2-2. Tortuosity (τ) can be calculated using the porosity of the material (ε), effective gas diffusivity (D^{eff}) and gas-free space diffusivity (D) [84].

$$\tau = \frac{\varepsilon D}{D^{eff}} \tag{2.3}$$

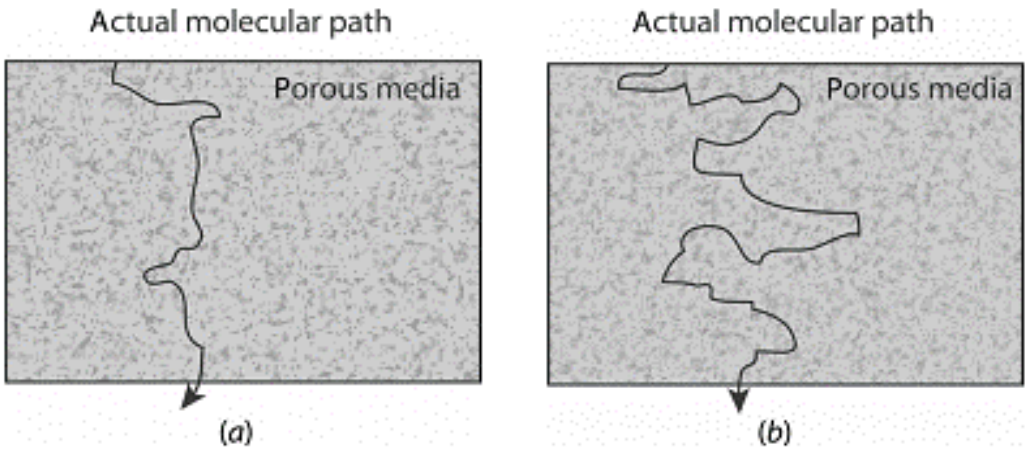

Figure 2-2 Porous substrate with (a) low tortuosity and (b) high tortuosity [42].

Espinoza et al. [85] carried out simulations to assess how the structural parameters of the GDL, in particular the tortuosity, affect overall fuel cell performance. The study concluded that when the GDL was compressed, gas-phase tortuosity increased, as there was an increase in the gas-phase transport resistance.

An experimental investigation was carried out by Zenyuk et al. [86] to compare different GDL characteristics including tortuosity values. Various GDLs were tested under compression and it was found that the tortuosity values varied between 1.5 to 3 for the least compressed and the most compressed, respectively. However, overall there was little deviation between the different GDL samples [86]. Tortuosity was also evaluated by Didari et al. [83] where it was found that the tortuosity property can be affected by the anisotropic nature of a GDL. The through-plane tortuosity can be a factor of between 2 and 3 times larger than in-plane for a standard GDL [83].

Tortuosity in the GDL can impact the mass transport efficiency and is linked closely to the porosity and diffusivity. High tortuosity leads to more convoluted pathways, which can slow gas diffusion to the catalyst layer. A high tortuosity and low porosity can result in significantly restricting the gas diffusion [42]. Optimising tortuosity is key to balancing the gas diffusion and electrical conductivity for efficient fuel cell operation. Additionally, as new materials and microstructures are being explored for usage in an MPL, it is important to measure and compare the tortuosity to achieve the best designs.

2.1.5 Hydrophobicity

As discussed in Section 1.3.5, the GDL must be able to reject the excess liquid water by-product, produced by the electrochemical reactions. This means that it must have hydrophobic properties. This is important at high current densities when more liquid water is produced and needs to be removed to prevent concentration polarisation losses.

Accumulation of liquid water in the fuel cell can lead to flooding. This is particularly prominent in the cathode due to the slow kinetics of the oxygen reduction reaction. Water is also generated at the cathode by electroosmotic drag. For this reason, water flooding is more likely to occur at the cathode. Water flooding can cause the reactant gases to be distributed in a non-uniform fashion at the catalyst. A non-uniform distribution can cause a decrease in individual cell performance as well as variations within the stack itself.

There are two main strategies to mitigate flooding in the fuel cell [87]. The first option is based on the overall system engineering of the fuel cell, including external supporting equipment. However, this can result in parasitic power losses. The second option is to focus on the overall design of the MEA. This mainly involves modifying the materials or the structural properties of the GDL, this is the preferred method as it avoids parasitic power losses.

The hydrophobicity of the GDL can be measured by the contact angle. Contact angle is defined as the angle between the gas-liquid interface and the solid surface [42]. Contact angles depend greatly on the base material, surface temperature, surface impurities, and surface morphology [[42], [88], [89]]. As shown in Figure 2-3, if the contact angle is less than 90° the substance is considered hydrophilic. A contact angle greater than 90° and the substance is deemed hydrophobic [90].

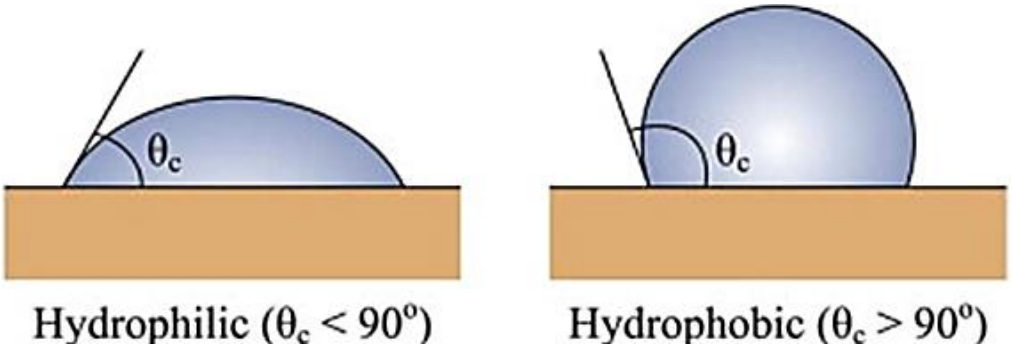

Figure 2-3 Hydrophilic vs hydrophobic surface demonstrated by the water droplet contact angle [91].

GDLs due to their porous nature, tend to soak up water causing mass transport resistance and a reduction of membrane hydration. As a result, a GDL is treated with PTFE to provide it with hydrophobic properties [91]. A study by Mortazavi et al. [92] found that for a Toray carbon paper GDL, the contact angle can be increased from 130° for untreated GDL to 153° when treated with PTFE. However, the GDL cannot be too hydrophobic, as it needs to retain some water to keep the membrane hydrated. The hydrophobicity of the GDL must be optimised to remove excess water whilst keeping the membrane hydrated.

Bevers et al. [93] examined carbon paper with different PTFE loadings. The carbon papers were characterised by, gas permeability, wettability, and electronic conductivity. The results showed that higher PTFE content reduced water saturation but simultaneously caused poor gas transport and higher electrical resistance.

The treatment of a GDL with PTFE not only improves hydrophobicity but can also affect GDL properties such as porosity, tortuosity and conductivity. Porosity can be reduced by the PTFE blocking the pores and tortuosity reduction occurs in the blocking of the longer pores [94]. The addition of PTFE to a GDL can help with water management however there is a trade-off with the other properties of the GDL.

It was found by Alhzami et al. [94] that the addition of PTFE decreased the through-plane thermal conductivity of the GDL, this is because PTFE is a natural insulating material with low thermal conductivity, approximately 0.25 W/mK. Velayutham et al. [88] further confirmed that increased usage of PTFE can decrease both the thermal and electrical conductivity of the GDL. However, these studies did not consider the anisotropic nature of the GDL. Ismail et al. [89] addressed this by examining the through-plane and in-plane effects of PTFE content. It was

found that the addition of PTFE contributed to a decrease in through-plane conductivity but had little effect on the in-plane conductivity of the GDL.

Yoosefabadi et al. [80] used a microstructural GDL model to determine the characteristics of a PTFE-treated GDL. It was found that liquid water acted as a barrier to gas diffusion. It was also shown that the presence of liquid water helped to improve thermal conductivity by reducing thermal resistance between the GDL fibres. The simulations also showed that with the addition of PTFE, there is an important trade-off between improved hydrophobicity and a reduction in reactant gas diffusivity.

Chen et al. [90] carried out a simulation using a 3D multiphase lattice Boltzmann model. It was used to evaluate the impact of PTFE content and the liquid/gas transport in the GDL. The PTFE content in the GDL was found to reduce the gas phase permeability and it was deduced that determining the optimum PTFE content in GDL must consider many different factors and should not rely solely on liquid water saturation levels.

The addition of PTFE to the GDL has been shown to affect the overall properties in different ways, consequently, optimisation of PTFE loading on the GDL is crucial. PTFE content has undergone many investigations and convention shows that the ideal PTFE content for a GDL ranges between 10 – 20 wt. % [[95], [96], [97]].

Alternative hydrophobic agents to PTFE have been explored for use in the GDL, to mitigate some of the negative effects that PTFE can have on the mass transport properties, and thermal and electrical conductivity. Perfluoropolyethers (PFPEs) present a viable substitute for PTFE in hydrophobic coatings due to their thermal and chemical stability, along with significant hydrophobic properties [98]. Additionally, their liquid state allows for straightforward application and enhances the gas permeability of the GDL when used as a coating [98].

A study by Stampino et al. [99] used PFPE derivatives as hydrophobic surface treatments for GDLs in PEM fuel cells, comparing them to traditional PTFE coatings. The experimental setup involved applying these coatings to carbon cloths through wet chemical methods. The performance of the coated GDLs was evaluated in a lab-scale fuel cell under varying conditions, specifically at 60°C and 80°C with relative humidity settings of 80/100% for hydrogen/air. Results indicated that PFPE coatings significantly enhanced cell performance, particularly at the lower temperature of 60°C. The study also noted that a minimal PFPE concentration (1 wt. % relative to the 10 wt. % typically used for PTFE) could markedly improve electrochemical performance.

Polyvinylidene fluoride (PVDF) is also recognised as a promising alternative to PTFE, given its high chemical stability, thermal resistance, and hydrophobic characteristics. Bottino et al. [100] created MPLs made from PVDF and sulfonated PVDF (PVDFS) were developed for PEMFC applications using the phase inversion method. The samples were assessed through scanning electron microscopy (SEM) imaging, water contact angle tests, electrical resistance, and gas permeability evaluations. The best PEMFC performance was observed with highly porous and gas-permeable MPLs, particularly those made from PVDFS. For example, at a current density of 0.60 A/cm², the voltage of a single cell using a PVDF-MPL increased from 0.43 V to 0.60 V when coated with a PVDFS-MPL.

Novel hydrophobic agents display promising properties which can mitigate some of the challenges posed by PTFE, but they are still in the early stages of development. They require

further research before they can replace PTFE as the standard choice for hydrophobic treatments in GDL fabrication.

Mass transport processes in the GDL is a complex process due to the two-phase flow conditions, this makes it particularly hard when characterising water transport. As mentioned previously, the GDL must have multiple properties in order to fulfil the many functions required of it. Several of them are related to water management, including hydrophobicity, permeability, porosity, pore size distribution and thickness. This makes the understanding of water management a critical factor to consider.

2.2 Transport Properties

2.2.1 Gas Permeability

Permeability is the ability of a porous material to allow fluid to move through its pores. A porous medium with high porosity will better facilitate the transportation of fluid as opposed to a medium with low permeability [42]. High permeability is an important property for a GDL as it allows more reactant gases to flow through to the CL and for liquid water to leave the CL. The low permeability of a GDL can cause an increase in pressure, thus requiring an increase in power input to keep the flow of reactant gases moving towards the catalyst, ultimately this decreases the performance of the fuel cell. GDL permeability is an important factor to characterise and optimise to have an efficient fuel cell.

Permeability can be estimated using Darcy's law. Darcy's law states that a flow rate (Q) through a porous substance is equal to the product of the permeability (k), cross-sectional area (A) and pressure gradient (ΔP) divided by the product of viscosity (μ) and thickness (L) of the substance [42].

$$Q = \frac{kA\Delta P}{\mu L} \tag{2.4}$$

The permeability can be measured experimentally; Figure 2-4 shows an experimental set-up used by Orogbemi et al. [101] The GDL sample with a sealing gasket is clamped between two plates in the middle of the lower fixture and air is then passed through using a mass flow controller [102].

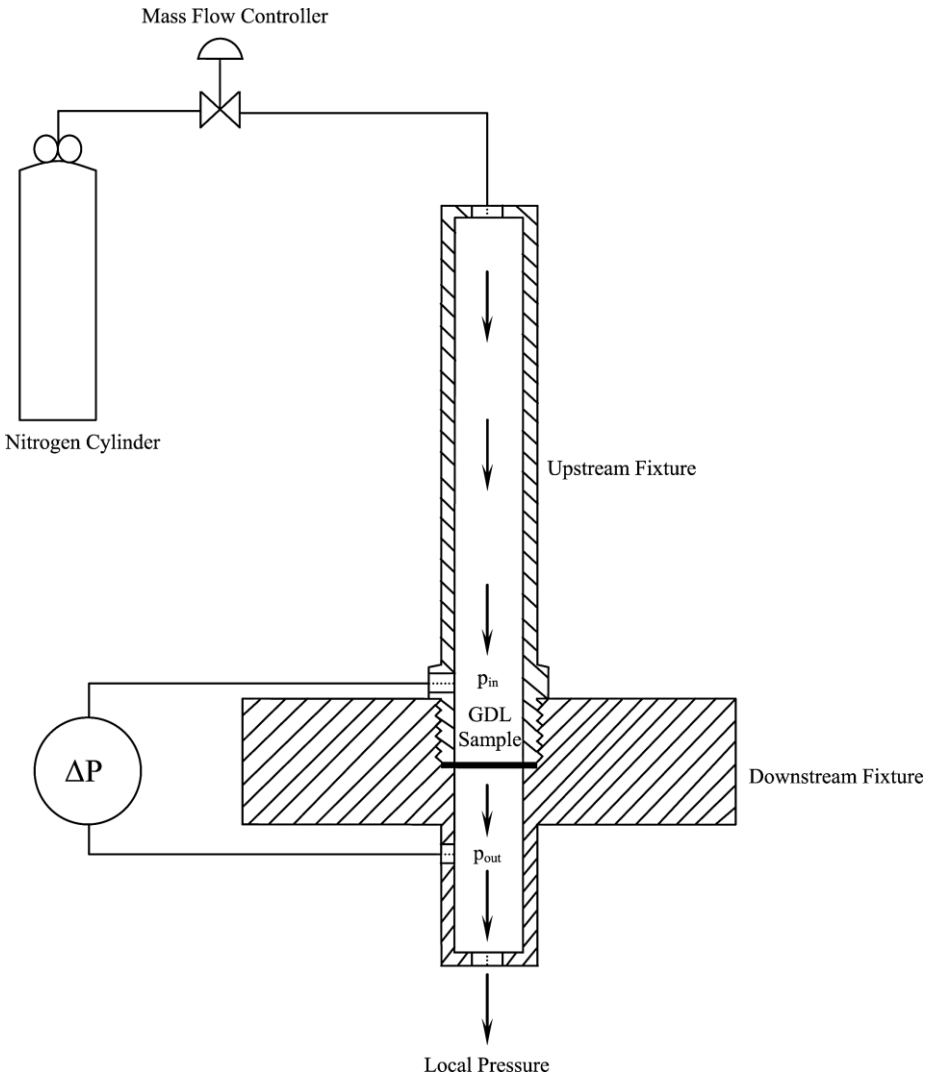

Figure 2-4 Permeability experimental set up to measure through-plane permeability [101].

Taira et al. [103] used an innovative experimental setup to measure directly the permeability of the GDL (E-TEK ELAT carbon cloth) as well as the cross-flow rate beneath the lands. The findings indicate that the effective permeability of the GDL changes with the width of the land and the conditions of humidification. Typical GDL permeability values were found to be in the range of 1×10^{-12} m^2 and 7×10^{-13} m^2 [103].

Ahmad et al. [63] conducted a detailed ex-situ evaluation of a broad range of GDLs, focusing on their physical and electrical attributes. It was found that uncoated Toray carbon paper (TGP-H060) had a permeability value of 6.15×10^{-12} m^2 whereas the thicker Toray TGP-H120 had a lower value at 3.90×10^{-12} m^2. The results indicated that the substrate's structure significantly affects the permeability values. Furthermore, the surface roughness, as well as the permeability and porosity of the GDL, are influenced by the addition of an MPL. An MPL decreases both the porosity and permeability Also the application of PTFE to the substrate increases the GDL's hydrophobicity and permeability but reduces its porosity and resistivity.

It was further studied that the addition of PTFE and MPL to the GDL can affect the permeability. Ismail et al. [102] found that increased amounts of PTFE in the MPL will increase the overall through-plane permeability of the GDL [102]. It was also found that the through-plane

permeability of the MPLs in the coated GDLs was 2 – 3 orders of magnitude lower than uncoated GDL [102].

Anisotropy can also affect the overall permeability of a GDL. Gostick et al. [65] investigated through plane and in-plane permeability. It was found that most substrates showed a higher in-plane permeability than through-plane permeability [65]. Substrates with the most highly aligned fibres showed the highest anisotropy leading to the permeability differing by as much as a factor of 2 [65].

Hossain et al. [104] further investigated the anisotropic nature of permeability through two-phase modelling. They found that for improved PEMFC performance, the permeability of the GDL is required to be high in both through-plane and in-plane. High in-plane and low through-plane permeability also gave good PEMFC performance. While high through-plane and low in-plane permeability gave a poorer PEMFC performance [104]. Opposingly, Holzer et al. [105] determined that the through-plane permeability was more critical to PEMFC performance, especially concerning liquid water permeability. This is a point of debate between researchers and was further studied by Rama et al. [106]. They conducted a numerical study to show gas transport in 3D structures. They compared the numerical study with measured data, which showed good agreement. They further pointed out that the through-plane tortuosity of the GDL would increase as the porosity decreased when under compression.

Furthermore, the addition of an MPL to the GDL can influence the permeability properties. Nanadegani et al. [107] found that the permeability and porosity of an MPL are influential to the operation of a GDL. Increasing MPL porosity would allow for better transfer of oxygen through the GDL. Also, decreasing the permeability would help reduce the liquid saturation. However, a reduction in permeability increased the overall PEMFC ohmic resistance, thus slightly decreasing overall performance [107]. Orogbemi et al. [101] also examined the effects on permeability with the addition of an MPL. It was found that the permeability of the GDL decreased by one order of magnitude after the addition of an MPL. Moreover, the permeability of an MPL was deduced to be between 2 – 3 orders of magnitude lower than the GDL substrate [101].

The gas permeability of GDLs has been studied extensively, as there is a critical relationship between the permeability characteristics of the GDL and the materials and structures that it is made from. This highlights the necessity of optimising GDL configurations for better fuel cell performance.

2.2.2 Effective Diffusivity

Oxygen transport is an important factor when considering PEMFCs and GDL functions. It is particularly important at high current densities. As oxygen is consumed at the catalyst, its concentration diminishes, ultimately leading to the current limiting density [23]. The reaction's kinetics and the oxygen concentration at the catalyst largely influence the slow oxygen reduction reaction, a significant performance bottleneck in PEMFCs. In the GDL, when the gas permeability is low, diffusion becomes the principal mechanism for oxygen transport. The resistance of the porous media to the diffusive flow of oxygen is characterised by the effective diffusivity, an essential material constant. The effective diffusivity (D_{eff}) in a porous medium (ε) takes into account the solid-phase obstacles, diffusivity in gas (D), and tortuosity (τ). These solid obstacles not only reduce the effective area for flux but also extend the length of diffusion pathways, which can be expressed as [42]:

$$D_{eff} = D\frac{\varepsilon}{\tau} \tag{2.5}$$

Ismail et al. [108] investigated the effective diffusivity of the porous layers in the PEMFC, in particular the GDLs. The main finding was that the commonly used Bruggeman relation significantly overestimates the effective diffusivity of the GDL, especially in the through-plane direction. To evaluate how this overestimation of the GDL effective diffusivity impacts the performance of the PEMFC, a two-dimensional model for a cathode was built. The polarisation curve for the model simulated with the Bruggeman relation was compared with an empirically-based equation for the effective diffusivity of Toray carbon papers. The results obtained have shown that the use of the Bruggeman relation significantly overestimates the performance of the fuel cell, up to a factor of 2 [108]. The capture of the anisotropic effective diffusivity of the GDL improves the performance of the modelled fuel cell.

Gao et al. [109] used simulations to examine the impact of GDL microstructure on its transport properties, focusing on how porosity and thickness influence the effective diffusivity. The simulations, varied GDL thickness from 88 μm to 352 μm. It demonstrated that an increase in thickness leads to a decrease in average velocity, with a more pronounced effect in the through-plane direction than in the in-plane direction. Additionally, flux values showed significant variation with increasing porosity, particularly at higher porosity levels. At higher porosities, flux reduction is linked to the water hindrance effect, with lower-porosity GDLs showing greater velocity disparities between inlet and outlet sections compared to higher-porosity GDLs, where the velocities tend to equalise when the porosity exceeds 0.8.

Mangal et al. [110] used an experimental setup called a diffusion bridge, to assess convective-diffusive in GDLs. Particularly focusing on measuring molecular diffusivity in the through-plane direction. The study evaluates the impact of varying PTFE concentrations (0, 10, 20, and 40%) on the transport properties of Toray 090 samples. Molecular diffusivity is measured by introducing a mix of nitrogen and oxygen into the system, followed by monitoring the pressures and oxygen concentration using an oxygen sensor. The findings indicated that diffusivity values decreased from 0.248 to 0.086 with increasing PTFE content.

The extensive literature on gas diffusivity in GDLs includes numerous experimental and numerical studies that have enhanced our understanding of this topic. Effective diffusivity is a crucial material constant, characterising the resistance of the porous media to diffusive oxygen flow.

2.2.3 Thermal Conductivity

Temperature gradient is an important parameter in a fuel cell, it simultaneously affects water and heat transport, which in turn affects the durability of a fuel cell. Therefore, efficient heat management is an important factor for fuel cells, this can be carried out by excess heat removal from the fuel cell [111]. The GDL has an important part to play in thermal conductivity as most of the heat generated is in the MEA, the GDL can thermally conduct this heat away from the MEA and out of the fuel cell. Thermal conductivity can be expressed as follows [42]:

$$Q_x = -KA\frac{dT}{dx} \tag{2.6}$$

It shows that the heat transferred is proportional to the change in temperature (dT), thermal conductivity (K) and the cross-sectional area (A). Thermal conductivity is dependent on the structural properties of the GDL and thermal conductivity will decrease if the porosity of the GDL increases. Thermal conductivity is also influenced by the anisotropic nature of the GDL, the orientation of the woven carbon fibres can result in a higher in-plane conductivity rather than through-plane [42].

Thermal conductivity has been estimated both theoretically and experimentally. Theoretical values range between 0.15 W/mK – 65 W/mK [[112], [113], [114], [115]]. Ramousse et al. [116] experimentally investigated the thermal conductivity of four carbon paper samples, comparing PTFE contents and the manufacturing process. They found a maximum thermal conductivity between 0.20 – 0.36 W/mK and a minimum between 0.3 – 1.36 W/mK.

Khandelwal et al. [117] measured the through-plane thermal conductivity from two different GDL manufacturers, with differing PTFE contents. The effective thermal conductivity of Toray carbon paper was found to decrease from 1.8 to 1.24 W/mK when there was an increase in temperature from 26 °C to 73 °C. It was also found that the addition of PTFE reduced the thermal conductivity [117].

Karimi et al. [118] experimentally measured the in-plane thermal conductivity for carbon paper. It was found that the in-plane thermal conductivity would vary depending on the manufacturing process, and the treatment and orientation of the paper. Results ranged from 3.54 W/mK – 15.1 W/mK [118].

The addition of MPL can also affect the thermal conductivity of a GDL. Sadeghifar et al. [119] created a model that determined that the addition of an MPL would reduce overall thermal conductivity and increase thermal contact resistance compared to an uncoated GDL [119]. Unsworth et al. [120] also investigated the thermal conductivity with the addition of an MPL. They concluded that a GDL with MPL coating had lower bulk thermal conductivity at high compressions. However, at low compression, the difference was negligible [120]. Despite the lower bulk thermal conductivity with the addition of an MPL, thermal management of the GDL can still be improved due to the improved surface contact of the MPL. This in turn lowers the thermal contact resistance and can assist in the dissipation of heat [120].

The thermal conductivity of a GDL is influenced by its morphological properties, such as porosity, tortuosity, and wettability. Effective thermal management is crucial for fuel cell performance, as poor heat management can reduce the fuel cell's lifespan [42]. Waste heat production and proper thermal management are critical challenges in PEMFC technology. In

PEMFCs without active cooling, the GDL conducts heat away from the MEA, making good thermal conductivity an essential property for the GDL.

2.2.4 Electrical Conductivity

The GDL is made from electrically conductive carbon fibres. These fibres allow electrons to travel from the CL and out to the external circuit. The electrical conductivity of the GDL is dependent on the material used, porosity and anisotropy. The GDL has carbon fibres aligned in specific directions, this gives rise to an anisotropic structure which affects the electrical conductivity in the in-plane and through-plane directions. Therefore, the electrical conductivity of the GDL thus exhibits noticeable differences in the different planes, such that the conductivity obtained from in-plane can differ by a factor of around two compared with through-plane [121].

A method was developed by Van der Pauw (VDP) to measure in-plane electrical conductivity for isotropic materials. The method assumes that samples are semi-infinite and thin, the equation is expressed as follows [89]:

$$\rho = g\frac{\Delta V}{I} \tag{2.7}$$

This describes the electrical resistivity (ρ) that can be calculated by dividing the potential difference (ΔV) by the applied current (I) and multiplying by a geometrical factor (g).

To experimentally measure the in-plane electrical conductivity of a sample, the four-point probe method is used. Figure 2-5 shows what the setup with the probes would look like.

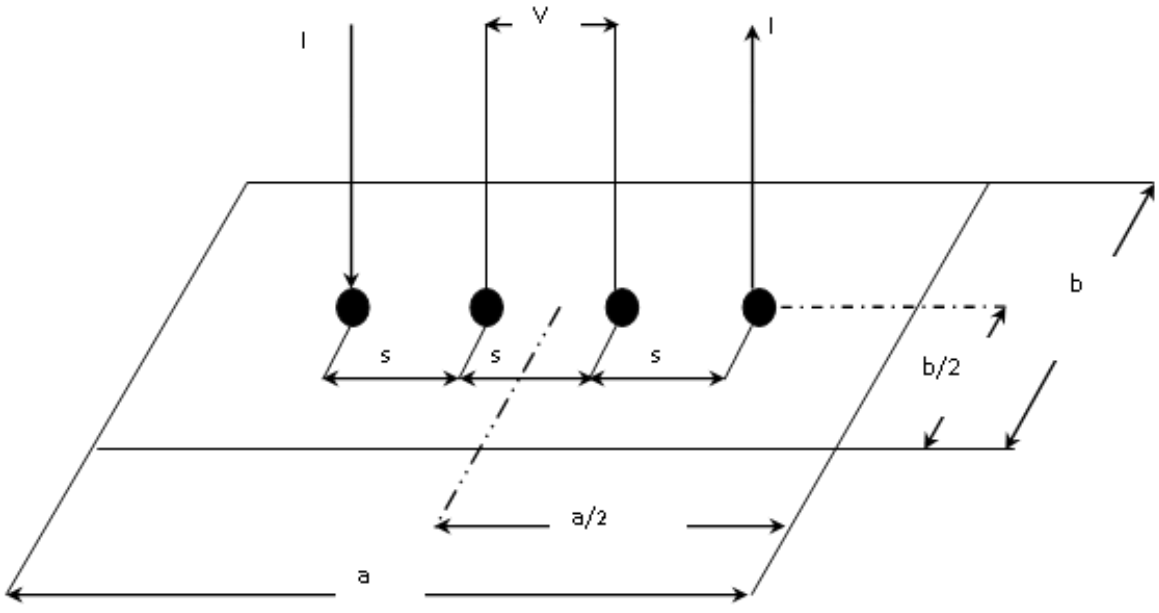

Figure 2-5 In-plane electrical conductivity experimental set-up [89].

As can be seen in Figure 2-5, two adjacent probes supply a constant current, while the other two probes measure electrical potential. The probes are placed equidistant and in a straight line, they are also required to be placed at the periphery of the sample and the probe contact areas

must be minimised. The VDP method is versatile and allows for samples of a range of different sizes and shapes to be examined [89].

The through-plane electrical conductivity of a GDL can also be measured using the 4-probe method, but the set-up is slightly different as shown in Figure 2-6.

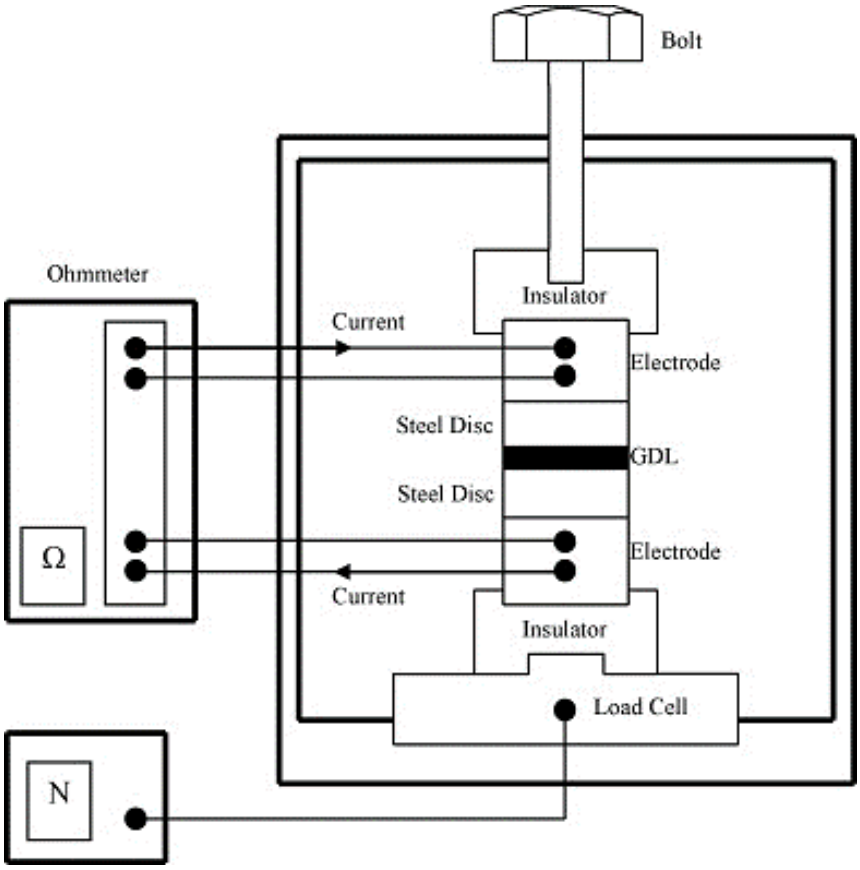

Figure 2-6 Through plane electrical conductivity experimental set-up [89].

A GDL sample is placed between two stainless steel discs and subsequently, two copper electrodes and two probes are placed on each side of the electrodes. A bolt can be used to increase the pressure of the sandwiched GDL to take measurements of electrical conductivity as a function of pressure [89].

The electrical resistance can be directly read from an Ohmmeter. Subsequently, the electrical resistivity of the GDL can be calculated [89]:

$$\rho = CtR \tag{2.8}$$

Where the resistivity (ρ), is the correction factor (C) multiplied by the thickness (t) and the measured electrical resistance (R). The correction factor is dependent on the ratio of the length of the GDL to its width and the width of the GDL to the spacing between probes. Following this, the electrical conductivity of the GDL can be found by the reciprocal of the resistivity [89].

$$\sigma = \frac{1}{\rho} \tag{2.9}$$

Morris et al. [69] used VDP to measure the in-plane electrical conductivities for different types of GDLs. They found pronounced anisotropy in the in-plane electrical conductivity for all GDL

samples [69]. Yoosefabadi et al. [80] also looked at the effects of anisotropy. They created a model to simulate the effective electrical conductivity of the GDL. It was found that the through-plane electrical conductivity was estimated at 600 S/m. Whereas the in-plane conductivity was 4 times higher due to the anisotropic nature of the GDL fibre structure [80].

Nitta et al. [122] measured the in-plane and through-plane electrical conductivity of a carbon paper (SGL Sigracet 10-BA) as a function of different compression pressures. They found that the electrical conductivity increases with increasing pressure and is thus, linearly dependent on the compressive force [122]. Ismail et al. [89] similarly measured the electrical conductivity of SGL carbon paper but considered the effect of PTFE content. It was found that PTFE decreased the through-plane conductivity but had no effect on the in-plane conductivity. This is expected as PTFE is naturally an insulating material and the decrease in the through-plane electrical conductivity is due to the electrical resistance that the PTFE creates between the carbon fibres [89].

Aydin et al. [123] addressed challenges associated with the accuracy of GDL electrical conductivity measurements. They used three variations of the VDP four-point probe method to measure the through-plane resistivity for different GDL samples. The three different methods used the same fundamental four-point probe technique with a modification in voltage sense probes, these probes were: gold-coated electrodes, contact pins, and micro-wire probes [123]. It was found that the accuracy of the results is highly dependent on the measurement method and probes used. The gold-coated probes helped reduce the electrical contact resistance between the probes and the samples but did not completely eliminate it [123]. The contact pins were found to be more suitable for measuring the in-plane conductivity [123]. The micro-wires were found to be best used in situations where samples had a lower in-plane resistance [123]. All things considered, the results indicated an inherent electrical contact resistance between the electrode probes and the GDL existed and could affect measurements. The optimum way to measure the GDL electrical conductivity should be taken on the surface of the sample using the micro-wires [123].

The addition of an MPL to the GDL has been shown to reduce the interfacial electrical contact resistance between the GDL and neighbouring components, thus improving overall through-plane conductivity. This was shown by Ismail et al. [124] where an addition of MPL between the GDL and the BPP improved the electrical conductivity of the overall setup. This was due to the fact that the MPL could establish good contact between the GDL and BPP. Ye et al. [125] carried out studies into MPL addition and reached a similar conclusion. The addition of an MPL to the GDL does not alter the bulk resistivity of the GDL. However, it did reduce the contact resistivity. The contact resistance and the effect it has on electrical conductivity will be discussed in further detail in Section 2.4.

The electrical conductivity of a GDL has been extensively studied, as it is a key design parameter for PEMFC operation. The GDL consists of densely packed carbon fibres that facilitate electron transport for the current collection. The capacity of the GDL to transport electrons is determined by its carbon fibre structure, which can be assessed through in-plane, through-plane, and contact resistance tests. Electron transport depends on the GDL's electrical conductivity, thickness, porosity, and heterogeneous anisotropic structure.

2.3 Microporous Layer

The MPL is composed of carbon black particles and PTFE. It is a thin layer applied to the surface of the GDL facing the CL and aids the overall functioning of the GDL. Ideally, an MPL should improve PEMFC performance in several ways [126]:

- By facilitating oxygen distribution to the cathode CL.
- Reducing liquid water saturation between the CL and the BPP through increased capillary pressure due to its hydrophobic nature and small pore sizes (1 – 10 μm) that are smaller than those in the gas diffusion layer (GDL, 10 – 100 μm) but larger than those in the CCL (0.001 – 5 μm) [126].
- Reducing electrical resistance at the interface between the CL and GDL.
- Improving the mechanical fit between the GDL and CL.
- Providing structural support to the fragile catalyst layer.
- Maximising catalyst usage by preventing the migration of precious metal catalysts into the GDL.

The MPL can be optimised in different ways to enhance the overall fuel cell performance. This includes modifying the MPL materials and microstructure.

2.3.1 Conventional MPL Materials

Carbon black is a commonly used material for components in PEMFC fabrication. It is used for both the catalyst support and to fabricate the MPL. Carbon black is produced through the pyrolysis of hydrocarbons such as natural gas or petroleum fractions. These materials typically have very low ash content, often under 1 wt. % [127]. The primary production techniques include the oil-furnace and acetylene processes, with the furnace black process being the most prevalent. In this method, the raw material is introduced into a furnace and combusted at approximately 1400°C with a restricted air supply [127]. Carbon black is known for its advantageous physical properties, such as high electrical conductivity, porosity, large surface area, low cost, and relative abundance [127]. Due to these characteristics, it is typically used as the primary material in the MPL. The MPL, which is positioned between the carbon substrate and the electrocatalyst layer, facilitates optimal contact with the electrocatalyst, enhancing the GDL function [127]. Typically, to form the MPL, carbon black particles are mixed with a polymeric hydrophobic binding agent, usually PTFE. The hydrophobic nature of the MPL creates high capillary pressure, which helps maintain membrane hydration and prevents water flooding in fuel cells. This configuration has been demonstrated to substantially enhance both the performance and durability of fuel cells [128]. Table 2-1 gives a summary of prevalent carbon blacks used as the MPL material for PEMFCs.

Table 2-1 Physical properties of different carbon blacks [129].

Carbon Black Type	Particle Size (nm)	Specific Surface Area (m^2/g)
Vulcan Black XC-72	30	254
Ketjenblack	34	1311
Acetylene Black	43	62
Black Pearls	15	1475

Vulcan black is a popular choice of carbon black in electrochemical applications due to its balanced properties, offering a high surface area of approximately along with good electrical conductivity [127].

There have been investigations into the properties of the carbon black particles and how they affect the performance and fabrication of the MPL. Wang et al. [129] carried out an investigation exploring the impact of various carbon blacks used in MPL fabrication. They examined the physical properties of the carbon black and the corresponding electrochemical performance in fuel cells. It was found that the key factor contributing to good MPL performance was an optimal pore size distribution, which favoured a good distribution of mesopores and macropores. These characteristics facilitated efficient gas and water transport. Similarly, Passalacqua et al. [130] explored various carbon blacks, including Vulcan XC-72, Acetylene Black and graphite for use in MPLs. The electrochemical tests showed that the behaviour of cells with these MPLs confirmed that the type and specifications of the carbon powder impacted performance. High pore volume and small average pore size, notably improved the cell performance

Chen et al. [131] demonstrated the importance of a consistent MPL distribution to ensure good PEMFC performance, but also the challenge associated with the formation of MPL cracks. The study found that regardless of the carbon black particle, the formulation of MPL ink will have some cracks and this can affect homogeneity, as well as the PTFE distribution. Additionally, the interaction between the carbon black and PTFE enhances PTFE distribution homogeneity. The study concludes that adjusting the ink polydispersity index can lead to a more homogeneous MPL structure, which is crucial for high-performance fuel cells.

Jordan et al. [[132], [133]] conducted studies for MPLs with different carbon powders (Vulcan XC-72 and Acetylene Black) with a 10 wt. % PTFE loading. The MPL which contained Acetylene Black led to higher power density than that with Vulcan XC-72 due to the less porous structure in the MPL. Furthermore, when the MPL was heat-treated at 350 °C for 30 minutes, an enhancement in performance was observed. It was evaluated that uniform distribution of the PTFE throughout the MPL by sintering made the MPL more hydrophobic, resulting in better water management. This highlighted the significant impact of MPL composition and treatment on overall fuel cell performance.

Various techniques can be used to apply the MPL to the carbon substrate, including brush coating, spray coating, the doctor blade technique, rod coating, and screen printing [134]. The method used to apply the MPL to the carbon substrate depends on the viscosity of the MPL ink. Thicker, more viscous inks are typically applied using the doctor blade coating technique, brush or screen printing. Thinner and less viscous inks are suitable for spray coating. After the application of the MPL to the GDL substrate. The MPL coated GDL then undergoes heat treatment and is sintered at approximately 350 °C to melt and evenly distribute the PTFE. The PTFE assists in binding the carbon black particles in the MPL and laminates the MPL onto the carbon substrate.

2.3.2 Novel Materials

Currently, studies of MPLs are typically limited to conventional carbon black materials, there has been little consideration for novel materials. Novel materials usage in MPL fabrication are becoming more widespread as they are shown to increase the capabilities of the MPL. In particular, carbon nanotubes and graphene show great promise.

2.3.2.1 Carbon Nanotubes

A carbon nanotube (CNT) is a cylindrical tube at the nanoscale made from a single atomic layer of carbon atoms. CNTs have several unique characteristics: high electrical conductivity, high thermal conductivity, chemical stability, excellent mechanical strength, and a high surface area [135]. These characteristics have caused CNTs to be an interesting area of research when choosing candidates for novel fuel cell materials.

Gao et al. [136] developed carbon paper made from CNTs, polyacrylonitrile-based carbon fibre and PTFE. Compared with a standard carbon paper of Toray (TGP-H-060), it showed a higher electronic conductivity than and larger pore volume with pore diameters between 0.03 μm – 3 μm. The GDL were tested in a DMFC and EIS showed that the GDL with CNTs had better electrical conductivity and mass transfer ability than the Toray GDL. As a result, the limiting current density increased by 40% and peak power density increased by 27%.

Kannan et al. [137] used chemical vapour deposition to grow multi-walled CNTs (MWCNTs) as an MPL on the GDL. The GDLs with in-situ growth of MWCNTs as the MPL had a natural hydrophobicity so no PTFE was added. It showed stable fuel cell performance in 70% – 100% relative humidity. It also exhibited mechanical robustness at elevated temperatures and lower relative humidity conditions. SEM was used to examine the surface and it displayed excellent surface morphology and homogeneity with no cracks.

Similarly, Tang et al. [138] fabricated an in-situ grown CNT layer and applied it to a commercial Toray carbon paper (TGP-H-090). SEM and Brunauer–Emmett–Teller (BET) analysis showed that the CNT layers exhibited extremely high porosity and surface area. This can allow for enhanced catalyst utilisation and electrical conductivity compared with standard carbon blacks.

Du et al. [139] prepared a CNT-based MPL without any hydrophobic agent. They used the CNT-based MPL to serve as a support for a thin CL and deposited Pt particles using physical vapour deposition. This enabled higher catalyst utilisation and enhanced electrical conductivity. The MPL made from CNT showed intrinsic hydrophobicity and high electrical conductivity with a continuous interface layer resulting in excellent performance. Maximum power densities of 902 mW/cm^2 were achieved for the fuel cell operating at 70 °C with a H_2/O_2 inlet.

Schweiss et al. [140] modified an MPL by the addition of MWCNTs to conventional carbon black, this was then coated onto a GDL surface. With the addition of MWCNTs, it was found that the electronic resistance of the GDL was significantly reduced. Also, a larger mean pore diameter was observed. Overall the fuel cell performance improved considerably with the addition of MWCNTs. This was attributed to the synergetic effect of increased electronic conductivity and improved mass transport.

2.3.2.2 Graphene

Similar to CNTs, graphene has excellent properties such as high electrical and thermal conductivity, high surface area, chemical stability and mechanical strength [141].

Leeuwner et al. [142] identified the contact resistance between the MPL and CL as an area of poor electrical conductivity. They carried out a comparative study of different MPLs created from conventional carbon black, graphene foam and graphene sheets. The graphene foam showed beneficial interfacial properties that contributed to enhanced electrical conductivity. This can be attributed to the graphene's ability for excellent interfacial adhesion combined with high electrical conductivity. This created an optimal combination, which enhanced overall performance.

Similarly, Ozden et al. [143] investigated water management and overall performance enhancement for a graphene-based MPL. The graphene-based MPL was characterised by examining morphological, structural, physical and electrochemical properties. It was also compared to a conventional MPL made from Ketjenblack. It was found that the graphene had higher in-plane electrical conductivity and better water-retaining abilities compared with Ketjenblack. In high humidity conditions, the graphene-based MPL showed comparable performance to the conventional Ketjenblack MPL. Under low to medium humidity conditions, graphene showed a peak power density improvement of 55%. Overall, it was found that the graphene MPL has significant potential to meet performance demand under a wide range of operating conditions. Ozden et al. [143] further examined, through characterisation and performance, a graphene MPL compared to a conventional MPL made from Vulcan black. The results showed that the graphene MPL had a unique morphology composed of horizontally packed graphene flakes that improved in-plane electrical conductivity by 2 times. The graphene MPL also performed better in fully and partially humidified conditions, with peak power densities of 43% higher than those obtained for Vulcan black MPL. This was due to the graphene having less ohmic resistance, particularly under partially humidified conditions.

Based on the aforementioned, it is clear that there is growing interest in the role that novel materials will play in the enhancement of the GDL. Particularly, because they can improve the surface contact and have intrinsic higher electrical conductivity. Despite this, they are still in the early stages of development and require further research to determine if they are suited for use as an MPL material. Furthermore, since they are relatively new materials, manufacturing costs are still high, which makes them commercially uncompetitive with conventional carbon black particles.

2.3.3 Novel Water Management Designs

Hydrophobic additives such as PTFE are conventionally used in the GDL/MPLs to enhance the water drainage rate and decrease the water condensation within the PEMFC [60]. The liquid water that accumulates can easily be expelled due to the low adhesion of the water on the hydrophobically treated surfaces. However, it must be considered that PTFE coating can affect other properties of the GDL by changing pore size distribution, bulk and contact resistance. This is due to the electrical insulating nature of the PTFE [[89], [144]]. Some researchers have carried out studies to examine novel water management GDL designs to further improve fuel cell performance.

2.3.3.1 Hydrophilic Treatment

Hydrophilic treatment of the GDL can aid PEMFC operation under low relative humidity and high current density conditions. However, it could be less beneficial for gas transport at high current densities. Therefore the optimisation of hydrophilic treatment should be balanced so that the PEMFC can operate efficiently in a wide range of current densities [60].

The mass transfer ability of MPL can potentially be further improved with hydrophilic treatment. The incorporation of hydrophilic agents into the MPL has been investigated [[140] ,[145], [146], [147], [148], [149]]. In these studies, the conventional PTFE-coated MPL had hydrophilic sites incorporated into it. These hydrophilic areas functioned by absorbing water whilst simultaneously leaving pores available for gas transport.

Schweiss et al. [140] fabricated hydrophilic wicking areas within the MPL. This helped to improve the water permeability of the MPL which in turn reduced the flooding of the catalyst layer [140]. Schweiss et al. [147] also further examined the effect of doping the MPL with hydrophilic agents. This was done using aluminosilicate fibres. The introduction of these fibres as a hydrophilic area helped to enhance water removal through the MPL. This was because the liquid water had a stable pathway to escape through and the hydrophobic pores remained open for gas transport. At low humidity conditions, the MPL with hydrophilic areas performed better at high current densities. This was because the hydrophilic areas helped keep the membrane hydrated.

Spernjak et al. [145] also used hydrophilic agents (aluminosilicate fibres) incorporated into the MPL. This helped to improve the performance of the PEMFC at high current densities by overcoming the high capillary pressures of the MPL [145]. However, if the aluminosilicate fibres detach from the MPL and migrate to the catalyst layer they can cause catalyst poisoning.

Ahn et al. [149] compared PTFE and Nafion used as binders in MPL. The binder is an important component in MPL fabrication and can influence the performance of the GDL. Nafion has a hydrophilic nature due to the sulfonate functional groups. It was found that there was a reduction in ohmic losses in the MPLs treated with Nafion as compared to those treated with PTFE. Furthermore, they found that at high humidity conditions, the Nafion facilitated liquid water removal from the CL and allowed reactant gasses to reach the CL. The hydrophilic Nafion was also able to retain water in low humidity conditions. This allowed the membrane to keep hydrated and improve overall PEMFC performance. However, using Nafion as a binder in the MPL proved problematic during the sintering stage of fabrication, which takes place at 350°C. This was because the Nafion started to degrade at temperatures above 280°C. Therefore, a uniform distribution cannot be achieved by using Nafion.

Similarly, Simon et al. [150] investigated MPLs which consisted of PTFE and hydrophilic perfluorosulfonic acid (PFSA). It was found that all the samples performed similarly at higher temperatures. However, when replacing PTFE with a PFSA binder there was increased oxygen transport resistance. This could be due to the hydrophilic PFSA accumulating too much water in the MPL which inhibited the flow of oxygen.

Hou et al. [146] investigated the influence of an ultrathin hydrophilic titanium dioxide layer in the MPL and the performance of the PEMFC at low humidity conditions. It was found that the hydrophilic doped MPL was better at self-humidification at lower relative humidity than the conventional MPL. The hydrophilic doped MPL was able to keep the membrane suitably hydrated at low humidity conditions and improve the overall PEMFC performance.

Hydrophilic treatment of the GDL has been shown in some cases to improve the overall PEMFC performance, particularly in low relative humidity and high current density scenarios. However, at high current density, the hydrophilic nature could trap water and inhibit the mass transport of reactant gases. Therefore, an optimum balance must be found between the hydrophilic and hydrophobic treatment for the PEMFC to perform well in a range of different conditions. There is significant research potential in exploring the interaction between hydrophobic and hydrophilic properties of GDLs, especially through engineering designs of materials for the GDL/MPL. This topic remains largely unexplored and warrants further investigation.

2.3.3.2 Graded Wettability

As discussed, several research findings showed that the incorporation of a hydrophilic layer in an MPL can improve the performance of the PEMFC at both relatively low and high humidity conditions [[151], [152], [153], [154], [155], [156]]. This hydrophilic MPL layer is helpful in the removal of water at high humidity and hydration of the MEA at low humidity conditions. In order to optimise the balance of hydrophobicity and hydrophilicity, some researchers have investigated graded wettability [[151], [156], [157], [158]].

It was shown that graded wettability in layers of hydrophobic and hydrophilic were effective at water management at different humidity conditions within the PEMFC. In particular, a hydrophilic layer between the catalyst and a hydrophobic layer acted as an internal humidifier. This helped to keep the membrane hydrated at low humidity conditions. When the fuel cell operates at high humidity conditions, the water is expelled by the hydrophobic layer.

Kitahara et al. [151] fabricated a double-layered MPL consisting of a hydrophilic and hydrophobic layer (Figure 2-7). The double-layer MPL was made to improve the PEMFC's performance at low humidification conditions.

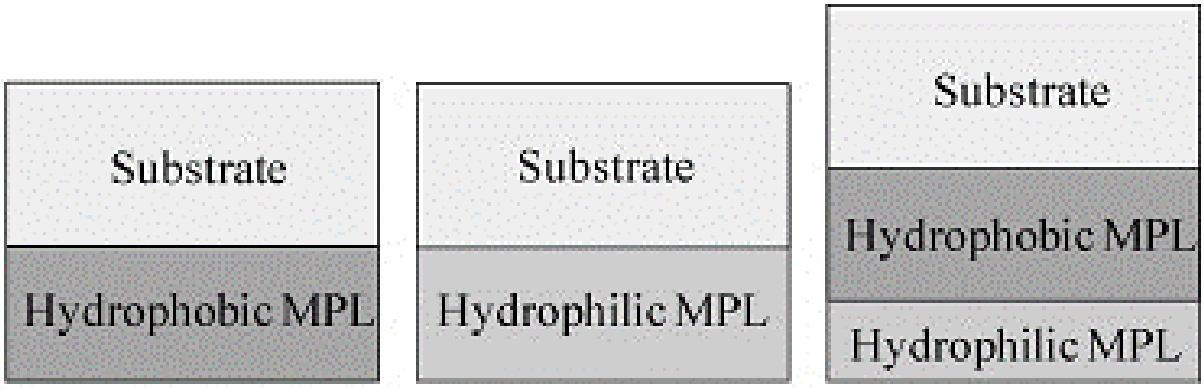

Figure 2-7 The structure of single-layered MPLs and a double-layered MPL with hydrophobic and hydrophilic treatment [151].

The GDL used at the anode was a commercial carbon paper without the MPL (SGL SIGRACET® 24BA) with 5% PTFE loading. The 24BA GDL had a thickness of 190 μm, areal weight of 54 gm^2, porosity of 84% and maximum pore diameter of 110 μm [151].

The hydrophobic MPL consisted of 20% PTFE and 80% carbon black. The hydrophilic MPL consisted of 5% PVA and 95% carbon black. Polyvinyl alcohol (PVA) was used instead of PTFE as the MPL binder. This enables hydrophilicity to be imparted without a reduction in the binder force between the MPL and the substrate [151].

For the hydrophilic and hydrophobic double-layer MPL, the hydrophilic layer was coated on the hydrophobic MPL. The PVA content in the hydrophilic layer was varied between 2 – 10%. The PTFE content in the hydrophobic intermediate layer was varied between 10 – 40% [151].

Contact angle measurements were carried out. It was found that when the PTFE content in the hydrophobic MPL increases from 10 – 40%, the contact angle increased from 123° to 142°. When the PVA content in the hydrophilic MPL increases from 2 – 10%, the contact angle is reduced from 56° to 42° [151].

It was found that the hydrophobic layer avoids excessive discharge of water, and the hydrophilic layer maintains the humidity of the membrane. One thing that must be considered is that the mass transfer resistance increases with thickness. The optimum thickness of the hydrophilic layer for this MPL was determined to be 5 μm. Although the ability of the hydrophilic single MPL coated GDL to conserve the humidity at the catalyst layer is enhanced, it is relatively easy for the water in the hydrophilic layer to be expelled to dry air in the GDL substrate. The hydrophilic layer is effective for conserving humidity at the catalyst layer, while the dense hydrophobic intermediate layer between the hydrophilic layer and the substrate prevents the removal of water in the hydrophilic layer via dry air in the substrate. This results in a significant enhancement of PEFC performance [151].

In a similar study, Chun et al. [156] investigated a bilayer-graded wettability MPL. They examined the PEMFC performance at high and low relative humidity conditions (wet condition RH = 100%, dry condition RH = 50%). A hydrophilic layer was placed between the hydrophobic layer and the CL. The hydrophilic layer was then placed between the GDL and the hydrophobic MPL layer (Figure 2-8). It was found that there was better performance in both wet and dry conditions when the hydrophilic layer was placed between the GDL and the

hydrophobic MPL. It was concluded that the top layer of hydrophobic MPL was beneficial in removing excess water during high humidity.

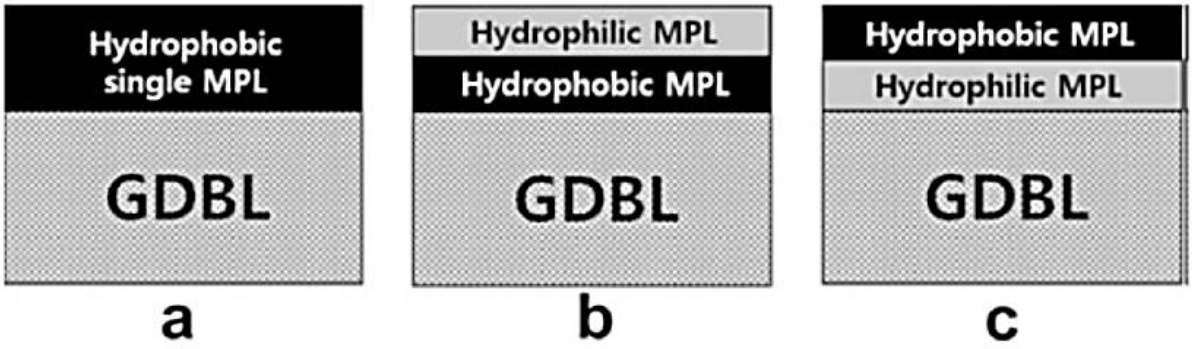

Figure 2-8 Single and double MPLs with hydrophobic and hydrophilic layers [156].

Hirakata et al. [[154], [155]] compared GDLs from SGL Group at low and high humidity conditions with a cold start-up. One GDL had a hydrophilic layer between the substrate and the MPL. The other GDL had a single conventional hydrophobic MPL. Similar to Chun et al. [156], it was found that a hydrophilic layer was effective at improving overall PEMFC performance at low and high humidity conditions. A cold start-up was also investigated at 10°C. It was found that there was a significant improvement with the use of a hydrophilic layer as it helped to remove liquid water from the CL which forms at low temperatures.

Weng et al. [157] fabricated a triple-layer MPL, each with different loadings of PTFE. The layer directly on the GDL was at 30 wt. % PTFE followed by 25 wt. % and 20 wt. % facing the catalyst layer. It was concluded that an MPL with a hydrophobicity gradient helped improve the overall water management. This was because, under low humidity conditions, the layers with lower PTFE loading helped keep the CL and membrane hydrated. However, the grading of PTFE content needs to be carefully optimised depending on the conditions of the PEMFC.

Similarly, Kitahara et al. [158] also investigated the effect of hydrophilic and hydrophobic triple layers MPL on the performance of PEMFCs under high humidity conditions (Figure 2-9).

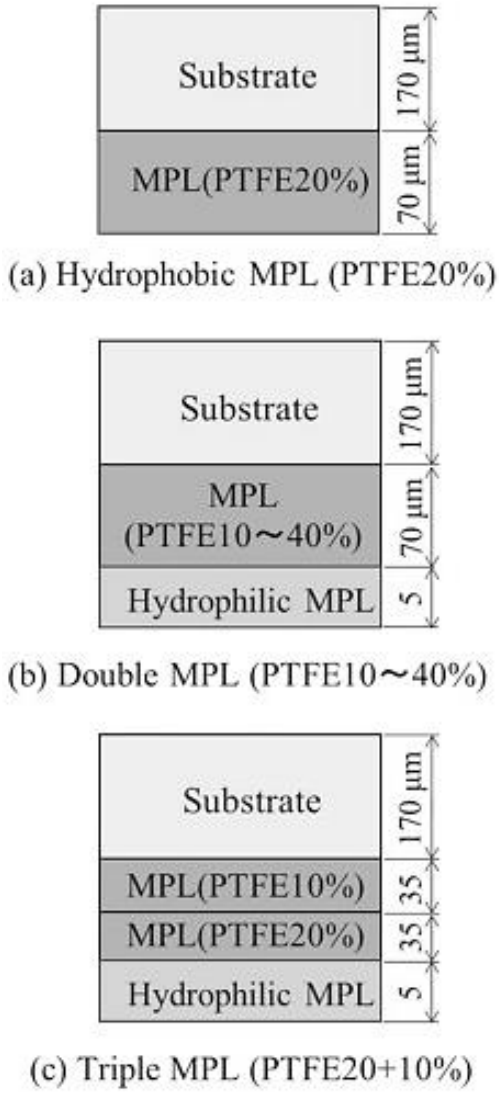

Figure 2-9 Different MPL configurations showing: (a) hydrophobic MPL, (b) double-layer MPL and (c) triple-layer MPL [158].

The MPL thickness of the hydrophobic MPL was set at 70 μm. The thickness of the hydrophobic intermediate MPL in the double MPL coated GDL was also set at 70 μm. In the case of the triple MPL coated GDL, the thickness of the hydrophobic MPL containing 10% PTFE after the first MPL coating was set at 35 μm, and that of the hydrophobic MPL containing 20% PTFE content after the second MPL coating was set at 35 μm. The hydrophilic layer thickness was 5 μm and the total thickness of all the double and the triple MPL coated GDLs was 245 μm [158].

The results of previous studies showed that graded wettability in the MPL, particularly with a hydrophobic and hydrophilic layer enhances the overall performance of a PEMFC in a wider range of RH conditions. The double MPL layers, in which a hydrophobic layer is located in between the hydrophilic layer and gas diffusion substrate, are effective at improving the water drainage ability of the catalyst layer and decreasing the oxygen transfer resistance. In addition,

the triple MPL coated GDL can expel excess water from the catalyst layer and the oxygen transport resistance is reduced effectively inside the MPL under high humidity conditions.

A trade-off must be considered, as the extra layers of MPL will increase the overall thickness of the GDL which can have a negative effect on water management and mass transport of reactant gases. It was found by Kitahara [151] that the optimum thickness of the hydrophilic layer was 5 μm.

Overall, it was found that creating a composite layered MPL can aid with water management within the GDL. The composition of the MPLs has been tested and optimised to find the best solution to water management whilst considering the gas transport trade-offs.

Graded wettability designs of MPLs are increasingly researched due to their potential benefits, particularly to ensure that GDL/MPLs can operate effectively across a wide range of humidity conditions, without compromising the PEMFC performance. Successfully implementing these designs is crucial for practical applications and could significantly boost PEMFC usage. However, further studies are needed to determine the optimal engineering approaches for maintaining high performance and to mitigate the trade-offs due to the extra thickness of the GDL.

2.3.3.3 Thickness of MPL

The thickness and loading of the MPL onto the GDL surface can be a critical factor in the overall fuel cell performance. It can impact functions such as mass transport and heat transfer.

Deevanhxay et al. [57] found that liquid water accumulation at the GDL/CL interface has a critical effect on the PEM fuel cell performance. The MPL helps reduce water accumulation, which gives better overall fuel cell performance. The liquid water accumulation at the GDL/CL interface without an MPL was shown to have a detrimental effect on the fuel cell performance. The MPL reduced the water accumulation at the GDL/CL, making the performance of the fuel cell with MPL better than that of the cell without MPL [159].

Lee et al. [160] carried out a study utilising synchrotron X-ray imaging to explore how different thicknesses of the MPL influence water management in a PEMFC. A custom miniature fuel cell with a 0.48 cm^2 active area was created, and radiographic images were taken at high resolution to track water behaviour. MPL thicknesses were varied (0, 50, 100, 150 μm, and 50 μm MPL without a substrate) across different ranges of varying current densities (0.5, 1.2, and 2.0 A/cm^2). Results showed that when an MPL was added, regardless of thickness, it helped to reduce liquid water buildup at the catalyst layer–GDL interface. Thicker MPLs were particularly good at minimising water accumulation at the transition region between the MPL and the GDL substrate. Under high current densities, water condensed near the flow fields and migrated towards the substrate. Interestingly it was observed that a GDL composed solely of an MPL significantly lowered the overall water buildup compared to MPLs with substrates.

Nam et al. [78] studied water formation in a GDL treated with PTFE using simulation modelling. It was also demonstrated that the MPL lowers liquid water saturation at the interfaces between the MPL and the MPS and also between the CL and MPL. This helped reduce the chances of severe water flooding in the fuel cell which in turn aids overall performance.

Research carried out by Nanadegani et al. [107] utilised three-dimensional, steady-state, non-isothermal simulations to investigate two-phase flow in PEMFCs. The study employed a two-fluid model to analyse the thermal and water transport dynamics and their impact on the performance of the cell. It was found that the incorporation of an MPL into a fuel cell promotes a more even temperature distribution and enhances the thermal conductivity of the membrane. This occurs as the increased thermal conductivity allows for greater heat dissipation from the MEA, resulting in a more uniform temperature across the membrane. Consequently, this leads to enhanced humidification of liquid water and an increase in liquid water saturation.

Thicker MPLs tend to be more suited for low humidity conditions as they can keep the membrane hydrated. In contrast, thinner MPLs are more suited to high humidity conditions to help with water removal. In general, lower MPL loadings with small to medium carbon particle sizes are preferred in humid conditions. Larger particles, with medium PTFE loadings, are better under dry conditions to help keep the membrane suitably hydrated [161].

GDL thickness is relative and varies for different scenarios, it is very much dependent on the fuel cell design and operating conditions. Experimental studies on GDL thickness have shown that there is an optimal MPL thickness to achieve the best fuel cell operation results [[162], [163], [164]].

The findings of Antonacci et al. [162] on changing the MPL thickness with respect to the overall PEMFC performance, using experimental techniques of EIS and synchrotron X-ray radiography. The results found that increasing the MPL thickness from 30 μm to 50 μm lowers the liquid water volume by 8% in the GDL on the cathode side. At a current density of 2.0 A/cm^2, this gave rise to a 50% decrease in the oxygen mass transport resistance. It was also reported that an MPL thickness greater than 50 μm at 2.0 A/cm^2 did not give any further reductions in the liquid water volume in GDL. However, ohmic resistance significantly increased by 16%. The optimum MPL thickness was found to be 50 μm as this gave the best trade-off between water removal and membrane hydration.

Weber et al. [164] showed similar results. However, they concluded that the optimal MPL thickness was 20 μm for efficient PEMFC performance. They asserted that the MPL needs to be thin enough for improved oxygen transport and thick enough for enhanced water management.

Park et al. [165] experimentally examined the effect of an MPL made from Acetylene Black for fuel cell performance. It was demonstrated that carbon loading of 0.5 mg/cm^2 at 75 °C and ambient pressure leads and air as the oxidant leads to the best fuel cell performance, according to polarisation curve measurements.

A numerical simulation conducted by Wang et al. [166], also showed agreement with these findings. It was reported that an MPL thickness between 30 μm – 45 μm was the optimum level in which the cathode liquid water saturation would be minimised and overall PEMFC performance would not be compromised.

Given these factors, determining the optimal MPL thickness is crucial. It must be thick enough to perform its functions effectively, but not so thick that it impedes the gas flow, increases the resistance, or hinders water management. The thickness has been an extensively researched topic in the MPL design and the implications of modifying the thickness are well understood.

2.3.4 Microstructure Modification

2.3.4.1 MPL Perforations and Cracks

Research has also shown [[128], [167], [168], [169], [170]] that perforations and cracks in the MPL can benefit water management by serving as preferential pathways for liquid water movement away from the CL. However, these cracks, while useful for water transport, may compromise the mechanical durability of the MPL.

Gerteisen et al. [167] created laser-perforated GDL and tested it in a 1 cm^2 test fuel cell. It had precisely spaced 1 μm holes with a distance of about 1 mm to improve water management. Voltammetry experiments conducted at various humidification levels of inlet gases revealed that the perforated GDL effectively reduces saturation at the cathode. Compared to a standard GDL, the modified version showed enhanced performance due to reduced liquid water accumulation, evidenced by a lower cathode overpotential and an 8 – 22% increase in limiting current density. This suggests a potential for further optimisation of GDL structures to decrease water accumulation and enhance oxygen diffusion.

Similarly, Manahan et al. [168] studied laser treatment of the cathode GDL. The laser treatment forms hydrophilic heat-affected zones that promote localised water redistribution. Experiments comparing non-perforated GDLs to one with 100 μm diameter perforations show that at lower humidity and currents, the non-perforated sample increases water back diffusion from cathode to anode. At higher current densities, it acted as a barrier to prevent cathode water from moving to the anode.

Lu et al. [169] also utilised laser perforation specifically on the MPL, leaving the substrate untouched. They employed neutron imaging to monitor water distribution during operation and observed improved performance under both dry (90°C cell temperature with 100% RH for hydrogen and 30% RH for air) and wet conditions (40°C cell temperature and 100% RH for both gases), particularly under wet conditions. The treatment notably enhanced the uniformity of water distribution across the CL, membrane, and GDL, compared to non-treated GDL samples.

Owejan et al. [128] explored the impact of MPL cracks on the performance of PEMFCs by comparing cracked and crack-free MPLs under both dry (80°C fuel cell temperature and RH of 66%) and wet conditions (60°C fuel cell temperature and RH of 100%). It was found that performance was similar in both types of MPLs, suggesting a minimal contribution from the cracks since most of the water was seen to be removed from the CL in vapour form. They also noted that the MPL helps prevent liquid water that condenses in the substrate's pores from reaching the CL and obstructing reactant delivery.

On the other hand, Markötter et al. [170] found that cracks in the MPL were beneficial. Water transport in the GDL was visualised using synchrotron X-ray radiography. The experiment revealed that these cracks significantly impacted liquid water movement through the GDL and into the gas channels. Cracks in the MPL were identified as the initial points for effective liquid water transport through the gas diffusion layer. The structural properties of MPL cracks, such as size, density, and distribution could be intentionally designed to enhance GDL performance, paralleling strategies like GDL perforation. These insights offer a new avenue for optimising fuel cell materials.

2.3.4.2 Pore Forming Agents

Several researchers have explored the use of different pore-forming agents within the MPL [[161], [171], [172], [173]]. Use of pore-forming agents can artificially modify the porosity and pore size distribution of the MPL, this in turn affects the overall fuel cell performance.

Simon et al. [171] enhanced oxygen transport in PEMFCs by using polymeric pore formers, with the materials assessed through MIP, nitrogen adsorption, and SEM. Their findings indicated that while all MPLs performed similarly under dry conditions, the samples with larger pores showed better performance under high water saturation, due to effective liquid water removal via the larger pores, facilitating oxygen transport through the smaller ones.

Chun et al. [172] produced a porosity-graded MPL using a double coating method to improve the water removal capability of the GDL. The porosity in each MPL layer was adjusted using thermal expandable graphite, which creates pores upon heating. The inner MPL layer, closer to the catalyst, was less porous than the outer layer adjacent to the gas diffusion backing layer, creating a gradient in porosity. This structure enhanced water permeability and performance, particularly at high current densities by reducing concentration losses from water flooding. Overall, the porosity-graded MPL proved advantageous for operating in high current density regions.

Morgan et al. [161] also observed improved performance in PEMFC by using a dual-layer MPL with varying pore sizes. Their findings indicated that this configuration enhanced cell performance at current densities above 0.4 A/cm². They suggested that the dual-layer MPL effectively reduced liquid water content in the CL and increased air humidity near the CL, thereby improving proton and oxidant transport within the CL.

Tang et al. [173] created a porosity-graded MPL and tested the performance on a PEMFC. Graded MPLs were created by printing layers with varying NH_4Cl pore-former concentrations, resulting in decreasing porosity from the membrane/MPL interface to the GDL/MPL interface. The structure and porosity of the graded MPL were analysed, and cell performance with graded MPLs was benchmarked against cells with uniform MPLs. Results showed that cells with graded MPLs outperform those with conventional MPLs, particularly at higher current densities. This was found to be due to enhanced water and gas management within the graded porosity layers.

Microstructural modifications, such as perforations, cracks, and pore-forming agents, can significantly impact the performance of the MPL. These changes primarily affect the porosity and pore size distribution, which are crucial characteristics of the GDL. Alterations in these properties influence the GDL's capacity for water and gas transport. Additionally, variations in the hydrophilic and hydrophobic properties of the pores greatly affect the mass transfer performance. There is considerable potential for further research by artificially modifying the MPL's microstructure to enhance the performance and address design issues related to the thickness. Microstructural modifications of the MPL are promising topics of research that deserve further exploration.

2.3.4.3 Degradation

The GDL and MPL can be subject to various processes that cause degradation. These include chemical degradation and mechanical degradation caused by external forces acting on GDL during assembly and operation. Many studies have been conducted [[174], [175], [176], [177], [178]] to analyse the effect of chemical and mechanical degradation on the MPL and fuel cell performance.

Ha et al. [174] investigated the impact of electric potential corrosion on the GDL of PEM fuel cells, focusing on how this degradation influences cell performance. Employing accelerated carbon corrosion tests, the study reveals significant GDL degradation, including a 13.5% reduction in thickness and a 5.8% decrease in total weight, predominantly centred around the middle of the GDL sample. Techniques such as SEM, thermogravimetric analysis, and tensile stress tests were used to analyse the degradation. There was a decrease in mechanical strength by up to 38%. This structural weakening of the GDL resulted in reduced mechanical properties and impaired water removal capabilities. Consequently, the overall fuel cell performance decreased.

Arlt et al. [175] explored the effects of artificial ageing of GDLs on PEM fuel cell performance, using high-resolution synchrotron radiography. A Sigracet SGL 25BC was used for the GDL samples. They were aged in a hydrogen peroxide solution for durations of 0, 16, and 24 hours before being tested in fuel cells. The research combined radiographic, voltage, and contact angle measurements to investigate ageing conditions. Findings indicated that water films formed at the interfaces between the GDL and the membrane, and the GDL and the BPP, mainly due to MPL cracks and large pores within the GDL. These caused water to block gas pathways, resulting in a reduced supply of reactant gases.

Liu et al. [176] similarly investigated the effects of accelerated ageing of GDLs and characterised the samples using synchrotron X-ray radiography and EIS. The GDLs were subjected to an accelerated ageing process by soaking them in a 35 wt. % solution of H_2O_2 at 90°C for 12 hours. The synchrotron X-ray imaging revealed that aged GDLs reached a terminal liquid water saturation at lower current densities compared to pristine GDLs, indicating a higher susceptibility for water accumulation. This was particularly evident at the interfaces between the GDL/BPP and MPL/MPS, where aged GDLs showed significantly higher liquid water content even at low current densities. EIS measurements confirmed an increase in mass transport resistances in aged GDLs, up to 10%, which correlated with the observed trends in liquid water accumulation. These findings suggest that the reduction in hydrophobicity due to ageing significantly impacts the liquid water transport behaviour and overall performance of fuel cells.

Wu et al. [177] explored the impact of GDL mechanical degradation under conditions of elevated temperature and flow rate. Degradation was assessed using electrical resistivity measurements, MIP, humidity sensitivity, and polarisation curves. Following 200 hours of accelerated degradation testing, a significant decrease in through-plane conductivity was observed in degraded GDL samples, particularly in those subjected to mechanical stress. The degradation process, characterised by the corrosion of carbon materials, leads to the loss of non-conductive PTFE. This results in notable mass transport losses, as evidenced by the polarisation curve measurements. The paper concludes that the primary mechanism of GDL degradation during ageing is the loss of nonconductive PTFE.

Radhakrishnan et al. [178] examined how cyclic compression affects the structure and properties of a GDL. The study found that cyclic compression leads to irreversible alterations in the GDL surface morphology, pore size, porosity, thickness, electrical resistance, contact angle, water uptake, and in-plane permeability. Notably, the impact of cyclic compression on the GDL hydrophobicity was found to be more significant than that of electrochemical effects.

The study on the durability of GDLs focuses on understanding the mechanisms behind their degradation. Much research has been conducted on the degradation phenomena of GDLs, the specific causes of degradation under the actual operating conditions of PEMFCs require further investigation.

The addition of an MPL is crucial for managing water in PEMFCs, besides reducing the electrical contact resistance and minimising the loss of catalyst layer particles. While numerous studies confirm that MPLs enhance PEMFC performance under various operating conditions (by maintaining membrane hydration in dry conditions or removing excess liquid water in wet conditions) the impact on water management is not completely understood. Research findings are inconsistent, indicating a need for further investigation into how different MPL properties affect the fuel cell performance across varying operating conditions.

The inclusion of an MPL is essential for the GDL architecture. Numerous studies have shown that MPLs boost PEMFC performance. Most of the strategies mentioned above have been adopted to enhance or modify the MPL. There are many engineering challenges and trade-offs when modifying the MPL, as outlined in Figure 2-10, and the specific effects of MPLs on mass transport and electrical conductivity are not fully understood. This highlights the need for further exploration into how different MPL characteristics influence the fuel cell performance under various operating conditions.

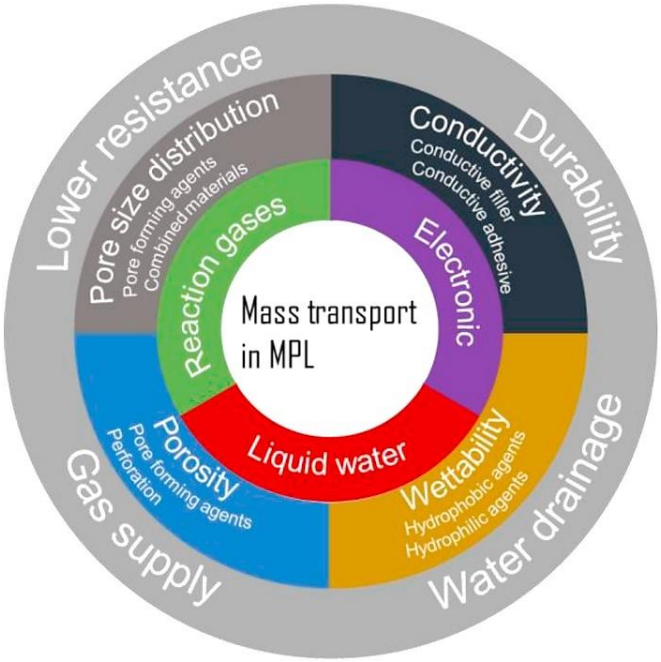

Figure 2-10 Schematic of the engineering challenges associated with the MPL [179].

2.4 Contact Resistance

Contact resistance between components in fuel cells is one of the primary challenges that need to be overcome before fuel cells can be successfully commercialised. Fuel cells are limited by several losses, as discussed in Section 1.3.3.2. These losses can be classified as irreversible and reversible. Irreversible losses are due to the thermodynamics of the system and cannot be reduced. For example, entropy losses and losses due to deviation from operating standard temperature and pressure (STP) conditions. On the other hand, reversible losses can be reduced. These are due to factors such as materials used, manufacturing methods and design of fuel cell [180].

The ohmic loss is a reversible loss, it is the sum of voltage lost due to the resistance from the fuel cell components and their contact resistances. The contact resistance is caused by imperfectly matched component interfaces within the fuel cell. It occurs because of differences in the morphological, structural, physical, and chemical properties of the different fuel cell components that encounter one another. Between these differing components, noncontinuous contact is formed giving rise to contact resistance. When these morphologically and structurally different components are in contact, a transition region forms between them, causing electron transport to be noncontinuous. This causes more complex electron pathways, hence the electrical resistance is increased [181]. Figure 2-11 shows how the noncontinuous contact between the MPL and CL can cause difficulties for electrons to pass through.

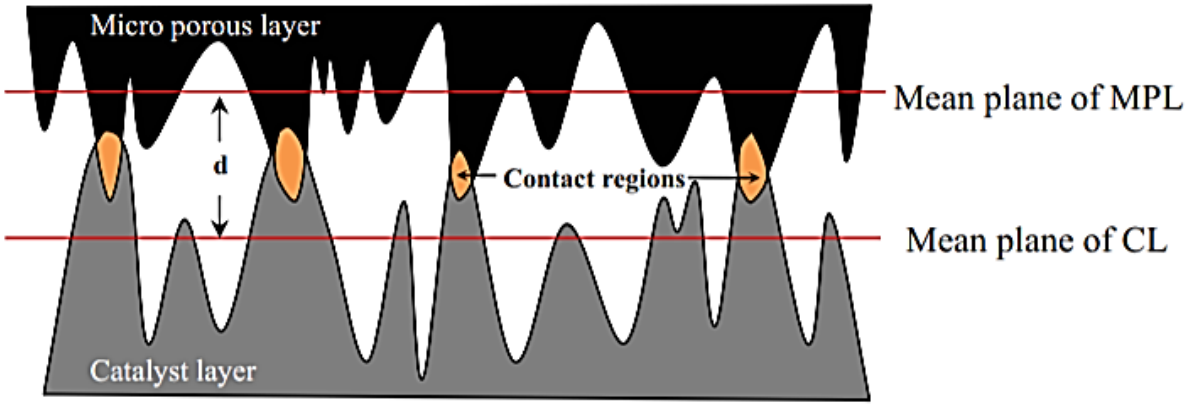

Figure 2-11 Schematic of contact interface between MPL and CL [181].

Swamy et al. [181] created an analytical simulation that examined the MPL and CL interface as a function of compression. They observed that a 50% drop in the surface roughness of the MPL and CL resulted in a 40% drop in the contact resistance at the MPL/CL interface [181].

As a result, it was found that the contact resistance is a function of the material surface and roughness and the contact pressure between the components. Therefore, the materials used and their corresponding surface roughness and contact points are major factors that need to be studied.

The importance of contact resistance was studied by Netwall et al. [182], and the contributions of component resistances to the total ohmic losses were examined. It was found that approximately 55% of the ohmic losses came from the interfacial contact between the fuel cell components: GDL/BPP, GDL/CL and membrane/CL. Bulk resistances of the individual components accounted for 45% of the ohmic resistances [182] and this is displayed in Figure 2-12.

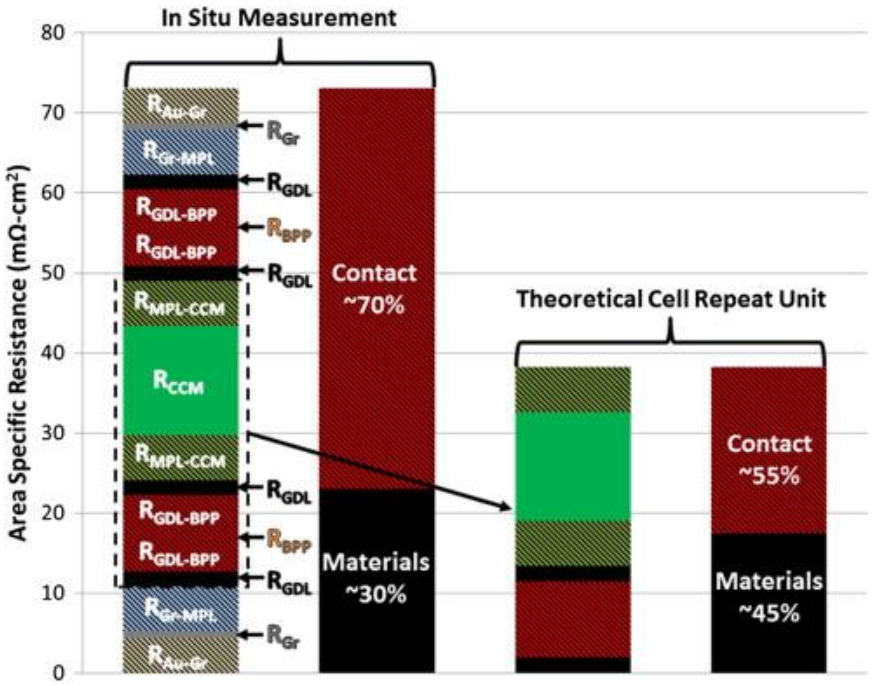

Figure 2-12 Contributions of bulk and contact resistance to the overall ohmic losses [182].

The contact resistance between the GDL/BPP and GDL/CL predominantly contributes to the ohmic losses. Such losses must be minimised in order to maximise the conversion of chemical energy to electricity rather than to waste heat. The GDL acts as a mediator between the CL and the BPP, so it is important to address the contact resistance in these regions. If not addressed properly, the contact resistance can cause severe losses for the fuel cell during operation and potentially contribute to material degradation [183].

Additionally, it must be noted that gaps and cracks can form at the interface of the MPL and catalyst layer. The cracks at the interface could be an ideal location for water accumulation, this in turn can prevent reactant gases from reaching the catalyst layer and it could also potentially affect the contact resistance values. It was studied by Hizir et al. [184] that the gaps at the interface of the MPL and catalyst layer could potentially have a relatively large water storage capacity. Swamy et al. [181] also showed that the interfacial contact area between the MPL and catalyst layer could hold between 6% – 18% of the total water content in a fuel cell.

2.4.1 Contact Resistance Between the GDL/BPP and GDL/CL

BPPs are important components of the fuel cell, their functions are described in detail in Section 1.3.4.1. Two main types of BPPs are used in fuel cells: graphite and metal. However, contact resistance can form between these materials and the GDL. In particular, metal BPPs tend to form a passive layer on the surface, due to the acidic environment of a PEMFC. Further to this, metals have a high surface roughness, both of these factors will contribute to an increased contact resistance when using metal-based BPP. Graphite composites are currently the standard choice for PEMFC bipolar plates due to their low surface contact resistance and excellent corrosion resistance. These properties make them highly suitable for use in fuel cell applications [185]. Despite this, 59% of total power loss from the fuel cell is due to contact resistance between the GDL and BPP [186].

To reduce the contact resistance, the contact points on the surfaces between GDL and BPP must be increased. More contact points across the surfaces will provide more pathways for electrons to travel across, which in turn will lower the contact resistance. To achieve this, BPP made from metal are typically coated with highly conductive and anticorrosive coatings [187]. These surface coatings lower the roughness of the metal and increase the contact points with the GDL thus reducing the contact resistance.

There have been many investigations into how best to decrease the contact resistance between the GDL and BPP, investigations have been carried out using simulations [[188], [189], [190]] and experimentation [[121], [122], [191], [192], [193]]. The main finding from these studies is that the contact resistance decreases as the compression pressure is increased. This was due to the compression creating more points of contact across the interface layer. Moreover, the contact resistance was also affected by the PTFE loading in the GDL, the BPP material used and the presence of an MPL.

Zhang et al. [188] carried out an investigation to calculate the contact resistance between the GDL and BPP, as a function of pressure. A hydraulic press was set up with insulating plexiglass. The GDL was then sandwiched between two graphite plates and subsequently gold plates. A micro-ohmmeter was installed to measure the resistance of the setup. Figure 2-13 shows a schematic diagram of the setup.

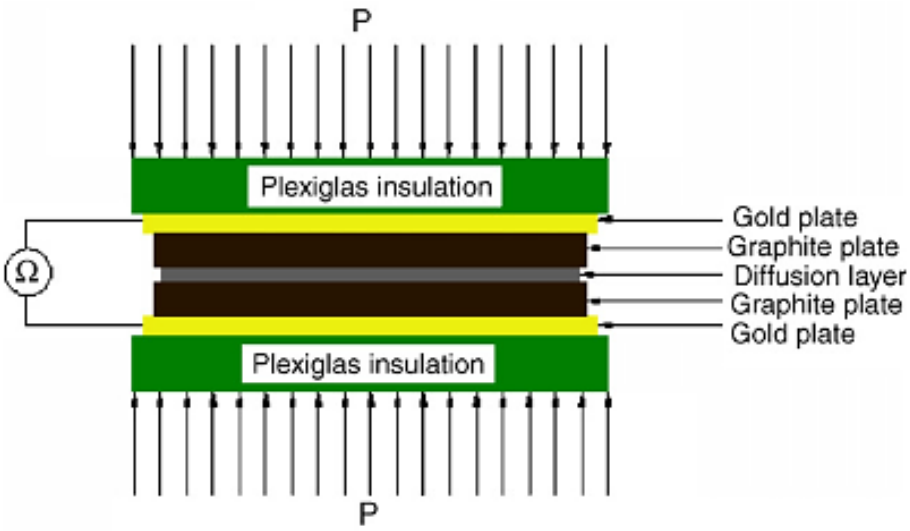

Figure 2-13 Contact resistance experimental measurement setup [188].

The bulk resistances of the components were known, these consisted of the two graphite plates ($2R_{Gr}$) and the GDL (R_{GDL}). The total resistance of the setup is also known (R_{Total}) as it can be directly measured. Equation 2.10 expresses the overall resistance as a function of the bulk resistances and contact resistances [188].

$$R_{Total} = 2R_{Gr} + R_{GDL} + 2R_{GDL/Gr} + 2R_{Au/Gr} \tag{2.10}$$

Rearranging for the contact resistance between the GDL and graphite plate:

$$R_{GDL/Gr} = \frac{R_{Total} - 2R_{Gr} - R_{GDL} - 2R_{Au/Gr}}{2} \tag{2.11}$$

The contact resistance between the Gold plate and the graphite current collector is measured in a separate setup consisting only of one graphite current collector sandwiched between two gold plates. This gives the contact resistance of the gold and graphite as follows:

$$R_{Au/Gr} = \frac{R_2 - R_{Gr}}{2} \tag{2.12}$$

All unknowns are now accounted for and equation 2.12 can be substituted into equation 2.11 to determine the contact resistance of the GDL and graphite [188].

$$R_{GDL/Gr} = \frac{R_{Total} - R_{Gr} - R_{GDL} - R_2}{2} \tag{2.13}$$

The study concluded that contact resistance is greatly influenced by the assembly clamping pressure and variation of pressure had a small impact on the contact resistance [188].

On the other hand, Nitta et al. [193] experimentally investigated the contact resistance between the GDL and the CL. An H_2/H_2 fuel cell was used with AC impedance measurements as a function of GDL compression. The AC impedance allowed for the measurement of total fuel cell electrical resistance. Membrane parameters were assumed to be constant under compression. The contact resistance between the GDL and the CL was calculated by subtracting the membrane resistance, individual component bulk resistances and the contact resistance of the GDL and graphite current collector from the total fuel cell resistance [193].

$$R_{GDL/CL} = R_{Cell} - R_m - R_{GDL/GR} \quad (2.14)$$

It was found that contact resistance at the GDL/CL interface decreases non-linearly with increased compression [193]. The contact resistance between the GDL/CL was found to be between 14 - 60 times larger than the contact resistance between the GDL/BPP.

Similarly, Makharia et al. [194] used EIS to estimate contact resistance between both the GDL/CL and GDL/BPP [194]. The GDL was made from Toray carbon paper treated with PTFE. It was found that the contact resistance between the GDL/BPP was 13.0 mΩ/cm^2 and between the GDL/CL was 3.4 mΩ/cm^2 [194]. Nevertheless, measurement of the contact resistance between the GDL/CL is challenging and there have been limited studies covering this area.

In general, it is difficult to accurately assess the contact resistance between the different PEMFC components. This is an ongoing topic of research for PEMFCs and various research groups have investigated it, as it is an important engineering parameter to consider. The investigations have required specially designed setups with sophisticated measuring.

As a whole, the two main techniques used to mitigate contact resistance are compression or the addition of an MPL to face the BPP, these two techniques will now be discussed in more detail.

2.4.2 Compression

As discussed in Section 2.4, contact resistance can be reduced by increasing contact points between components. One such way to achieve this is to increase the compression of the fuel cell. The compression force enhances the contact between the carbon fibres of the GDL and its neighbouring components. These enhanced contact areas will in turn improve the electrical transport through the interface thus reducing contact resistance and ultimately ohmic losses [195]. The effects of compression on a GDL and its transport properties have been thoroughly researched [[195], [196], [197], [198], [199]].

Chang et al. [199] investigated the contact resistance between a graphite BPP and a GDL. Results showed that the contact resistance between the BPP and GDL caused serious voltage losses across the fuel cell. It was also shown that low compression resulted in a higher contact resistance and high compression reduced the contact resistance. High compression also decreased diffusion pathways for mass transfer to take place from gas channels to the CL [199].

A high compression force in a fuel cell not only increases electrical contacts but also changes the morphological and structural properties of the GDL. For example, GDL thickness can potentially be reduced by half. This occurs because of degradation, as discussed in Section 2.3.4.3, the GDL is naturally a porous material, many of the GDL characteristics that affect its overall performance, such as thermal conductivity, permeability and electrical can be affected due to compression [122].

Under low compressions of approximately 8%, the oxygen transport resistance in a GDL coated with an MPL is very high for high current densities. This is because a lot of water condensation in the porous substrate will take place. An uncoated GDL also exhibits similar behaviour but for compression at around 22%. Based on this, it shows that the MPL substantially helps to reduce the water condensation by providing uniform contact between the GDL and the catalyst layer. The MPL also allows for the water to accumulate within the carbon fibres of the substrate rather than at the surface of the electrode. At lower compression, a liquid water film can form during the electrochemical reaction inhibiting the oxygen mass transport at the catalyst

interface. However, an MPL aids in the dissipation of the water more effectively than an uncoated GDL [200].

X-ray imaging carried out showed that gaps at the interfacial region of the MPL and catalyst can serve as small water reservoirs. Not only can the gaps cause poor interfacial contact and higher contact resistance, but can also hinder the transport of oxygen with the trapped water [200].

Therefore, utilising compression will establish a trade-off between the characteristics of a GDL and ultimately balancing ohmic polarisation losses vs concentration polarisation losses. This indicates that there is an optimum compression force for ideal fuel cell performance [199]. Bates et al. [201] experimentally analysed the compression between the GDL and BPP, it was found that 1 MPa was an optimum average contact pressure. Figure 2-14 shows the trade-offs associated with the compression of the fuel cell.

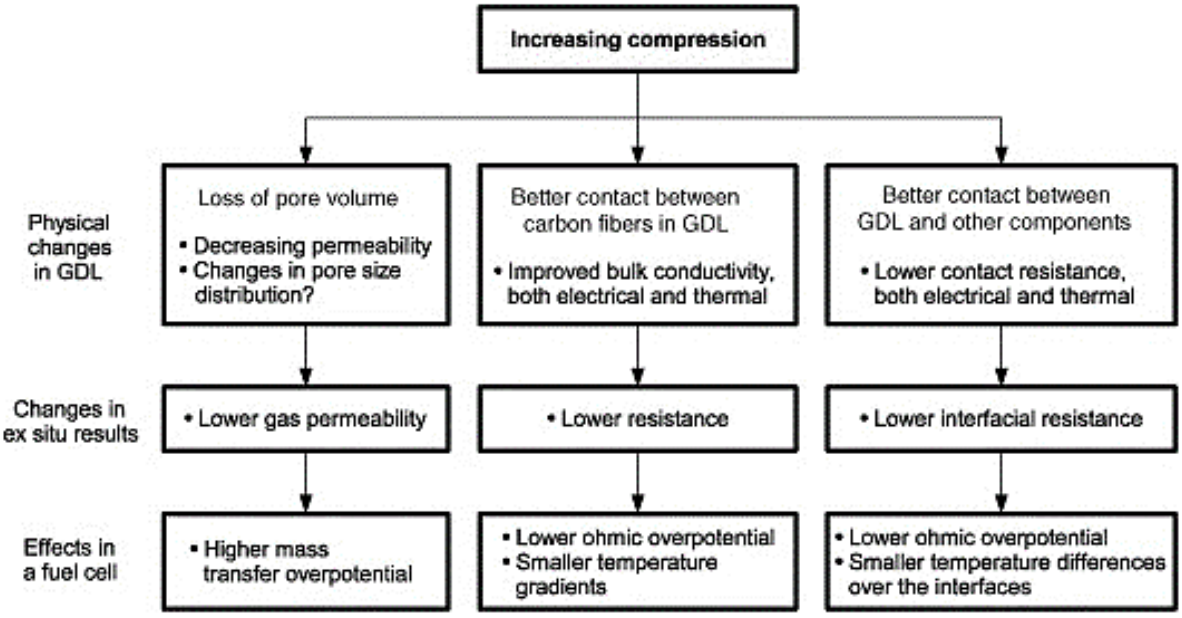

Figure 2-14 Compression trade-offs [122].

The GDL inherently has a delicate architecture, so even if the fuel cell is assembled with the optimum compression force the GDL can potentially GDL suffer from mechanical degradation/failure. Degradation of the GDL due to compression can lead to a breakup of fibres and deterioration of the PTFE coating. Compression not only affects the contact resistance but also the GDL porosity and ultimately fuel cell performance. Moreover, minor compression forces can be reversible, with a GDL returning to its original state once compression is lifted. Despite this, in general, the deformation of the GDL structure caused by fuel cell compression is not reversible [202]. El-Kharouf et al. [63] established that the contact resistance decreases with each compression cycle reaching stabilisation, between 3 – 5 cycles [63]. However, this resulted in an irreversible deformation effect on the GDL. In addition to the GDL deformation, excessive compression can also create hot spots within the MEA due to uneven production of current. This can ultimately lead to an MEA puncture [128] and overall fuel cell degradation.

It was reported by Nitta et al. [122] that the GDL also undergoes inhomogeneous compression. The GDL suffers very little compression under the BPP channels. But under the ribs, it is

compressed to gasket thickness. GDL compression reduces gas permeability but improves bulk conductivity and contact resistance. Inhomogeneous compression can lead to changes in the GDL electrical and mass transport properties thus increasing the rate of degradation [122].

Ismail et al. [89] investigated the contact resistance with respect to compression and an additional MPL to the GDL. Figure 2-15 highlights how the different MPL samples (SGL 10BA, SGL 10BC and SGL 10BE) decreased in contact resistance with increasing pressure. At 10 bar, the SGL 10BA when coated with an MPL, to become SGL 10BC and SGL 10BE, experiences a reduction of approximately 15% and 40%, respectively. This reduction in resistance is likely due to the presence and higher concentration of carbon particles in the MPL, which allows for easier transfer of electrons. Additionally, the contact resistance increased with increasing PTFE content [[89], [119]]. This is due to PTFE being a natural electrical insulator, so the higher the content of PTFE the lower the overall conductivity on the GDL.

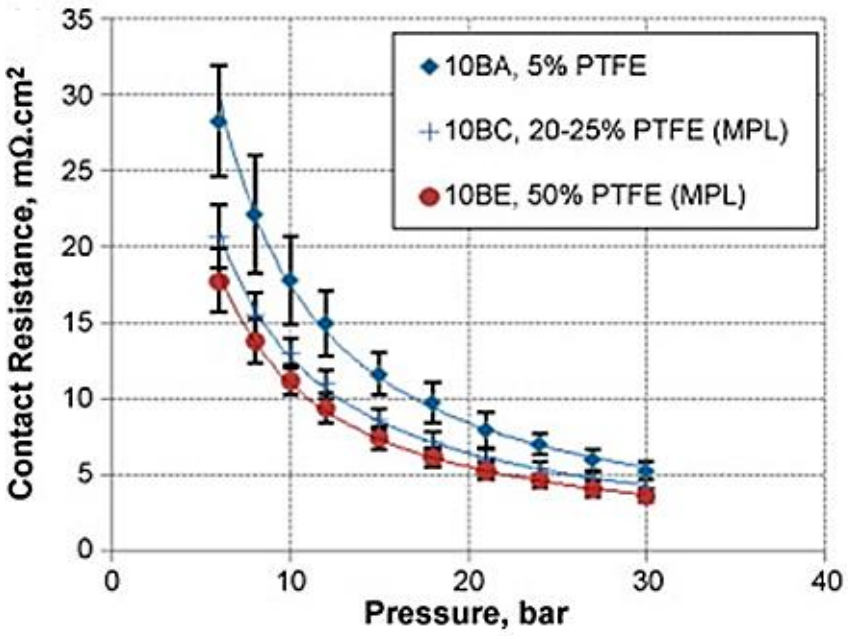

Figure 2-15 The effect of MPL coating on the contact resistance of carbon substrate SGL 10BA [89].

2.4.3 Double-Sided MPL Coated GDL

As discussed in Section 2.3, the addition of an MPL to a GDL is of great importance in PEMFCs especially concerning the enhancement of mass transport and reducing electrical contact resistance. Typically, an MPL is placed between the GDL and the CL. An addition of an MPL facing the CL has been proven to decrease the contact resistance due to increasing contact points between components and therefore allowing more pathways for electrons to travel through, which in turn enhances the overall capabilities of a fuel cell.

The application of the MPL facing the BBP side can also decrease the contact resistance, but it is also possible for it to affect the water removal mechanism on the BPP side. Owejan et al. [128] investigated water removal on the BPP side. They showed that using a 50 μm free-standing MPL between the GDL and BPP can reduce the performance of the fuel cell as water becomes trapped. However, they only applied the MPL on one side facing the BPP and not both sides of the GDL. Also, the use of a free-standing MPL could have left cavities between the MPL and GDL in which water could accumulate.

Some researchers have suggested creating a double-sided MPL by applying MPL on both sides of the GDL. One side of the MPL will contact the CL and the other with the BPP. Wang et al. [76] used a carbon fibre paper (TGPH-030, Toray) as the GDL and applied an MPL on both sides. The MPL was made from a composite of two different carbon blacks: Acetylene Black and Black Pearls 2000 with 30 wt. % PTFE loading. The operating temperature was set at 80°C with an air inlet temperature of 85°C and hydrogen inlet temperature of 90°C, supplied at 0.2 MPa. The membrane active area was set at 5 cm^2. It was reported that a double-sided MPL improved the fuel cell performance more so than a single-sided MPL facing the CL. This is due to the improved contact interfaces between the GDL/BPP. It should be noted that total carbon loading was kept constant in this experiment at a total of 1 mg/cm^2. This would have put limitations on the optimisation of the MPL compositions. For example, the first scenario had 1 mg/cm^2 MPL loading facing the CL and no MPL facing the BPP. The second scenario had 0.7 mg/cm^2 facing the CL and 0.3 mg/cm^2 facing the BPP. The final scenario had a 0.5 mg/cm^2 on both sides. The second scenario gave the best performance results [76].

Figure 2-16 shows a comparison of the different loadings for the double-sided MPL-coated GDL. It can be seen that sample CC2 (0.7 mg/cm^2 facing the CL and 0.3 mg/cm^2 facing the BPP) performs the best.

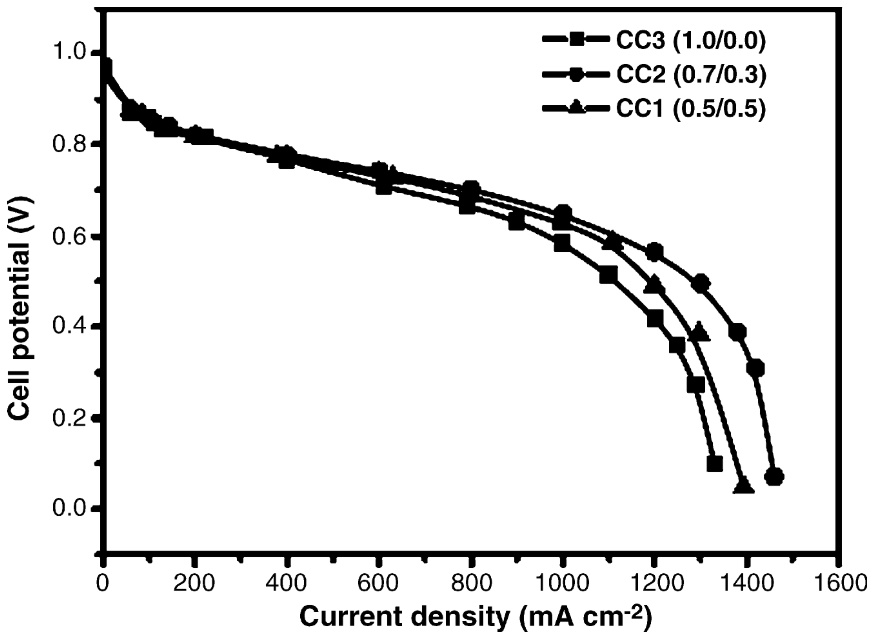

Figure 2-16 Polarisation curves showing the performance of different MPL structures [76].

Despite these measurements, the characteristics of the double-sided MPL coated GDL were not explored. MPL thickness can potentially have a negative impact on overall fuel cell performance by lowering gas permeation. As a result, different losses were not reported which are critical to a sound interpretation of the results.

Chang et al. [47] carried out a similar study and applied an MPL on both sides of the GDL. In this scenario, they did not keep the total carbon loading constant. An SGL 10BA carbon paper GDL was used and three different carbon blacks were assessed to see which performed the best: Acetylene Black, Black Pearls 2000 and Vulcan XC 72B. The active area of the fuel cell was kept constant at 5cm x 5cm. Both inlet gases were humidified and at a constant temperature of 70°C and the temperature of the fuel cell was also kept at 70°C. PTFE content was kept constant in all MPLs at 20 wt. %. It was found that Acetylene Black gave the best performance out of the different carbon blacks. Chang then went on to optimise the loading of Acetylene Black for the two MPL coatings [47]. Figure 2-17 shows that the optimal loading of MPL is 1.25 mg/cm^2 facing the CL and 0.25 mg/cm^2 facing the BPP.

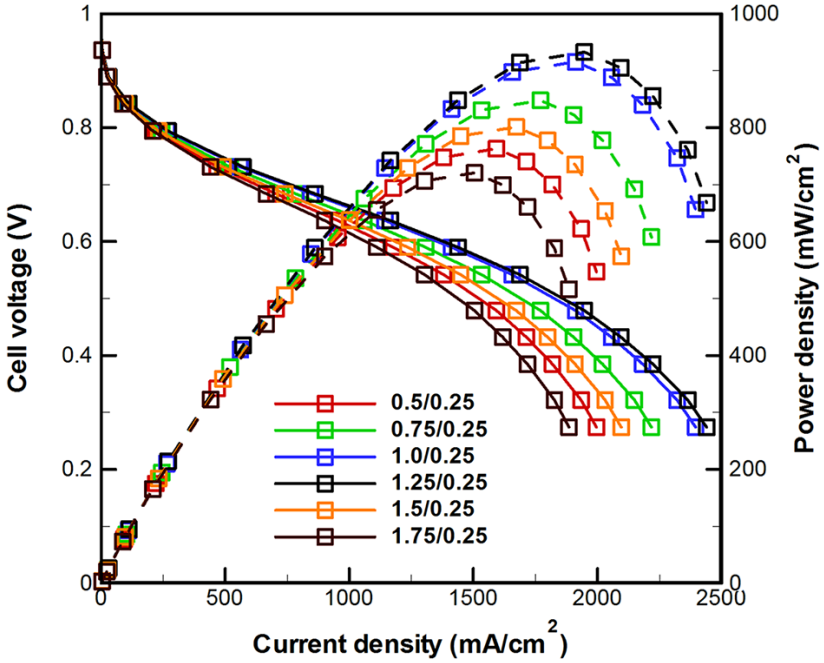

Figure 2-17 Polarisation and power density of double-sided MPL coating for optimal loading [47].

Figure 2-17 also shows that the 1.25/0.25 loading can reach maximum power densities of around 900 mW/cm^2 compared to a conventional single side loading of MPL at 1 mg/cm^2 facing the catalyst side of around 750 mW/cm^2 [47]. This shows that an MPL loading on the surface facing the BPP is generally less than the surface facing the CL and helps reduce contact resistance. However, there is an optimum ratio before performance declines due to the GDL becoming too thick and suffering from mass transport losses. PTFE content was also examined and it was found that loading of 20 wt. % was the most effective. Figure 2-18 shows a varying PTFE content from 5 wt. % – 40 wt. %. It can be seen that an optimum is achieved at 20 wt. % and there is a drop off in effectiveness at higher and lower PTFE content.

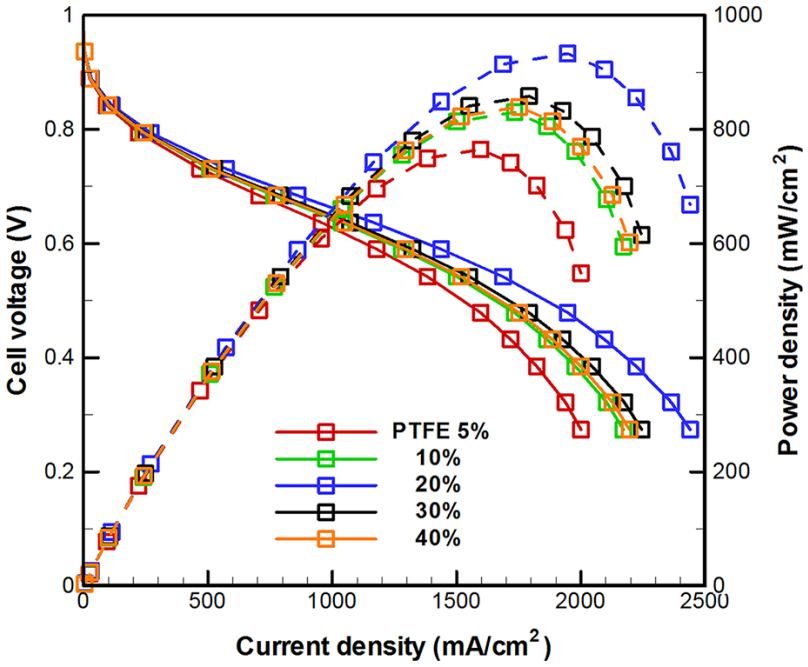

Figure 2-18 Polarisation curves comparing the varying content of PTFE [48].

Huang and Chang [48] further investigated the double-sided MPL coating under different humidity conditions. Carbon paper (SGL 10BA) was used as the MPS. It was then coated on both sides with an Acetylene Black MPL with different carbon and PTFE loadings. Temperatures of gas inlets and overall fuel cell temperature were kept constant at 70°C. Air humidification temperature was adjusted in the range of 30°C – 70°C allowing relative humidity to range between 13.6% – 100% [48].

Different amounts of MPL carbon loadings on both sides of GDL were tested. The results showed that optimum carbon loading was 1.2 mg/cm^2 facing the CL and 0.3 mg/cm^2 facing the BPP [48]. In all the different relative humidity scenarios, this ratio gave the best performance. This shows that a small MPL facing the BPP is beneficial for improved fuel cell performance, not only at low air relative humidity but also when the airflow is fully humidified. Figure 2-19 displays a comparison between the different MPL loadings, comparing power density and relative humidity.

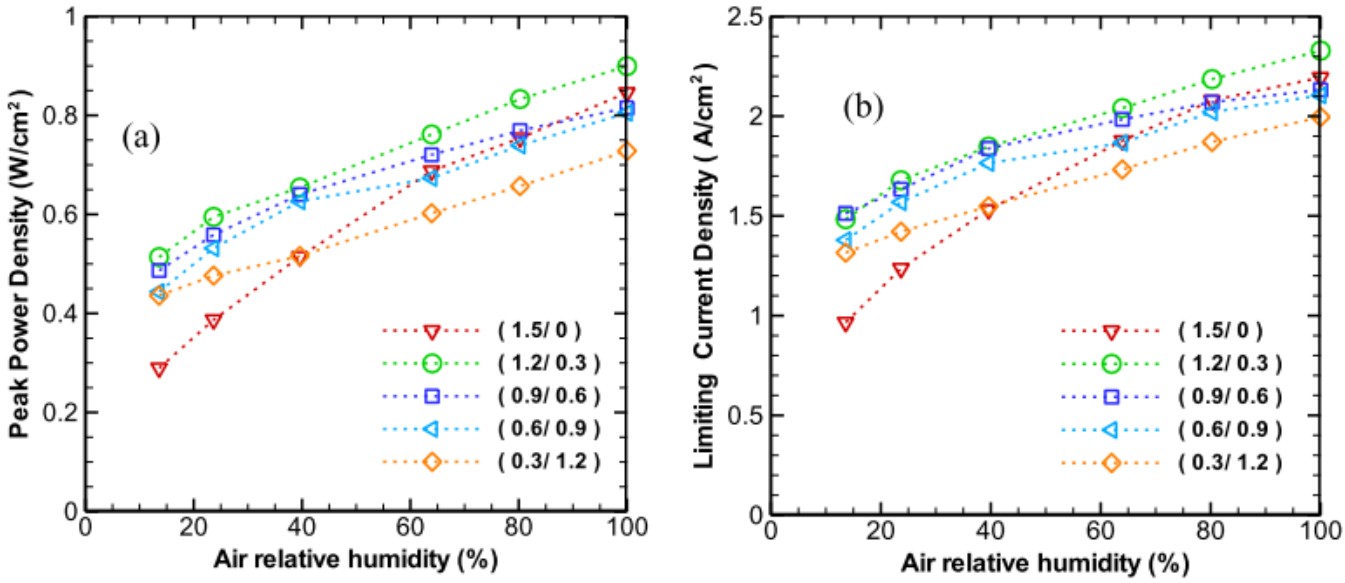

Figure 2-19 Peak power densities with varying humidity levels(a) peak power density and (b) limiting current density [48].

For instance, at a very low air relative humidity of 13.6%, a traditional single-side MPL-coated GDL with a carbon loading of 1.5 mg/cm² facing the catalyst layer typically achieves a peak power density of only about 0.28 W/cm². However, by applying a small amount of MPL on the opposite side of the GDL facing the flow channel, cell performance significantly improves, nearly doubling the peak power density to approximately 0.52 W/cm², as demonstrated with a coating of 1.2/0.3 mg/cm².

PTFE content was also examined. It was found that the optimal PTFE loadings are the same on both sides of the MPL at 20 wt. % [48]. Peak power density at very low air relative humidity conditions can be increased by more than 85% compared to that of a conventional single-sided MPL coated GDL [48]. Furthermore, EIS showed that the double-sided MPL at optimum composition always exhibit the lowest ohmic resistances [48].

These investigations show the promise of reducing the contact resistance, especially by increasing the contact point between the components without the need to risk compression and the deformation of the GDL. However, unlike compression tests, no in-depth characterisations were carried out for the double-sided MPL coating of the GDL for different operating conditions and different MPL materials. The main metrics of measurements were polarisation curves and impedance spectra. This does not give a holistic characterisation as to how the double-sided MPL coated GDL performs and needs to be further investigated particularly for different designs and operating conditions.

2.5 Summary of the Literature

This chapter has reviewed a wide range of the literature concerning the characterisation of the GDL and MPL for PEMFCs. This research includes both experimental and computational studies and has significantly deepened our understanding of how GDLs function in fuel cells. These well-proven tools are essential for accurately characterising GDLs.

In-depth evaluations of the MPL have also been conducted, focusing on the use of both conventional and novel materials, adjustments in thickness, microstructural modifications, and the implications of these changes on degradation. Extensive research has been directed towards MPL modifications aimed at improving electrical conductivity and optimising mass transport. It is acknowledged, however, that while modifications can cause considerable advantages, they also involve trade-offs.

One of the primary challenges in fuel cell design is minimising electrical contact resistance among the various layers that comprise the cell. MPL modifications can play a crucial role here, especially in reducing contact resistance. Strategies such as applying compressive forces and using double-sided MPL coated GDL have been explored. The latter seems to be a better choice as it is least likely to cause long-term structural damage to the GDL.

Despite the promise shown by double-sided MPL coated GDLs, research in this area remains limited, highlighting a significant opportunity for further investigation. Characterisation techniques can be used to analyse the double-sided MPL coated GDL and determine the engineering trade-offs that need to be made in order to create an improved GDL.

2.6 Knowledge Gap, Novelty and Importance

The GDL is a critical component of the PEMFC and optimal operation of the fuel cell with limited ohmic losses largely depends on the efficient design of the GDL. It has been shown that contact resistance losses account for a large portion of ohmic losses. As the GDL is situated between the BPP and CL, it is an important medium in which the contact resistance manifests. Therefore, it is critical to minimise the contact resistance to improve the overall fuel cell performance. Compression of a fuel cell is one way to increase electrical conductivity and decrease contact resistance. However, there is maximum pressure that can be applied, after which irreversible damage can be done to the MEA. It has even been shown that small amounts of compression can damage the delicate structure of the MEA thus increasing fuel cell degradation rates.

Previous studies have highlighted that the addition of an MPL to the interface between the GDL/BPP shows promise in reducing the contact resistance, without the GDL degradation risks trade-offs when increasing compression. Experimental studies were carried out to test the capabilities of a GDL with a double-sided MPL. The double-sided MPL coated GDL showed improved performance in fuel cell operation as contact resistance was reduced. It was also shown that there is an optimal ratio when applying two MPLs. A trade-off between improved electrical conductivity and a thicker GDL, which can potentially start to inhibit mass transport, needs to be found.

The previous studies for a double-sided MPL coated GDL focused on in-situ testing such as polarisation curves and EIS as the main mode of characterisation. There is little or no work that has been undertaken to specifically characterise the double-sided MPL coated GDL, using both ex-situ and in-situ methods. Subsequently, there is little knowledge of the effect of the double-

sided MPL coated GDL and of its main properties, for example: pore size distribution, permeability, porosity, hydrophobicity, structural properties, and electrical conductivity.

Furthermore, current studies for double-sided MPL coated GDLs use conventional carbon-based MPLs. Novel materials, such as graphene, show great promise for GDL usage because of their excellent inherent properties of high electrical conductivity, mechanical strength, large surface areas and natural hydrophobicity [[135], [141]]. Characterisation and performance metrics of double-sided MPL coated GDLs made from novel materials have not been explored. However, the use of novel materials could help optimise the trade-off between electrical conductivity and mass transport processes.

The double-sided MPL coated GDL applies a microstructural modification to the overall GDL structure. Further microstructural modifications could be made to this configuration by the introduction of pore-forming agents. MPL microstructural modifications using pore-forming agents have been shown to improve the mass transport within the GDL. The double-sided MPL coated GDL improves the electrical contact of the GDL. Microstructure modifications of this GDL could also help improve the mass transport process and help mitigate the trade-off between improved electrical contact and the mass transport processes within the GDL (governed mainly by thickness, porosity and pore size distribution).

The novel double-sided MPL coated GDL, which alters the GDL configuration by adding a small loading of MPL coating facing the BPP, is not well understood, nor have there been extensive studies to optimise the configuration. Despite minimal manufacturing changes from the single-sided MPL, to the double-sided MPL located GDL, this adjustment could significantly enhance the overall fuel cell performance.

2.7 Research Objectives

After identifying the gaps in the knowledge, as previously discussed, this thesis aims to improve the performance of the PEMFC by reducing the contact resistance, with the application of a double-sided MPL coated GDL. Reducing ohmic losses with the PEMFC has been the focus of many research groups. However, as mentioned in Section 2.4.3, the reduction of ohmic losses via the reduction of contact resistance using a double-sided MPL coated GDL is still not fully understood. The MPLs will be fabricated in laboratory facilities, following this, ex-situ experiments will assist in analysing and characterisation of the double-sided MPL-coated GDLs. The samples will then be employed in-situ for fuel cell performance testing. Consequently, one of the major objectives of this work is to characterise double-sided GDLs and evaluate the effect of the double-sided GDL on overall fuel cell performance.

This study aims to provide greater insight into the development of alternative MPL coated GDLs to improve interfacial characteristics. Any alternative MPL should ultimately achieve improved overall fuel cell performance.

Chapter 3: Characterisation of Novel and High Performing Double-sided Microporous Layer Coated Gas Diffusion Layers for Polymer Electrolyte Membrane Fuel Cells

3.1 Abstract

This study aims to experimentally evaluate the impact of a double-sided microporous layer coating on gas diffusion layers in terms of their key properties and fuel cell performance, in comparison to conventional single-sided coated gas diffusion layers (GDLs). Vulcan black and Ketjenblack were used as the carbon black materials. This was to investigate the sensitivity of the results with respect to the type of carbon black used. The results showed that the in-plane electrical conductivity is almost insensitive to microporous layer (MPL) loading and carbon black type. Furthermore, the electrical conductivity of all the MPL-coated GDLs is slightly lower than that of the uncoated GDL. The Ketjenblack black MPL samples were found to demonstrate higher gas permeability than Vulcan black samples. The addition of the MPL resulted in a favourable shift in pore size distribution, with prominent micropores observed in both single and double-sided MPL coated GDLs. Contact angle measurements indicated a slight increase in the hydrophobicity with the addition of a microporous layer but without significant differences between carbon black types or loading levels. Cross-sectional SEM images showed that there was a higher level of MPL penetration into the carbon substrate for the GDLs coated with Vulcan black as compared to a Ketjenblack coating. In-situ fuel cell testing demonstrated the superior performance of the double-sided Vulcan black MPL coated GDL under high humidity conditions, while single-sided Vulcan black MPL coated GDL exhibited better performance at low humidity conditions. All the above findings have been thoroughly discussed and justified.

3.2 Introduction

To reduce or eliminate the reliance on fossil fuels, numerous initiatives and projects have recently emphasised the production and utilisation of green hydrogen. Green hydrogen is produced from water electrolysis, using electricity generated by renewable energy sources such as wind or solar power. Given the intermittent nature of these renewables, green hydrogen is typically stored and deployed as needed through fuel cells [203].

Polymer electrolyte membrane fuel cells (PEMFC) are of major interest for the utilisation of low-carbon hydrogen. This is due to their high efficiency, low operating temperature and ease of assembly [203]. PEMFCs are well placed to enable the use of hydrogen, as they can be applied in a wide variety of stationary, automotive and portable applications [23].

The gas diffusion layer (GDL) is a vital component of the PEMFC. It carries out many different roles within the fuel cell. Firstly, it uniformly distributes the reactant gasses (hydrogen and oxygen) to the catalyst layer (CL) active sites. It is also crucial to water management; the GDL should ideally expel excess water whilst simultaneously keeping the membrane hydrated. Water flooding, when it occurs, has the potential to hinder the transport of reactant gases to the catalyst layers due to the partial/complete blockage of the pores within the porous media, particularly the gas diffusion layers. This in turn degrades the performance of the fuel cell especially when operating under high current densities. Therefore, effective management of liquid water within the GDLs in the fuel cell is of paramount importance in order to maintain optimal operation [23].

Finally, the GDL provides structural support to the delicate membrane and catalyst layers [54]. Due to the multifaceted nature of the GDL, it is typically comprised of a carbon fibre material, as this best fulfils the multiple functions it must provide. GDLs are usually made from a carbon cloth or carbon paper.

Typically, a microporous layer (MPL) is added to the GDL. MPLs comprise a carbon black slurry combined with polytetrafluoroethylene (PTFE). It was found that MPLs, which are conventionally applied to the surface of the GDL facing the catalyst layer (CL), enhance water management within the membrane electrode assembly (MEA) [[165], [158]], boost electrical contact between the GDL and the catalyst layer [[89], [204]], thus improving overall fuel cell performance [[182], [204]]. Figure 3-1 shows a schematic representation of typical components of a PEMFC, including the GDL/MPL.

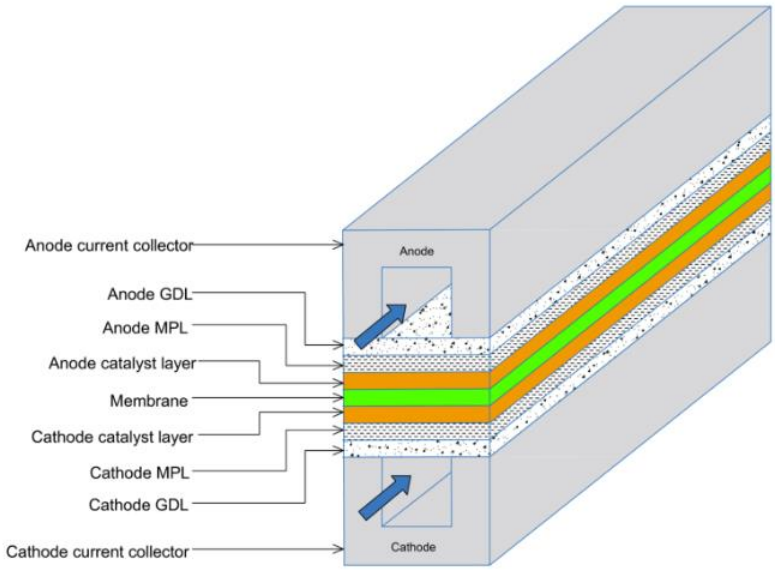

Figure 3-1 Schematic representation of a PEMFC, highlighting key components, including the MPLs [205].

Fuel cells experience irreversible and reversible losses. Irreversible losses are caused by entropy and deviations from operating conditions, these cannot be reduced. Reversible losses on the other hand, such as ohmic polarisation, can be minimised. Ohmic polarisation is caused by contact resistances between fuel cell components and the bulk resistances of conducting materials. Morphological and structural differences create transitional regions, increasing electrical contact resistance [180]. The GDL between the CL and bipolar plate (BPP) is particularly affected. Contact resistance in fuel cells depends on the material surface, roughness, and contact pressure between components. Netwall et al. [182] found that 55% of ohmic losses stem from interfacial contact resistances (GDL/BPP, GDL/CL, and membrane/CL), while 45% come from bulk resistances. GDL/BPP and GDL/CL contact resistances have a significant impact on ohmic losses. Properly addressing these resistances is crucial to avoid substantial losses during fuel cell operation [183]. There have been many investigations into how best to decrease the contact resistance between the GDL and BPP; investigations have been carried out using simulations [205] and experimentation [[63], [79], [89], [90], [101], [206], [207], [208]]. The main finding from these studies is that the contact resistance can be decreased with the application of an MPL, in particular a double-sided MPL coated GDL.

Nitta et al. [193] experimentally investigated the contact resistance between the GDL and the CL. They found that contact resistance at the GDL/CL interface decreases non-linearly with increased compression. They also showed that the contact resistance between the GDL/CL is between 14 – 60 times larger than the contact resistance between the GDL/BPP. On the other hand, Makharia et al. [194] used electrochemical impedance spectroscopy (EIS) to estimate the contact resistances GDL/CL and GDL/BPP [194]. The GDL was made from Toray carbon paper treated with PTFE. They estimated the contact resistance GDL/BPP to be around 13.0 $m\Omega.cm^2$ and the contact resistance GDL/CL to be around 3.4 $m\Omega.cm^2$ [194]. The reasons behind the discrepancy of the findings between Nitta et al. [194] and Makharia et al. [194] is that the former did not use an MPL whereas the latter researchers utilised an MPL coating on the GDL, this helped reduce the contact resistance at the GDL/CL interface.

Ismail et al. [89] found that the contact resistance decreased when an MPL-coating was added to the GDL [89]. This is due to MPL conformability, which allows easier transfer of electrons. Additionally, the contact resistance was found to increase with increasing PTFE content [89] [207]. This is due to PTFE being a natural electrical insulator. Therefore, the higher the PTFE content, the lower the overall conductivity of the GDL.

A three-dimensional numerical model of a PEMFC was developed by Okereke et al. [205]. The aim was to computationally investigate the effects of a double-sided MPL coating on overall fuel cell performance and the distribution of current and oxygen concentration within the cathode GDLs. The results revealed that the double-sided MPL coating significantly improved fuel cell performance by up to 30%. However, neglecting the contact resistance between the MPL and the catalyst layer could result in an overestimation of performance up to 6%. Additionally, the study found that the fuel cell's performance and oxygen distribution were more sensitive to the porosity of the MPL facing the bipolar plate than the MPL facing the catalyst layer. Incorporating an extra MPL at the GDL-bipolar plate interface has the potential to greatly enhance fuel cell performance.

The application of the MPL to the surface of the GDL facing the bipolar plate was shown to reduce the relevant contact resistance and improve the fuel cell performance. However, it is also possible for it to affect the removal of excess water. For example, Owejan et al. [128] investigated the addition of a 50 μm free-standing MPL between the GDL and the bipolar plate and it was shown that the performance of the fuel cell was reduced as the water was trapped between layers. However, they only applied the MPL to the side facing the BPP. Also, the use of a free-standing MPL could have left cavities between the MPL and GDL in which water could accumulate. An improved solution would be to apply the MPL directly to the GDL to avoid these cavities. On the other hand, Wang et al. [76] used a carbon fibre paper (TGPH-030, Toray) as a macroporous substrate (MPS) and applied MPLs on both sides. The MPL was made from a composite of two different carbon blacks: Acetylene Black and Black Pearls 2000 with a 30 wt. % PTFE loading. It was shown that the double-sided MPL coating improved the fuel cell performance; the current density with double-sided MPL coating was 1500 mA/cm^2 and with the single-sided coating was 1300 mA/cm^2 at 0.2 V. This is evidently due to the improved contact between the GDL and both the BPP and the CL [76]. It was also highlighted by Wang that the double-sided MPL coating allowed for a gradually changing porosity from the catalyst to the bipolar plate, thus maintaining satisfactory levels of mass transport management [76]. Maintaining a constant total MPL loading of 1 mg/cm^2, the MPL loading of 0.7 mg/cm^2 facing the CL and 0.3 mg/cm^2 facing the BPP gave the best overall fuel cell performance [76].

Chang et al. [47] did a similar study and applied an MPL on both sides of the GDL. In this scenario, they did not keep the total carbon loading constant. An SGL 10BA carbon paper was used and three different carbon blacks were assessed to see which performed the best: Acetylene Black, Black Pearls 2000 and Vulcan XC 72B. The PTFE content was kept constant in all MPLs at 20 wt. %. It was found that Acetylene Black was the best-performing carbon black. They then optimised the loading of Acetylene Black for the two MPL coatings [47]. They reported that an MPL loading of 1.25 mg/cm^2 facing the CL and 0.25 mg/cm^2 facing the BPP gave the best fuel cell performance. PTFE content was also examined and it was found that loading of 20 wt. % was the most effective. The double-sided MPL coating with 1.25/0.25 mg/cm^2 loading could reach a maximum power density of 900 mW/cm^2 compared to a conventional single-sided MPL coating (with 1 mg/cm^2 loading) which had a maximum power

density of 750 mW/cm^2 [47]. The authors showed that there is an optimum ratio of loading before fuel cell performance starts to decline due to the GDL becoming significantly thick and suffering from mass transport losses.

Huang and Chang [48] further investigated the double-sided MPL coating under different humidity conditions. SGL 10BA carbon paper was coated on both sides with an Acetylene Black MPL with different carbon and PTFE loadings. Different amounts of MPL carbon loadings on both sides of GDL were tested. The results showed that over a large range of relative humidities, the optimum MPL loading was 1.2 mg/cm^2 facing the CL and 0.3 mg/cm^2 facing the BPP [48]. This again showed that a small amount of MPL loading facing the BPP is beneficial for improved fuel cell performance, not only at low relative humidities but also when the relative humidity of air is high. PTFE content was also examined. It was found that the optimal PTFE loadings are the same on both sides of the MPL: 20 wt. % [48]. The peak power density at very low air relative humidity conditions, 13.6% RH, was 0.28 W/cm^2 for a single-sided MPL coating, whereas it was 0.52 W/cm^2 for the double-sided MPL coating which is an 85% increase [48]. Furthermore, EIS showed that the double-sided MPL at optimum composition always exhibits the lowest ohmic resistances [48].

Further research is needed to fully understand the potential of double-sided MPL coated GDLs in reducing contact resistances and minimising the need for increased compression in fuel cells. The existing investigations primarily relied on polarisation curves and EIS, providing limited insights. This study aims to comprehensively characterise double-sided MPL coated GDLs through ex-situ and in-situ analyses, including measurements of pore size distribution, permeability, porosity, contact angle, morphology, electrical conductivity, as well as polarisation curves and EIS.

3.3 Materials and Methods

3.3.1 Fabrication Procedure

The GDL used for all of the samples was Toray Carbon Paper 060 PTFE 10 wt. % (Fuel Cell Earth, USA). Two different types of carbon black were used for the MPL coatings: Ketjenblack and Vulcan Black XC 72 R (Sigma Aldrich®, UK). The categories of samples that were used for the characterisations are shown in Table 3-1.

Table 3-1 GDL samples prepared for the investigation.

Sample Type	Abbreviation	GDL Substrate	MPL Material	MPL Loading Side 1 (mg/cm^2)	MPL Loading Side 2 (mg/cm^2)
Uncoated GDL	GDL	Toray Carbon Paper 060 PTFE 10 wt. %	-	-	-
Single Sided MPL coated GDL	SVB	Toray Carbon Paper 060 PTFE 10 wt. %	Vulcan Black PTFE 20 wt. %	1.25	-
Single Sided MPL coated GDL	SKB	Toray Carbon Paper 060 PTFE 10 wt. %	Ketjenblack PTFE 20 wt. %	1.25	-
Double Sided MPL Coated GDL	DVB	Toray Carbon Paper 060 PTFE 10 wt. %	Vulcan Black PTFE 20 wt. %	1.25	0.25
Double Sided MPL Coated GDL	DKB	Toray Carbon Paper 060 PTFE 10 wt. %	Ketjenblack PTFE 20 wt. %	1.25	0.25

For the coated GDLs, the loadings of 1.25 mg/cm^2 and 0.25 mg/cm^2 were selected based on the previous study by Chang et al. [[47], [48]]. PTFE content in all of the MPLs was kept constant at 20 wt. %. Carbon black (800 mg), 60 PTFE wt. % dispersion (200 mg) (Sigma-Aldrich®, UK), methylcellulose (Sigma Aldrich®, UK) and Triton X 100 (21.6 µg) (Sigma Aldrich®, UK) were mixed with deionised water. The solution was magnetically stirred at 800 rpm for half an hour with small additions of deionised water until a viscous consistency was achieved. This amount of MPL ink would then be enough to make up to 5 samples of a single-sided MPL coated GDL.

The Toray carbon paper was secured to a hot plate, which was set at 90°C. MPL slurry was applied to one side of the GDL and the doctor blade apparatus was used to spread it evenly across the surface. This was repeated until the desired MPL loading was achieved. The samples were sintered in a furnace at 350°C for half an hour with a flow of nitrogen at 1 bar. Each category described in Table 3-1 was comprised of 5 samples with dimensions of 7.0 cm × 2.5 cm. In the case of the double-sided samples, the 1.25 mg/cm^2 loading was applied first. The sample was allowed to dry thoroughly before being flipped and the 0.25 mg/cm^2 coating was applied to the opposite side. This was to ensure that the first side had dried out properly so that it would not be damaged when the 0.25 mg/cm^2 coating was applied. All of the MPL slurries contained PTFE at 20 wt. %. Figure 3-2 shows photos of the double-sided MPL coating carried out in the laboratory. The example shows Ketjenblack used for the MPL coating, image A shows a 1.25 mg/cm^2 loading and image B a 0.25 mg/cm^2 loading. It can be seen by visual inspection, that side B has less coverage than side A. However, it still has good overall coverage over the GDL substrate. This will be investigated further with scanning electron microscope (SEM) imaging.

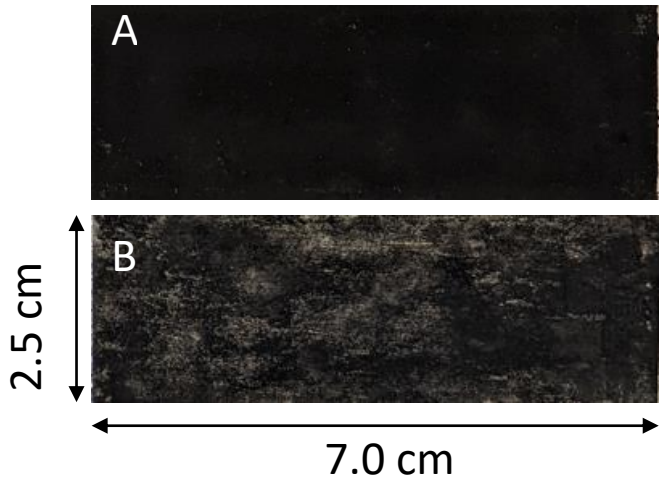

Figure 3-2 Picture of the two sides of a double-sided MPL coated GDL. Featuring Ketjenblack. A: 1.25 mg/cm^2 B: 0.25 mg/cm^2.

3.3.2 In-plane Electrical Conductivity

The in-plane conductivity of the GDL samples was measured using the 4-probe method as described by Smits [209]. To experimentally measure the electrical conductivity of a sample, the method uses four probes spaced at equal intervals as shown in Figure 3-3.

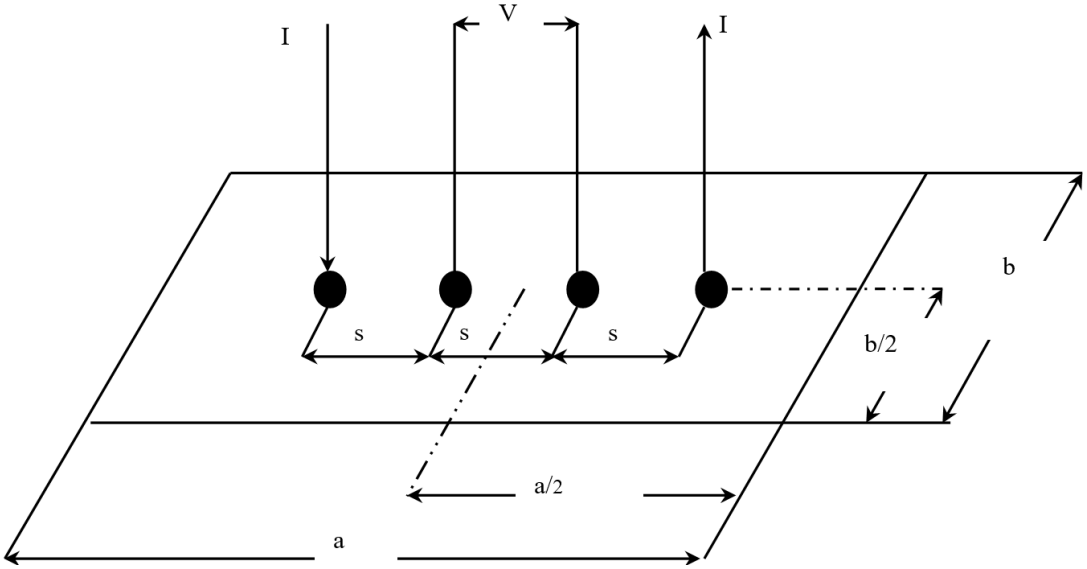

Figure 3-3 In-plane electrical conductivity experimental set-up [89].

The correction factor also needs to be evaluated; it is a function of two ratios. The first ratio is between the length of the sample and its width (a/b). The second shows the ratio between the width of the sample and the spacing between the probes (b/s) [209]. In this study, these ratios were found to be 3 and 1.25 respectively. This gave a correction factor of 0.9973. The resistivity (ρ) can be calculated using the following formula [209]:

$$\rho = CtR \tag{3.1}$$

Where C is the correction factor, t is the thickness of the sample and R is the electrical resistance. Following this, the electrical conductivity, σ, of the GDL can be found by the reciprocal of the resistivity:

$$\sigma = \frac{1}{\rho} \tag{3.2}$$

Sample thickness was measured using a micrometre. However, the GDL thickness varied from one GDL type to another and even from one sample to another. Also, within the sample itself, there was a slight variation in the thickness from one position to another. Therefore, the thickness of each GDL sample was measured at five equally spaced positions and the average value was taken. Following this, the GDL samples were positioned on an insulating plate. Copper electrodes (10 mm × 10 mm × 5 mm) were then placed onto the GDL sample. The distance between the probes was kept constant; this was done by fixing the probes in a rectangular plastic body. The spacing between the probes was 2 cm. A high-resolution ohmmeter (RS Pro 804, RS Components, UK), with a resolution of 0.01 mΩ, was used to read the electrical resistance of the sample. An electrical current passed through the sample via the copper electrodes and the voltage between the internal probes (see Figure 3-3) was measured. This allows for the resistance to be calculated using Ohm's law.

3.3.3 Permeability

Permeability can be estimated using Darcy's law. Darcy's law states that a flow rate (Q) through a porous substance is equal to the product of the permeability (k), cross-sectional area (A) and pressure drop (ΔP) divided by the product of viscosity (μ) and thickness (L) of the sample [42].

$$Q = \frac{kA\Delta P}{\mu L} \tag{3.3}$$

The permeability can be measured experimentally; Figure 3-4 shows an experimental set-up used by Orogbemi et al. [101]. The GDL sample is clamped between two plates in the middle of the lower fixture and nitrogen is then passed through using a mass flow controller [101].

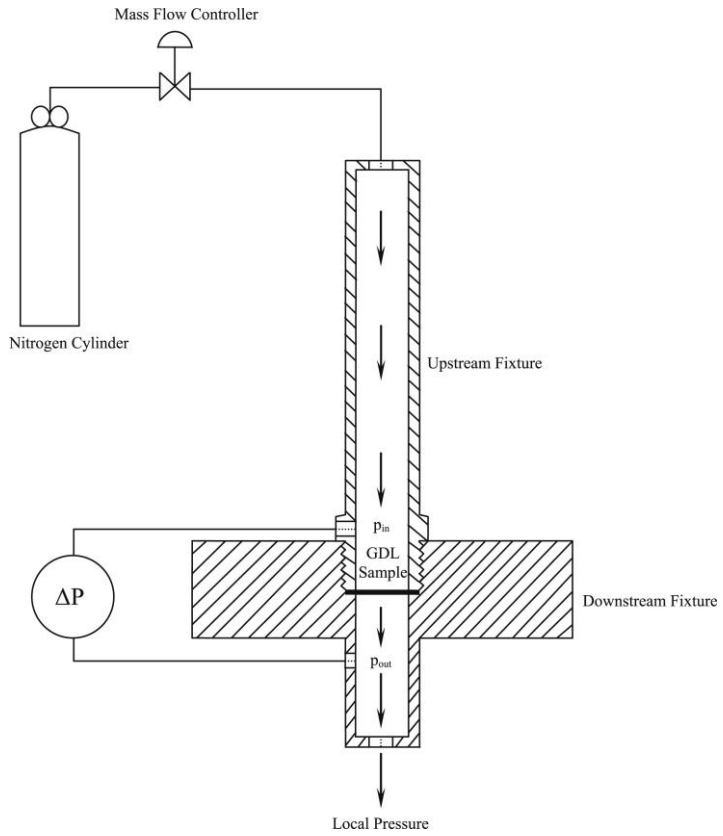

Figure 3-4 Experimental setup used to measure through-plane permeability [101].

The experimental setup depicted in Figure 3-4 consists of two fixtures, one positioned upstream and the other downstream. This arrangement allows for the controlled flow of air through the sample, with the resulting pressure drop being measured. The sample used was obtained using a circular punch with a diameter of 25.4 mm. However, when the sample is fixed between the fixtures, only a 20 mm diameter area is exposed to the airflow. To ensure accurate measurements, the pressure drop is recorded at multiple flow rates, using extremely low rates to minimise inertial losses which enables the use of Darcy's Law. To control the flow rate of nitrogen gas, an HFC-202 flow controller is utilised, providing a range of 0.0-0.1 SLPM (standard litre per minute). The pressure difference across the sample is measured by employing a PX653 differential pressure sensor, capable of measuring within a range of ±12.5 Pa. By applying Darcy's Law (Equation 3.3), the gas permeability of the sample can be calculated. The permeability is determined for each sample at different flow rates and then the

average value is calculated. The entire process is repeated for all five samples in each category, as outlined in Table 3-1.

3.3.4 Pore Size Distribution

Pore size distribution is an important characteristic to understand as it provides insights regarding the mass transport modes of gas and liquid water within the fuel cell porous media. Further, it is a major parameter when it comes to the modelling and optimisation of mass transport processes in the fuel cell [126]. Mercury intrusion porosimetry (MIP) is a widely used method to determine pore size distribution within a material. It is based on the high surface tension of mercury. In the process of MIP, a small sample of the GDL is immersed in mercury. Due to the high surface tension of mercury, it does not readily enter the pores of the GDL. The mercury pressure is then increased in increments. This causes the mercury to enter into the pores of the GDL, the larger pores are initially filled, gradually followed by subsequently smaller pores [126]. The pore size distribution is found by measuring the intrusion pressure of the mercury which is inversely proportional to the pore size. A key assumption made when using this method is that the pore shape is cylindrical. Also, MIP does not account for closed pores. However, this is acceptable when considering carbon papers [207]. The pores of a GDL typically fall into three main categories: pores with radii less than 50 nm are micropores; pores with radii ranging between 50 and 7000 nm are mesopores; and pores that have a radius larger than 7000 nm are designated as macropores [63]. The GDL mainly consists of macropores [79] but the addition of an MPL can influence the pore size distribution by increasing the amount of micropores and mesopores. In general, macropores facilitate the diffusion of gases, whereas micropores allow for the removal of liquid water [208].

3.3.5 Contact Angle

The contact angle is a measure of the wettability of the material in question. If the contact angle is less than 90° the substance is considered hydrophilic. A contact angle greater than 90° and the substance is deemed hydrophobic [90]; see Figure 3-5. Determination of the contact angle for the samples was carried out using the sessile drop method. Single drops of water were placed on the surface of the GDL sample. High-resolution photographs were then taken within the first three seconds of the droplet settling on the surface to account for the transient behaviour of the water [208]. Contact angle values were then measured. Each sample underwent five measurements and then an average value was taken.

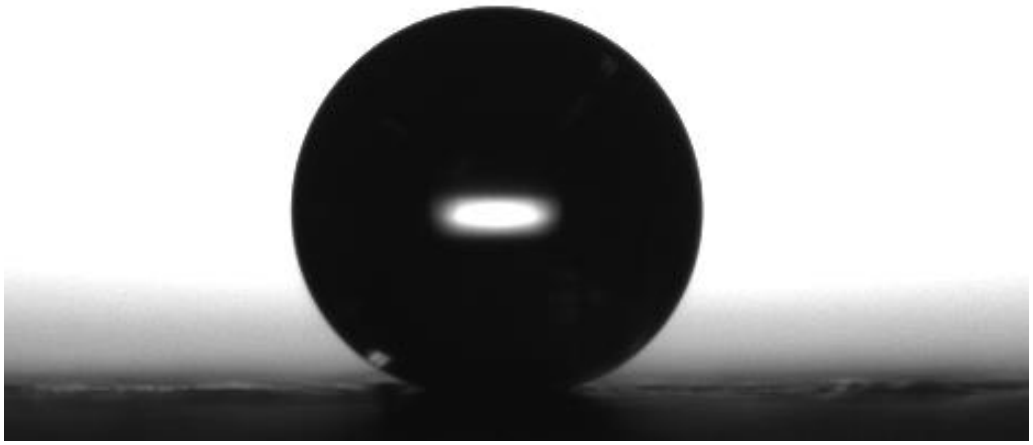

Figure 3-5 A typical water droplet on the surface of a GDL sample.

3.3.6 Morphology

SEM imaging is a good way to analyse the surface morphology and fibre structure of the GDL/MPL. The SEM micrographs often assist in analysing the characteristics of the GDL materials and/or the fuel cell performance [[203], [210], [211]]. The morphological characteristics of the GDL were analysed using a scanning electron microscope (JEOL - Model JSM-6010LA). GDL samples were cut into 1 cm x 1 cm squares. The squares were then attached to SEM stubs and secured in the specimen stage. The SEM was then set at 10 kV and each sample was examined at various magnifications.

To obtain the cross-sectional images of the GDL samples, the samples were first frozen in liquid nitrogen and then cut with a scalpel. This helped preserve the cross-section of the GDL for clear imaging.

3.3.7 In-situ Fuel Cell Testing

The membrane electrode assembly (MEA) was prepared by assembling the cathode and anode side GDLs with the catalyst coated membrane (CCM). GDL coated with MPL samples investigated in this study were placed on the cathode side, while Freudenberg H2315 C2 MPL coated GDL was placed on the anode side. A CCM (Johnson Matthey) was used, comprising a 211 Nafion membrane with a thickness of 25 μm. Catalyst layers with a platinum loading of 0.2 mg/cm^2 were applied to both sides of the Nafion membrane. The active area for the fuel cell was 2.25 cm x 2.25 cm. The MEA was then hot pressed at 140°C for 2 minutes. The MEAs were fitted into a PaxiTeck single-cell fixture. This consisted of graphite monopolar plates containing a single serpentine flow field channel measuring 1 mm in width and depth. The current collector plates were made of gold-plated copper, while the end plates were made of aluminium, which allowed for the use of electric heating elements to separately control the anode and cathode temperatures. The cathode graphite monopolar plate was fitted with a Negative Temperature Coefficient (NTC) sensor to measure the cell temperature, while the cell potential was measured between the monopolar plates. The cell was connected to a Bio-logic FCT-50S test station that had a maximum load current of 50 A and 250 W power, which was computer-controlled using FC-lab® software. The reactant temperature and humidity were regulated by sensors and electrical heaters, which measured and controlled the temperature of the anode and cathode humidifiers and reactant lines. The fuel cell system operated with a specific backpressure of 1.5 bar on the anode side and 1.3 bar on the cathode side. Gas flow rates were set based on stoichiometric ratios. For hydrogen, the stoichiometry ratio is 1.3, resulting in an estimated flow rate of 120 mL/min. For air, the stoichiometry ratio is 1.5, leading to a flow rate of approximately 300 mL/min.

The fuel cell was then set to a temperature of 80°C. The inlet gas humidifiers (hydrogen and air) were also set at 80°C, this was subsequently changed to vary the relative humidity conditions. Following this, the polarisation and EIS data were collected for four different relative humidity (RH) conditions: 25, 50, 75 and 100%.

3.4 Results and Discussion

The abbreviations of the samples are shown in Table 3-2, these will be referred to throughout this section.

Table 3-2 Abbreviations of the samples used in this investigation.

Sample Type	Abbreviation
Uncoated GDL	GDL
Single sided MPL coated GDLs	
Single Sided Vulcan black MPL coated GDL	SVB
Single Sided Vulcan black MPL with a 1.25 mg/cm^2 loading	SVB 1.25
Single Sided Ketjenblack MPL coated GDL	SKB
Single Sided Ketjenblack MPL with a 1.25 mg/cm^2 loading	SKB 1.25
Double sided MPL coated GDLs	
Double Sided Vulcan black MPL Coated GDL	DVB
Double Sided Vulcan black MPL with a 1.25 mg/cm^2 loading	DVB 1.25
Double Sided Vulcan black MPL with a 0.25 mg/cm^2 loading	DVB 0.25
Double Sided Ketjenblack MPL Coated GDL	DKB
Double Sided Ketjenblack MPL with a 1.25 mg/cm^2 loading	DKB 1.25
Double Sided Ketjenblack MPL with a 0.25 mg/cm^2 loading	DKB 0.25

3.4.1 In-plane Electrical Conductivity

The in-plane conductivity was measured for all five samples of each category of GDL. Each sample was measured five times and the values of the resistance were averaged. The results for the in-plane conductivity per category are displayed in Figure 3-6. It can be seen from the results that there is a difference of around 5000 S/m between the highest value and the lowest value for the average conductivity. In general, there are no recognisable trends: regardless of loading or the fact that it is single-sided or double-sided. The conductivities of all the MPL-coated GDL samples are similar to each other and are within the error bars ranges. Notably, the in-plane conductivity of all the MPL coated GDLs is less than that of the uncoated GDL. This could be attributed to the fact that the MPLs contain a sizable amount of the electrically insulating PTFE (20 wt. %) compared to the carbon substrate (10 wt. %). It is noteworthy that the conductivity of the uncoated GDL (~ 20000 S/m) fits closely with values from the literature for the same type of Toray GDL [63]. It should also be noted that the through-plane conductivity of the MPLs applied to the GDL is highly expected to be similar to the in-plane conductivity, this is due to the uniformity of the MPL structure. Error bars of ±5 % have been added to the data reflecting the potential for uncertainty in the measurements. It can be seen that there is some overlap for the coated samples, both Vulcan black and Ketjenblack. However, the uncoated sample of GDL is distinctly outside of the error bar region, suggesting that statistically the value is distinctly higher than the MPL coated samples.

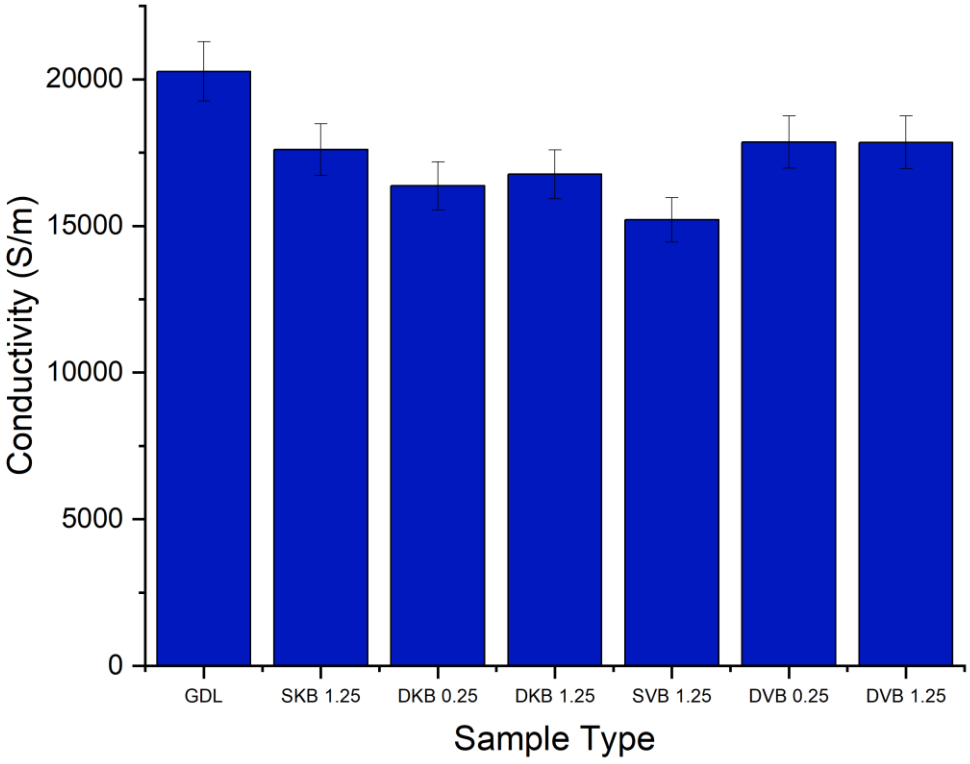

Figure 3-6 In-plane electrical conductivity of the tested GDL samples. Note that the numbers correspond to the MPL loading on either the GDL side facing the catalyst layer or the side facing the bipolar plate.

3.4.2 Gas Permeability

Figure 3-7 shows the permeability values for the different samples. It can be immediately seen that there is almost one order of magnitude difference between the permeability of the uncoated GDL and the permeability of the MPL coated samples; this is due to the addition of the less porous MPL to the carbon substrate. Interestingly, the results show that the gas permeability of the coated samples is more sensitive to the type of carbon black than to the GDL being single-sided or double-sided MPL coated. Namely, the permeability of the Ketjenblack GDL samples is significantly higher than that of the Vulcan black GDL samples. This difference is most likely due to the presence of a higher volume fraction of macropores in the former samples, as will be demonstrated in the next section. Furthermore, it appears that the addition of a second MPL does not make a significant difference to the mass transport resistance of the GDL sandwich. This is most likely due to the relatively low loading of the second MPL (0.25 mg/cm²).

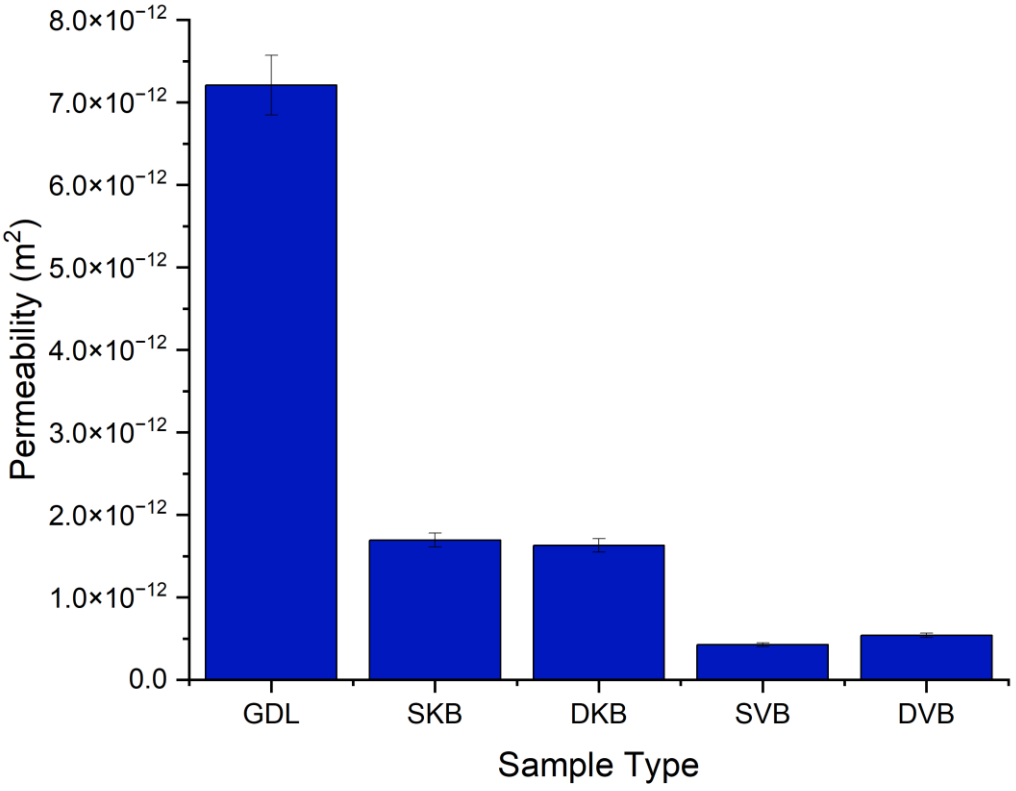

Figure 3-7 Gas permeability of the tested GDL samples.

3.4.3 Pore Size Distribution

The results of the MIP tests are displayed in Figure 3-8, which shows a wide distribution of pore sizes. This is in line with the literature as it has been found in previous studies that the microstructure of a GDL is anisotropic with a wide range of pore sizes [212]. Figure 3-8 also shows that the gas diffusion layer has a distinctive change in pore size distribution once the MPL coating is applied. To identify these structural changes in pore size Figure 3-8 has been divided into three pore categories: micropores, mesopores and macropores. They are divided based on the categories discussed above. It was found that the micropores and mesopores expectedly arise upon applying the addition of the MPL. The first observation is that the volume and size of macropores decrease with MPL addition. It could be also seen that the Ketjenblack samples, both single-sided or double-sided coating, have only micropores. On the other hand, Vulcan black samples were shown to have both micropores and mesopores. Furthermore, as expected, the volume of the micropores and/or mesopores was found to increase with the addition of the second 0.25 mg/cm^2 MPL; see Figure 3-8 (b). The variation appears to affect the efficiency of removing liquid water from the GDL to the flow channel, which, as demonstrated in the final section, subsequently influences fuel cell performance. Moreover, Table 3-3 displays the porosity and the average pore diameter for each of the samples. The porosity is the measure of empty spaces or voids within the material, typically expressed as a percentage of the material's total volume [213]. The introduction of an MPL to the samples results in an overall reduction in porosity. This outcome is in line with expectations as when the MPL is applied, it will naturally fill in the pores of the carbon substrate. Comparatively, there is a minimal difference between the porosities of the samples when looking at the type of carbon black used. There is also little difference between the single-sided and double-sided configurations. However, it can be seen that when a second coating is applied, there is a reduction in porosity. Ketjenblack experiences a 3.8% reduction in porosity when the second MPL is applied and Vulcan black shows a 2.1% reduction.

Table 3-3 The porosity of the GDL samples.

Sample Type	Porosity (%)
GDL	76.4
SKB	75.1
SVB	74.9
DKB	71.3
DVB	72.8

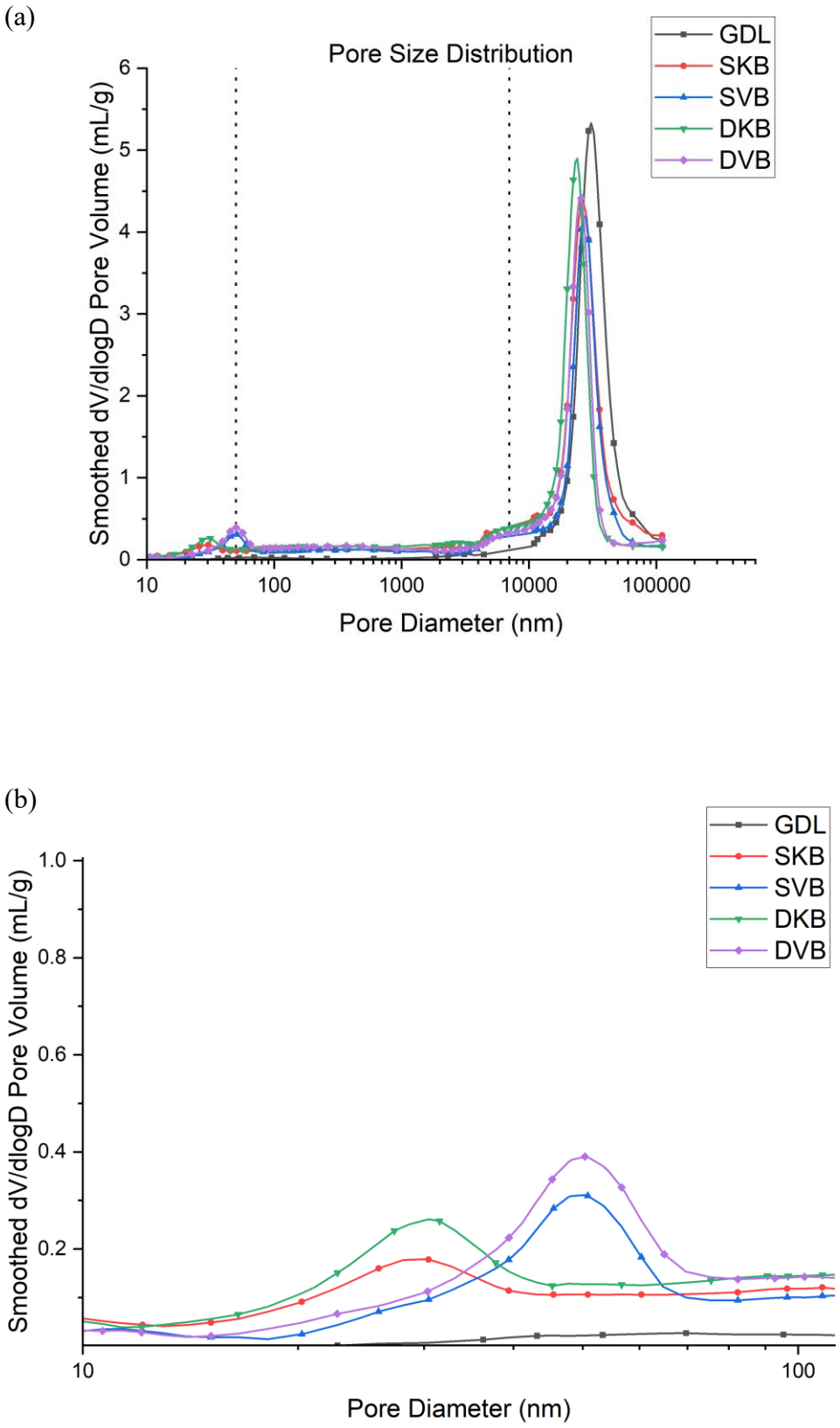

Figure 3-8 (a) Pore size distribution of the tested GDL samples and (b) micropores and mesopores ranges of the samples.

3.4.4 Contact Angle

From the contact angle measurements (Figure 3-9), it can be seen that the addition of an MPL generally increases the contact angle. The uncoated sample of GDL measures 138° and the coated samples measure between 139° and 142°. This could be attributed to the high amount of PTFE loading in the MPL (20 wt. %) compared to the carbon substrate (10 wt. %). Further, for the double-sided MPL coated GDLs, the 1.25 mg/cm^2 side was found to demonstrate a slightly higher contact angle than the 0.25 mg/cm^2. This is most likely because, as will be shown in the following micrographs, the MPLs with 0.25 mg/cm^2 do not fully cover the surface of the carbon substrate, thus allowing for the structure of the carbon substrate (which has a lower contact angle) to lower the contact angle of the latter MPL. It should also be noted that there is overlap between the ±5 % error bars which would suggest that the actual differences between the values may be statistical rather than observational.

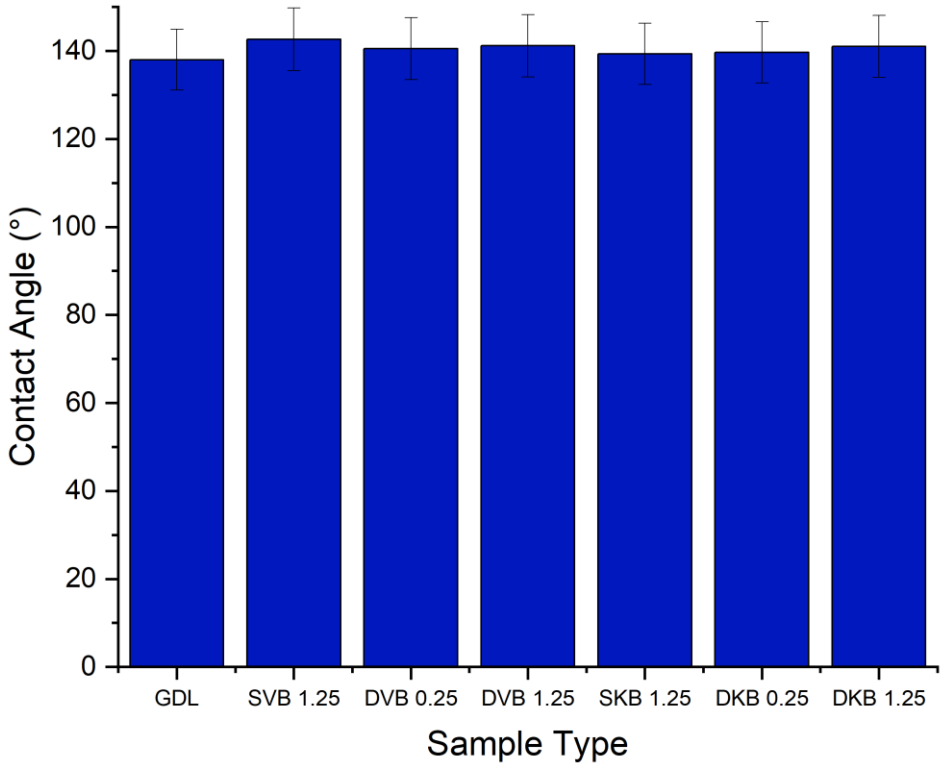

Figure 3-9 Contact angle of the tested GDL samples.

3.4.5 Morphology

The SEM images used to examine the morphology of the samples are displayed in Figure 3-10 and Figure 3-11. Figure 3-10 shows the uncoated Toray GDL and the conventional single coating of MPL of Vulcan black and Ketjenblack with an MPL loading of 1.25 mg/cm^2. Figure 3-11 shows both sides of the double-sided coating of MPL for both Ketjenblack and Vulcan black samples. The loading of these samples is 1.25 mg/cm^2 facing the catalyst layer and 0.25 mg/cm^2 facing the BPP. Firstly, it can be seen that for both the carbon blacks, the 1.25 mg/cm^2 has full uniform coverage of the substrate. In the case of the 0.25 mg/cm^2, it can be seen that there are protrusions of the carbon fibre strands from the substrate. This is expected as a lower loading would result in a thinner MPL. As discussed in the methodology, the loading of 1.25 mg/cm^2 was applied first. It was then allowed to dry out, flipped and the 0.25 mg/cm^2 was then applied. This had the potential to damage the MPL loading on the 1.25 mg/cm^2 side when the doctor blade applicator was being used. However, it can be seen from the SEM imaging, that there is no noticeable damage to the 1.25 mg/cm^2 MPLs. Furthermore, Figure 3-10 and Figure 3-11 show that Vulcan black has much finer particles than the Ketjenblack; the Ketjenblack appears slightly coarser on the surface. Upon examining the cross-sectional image presented in Figure 3-11, it is evident that the penetration of the Vulcan black MPL into the GDL substrate is more pronounced compared to the Ketjenblack. This is potentially the reason that the Vulcan black GDL samples have fewer macropores compared to Ketjenblack samples.

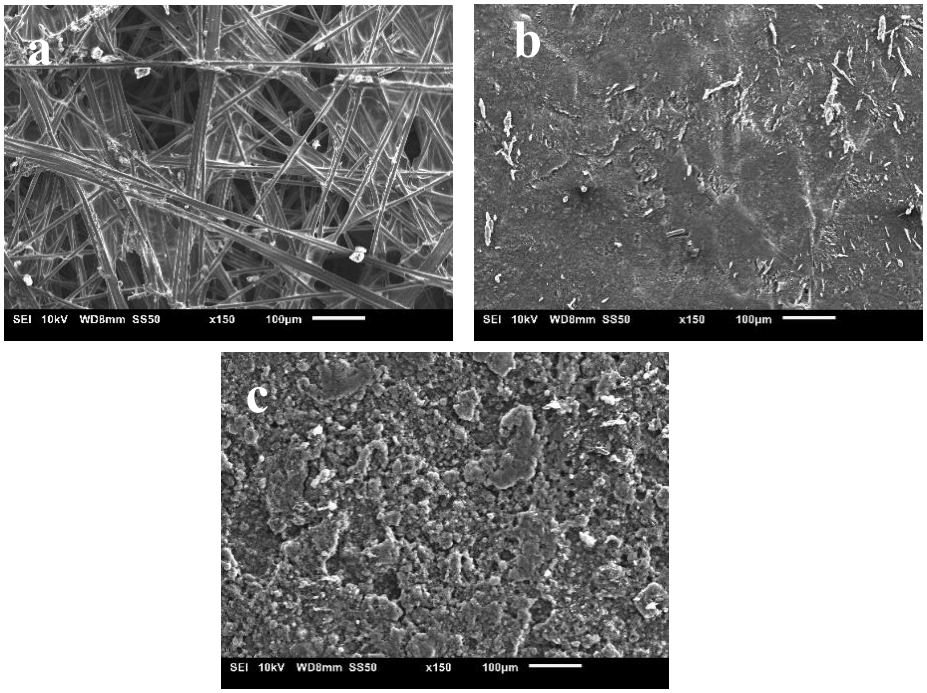

Figure 3-10 SEM images for (a) uncoated Toray GDL, (b) single-sided coated GDL with 1.25 mg/cm^2 Vulcan black and (c) single-sided coated GDL with 1.25 mg/cm^2 Ketjenblack.

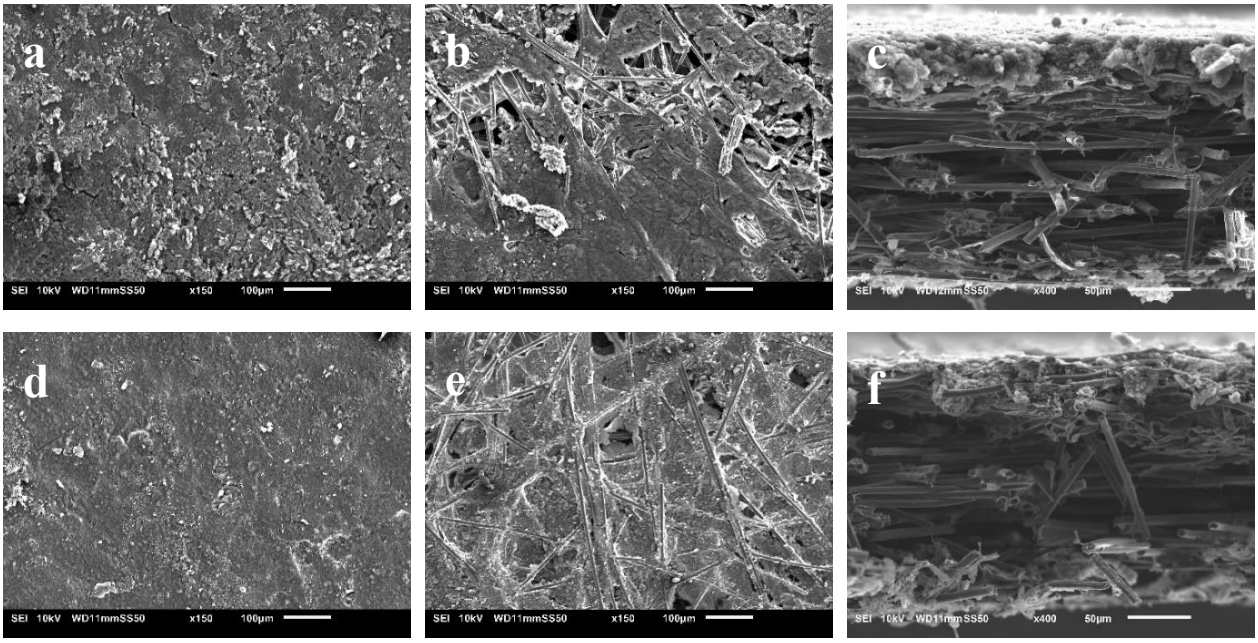

Figure 3-11 SEM images for (a) double-sided coated GDL with 1.25 mg/cm^2 Ketjenblack, (b) double-sided coated GDL with 0.25 mg/cm^2 Ketjenblack, (c) cross-sectional of double-sided coated GDL with Ketjenblack (d) double-sided coated GDL with 1.25 mg/cm^2 Vulcan black and (e) double-sided coated GDL with 0.25 mg/cm^2 Vulcan black (f) cross-sectional of double-sided coated GDL with Vulcan black.

3.4.6 Fuel Cell Performance

The fuel cell was tested for its performance at four different RH conditions (25, 50, 75 and 100%); Figure 3-12 shows the polarisation curves for the fuel cell operating with the investigated GDL samples at these humidity conditions. Furthermore, for reference, Table 3-4 shows the peak power density and the maximum current density (extracted from the corresponding polarisation curves) for each of the cases investigated. There are some observations that one could deduce from the polarisation curves. The first observation is that the fuel cell with the cathode uncoated GDL performs reasonably well at low humidity conditions (25% RH); however, the performance becomes worse as the relative humidity increases. The lack of the MPL renders the GDL unable to remove excess liquid water as effectively as compared to an MPL coated GDL, thus resulting in water flooding [87]. This result is corroborated by the EIS measurements (Figure 3-13) that show that the fuel cell operating with the cathode uncoated GDL demonstrates a significant charge transfer resistance at high humidity conditions (75 and 100% RHs). The second observation is that the fuel cell with double-sided Vulcan black coated GDL significantly outperforms all other GDL samples, as it shows the lowest charge transfer resistance (Figure 3-13). This could be attributed to the fact that this GDL lowers the contact resistance with the bipolar plate and has balanced volume fractions of micropores and mesopores (Figure 3-8); this turned out to be crucial when it comes to draining excess liquid water, particularly for the side facing the bipolar plate. Research has indicated that MPLs with a suitable combination of micropores and mesopores exhibit improved water removal capabilities in high-humidification conditions [81].

On the other hand, the fuel cell with double-sided Ketjenblack coated GDL does not perform as well as the double-sided Vulcan black coated GDL. The MIP results are shown in Figure 3-8, show that the Ketjenblack GDL samples have only micropores that are smaller than those Vulcan black samples. Such small micropores at both sides of the GDL appear to act as a trap for liquid water, which is an issue at higher current densities. This premise is corroborated by the fact that the single-sided Ketjenblack coated GDL performs slightly better than the double-sided Ketjenblack coated GDL at high humidity conditions (75 and 100% RH), implying that the second MPL facing the bipolar plate hinders the removal of liquid water from the GDL.

It is important to acknowledge that conducting fuel cell testing at lower relative humidity (RH 25%) is not ideal for optimal performance of the Nafion membrane [[214], [215]]. This suboptimal condition can impact the overall results due to membrane dehydration, leading to, membrane shrinkage, low ionic conductivity and poor contact between the membrane and electrode [[214], [215]]. Despite this limitation, it can be seen that SVB and DVB samples demonstrate satisfactory performance under these challenging conditions.

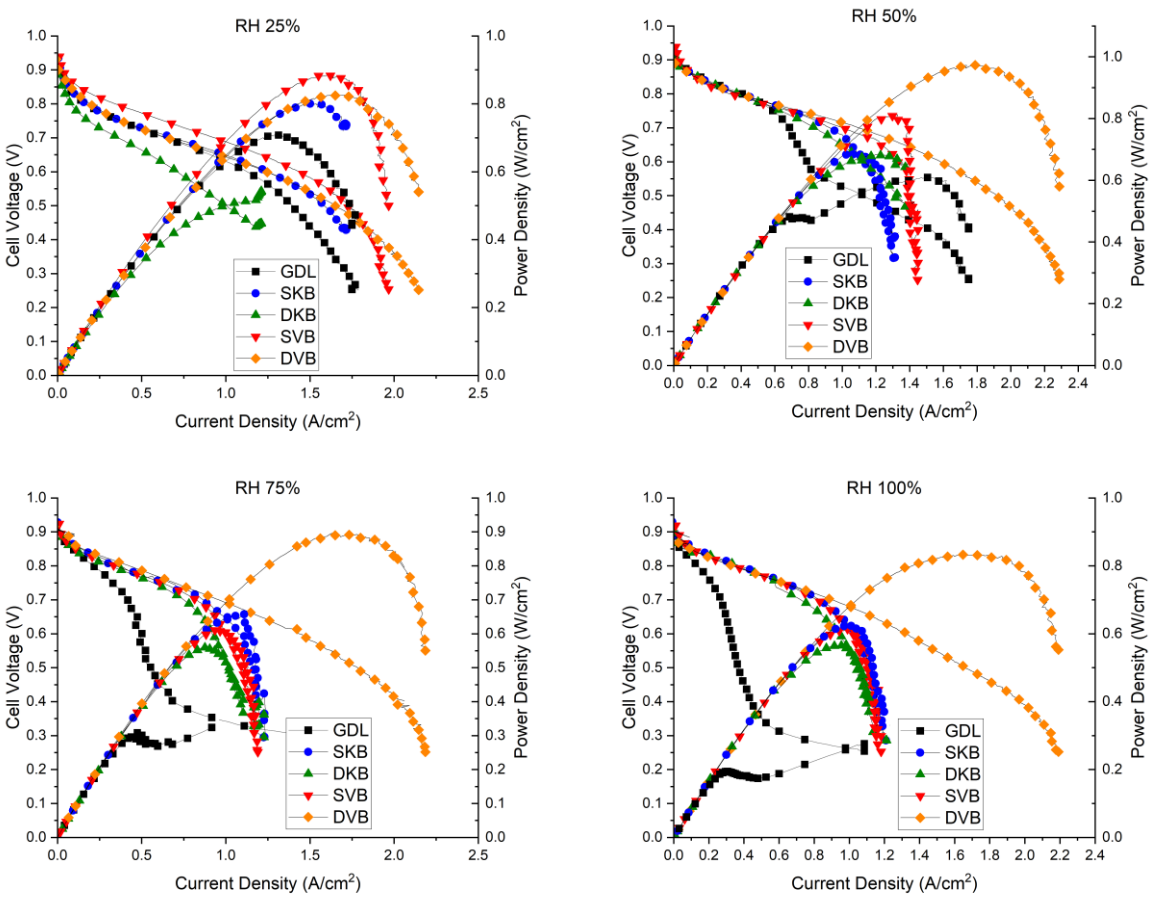

Figure 3-12 The polarisation curves of the fuel cell operating with the investigated GDL samples at various humidity conditions (RH 25%, RH 50%, RH 75% and RH 100%). Note that the cell temperature was kept constant at 80°C.

Table 3-4 The peak power density and maximum current density for the cases investigated.

Relative Humidity	Sample Type	Peak Power Density (W/cm^2)	Maximum Current Density (A/cm^2)
25%	GDL	0.71	1.33
	SVB	0.88	1.62
	SKB	0.79	1.52
	DVB	0.82	1.67
	DKB	0.51	1.13
50%	GDL	0.61	1.51
	SVB	0.79	1.36
	SKB	0.67	1.11
	DVB	0.96	1.85
	DKB	0.68	1.22
75%	GDL	0.32	0.91
	SVB	0.61	0.96
	SKB	0.66	1.10
	DVB	0.89	1.76
	DKB	0.55	0.89
100%	GDL	0.27	1.08
	SVB	0.62	1.01
	SKB	0.62	1.02
	DVB	0.83	1.74
	DKB	0.56	0.97

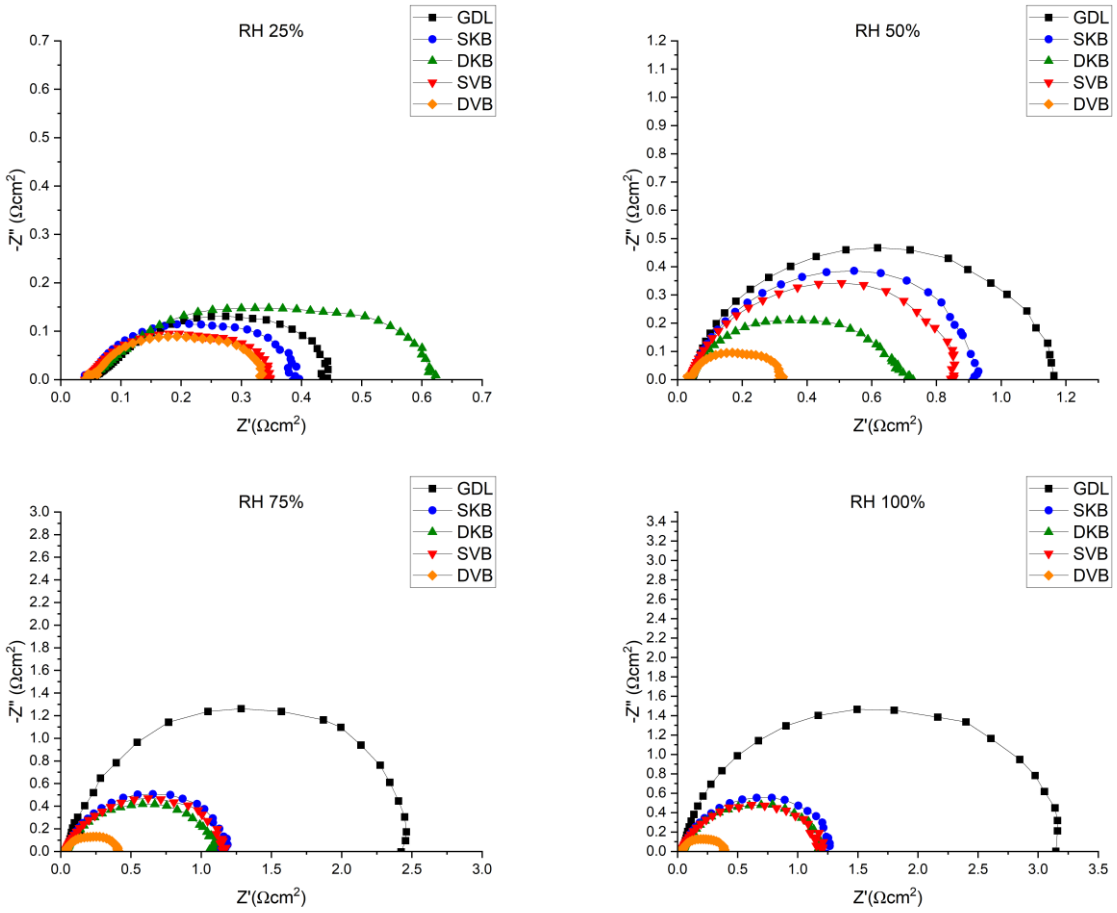

Figure 3-13 EIS measurements for the fuel cell operating with the investigated GDL samples at 0.6 V.

3.5 Conclusion

The impact of double-sided MPL on key properties and fuel cell performance has been investigated and compared with conventional single-sided MPL coatings. Two types of carbon black (Vulcan black and Ketjenblack) were employed to evaluate the sensitivity of the results to the type of carbon black. The MPL loadings applied to the surfaces of the GDL facing the catalyst layer and the bipolar plate were 1.25 and 0.25 mg/cm², respectively.

The results indicated that the in-plane electrical conductivity of all the MPL-coated GDLs is slightly lower than that of the uncoated GDL. This decrease was attributed to the lower PTFE content in the carbon substrate. Furthermore, the study demonstrated that the in-plane electrical conductivity exhibits minimal sensitivity to the MPL loading or carbon black type. The permeability measurements indicated that the permeability is almost insensitive to whether the GDL is single or double-sided MPL coated. It is more sensitive to the type of carbon black used. The MIP data showed that the addition of an MPL results in a favourable shift in pore size distribution, with prominent micropores observed in both single and double-coated MPLs. The double-sided MPL coating slightly increased micropores and mesopores when compared to the single-sided MPL coating. Contact angle measurements showed a slight increase in hydrophobicity with the addition of MPL, but no significant differences were observed between the carbon black types or loading levels. SEM imaging showed that the 0.25 mg/cm² loading does not fully cover the surface of the GDL. Also, the level of MPL penetration into the carbon substrate is higher in the case of Vulcan black compared to Ketjenblack. In-situ fuel cell testing revealed that the DVB case performed exceptionally well under high humidity conditions, outperforming SKB, DKB, and SVB at 50%, 75%, and 100% relative humidity. This can be attributed to the fact that, as indicated by the MIP results, the DVB case demonstrates a favourable balance of mesopores and micropores (when particularly compared to DKB) that is necessary for the effective management of excess water. At 25% relative humidity, the SVB case exhibited better performance than the DVB case, indicating its suitability for low humidity conditions. This is attributed to the shorter diffusion paths demonstrated by the former case.

Further investigations can explore the behaviour of double-sided MPL coated GDL with novel materials like graphene, providing insights for optimisation and enhanced performance in fuel cell applications. Such efforts hold potential for improved fuel cell efficiency and performance.

Chapter 4: Characterisation of Double-Sided Graphene Based Microporous Layer Coated Gas Diffusion Layers for the Improved Performance of Polymer Electrolyte Membrane Fuel Cells

4.1 Abstract

This study aims to experimentally evaluate the effects of double-sided microporous layer coated gas diffusion layers, comparing the addition of graphene in the microporous layer to traditional Vulcan black. Various key properties were analysed alongside the fuel cell performance. The findings indicated that in-plane electrical conductivity was enhanced with the inclusion of graphene. The graphene microporous layer samples displayed higher gas permeability than those using Vulcan black. Vulcan black microporous layers exhibited a favourable shift in pore size distribution, with significant micropores and mesopores present in both the single and double-sided microporous layer-coated gas diffusion layers. In contrast, pure graphene coatings did not generate as many micropores or mesopores. Contact angle measurements remained consistent across all microporous layer coatings, suggesting that this characteristic is more dependent on polytetrafluoroethylene content rather than the type of carbon employed. Scanning electron microscope images revealed that Vulcan black results in a smooth surface, whereas graphene exhibited numerous surface cracks. In-situ fuel cell testing revealed that the double-sided microporous layer, with Vulcan black facing the catalyst layer and graphene facing the bipolar plate, showed superior performance under high humidity conditions as it facilitates the expulsion of excess water through the cracks in the graphene layer. Furthermore, the single-sided Vulcan black microporous layer-coated gas diffusion layer performed better under low humidity conditions due to the presence of a good amount of micropores required to retain water for membrane humidification.

4.2 Introduction

Polymer electrolyte membrane fuel cells (PEMFCs) are a highly promising technology for harnessing hydrogen and playing a significant role in the transition to sustainable energy. PEMFCs can efficiently transform the chemical energy stored in hydrogen directly into electricity via electrochemical reactions, yielding only water and heat as its by-products [23]. PEMFCs are a particularly attractive technology due to their high efficiency, ability to operate at low temperatures, and ease of assembly [203]. PEMFCs are well adapted to facilitate the integration of hydrogen into a range of applications, such as stationary, automotive and portable use [23].

The gas diffusion layer (GDL) is an essential component of the PEMFC. The GDL serves multiple functions within the PEMFC. Firstly, it ensures the even distribution of hydrogen and oxygen to the active sites of the catalyst layer (CL). Additionally, it plays a pivotal role in managing water; ideally, it should remove excess water while keeping the membrane adequately hydrated. Lastly, it provides structural support to the delicate membrane and catalyst layers [54]. Due to the varied tasks it must perform, the GDL is typically made from carbon fibre material, as this best fulfils the multifunctional requirements. A microporous layer (MPL) is conventionally incorporated onto the surface of the GDL. The MPL consists of an ink composed of carbon black and polytetrafluoroethylene (PTFE). Research has shown that the addition of an MPL to the GDL improves water management within the membrane electrode assembly (MEA) [[158], [165]] and enhances electrical contact between the GDL and the catalyst layer [[89], [216]] consequently, leading to improved overall fuel cell performance [[130], [159], [151], [216], [217]].

During the operation of fuel cells, various types of losses occur. Ohmic polarisation losses primarily result from the bulk resistances from induvial fuel cell components and the contact resistance at the interfaces between these components. Contact resistance occurs because of the differences in structure and morphology of the different components. This leads to transitional regions forming at the boundary of these components, increasing the electrical contact resistance [180]. One area particularly affected by the contact resistance is the GDL. This is because it is positioned between the CL and the bipolar plate (BPP). Numerous studies have explored strategies to reduce contact resistance between the GDL and BPP. These investigations have utilised both simulation-based approaches (e.g. [188], [189], [190] and [205]) and experimental methods (e.g. [121], [122], [191], [192] and [193]). The primary consensus emerging from these research efforts is that the application of an MPL, especially a double-sided MPL-coated GDL, proves effective in decreasing contact resistance. Additional research is required to gain a comprehensive understanding of the potential of double-sided MPL-coated GDLs in reducing contact resistances and reducing the necessity for increased compression in fuel cells. The current studies have predominantly relied on polarisation curves and electrochemical impedance spectroscopy (EIS), offering only limited insights into this matter. Furthermore, these studies have only considered conventional carbon black as the main constituent of the MPL. This study aims to examine the use of the novel material of graphene in the context of the double-sided MPL coated GDL and seeks to further improve the contact resistance between the CL and the BPP.

Novel material usage in MPL fabrication is becoming more widespread, as they are shown to increase the capabilities of the MPL. In particular, graphene shows great promise [218]. The aim of using novel materials is to take advantage of their natural properties and increase the performance of the MPL, in particular, reducing contact resistance, improving bulk conductivity and enhancing mass transport processes. Graphene as a novel material for the MPL has recently been a subject of exploration [[142], [143], [211], [219], [220], [221], [222],

[223]]. Graphene consists of a two-dimensional monolayer of graphitic carbon atoms. Graphene has excellent properties such as high electrical and thermal conductivity, large surface area, chemical stability and mechanical strength [[141], [219], [224]].

Leeuwner et al. [142] identified the contact resistance between the MPL and CL as an area of poor electrical conductivity. They conducted a comparative analysis of various MPLs (conventional carbon black, graphene foam, and graphene sheets). Notably, graphene foam exhibited advantageous interfacial properties that contributed to improved electrical conductivity. This can be attributed to graphene's capacity for strong interfacial adhesion coupled with its high electrical conductivity. This combination proved to be optimal and resulted in enhanced overall performance [142]. Additionally, at mid-range current densities, graphene had a higher peak power density (graphene: 362 mW/cm^2, conventional carbon black: 334 mW/cm^2). However, at higher current densities, the conventional MPL outperformed graphene. This was because graphene was less efficient in expelling water. Leeuwner et al. [222] also investigated electrochemically exfoliated graphene and compared it with reduced graphene oxide and natural graphite as an MPL. The graphene samples were deposited onto the Toray TGP H-060 carbon paper with a PTFE loading of 20 wt. %. The graphene MPLs showed a reduced contact resistance and a lower in-plane electrical resistance, compared to a conventional MPL. However, at high humidity levels, flooding took place and this reduced mass transport; this was due to their lower hydrophobicity. A composite MPL made from a mixture of carbon black and graphene was shown to perform better at higher relative humidity.

Similarly, Ozden et al. [220] investigated water management and overall enhanced performance for a graphene-based MPL. The graphene-based MPL was characterised by examining morphological, structural, physical and electrochemical properties. It was also compared to a conventional MPL made from Ketjenblack. It was found that the graphene had higher in-plane electrical conductivity and better water-retaining abilities compared with Ketjenblack. In high humidity conditions, the graphene-based MPL showed comparable performance to the conventional Ketjenblack MPL. Under low to medium humidity conditions, graphene showed a peak power density improvement of 55%. Ozden et al. [143] further examined a graphene MPL compared to a Vulcan black MPL. The results showed that the graphene MPL had a unique morphology composed of horizontally packed graphene flakes that improved in-plane electrical conductivity by 2 times. The graphene MPL also performed better in fully and partially humidified conditions, with peak power densities 43% higher than those obtained for Vulcan black MPL. This was due to the graphene having less ohmic resistance, particularly under partially humidified conditions [143]. This could be attributed to the structure of the graphene flakes used in this study; they have a slightly different microstructure as compared to the platelet type of graphene.

Najafabad et al. [219] created an MPL from electrochemically exfoliated graphene. It was observed that the MPL with graphene saw a decrease in overall ohmic losses. However, graphene did not perform as well as the conventional MPL under high humidity conditions. Najafabad et al. [219] also made a composite MPL composed of graphene and carbon black in a 1:1 ratio. This composite MPL performed better than pure graphene and pure carbon black during the in-situ polarisation curve tests. Furthermore, it was found that the composite MPL provided optimal water management as it was able to prevent the PEMFC from flooding but also kept the membrane hydrated. At low relative humidity (20%) the composite MPL was shown to perform better than pure carbon black or graphene. The maximum power density at 20% RH was 1188 mW/cm^2 which changed very little from RH 100% at 1173 mW/cm^2. The optimum loading of the MPL with the additional graphene was found to be 1.5 mg/cm^2.

Mariani et al. [221] investigated three different types of graphene: small-size graphene nanoplatelets, medium-size graphene nanoplatelets and exfoliated graphite with average particle sizes of 5 μm, 25 μm and 500 μm respectively. These were examined individually and then also mixed in a 1:1 ratio with carbon black (Vulcan Black), with a 10 wt. % carbon nanotubes (CNTs). A 40 μm MPL coating was then applied to the GDL. The exfoliated graphene performed the worst out of all the MPL samples. At higher current densities, the fuel cell experienced a sharp voltage drop due to flooding. The small size of graphene nanoplatelets allowed for the maintenance of optimal membrane hydration under the different RH conditions. The medium-sized graphene nanoplatelets performed best overall in all the different RH conditions. However, there were issues with flooding at higher humidity for all graphene-based MPLs, as the MPL did not have sufficient micropores to transport the water away from reactive sites. The addition of carbon black to these samples had an overall effect of increasing the performance. The use of the combined MPL of carbon black and graphene can take advantage of a more favourable pore size distribution. The packing behaviour of the graphene plates helps to form more mesopores and macropores, which help in water retention. This is particularly beneficial at low relative humidities. The carbon black helps to create more micropores which helps to reduce the accumulation of excess water.

Lee et al. [223] experimentally determined the characteristics of graphene-based MPLs in order to optimise hybrid MPLs containing varying ratios of graphene to Vulcan black. Single-cell tests were conducted at different relative humidities and temperatures to understand how the graphene-based MPL composition affects fuel cell performance. Incorporating graphene into the MPL altered the pore size distribution, resulting in more mesopores (with pore sizes between 70 nm and 5000 nm). The findings showed that adding a small amount of graphene (30 wt. %) improved fuel cell performance at low humidity (RH 25%) conditions. Conversely, at high humidity (larger than RH 50%), higher graphene content (≥50 wt. %) enhanced performance by creating sufficient mesopores to manage excess water at high current densities. Higher graphene content in the MPL also improved electrical conductivity; it was shown that even a small addition of graphene (30%) could significantly improve the in-plane electrical conductivity of the sample.

The growing interest in enhancing the GDL and reducing contact resistance underscores the potential of novel materials, notably graphene, due to its improved surface contact and higher electrical conductivity. However, graphene's application in the MPL is still in its early stages and is limited in scope. More research is needed to determine the optimal graphene quantities for MPL, particularly in high-humidity conditions where efficiency may diminish. Surprisingly, there is a lack of studies on the impact of novel materials, especially in the context of a double-sided MPL-coated GDL. The double-sided MPL architecture has demonstrated improved PEMFC performance [[121], [122], [191], [192], [193], [225]] and graphene could further enhance this. Moreover, the double-sided MPL-coated GDL exhibits better performance across various humidity conditions compared to conventional MPL. Investigating how a graphene-based double-sided MPL performs under different relative humidities is an intriguing avenue for research. Mixing graphene with carbon black has the potential to optimise MPL, as previous studies have shown. Additionally, the unique architecture of the double-sided MPL-coated GDL could compound the advantages of a novel structure with novel material, further improving PEMFC performance.

4.3 Materials and Methodology

This investigation will systematically analyse the double-sided MPL coated GDL at the cathode side, to assess the overall performance resulting from the introduction of graphene. Also, it will be identified, if applicable, on which side of the GDL that graphene exhibits the most significant performance improvement. As detailed in Figure 4-1, one side of the double-sided MPL coated GDL will be maintained constant with the Vulcan black, whilst the other side will change composition (Vulcan black, graphene and Vulcan black/graphene). This approach is designed to facilitate an in-depth examination of the consequences arising from the introduction of graphene into the MPL.

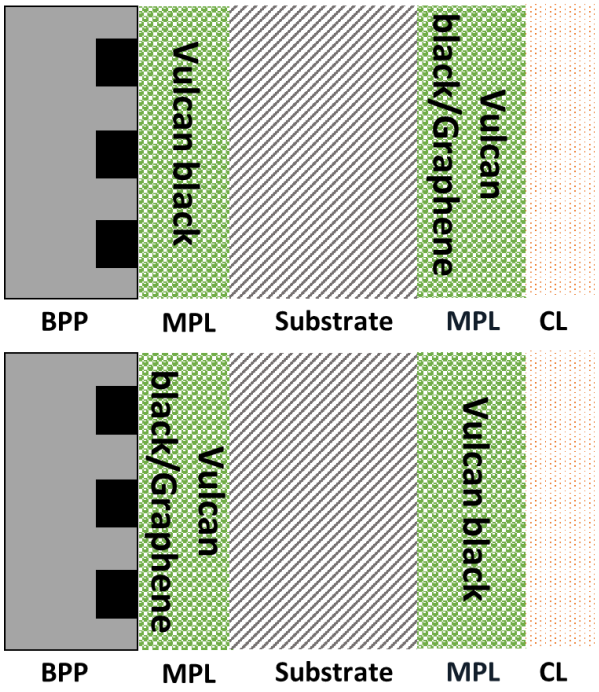

Figure 4-1 The two configurations used for double-sided MPL coated GDL.

4.3.1 Fabrication Procedure

The GDL used for all of the cathode samples was Toray Carbon Paper 060 PTFE 10 wt. % (Fuel Cell Earth, Woburn, MA, USA). The MPL coatings consisted of Vulcan Black XC 72 R (Sigma Aldrich®, Gillingham, UK) and graphene nanoplates (Sigma Aldrich®, Gillingham, UK). The categories of samples that were used for the investigation are shown in Table 4-1. The anode side GDL was kept constant: Toray Carbon Paper 060 PTFE 10 wt. % (Fuel Cell Earth, Woburn, MA, USA) was used. The loadings of each side of the MPL were kept constant at a 1.25 mg/cm^2:0.25 mg/cm^2 ratio as detailed in the previous study [225]. The PTFE content in all MPLs will be kept constant at 20 wt. %.

A mixture was prepared, consisting of 800 mg of Vulcan black (Sigma Aldrich®, UK), 200 mg of a 60 wt.% PTFE dispersion (Sigma Aldrich®, Gillingham, UK), methylcellulose (Sigma Aldrich®, UK), and 21.6 µg of Triton X 100 (Sigma Aldrich®, UK). This mixture was blended with deionised water and stirred at 800 rpm for 30 minutes until a viscous consistency was achieved. This MPL ink was then adequate to create up to five samples of a single-sided MPL-coated GDL. To create the graphene based MPL, the same procedure was followed, but with the substitution of Vulcan black for graphene nanoplates. In the case of the Vulcan black/graphene mixture, these were mixed in a 1:1 ratio. The MPL ink was then applied to Toray carbon paper after it was secured to a hot plate set at 90°C. The 1.25 mg/cm² loading was applied first using the doctor blade apparatus. If the sample was a double-sided MPL coated GDL, it was then flipped and the 0.25 mg/cm² loading of MPL was subsequently applied. The samples were then sintered in a nitrogen-rich environment at 1 bar and 350°C, for half an hour. Each category described in Table 4-1 was comprised of 5 samples with dimensions of 7 cm × 2.5 cm.

Table 4-1 GDL samples prepared for the investigation.

Abbreviation	MPL Material	Total MPL Loading Side 1 (CL) (mg/cm^2)	Total MPL Loading Side 2 (BPP) (mg/cm^2)	Graphene % in the MPL	Side the Graphene is Applied to
		Single sided MPL coated GDLs			
SVB	Vulcan black	1.25	-	-	-
SVBG	Vulcan black /Graphene	1.25	-	50%	-
SG	Graphene	1.25	-	100%	-
		Double sided MPL coated GDLs			
DVB	Vulcan black	1.25	0.25	-	-
D_VBG50_VB100	Vulcan black /Graphene	1.25	0.25	50%	Side 1
D_VB100_VBG50	Vulcan black /Graphene	1.25	0.25	50%	Side 2
D_VBG50_VBG50	Vulcan black /Graphene	1.25	0.25	50%	Side 1 and 2
D_G100_VB100	Vulcan black /Graphene	1.25	0.25	100%	Side 1
D_VB100_G100	Vulcan black /Graphene	1.25	0.25	100%	Side 2
DG	Graphene	1.25	0.25	100%	Side 1 and 2

4.3.2 Preparation of the Membrane Electrode Assembly

The catalyst ink was prepared by combining Pt/C (TEC10E50E, lot 1019-8581, 46.8 wt. Pt %, Tanaka, Japan), with 5 wt. % Nafion solution (Wako, Japan), deionised water, and super-dehydrated ethanol (99.5 vol%, Wako, Japan). To ensure thorough mixing, the catalyst ink was subjected to 30 minutes of sonication using an Ultra Sonic Homogeniser UH-600 from SMT Corporation. For the assembly of the MEA, Nafion 212 membranes were carefully positioned on a movable-hot plate and masked, leaving an exposed area of 1 cm^2. The catalyst ink, with a catalyst loading of 0.3 mg Pt/cm^2 and a Nafion content of 28 wt. % was then sprayed directly onto the Nafion membrane. This spraying process was carried out using the pulsed spray mode of an automated spraying device (Nordson K.K., C3J). Finally, the resulting MEAs were placed in a hot press at 132 °C and 0.3 kN for a duration of 180 seconds, using the Sinto Digital Press CYPT-10. This step ensured the proper bonding and integration of the components.

4.3.3 In-plane Electrical Conductivity

The GDL samples' in-plane conductivity was experimentally assessed through the utilisation of the 4-probe technique, as outlined by Smits [209]. This method employs four probes positioned equidistantly, as depicted in Figure 4-2.

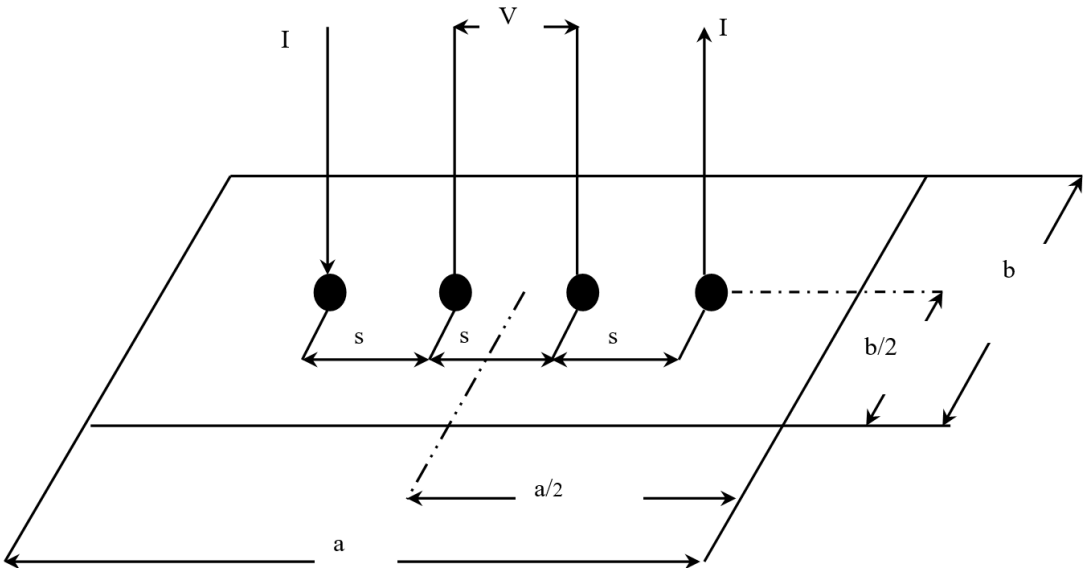

Figure 4-2 In-plane electrical conductivity experimental set-up [89].

When using the Smits method, the correction factor needs to be obtained which is based on two geometric ratios. The sample's length and width (a/b) give the initial ratio, while the sample's width and the spacing between the probes (b/s) give the second ratio [209]. In this investigation, these ratios were determined to be 3 and 1.25, respectively. Consequently, this gave a correction factor of 0.9973. The resistivity, denoted as ρ, can then be computed using the subsequent formula [209]:

$$\rho = CtR \tag{4.1}$$

Where C is the correction factor, t is the thickness of the sample and R is the electrical resistance. Following this, the electrical conductivity, σ, of the GDL can be found by the reciprocal of the resistivity:

$$\sigma = \frac{1}{\rho} \tag{4.2}$$

A micrometre was used to obtain the thickness of the samples. Notably, the thickness of the GDL varied among the different samples. Additionally, within each sample, slight thickness variations were observed at different positions. To account for this variability, thickness measurements of each GDL sample were taken at five evenly spaced positions and then an average was taken. Subsequently, the GDL samples were secured to an insulating plate. The copper electrodes measuring 10 mm × 10 mm × 5 mm were positioned onto the GDL sample. Using a high-precision ohmmeter (RS Pro 804, RS Components, London, UK) with a resolution of 0.01 mΩ, electrical resistance measurements of the samples were taken.

4.3.4 Permeability

The permeability of the samples can be estimated by using Darcy's law:

$$Q = \frac{kA\Delta P}{\mu L} \tag{4.3}$$

The flow rate (Q) through a porous material equals the product of the permeability (k), cross-sectional area (A), and pressure drop ΔP, all divided by the product of the sample's viscosity (μ) and its thickness (L) [102]. To help calculate the permeability of the samples, the experimental setup displayed in Figure 4-3 was used [101].

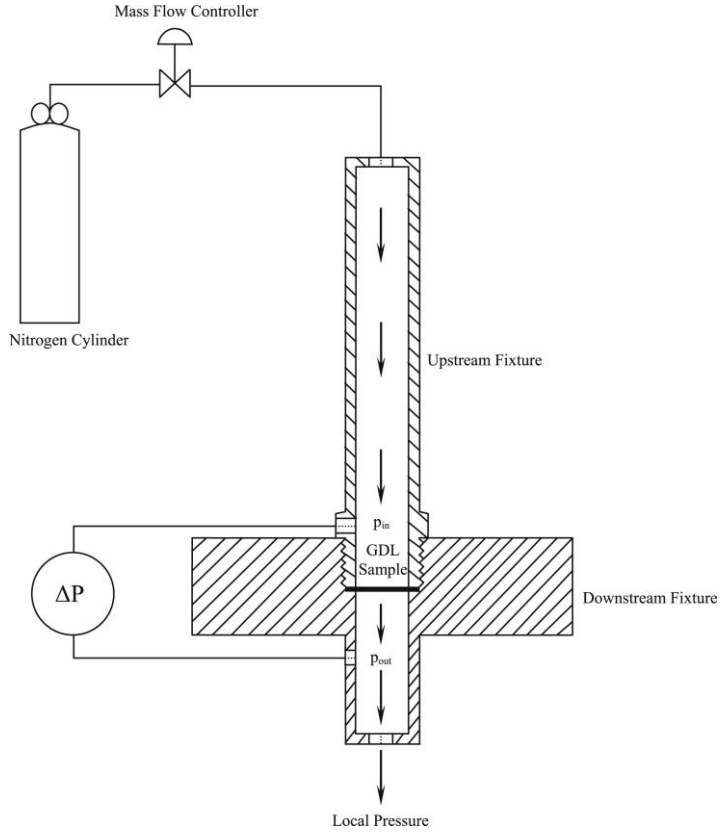

Figure 4-3 Experimental setup used to measure through-plane permeability [101].

The configuration of the experimental setup consists of two fixtures: one fixture is placed upstream and the other downstream. This enables controlled airflow through the sample and measurement of the resulting pressure drop. The sample itself is prepared using a circular punch with a 25.4 mm diameter, but when placed between the fixtures, only a 20 mm diameter area is exposed to the airflow. An HFC-202 flow controller is employed to control the flow rate of nitrogen gas, providing a range of 0.0-0.1 standard litres per minute (SLPM). Measurement of the pressure difference across the sample is carried out using a PX653 differential pressure

sensor, capable of measuring within a range of ±12.5 Pa. Utilising Darcy's Law (Equation 4.3), the gas permeability of the sample can be calculated. This permeability is determined for each sample at different flow rates, and an average value is taken. The entire process is replicated for all five samples within each category, as outlined in Table 4-1.

4.3.5 Pore Size Distribution

Mercury intrusion porosimetry (MIP) is a widely used technique for determining pore size distribution in materials. In the MIP process, a small sample of the GDL is immersed in mercury. Initially, due to mercury's high surface tension, it does not easily penetrate the GDL's pores. The pressure on the mercury is then incrementally increased, causing it to gradually infiltrate the GDL's pores, starting with the larger ones and progressively filling smaller ones [126]. The resulting pore size distribution is determined by measuring the intrusion pressure of the mercury, which is inversely related to pore size. It is important to note that this method assumes the pores to be cylindrical and does not account for closed pores. However, for materials such as carbon papers, this assumption is deemed acceptable [207].

Pore size distribution plays a crucial role in understanding the mass transport mechanisms of gas and liquid water within the porous GDL media. Additionally, it is a key parameter for modelling and optimising mass transport processes in fuel cells [126]. In general, the pores in a GDL can be classified into three main categories based on their radii: micropores (less than 50 nm), mesopores (50 to 7000 nm), and macropores (larger than 7000 nm) [63]. Macropores predominantly constitute the GDL [79], but the introduction of an MPL influences the pore size distribution of a sample by increasing the presence of micropores and mesopores. Macropores primarily facilitate gas diffusion, while micropores play a crucial role in liquid water removal [[208], [210]].

4.3.6 Contact Angle

The contact angle serves as a measure of a material's wettability. When the contact angle is less than 90°, the material is classified as hydrophilic. Conversely, if the contact angle exceeds 90°, the material is considered hydrophobic [90]. To determine the contact angle of the samples, the sessile drop (DMs-401, Kyowa Interface Science Co., Ltd, Japan) method was employed. In this method, individual water droplets were carefully deposited onto the surface of the GDL sample (Figure 4-4). High-resolution photographs were then captured within the first three seconds after the droplets settled on the surface; this is to account for the transient behaviour of the water [208]. Subsequently, contact angle values were measured, with each sample undergoing ten measurements, and then an average value was calculated.

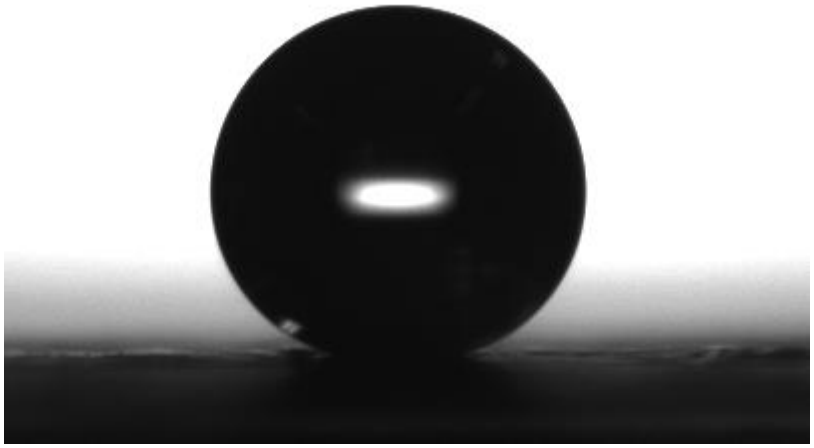

Figure 4-4 A typical water droplet on the surface of a GDL sample.

4.3.7 Morphology

Scanning electron microscopy (SEM) was utilised to scrutinise the morphological characteristics of the GDL samples. This enabled the analysis of the surface morphology and fibre structure of the samples. SEM micrographs play a significant role in evaluating GDL morphology and assessing fuel cell performance [[203], [210], [211]]. In this analysis, GDL samples were first cut into 1 cm^2 squares. These squares were then securely attached to SEM stubs using carbon tape and placed on the specimen stage. The SEM (JEOL - Model JSM-6010LA), operating at 10 kV, facilitated the examination of each sample at various magnifications. This method ensured the conservation of the GDL's delicate fibres when cut to examine the cross-section.

4.3.8 In-situ Fuel Cell Testing

A 1 cm^2 active area single cell was used for the testing from the Japanese Automotive Research Institute (JARI). The fuel cell was fitted with graphite bipolar plates with serpentine type flow fields. The fuel cell operated under counter flow conditions, with constant volumetric flow rates of 0.139 L/min for hydrogen at the anode and 0.332 L/min for oxygen at the cathode.

To ensure proper control of the experimental conditions, a fuel cell test station (AUTOPEM-CVZ01, Toyo Corporation, Japan) was employed. This test station allowed for precise regulation of humidification, cell temperature, and gas flow throughout the testing process. An electrochemical interface impedance analyser (Solartron SI-1287) was used to measure the polarisation curves. Before conducting the in-situ measurements, the cell underwent a conditioning process at a voltage of 0.6 V for a duration of 16 hours.

The fuel cell was set to an operating temperature of 80°C. The inlet gases (hydrogen and air) were also set at 80°C. The fuel cell was then humidified via the inlet gases. Once this had been done, the polarisation and EIS data were subsequently collected for four different relative humidity (RH) conditions: 25%, 50%, 75% and 100%. These varying humidity conditions allowed for a comprehensive assessment of the fuel cell's performance across different humidity levels.

4.4 Results and Discussion

The abbreviations of the samples used in this investigation are shown in Table 4-2, these will be referred to throughout this section.

Table 4-2 Abbreviations of the samples used in this investigation.

Sample Type	Abbreviation
Single sided MPL coated GDLs	
Single sided Vulcan black	SVB
Single sided Graphene	SG
Single sided Vulcan black and graphene composite	SVBG
Double sided MPL coated GDLs	
Double sided Vulcan black	DVB
Double sided coating with 50% composition of Vulcan black and graphene facing the CL and 100% Vulcan black facing the BPP	D_VBG50_VB100
Double sided coating with 100% Vulcan black facing the CL and 50% composition of Vulcan black and graphene facing the BPP	D_VB100_VBG50
Double sided coating with 50% composition of Vulcan black and graphene facing the CL and 50% composition of Vulcan black and graphene facing the BPP	D_VBG50_VBG50
Double sided coating with 100% graphene facing the CL and 100% Vulcan black facing the BPP	D_G100_VB100
Double sided coating with 100% Vulcan black facing the CL and 100% graphene facing the BPP	D_VB100_G100
Double sided coating with graphene	DG

4.4.1 In-plane Electrical Conductivity

In-plane electrical conductivity of the samples is displayed in Figure 4-5. Note that the error bars in this figure (and other figures) represent the 95% confidence intervals around an average value of the 5 samples that were measured. There is some overlap in the error bars which must be considered, as this could suggest that some of the differences in the data can be attributed to statistical factors. It can be seen that when graphene is introduced into the MPL, it leads to an enhancement in its electrical conductivity. This increase in electrical conductivity can reach a difference of approximately 800 S/m when compared to the conductivity of the pure Vulcan black (SVB, DVB) samples, emphasising graphene's conductive properties. This outcome aligns with expectations, given the excellent electrical conductivity of graphene, which is widely documented in scientific literature [211]. Therefore, it is expected that the inclusion of graphene in the MPL composition consistently enhances the in-plane electrical conductivity across all MPL samples that contain graphene. It is a particularly interesting observation, that when graphene is incorporated into a 50% composite with Vulcan black (SVBG, DVB100_GVB50, D_VB100_VBG50, D_VBG50_VBG50), the resulting electrical conductivity shows a comparable improvement to that observed with the pure graphene samples (SG, DG, D_G100_VB100, D_VB100_G100). This suggests that even a modest addition of graphene can elevate the conductivity levels to be on par with those achieved by pure graphene. Furthermore, it's worth noting that the variation in electrical conductivity is not so much influenced by whether the material is double-sided or single-sided, but rather by the type of carbon used in the MPL. This observation underscores the significance of the carbon source in determining the electrical conductivity of an MPL. Additionally, the through-plane electrical conductivity of the MPLs is highly expected to be similar to the in-plane conductivity, due to the uniformity of the MPL particle structure.

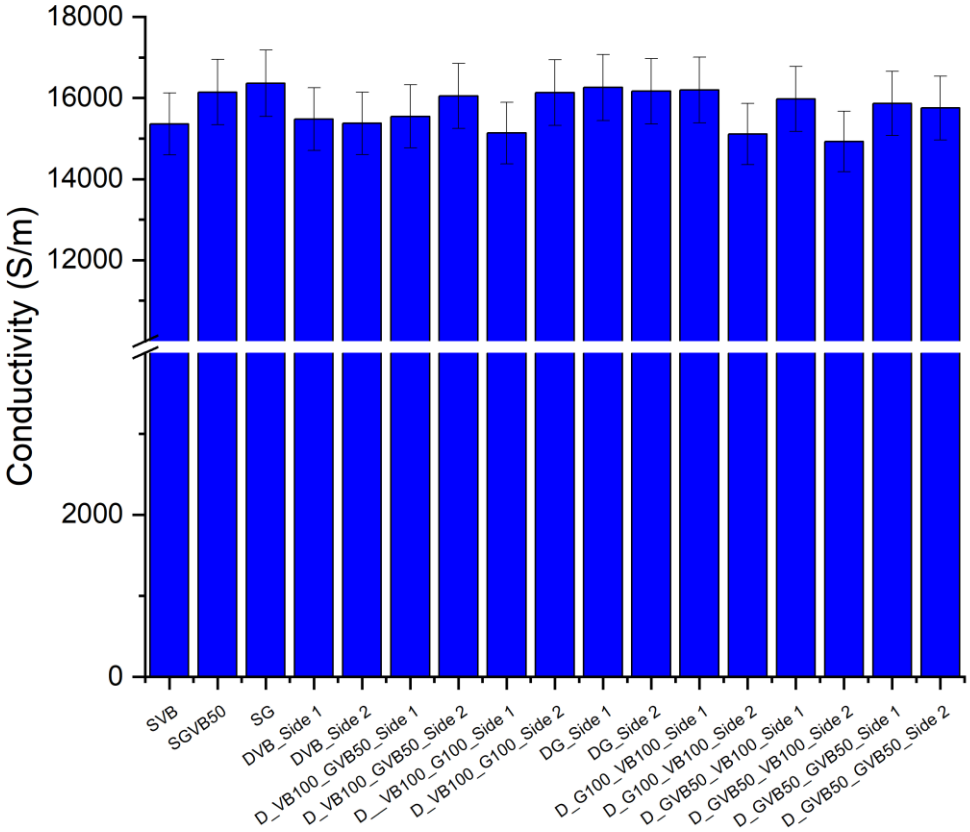

Figure 4-5 In-plane electrical conductivity of the MPL samples.

4.4.2 Gas Permeability

The permeability of the gas diffusion layer is intricately tied to its physical structure and morphology, particularly in relation to porosity and pore size distribution [89]. Firstly, it can be seen in Figure 4-6 that the double-sided configuration exhibits lower permeability compared to the single-sided configuration. This outcome aligns with expectations, as the addition of an extra layer of MPL facing the BPP not only increases the thickness of the GDL but also fills in the surface pores of the GDL substrate. Specifically, double-sided Vulcan black (DVB) has a difference of 0.9×10^{-13} m^2 decreasing permeability, compared to single-sided Vulcan black (SVB). Similarly, double-sided graphene (DG) experiences a decrease of 0.7×10^{-13} m^2, compared to single-sided graphene (SG). Additionally, the composite MPLs comprised of Vulcan black and graphene (DVB100_GVB50, D_VB100_VBG50, D_VBG50_VBG50), exhibit a similar decrease in permeability of around 1×10^{-13} m^2 compared to the single-sided MPL samples (SVB, SVBG, SG).

The second significant observation is that the introduction of graphene enhances the sample's permeability. For example, the permeability of single-sided graphene (SG) is higher than that of single-sided Vulcan black (SVB) increasing by 2.2×10^{-13} m^2. Similarly, the double-sided graphene sample (DG) has a greater permeability, by 2.4×10^{-13} m^2, compared to the double-sided Vulcan black (DVB). This phenomenon can be attributed to the morphology of graphene, which features more surface cracks and generally larger pores compared to Vulcan black. This will be elaborated on when exploring the morphology and pore size distribution of the samples. It can also be observed that the GDLs with a more predominant type of carbon in them, will behave more like the pure carbon counterparts. For example, GDLs with an MPL configuration

that contains more graphene than Vulcan black (e.g. DG, D_G100_VB100) will have a permeability more similar to the pure graphene samples than the pure Vulcan black samples (DVB). This would also suggest that permeability is primarily influenced by the type of carbon used rather than the double or single-sided structure.

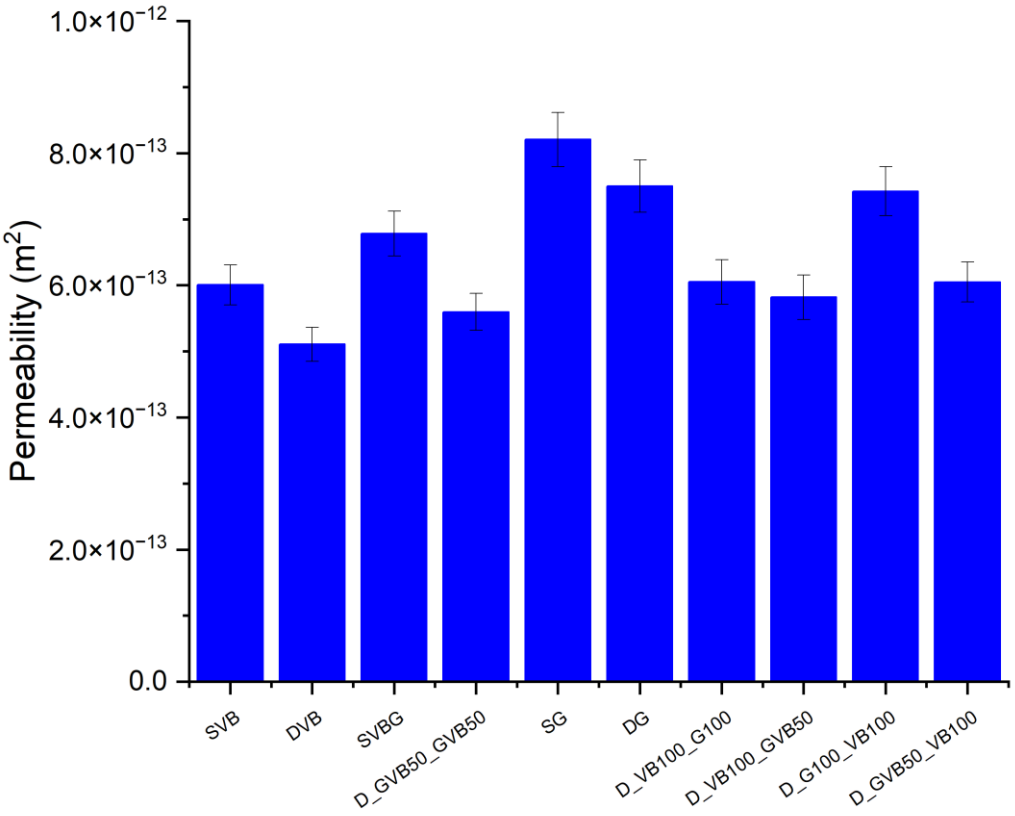

Figure 4-6 Permeability of GDL samples

4.4.3 Pore Size Distribution

Figure 4-7 shows the pore size distribution of the samples. Firstly, it is important to highlight that there is a broad spectrum of pore sizes; literature has identified the anisotropic microstructure of the GDL which gives rise to the range of pore sizes [212]. In order to delineate between the significant pore sizes, Figure 4-7 has been segregated into three distinct categories of pores: micropores (< 50 nm), mesopores (50 - 7000 nm), and macropores (7000 nm), aligning with the classifications discussed in above. Assessing the comparison between Vulcan black and graphene samples when it comes to the pore size distribution shows some significant results.

Vulcan black as an MPL material, tends to create a greater number of micro and mesopores in comparison to graphene based samples. Specifically, when examining single-sided graphene (SG) and double-sided graphene (DG), it becomes evident that they possess the lowest quantity of micropores among the samples. Contrastingly, the samples containing pure Vulcan black (SVB and DVB) display the highest proportion of micropores. Moreover, a clear trend can be seen, where the introduction of more Vulcan black into the MPL, leads to an increase in micropores, as demonstrated by DVB and D_VB100_GVB50, which exhibit the highest micropore counts and have the highest content of Vulcan black. The increase in the number of micropores has an impact on the transport of reactant gases and liquid water within the GDL,

thus leading to consequential effects on the fuel cell's performance, which will be discussed in further detail in the next sections.

The type of MPL configuration (single-sided and double-sided coating) also displays some differences. Examining the pure Vulcan black samples, the DVB shows an increase in the quantity of micropores compared to the SVB samples. This trend is also present in the SG and DG samples. As the second coating of MPL is applied to the GDL, this creates more micropores as more of the larger pores of the GDL are filled in with the MPL ink.

The porosity values displayed in Table 4-3, do not display much of a variation between the types of carbon black particles used for the MPL. They also do not highlight any differences between the single-sided or double-sided configuration.

Table 4-3 Porosity of the GDL samples.

Sample Type	**Porosity (%)**
SVB	72.8
SG	73.8
SVBG	73.9
DVB	71.3
D_VB100_GVB50	73.6
D_GVB50_VB100	72.8
D_GVB50_GVB50	73.1
D_G100_VB100	72.9
DG	73.2
D_VB100_G100	72.5

(a)

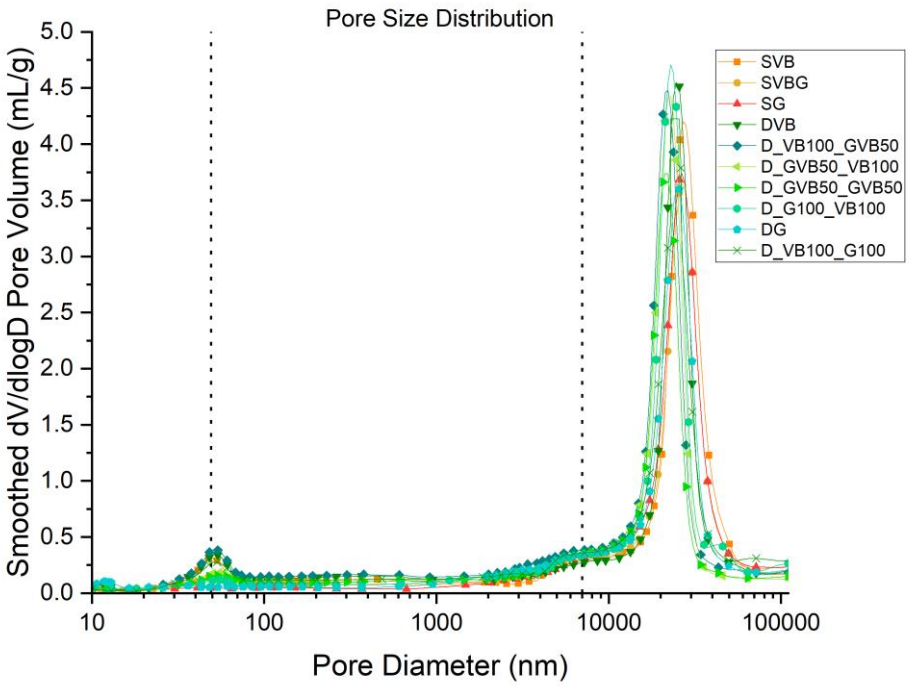

(b)

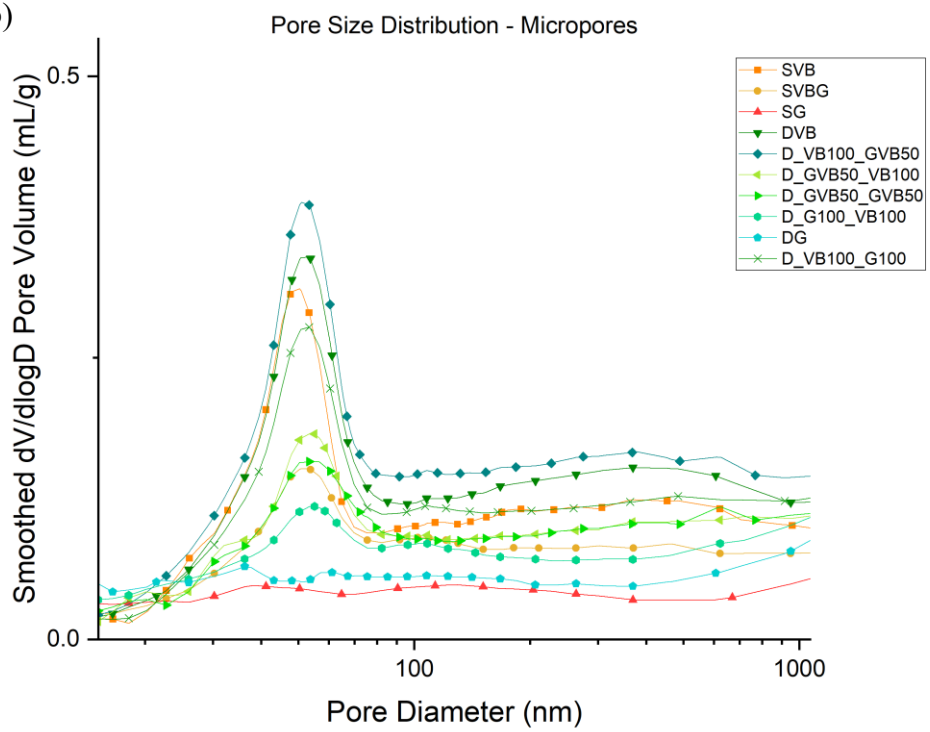

Figure 4-7 (a) Pore size distribution of the samples and (b) zoomed-in image highlighting micropores and mesopores ranges of the samples.

4.4.4 Contact Angle

The wettability of a GDL plays a pivotal role in overall PEMFC performance, especially concerning liquid water management. The wettability of a GDL depends upon a combination of the material's physical properties and the surface structure. These factors determine the interactions occurring between the MPL surface and water droplets. The results of these measurements, shown in Figure 4-8, revealed a consistent trend across all GDL samples. Each sample was hydrophobic, exhibiting a contact angle greater than 130°. The minor variations observed in the measured contact angles of MPLs containing graphene, Vulcan black and the composite mixture of Vulcan black and graphene, suggest that the primary factor governing wettability is the PTFE content which was made constant at 20 wt. %. Furthermore, when considering the error bars, there is significant overlap, suggesting that there is not much variability in the contact angle observations. This consistency in PTFE content implies that it plays a dominant role in dictating the wettability characteristics of these MPLs, rather than the type of carbon particles used in the fabrication of the MPL.

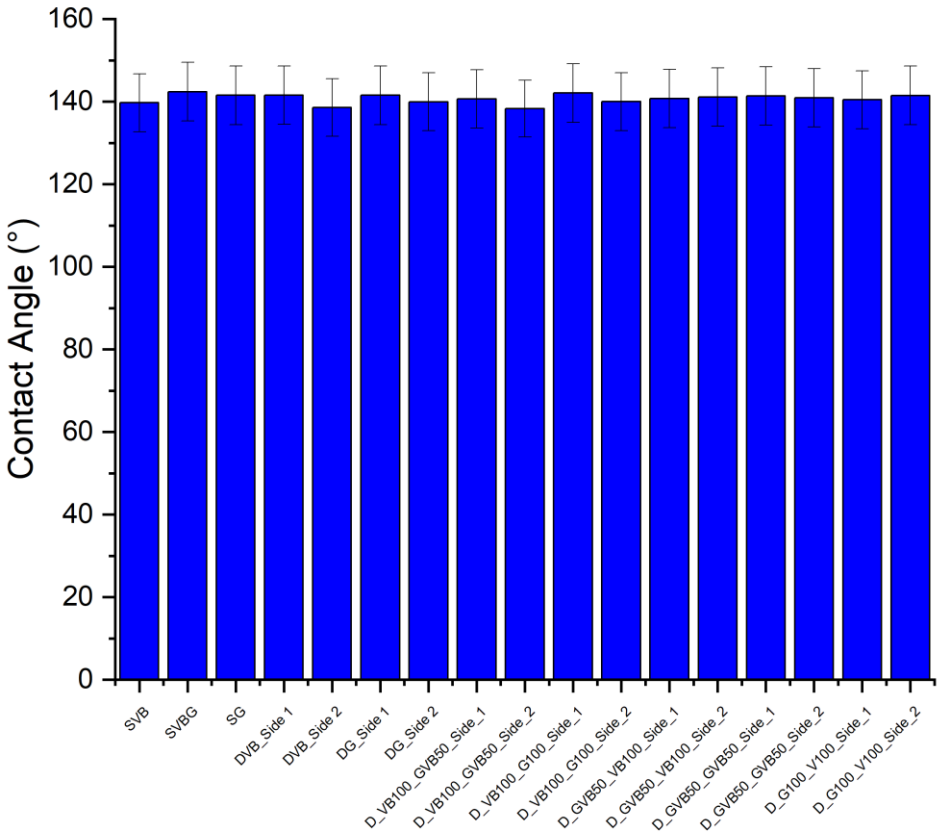

Figure 4-8 Contact angle measurements of the GDL samples.

4.4.5 Morphology

Scanning Electron Microscopy (SEM) was employed to visualise the surface structure and morphology of both the different MPL surfaces, as well as the GDL cross-sections. Figure 4-9 shows a series of SEM micrographs that compare the surface structures of Vulcan black, graphene, and Vulcan black/graphene for both the 1.25 mg/cm^2 loading and the 0.25 mg/cm^2 loading. These images reveal striking disparities in surface structure and morphology between the MPLs containing Vulcan black and those that incorporate graphene. These distinctions are contingent on the physical attributes of the different carbon materials. Vulcan black gives a smooth surface while graphene gives a much rougher surface with clusters of carbon which form on the surface. Also notable, is the graphene MPL structure has more micro-cracks on the surface. MPL surface cracks emerge naturally during the fabrication process. This arises as a result of solvent evaporation during the thermal treatment phase [226]. Such surface cracking is a common trait of MPLs based on carbon black and has been a subject of study in literature [[170], [226]]. With regards to the graphene MPLs, these cracks are more pronounced compared to Vulcan black MPLs. This could be due to the agglomeration of the graphene particles which means it does not fully spread over the surface of the substrate, thus lending itself to be more susceptible to surface cracks.

On the side facing the BPP, with the 0.25 mg/cm^2 loading, the carbon fibres of the GDL substrate can be easily seen, for all samples. This is expected as the lower the loading of the MPL, the lower the thickness of the coating on the surface. The pure Vulcan black exhibits a smooth surface much like in the 1.25 mg/cm^2 loading, the smooth surface allows for the effective filling of the substrate surface pores, despite the exposure of the carbon fibres. The graphene on the other hand, as it clusters, occupies fewer of these surface pores, allowing the substrate to remain more visible, with visibly larger pores present. The Vulcan black/graphene composite features a smooth surface, similar to the pure Vulcan black. However, there are small clusters of carbon forming on the surface, similar to the pure graphene samples.

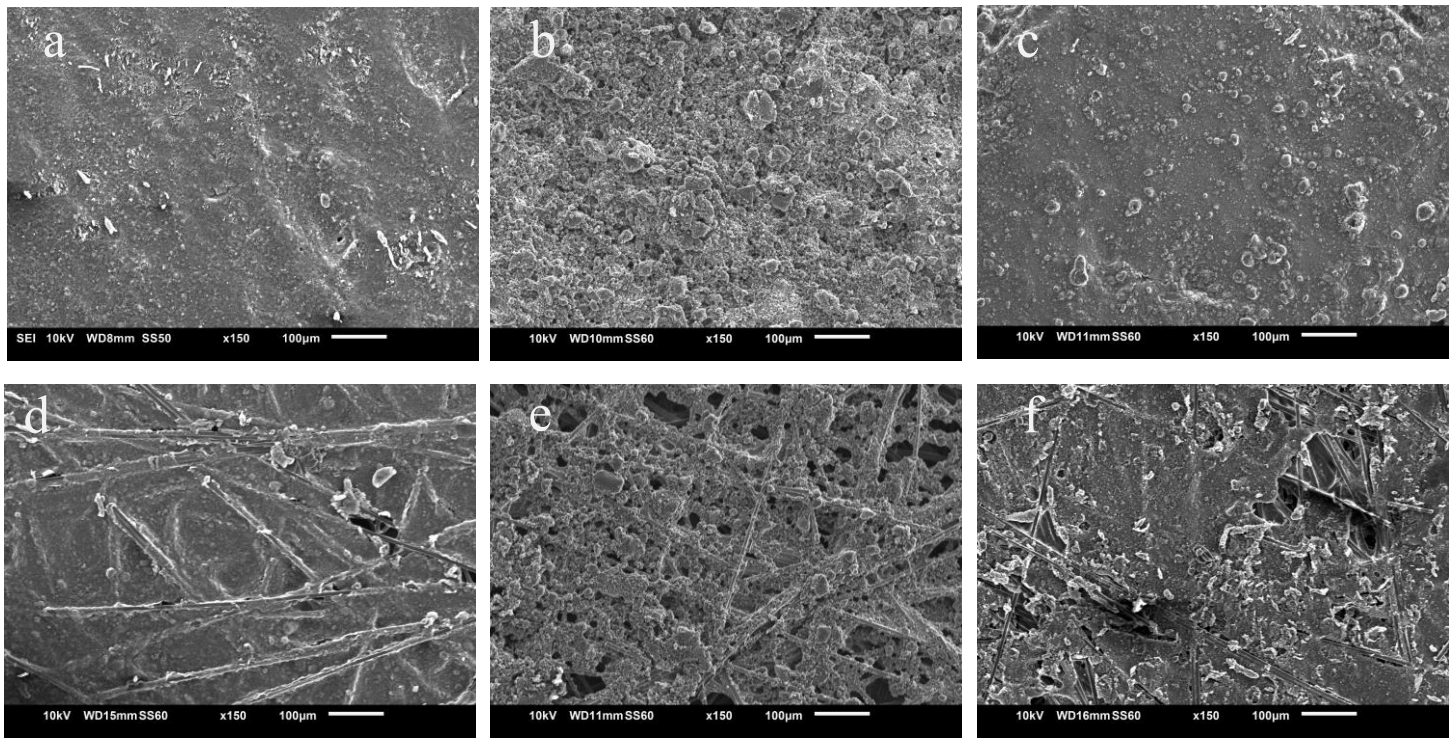

Figure 4-9 SEM images for (a) Vulcan black 1.25 mg/cm^2 loading, (b) Graphene 1.25 mg/cm^2 loading, (c) Vulcan black/Graphene 1.25 mg/cm^2 loading, (d) Vulcan black 0.25 mg/cm^2 loading, (e) Graphene 0.25 mg/cm^2 loading, (f) Vulcan black/Graphene 0.25 mg/cm^2 loading.

4.4.6 Fuel Cell Performance

Figure 4-10 displays the polarisation curves for the samples, at 25%, 50%, 75% and 100% RHs. Figure 4-11 shows the corresponding power density curves and Figure 4-12 displays the EIS data. Firstly, it can be seen that in general, the double-sided configuration exhibits better fuel cell performance compared to the single-sided counterparts, at relative humidities of 50%, 75%, and 100%; this is (given that the fuel cell is not membrane resistance limited) due to presence of MPLs facing the bipolar plates and consequently better electrical contact with these plates. Conversely, the single-sided configuration outperforms the double-sided samples at 25% RH; this is due to a lower diffusion path (i.e. lower mass transport resistance) demonstrated by the single-sided samples.

Considering the single-sided samples (SVB, SVBG, SG) at 25% RH, it can be seen that there is a trend where the SVB and SVBG perform the best and SG performs the worst. This could be attributed to the fact that the SVB and SVBG samples contain a high amount of micropores (Figure 4-7) that is necessary to retain water required for membrane humidification at relatively low humidity conditions [223]. This is corroborated by the EIS measurements at 25% RH (Figure 4-12) that show that the SVB and SVBG samples, compared to SG, have less ohmic resistance (represented by the left intercept of the semicircle with the x-axis) signifying better membrane humidification and consequently less membrane resistance.

Among the samples, D_VB100_G100 demonstrates the best overall performance, closely followed by the DVB sample. This could be attributed to the fact that, under relatively high humidity conditions, the double-sided MPL coating lowers the contact resistance with the BPP. Furthermore, these samples (D_VB100_G100 and DVB) have a good balance of micropores and mesopores, which is important for draining excess liquid water at high current densities, particularly for the side facing the catalyst layer. Research has shown that a combination of micropores and mesopores improves the water removal capabilities of a GDL in high humidity conditions [223]. The EIS measurements of the above samples (Figure 4-12) at high relative humidities (≥ 50%) show that they, compared to other samples, demonstrate less membrane resistance and less charge transfer resistance (represented by the diameter of the semi-circle). This signifies both adequate membrane humidification and mitigated water flooding at the catalyst layer. Additionally, the D_VB100_G100 sample, which contains graphene facing the BPP, performed slightly better than the DVB sample due to the combined positive effects of the enhanced conductivity and the presence of cracks (Figure 4-9) in the graphene layer facing the BPP; these cracks help expel excess liquid water.

Notably, samples containing pure graphene (SG and DG) consistently perform the worst across various humidity conditions. Despite graphene's enhanced electrical conductivity, its inferior mass transport properties offset this advantage. The very low content of micropores and mesopores in pure graphene samples (Figure 4-7), compared to the Vulcan black samples, results in less retention of liquid water produced at the cathode catalyst layer, thus lowering the ionic conductivity of the membrane electrolyte. The composite samples containing higher graphene content (D_G100_VB100, D_GVB50_GVB50) also behaved similarly to the pure graphene samples due to the decreased presence of micropores/mesopores in the MPL facing the catalyst layer, resulting in deteriorating performance due to poor retention of liquid water.

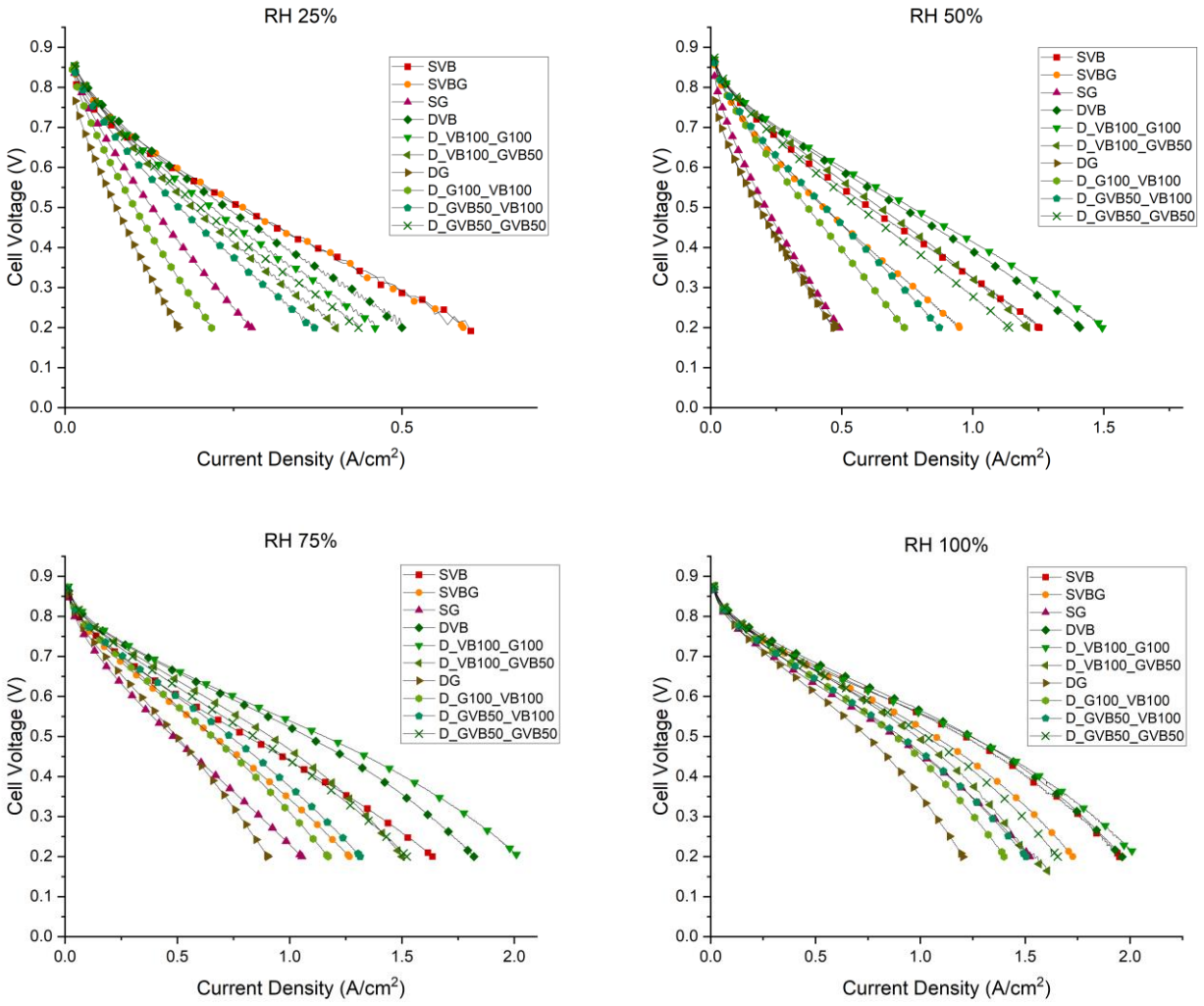

Figure 4-10 The polarisation curves of the fuel cell operating with the investigated samples at various humidity conditions (RH 25%, RH 50%, RH75% and RH 100%).

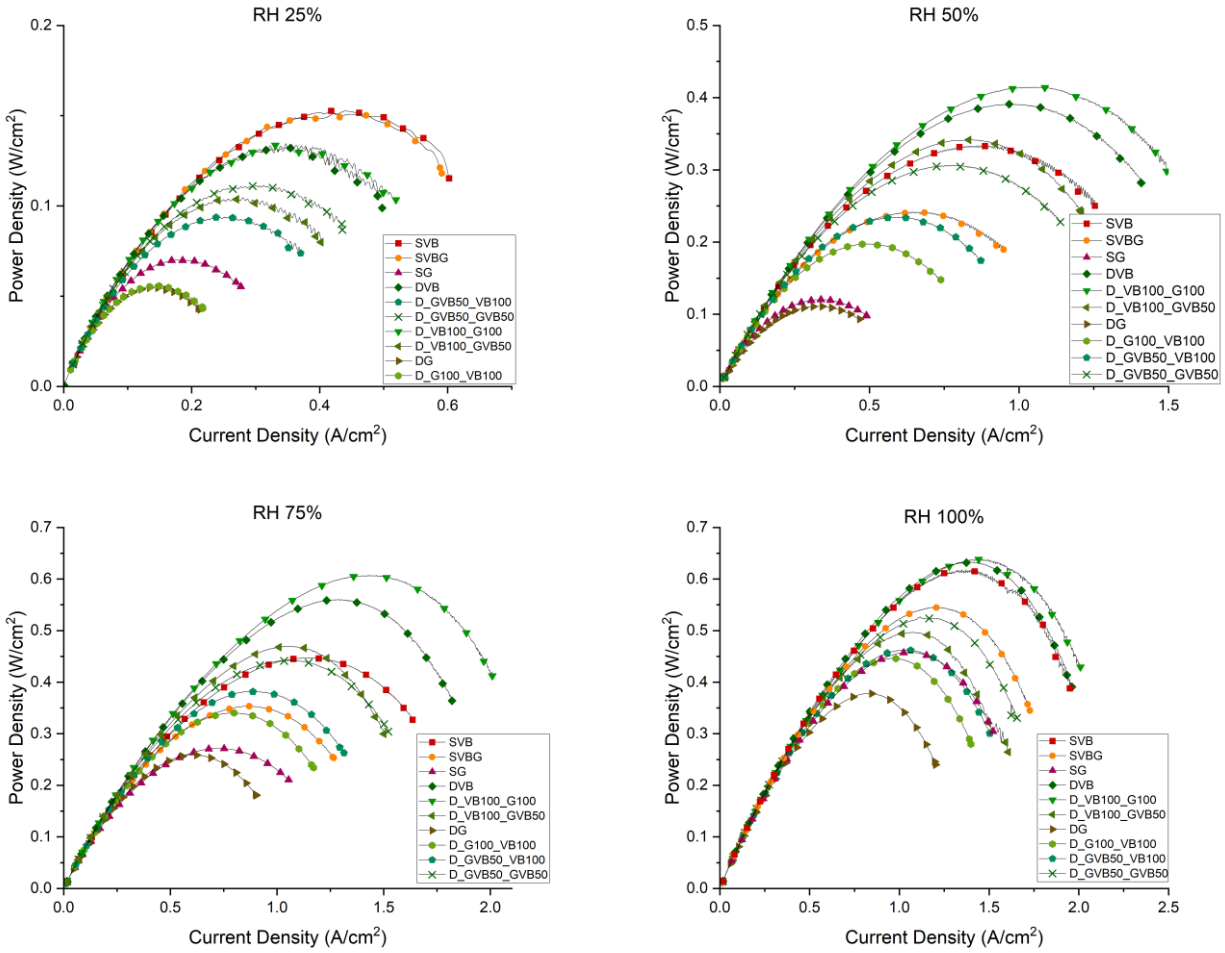

Figure 4-11 The power density curves of the fuel cell operating with the investigated samples at various humidity conditions (RH 25%, RH 50%, RH75% and RH 100%).

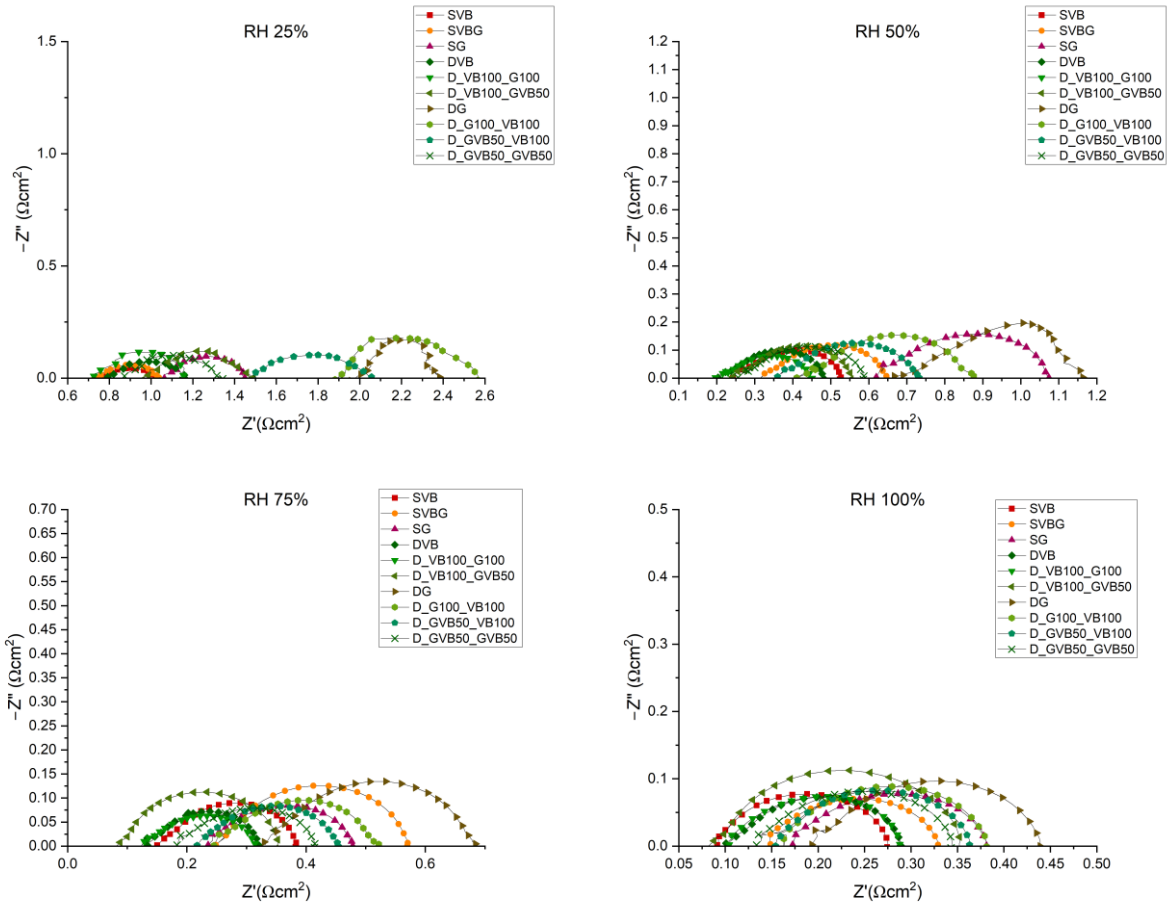

Figure 4-12 The EIS curves of the fuel cell operating with the investigated samples at various humidity conditions (RH 25%, RH 50%, RH75% and RH 100%).

4.5 Conclusion

The impact of double-sided MPL coated GDLs, compared to conventional single-sided MPL coated GDLs, was investigated in terms of key characteristics and fuel cell performance. Two types of carbon for the MPL coatings were employed, Vulcan black and graphene. This was to evaluate the effects of introducing a novel material to the double-sided MPL coating and to see where improvements could be made. The MPL loadings applied to the surfaces of the GDL facing the catalyst layer and the bipolar plate were 1.25 and 0.25 mg/cm², respectively. The following key findings were made from the ex-situ and in-situ tests:

- Graphene samples displayed a higher gas permeability compared to Vulcan black samples, this is due to the presence of a higher amount of cracks in the former samples. Expectedly, graphene samples displayed a higher in-plane electrical conductivity than the Vulcan black samples. Notably, the introduction of graphene at a 50% mixture with the Vulcan black results in a conductivity increase equivalent to that of a sample composed entirely of pure graphene. When analysing the contact angle, there is no notable variation. This suggests that contact angle is a factor more dependent on the PTFE content rather than the type of carbon used in the MPL.
- MIP analysis showed that for all samples, the addition of Vulcan black MPLs created micropores and mesopores that are essential for efficient water removal at high current densities. The double-sided Vulcan black MPL coating increased the amount of micropores and mesopores. On the other hand, the pure graphene samples produced the lowest content of micropores and mesopores. SEM micrographs of the samples showed that the graphene samples exhibited a higher number of surface cracks, while Vulcan carbon black samples displayed a smoother surface.
- Under low humidity conditions (25% RH), it is advisable to use single-sided MPL coated GDLs as the fuel cell, under these circumstances, is gas diffusion limited. These samples, compared to double-sided coated GDLs, offer lower diffusion paths and consequently lower mass transport resistance. Notably, the single-sided Vulcan Black (SVB) and the single-sided composite of Vulcan Black and Graphene (SVBG) samples performed significantly better than the single graphene (SG) sample. This is due to the presence of micropores necessary to retain water for membrane humidification under low humidity conditions.
- Under relatively high humidity conditions (≥ 50% RH), double-sided MPL coated GDLs generally performed better than single-sided MPL coated GDLs as they offer better electrical contact with the bipolar plates. Notably, the GDL with Vulcan Black MPL facing the CL and graphene MPL facing the BPP (D_VB100_G100) demonstrated the best overall performance. This configuration allowed for the correct water retention required for membrane humidification at the CL, yet it also facilitated the expulsion of excess water through the cracks available in the graphene MPL facing the BPP.

Chapter 5: Characterisation of Double-Sided Microporous Layer Coated Gas Diffusion Layers Treated with Pore Forming Agents for the Improved Performance of Polymer Electrolyte Membrane Fuel Cells

5.1 Abstract

This study experimentally evaluates the effects of double-sided microporous layer coated gas diffusion layers, incorporating pore-forming agents to modify the microporous layer facing the bipolar plate. The investigation utilised two different particle sizes of pore-forming agents, 10 μm and 30 μm, at varying concentrations to assess their impact on the structural and functional properties of the GDLs. Scanning electron microscope images confirmed that the pore-forming agents degraded under standard MPL sintering conditions, successfully leaving behind artificial pores. These artificial pores often expanded the naturally occurring pores, thus creating a distinct difference in pore structure between samples with smaller and larger pore-forming particles. Key properties characterised, included in-plane electrical conductivity, contact angle, permeability, porosity, and pore size distribution. The findings revealed that the in-plane electrical conductivity and contact angle remained unaffected by the addition of pore-forming agents. This stability is advantageous, as it ensures that the excellent electrical conductivity and hydrophobic properties of the MPL are maintained, even with the structural modifications made using the pore-forming agents. Pore size distribution analysis showed a well-balanced mix of micropores and mesopores across all double-sided samples. However, the introduction of pore-forming agents caused a slight shift, reducing the number of micropores while increasing the number of macropores. Permeability measurements indicated an increase when pore-forming agents were added, with the extent of the increase being more influenced by the concentration of the pore-forming agent rather than the particle size. This suggests that the overall porosity of the GDL can be effectively tuned by adjusting the amount of pore-forming agent used. The study also observed a direct correlation between the concentration and particle size of the pore-forming agents and the porosity of the GDLs. Higher concentrations and larger particle sizes resulted in increased porosity, with the highest porosity observed in samples containing the larger (30 μm) particles at higher concentrations.

5.2 Introduction

The drive to mitigate climate change has necessitated prioritising the reduction of fossil fuel use. In recent years, there has been an increasing shift towards generating and applying low-carbon hydrogen. This shift is partly due to the growing interest in polymer electrolyte membrane fuel cells (PEMFCs), which are recognised for their high efficiency, low-temperature operation, and ease of assembly [203]. The versatility of PEMFCs enables their use in stationary, automotive, and portable applications, making them particularly advantageous for promoting hydrogen adoption as a clean energy source [23].

The gas diffusion layer (GDL) plays a crucial role in the performance of PEMFCs. It carries out several critical functions, including the uniform delivery of hydrogen and oxygen gas to the catalyst layer's active sites. Additionally, the GDL is integral to water management, aiming to remove excess water while maintaining membrane hydration. It also provides essential structural support to the more fragile membrane and catalyst layers [54]. They are typically made from carbon fibre (carbon paper or cloth) to meet their functional requirements effectively. The GDL often incorporates a microporous layer (MPL) on its surface, facing the catalyst layer (CL). The MPL is made from a mixture of carbon black particles and polytetrafluoroethylene (PTFE). The MPL has been demonstrated to enhance the membrane electrode assembly's (MEA) water management [[158], [165]] and to improve electrical conductivity with the catalyst layer [[89], [216]]. These improvements are pivotal for optimising fuel cell performance [[130], [151], [159], [216], [217]].

During fuel cell operation, various losses occur, including ohmic losses. These losses mainly arise from the resistance encountered at the interfaces between different components of the fuel cell and the internal resistance of these components. The differences in structure and morphology at the interfaces create transitional regions, leading to increased electrical contact resistance [180]. A significant area of contact resistance is found in the GDL, located between the catalyst layer and the bipolar plate (BPP). Factors such as the surface material, its roughness, and the pressure exerted between components play crucial roles in determining the extent of contact resistance within fuel cells. A study by Netwall et al. [182] suggests that 55% of ohmic losses in fuel cells can be traced back to interfacial contact resistances, particularly between the GDL/BPP, GDL/CL, and membrane/CL interfaces, while the rest, about 45%, are due to bulk resistances within the components. The interaction between the GDL and both the BPP and CL significantly contributes to ohmic losses. Addressing these contact resistances is vital for reducing major losses and enhancing fuel cell performance [183].

A wide range of studies have been conducted to find ways to minimise the contact resistance between the GDL and the BPP, employing both simulations ([188], [189], [190] and [205]) and experimental techniques ([121], [122], [191], [192] and [193]). The primary consensus emerging from these studies is that using an MPL, particularly when applying a double-sided MPL to the GDL, significantly lowers the contact resistance.

To fully understand the impact of double-sided MPL-coated GDLs on reducing contact resistance, further research is needed. Current investigations mainly focus on in-situ characterisations such as polarisation curves and electrochemical impedance spectroscopy (EIS). In addition, these studies have generally focused on using conventional carbon black for the MPL, suggesting the exploration of MPL modifications could be beneficial. This study investigates the use of the double-sided MPL coated GDL and the treatment of the MPL facing the BPP with pore forming agents to modify the MPL structure. This study will explore this novel microstructure in an attempt to reduce contact resistance and improve the water management of the PEMFC.

Several researchers have explored the use of different pore forming agents within the MPL using a range of experimental methods to improve PEMFC performance [[81], [171], [173], [227], [228], [229], [230]]. Use of pore forming agents can artificially modify the microstructure of the MPL, in particular, the porosity and pore size distribution. This in turn affects the overall fuel cell performance.

According to research studies, the porosity and pore size distribution play a significant role in mass transport processes for PEMFCs [60]. A higher porosity in the MPL can facilitate the removal of water and improve the transport of oxygen, leading to better performance of the fuel cell [60]. Some researchers have also found that a larger median pore diameter and pore volume are necessary to prevent cathode flooding under high-humidity conditions [231].

Adding pore forming agents to the MPL can modify the pore structure and lead to improved performance of PEMFCs [227]. Typically, decomposable salts and polymers are used as pore forming agents, which generate gas when they decompose, creating pores on the substrate. It should be noted that an important property of a pore forming agent is that it can be removed from the MPL without compromising the overall structural integrity of the material.

Kong et al. [228] investigated the effects of using Li_2CO_3 as a pore forming agent to examine the effects of the pore size distribution of the samples and oxygen transportation [228]. They removed the pore-forming agent from the MPL via acid treatment. They found that they managed to increase the volume of macropores in the MPL, with diameters ranging from 5 to 10 μm. This, in turn, resulted in improved performance of the fuel cell when operating both under H_2/O_2 or H_2/air. They found that with the modifications, there was less oxygen diffusion limitation. This suggests that pore size distribution is an important factor in mass transport processes.

Simon et al. [171] conducted a study where they used a polymeric pore former to reduce oxygen transport resistance in MPLs. They characterised the materials using various techniques such as mercury intrusion porosimetry (MIP), nitrogen adsorption, and scanning electron microscope (SEM). Their results showed that all MPLs performed similarly under dry conditions. However, at high humidity conditions, MPLs with larger pore diameters exhibited increased performance. This was attributed to the effective removal of liquid water through the larger pores, while oxygen transport could still take place in the smaller pores.

Chun et al. [81] conducted a study on the impact of pore forming agents and drying conditions on the pore size distribution of MPLs and their effects on the performance of PEMFCs. They found that the contents of pore forming agents control the pore size distribution. The authors varied the sintering temperature to adjust the pore size distribution and characterised the samples using a field emission scanning electron microscope (FE-SEM) and MIP. Their results showed that increasing the sintering temperature led to higher macropore content (approximately 1000 – 2000 nm), which had a positive impact on gas supply, whereas moderate amounts of micropores were beneficial in removing water at high relative humidity. The performance of single cells with different MPLs was evaluated under two different humidification conditions, and they observed that the MPL treated at a higher temperature performed better under lower humidification conditions, while the MPL dried at a lower temperature performed better under high humidification conditions. The authors found that a moderate amount of micropores in the MPL is beneficial for removing water at high relative humidity, while macropores are effective in providing a gas supply.

Liu et al. [229] examined the influence on MPL pore structure using four different pore forming agents: PEG-200, $(NH_4)_2C_2O_4$), NH_4HCO_3, and NaCl. Their findings revealed that in all GDL samples, there was an increase in both the primary and secondary average pore diameters. The

modifications involving $(NH_4)_2C_2O_4$ displayed the most favourable activity for the oxygen reduction reaction. This result could be attributed to the MPL's increased pore volume and larger secondary pore diameter.

Li et al. [230] investigated the impact of hierarchical pore structures within the MPL. They constructed two layers of MPLs, with the layer closest to the carbon paper being modified using a pore forming agent. They carefully controlled the pore former content and the duration of sonication to create MPLs with varying levels of porosity. Their findings indicated that the modified MPL exhibited reduced transmission impedance across different humidity conditions. They proposed that the pore sizes within the range of 7 – 20 μm and 20 – 100 μm played crucial roles in facilitating gas and water transport, respectively. Therefore, enhancing the pore volume within these specific size ranges (7 – 20 μm and 20 – 100 μm) is advisable to enhance the performance of PEMFCs.

Tang et al. [173] utilised ammonium chloride (NH_4Cl) as a pore forming agent to create a porosity-graded MPL consisting of three layers with different porosities (the MPL next to the CL had 10 wt. %, the middle MPL contained 30 wt. %, and the MPL on the substrate had 50 wt. % of NH_4Cl). The performance of the fuel cell with the porosity-graded MPL was found to be better than homogenous MPLs containing only 10 or 50 wt. % NH_4Cl as a pore forming agent, especially at higher current densities (greater than 0.7 A/cm^2). The results indicated that the porosity gradient in the MPL, with thicker pores closer to the catalyst layer and thinner pores closer to the GDL, created a higher capillary pressure for water flow compared to MPLs with straight pores, resulting in improved water management at the cathode.

The high capillary pressure generated by the small, hydrophobic PTFE-treated pores in the MPL leads to the preferential transport of liquid water through sudden releases via larger pores and cracks. These larger openings can be inherent flaws within the GDL or intentionally constructed. X-ray imaging studies have detailed how liquid water moves through these perforations and fissures. Fuel cell experiments with materials featuring deliberately created larger pores within the MPL/GDL have demonstrated improvements in overall fuel cell efficiency, increased limiting current density, and reduced oxygen transport resistance. This can be attributed to the capillary pressure in hydrophobic pores and the release of water through the larger pores and cracks [171].

Porosity and pore size distribution are important characteristics of GDLs, with the former directly influencing the GDL's permeability and the latter affecting the gas and water mass transport properties. Variations across different pores considerably impact mass transfer capabilities, highlighting that changing the pore size distribution can affect the overall fuel cell performance. With regards to the double-sided MPL coated GDL, this is of importance to consider as there are two coatings of MPL. The use of pore forming agents could help modify the double-sided MPL coated GDL and thus improve water and gas management, whilst also keeping the benefits of good electrical contact with the CL and BPP.

5.3 Materials and Methodology

As mentioned, the use of pore forming agents in the context of a double-sided MPL coated GDL has not been explored. In this chapter, experimental studies were carried out to evaluate the effects of the MPL treated with pore forming agents facing the BPP. The loadings of each side of the MPL are kept constant at a 1.25 mg/cm^2: 0.25 mg/cm^2 ratio as detailed in the first study of this thesis [225]. PTFE content in all MPLs will be kept constant at 20 wt. %.

This investigation systematically analyses both sides of the double-sided MPL coated GDL in order to assess the overall performance resulting from the introduction of pore forming agents. The side facing the BPP will be modified with pore forming agents, whilst the side facing the CL remains constant. Figure 5-1, shows the configuration of the double-sided MPL coated GDL and where the pore forming agents are employed.

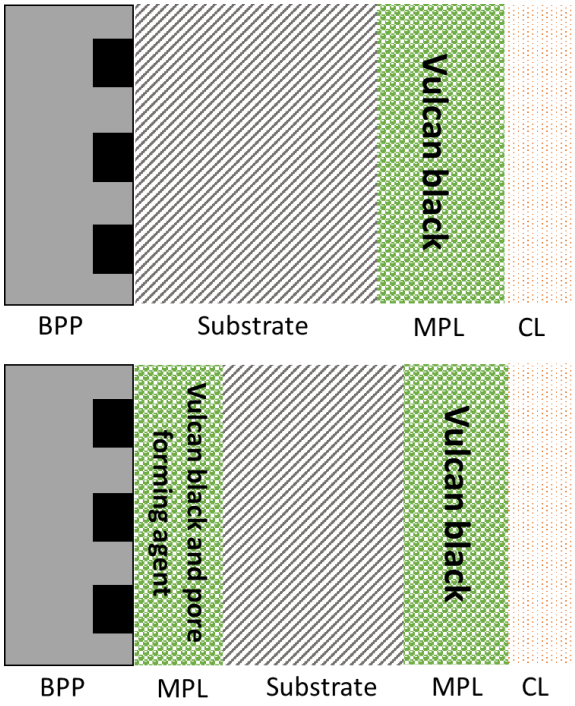

Figure 5-1 Double-sided MPL coated GDL configuration with the application of pore forming agents.

5.3.1 Fabrication Procedure

The GDL used for all of the samples was Toray Carbon Paper 060 PTFE 10 wt. % (Fuel Cell Earth, USA). The MPL coatings consisted of Vulcan Black XC 72 R (Sigma Aldrich®, UK) and PTFE dispersion (Sigma-Aldrich®). Pore forming agent, Chemisnow™ MX Series (Soken, Japan), was used to treat the MPL facing the BPP. Soken kindly provided pore forming agents from their MX series in two different particle sizes 10 µm (MX-10HN) and 30 µm (MX-30H). The categories of samples that were used for the characterisation study are shown in Table 5-1.

Table 5-1 GDL samples prepared for the investigation.

Abbreviation	Sample Type	Total MPL Loading Side 1 (CL) (mg/cm^2)	Total MPL Loading Side 2 (BPP) (mg/cm^2)	Pore Size	Content of Pore Forming Agent
		Single sided MPL coated GDLs			
SVB	Single Sided MPL coated GDL	1.25	-	-	-
		Double sided MPL coated GDLs			
DVB	Double Sided MPL Coated GDL	1.25	0.25	-	-
S10_10	Double Sided MPL Coated GDL	1.25	0.25	S (10 µm)	10%
S10_20	Double Sided MPL Coated GDL	1.25	0.25	S (10 µm)	20%
S10_30	Double Sided MPL Coated GDL	1.25	0.25	S (10 µm)	30%
L30_10	Double Sided MPL Coated GDL	1.25	0.25	L (30 µm)	10%
L30_20	Double Sided MPL Coated GDL	1.25	0.25	L (30 µm)	20%
L30_30	Double Sided MPL Coated GDL	1.25	0.25	L (30 µm)	30%

MPL loadings of 1.25 mg/cm² and 0.25 mg/cm² were chosen for all the samples. All of the MPLs contained a constant polytetrafluoroethylene (PTFE) content at 20 wt.% [225]. A blend including 800 mg of Vulcan black, 200 mg of a 60 wt. % PTFE dispersion (provided by Sigma-Aldrich®, UK), methylcellulose (Sigma Aldrich®, UK), and 21.6 µg of Triton X 100 (Sigma-Aldrich®, UK) were prepared. This mixture was diluted with deionised water and mixed at 800 rpm for 30 minutes until it reached a viscous consistency, suitable for generating up to five samples of the single-sided MPL-coated GDL.

The prepared MPL ink was then evenly spread on Toray carbon paper fixed on a hot plate with a temperature set to around 90°C. Utilising the doctor Blade apparatus, the ink for the 1.25 mg/cm² loading was first applied. For the double-sided MPL coated GDL samples, the carbon paper was then turned over for the subsequent application of the 0.25 mg/cm² MPL loading. Following application, the samples were sintered at 350°C for 30 minutes in a nitrogen-rich atmosphere at 1 bar pressure. Each category described in Table 5-1 was comprised of 5 samples with dimensions of 7 cm x 2.5 cm.

For the samples with the pore forming agents, they were created in the same way but with the addition of the pore forming agent to the MPL mixture. Table 5-2, shows the composition of the MPL inks with pore forming agent used to make up a mixture containing 0%, 10%, 20%, and 30% pore forming agent. This was repeated for particle sizes 10 µm and 30 µm. It is important to note that the samples treated with pore forming agent were also sintered at the same temperature of 350°C. This temperature was hot enough to cause pore forming particle degradation. The sintering process didn't need modifying for the pore forming agents, thus keeping the fabrication methodology consistent across all samples.

Table 5-2 Pore forming agent MPL compositions.

VB (mg)	PTFE (mg)	Pore Former (mg)	VB (%)	Pore Former (%)	PTFE (%)	Total (mg)
800	200	0	80	0	20	1000
700	200	100	70	10	20	1000
600	200	200	60	20	20	1000
500	200	300	50	30	20	1000

5.3.2 In-plane Electrical Conductivity

The in-plane conductivity of the GDL samples was evaluated using the 4-probe technique, as described by Smits [209]. This approach involves positioning four equidistant probes on the sample, a configuration of which is illustrated in Figure 5-2.

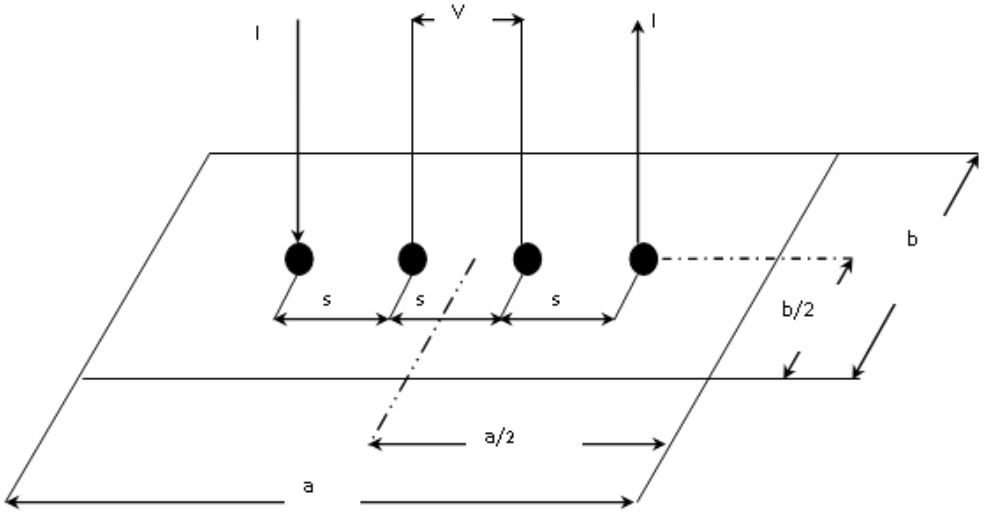

Figure 5-2 In-Plane Electrical Conductivity Experimental Set-up [89].

When applying the Smits method, obtaining the correction factor is crucial, which depends on two geometric ratios: the ratio of the sample's length to its width (a/b) and the ratio of the sample's width to the spacing between the probes (b/s) [209]. For this study, these ratios were calculated to be 3 and 1.25, respectively, resulting in a correction factor of 0.9973. The resistivity, represented by ρ, is then calculated using the formula provided [209].

$$\rho = CtR \tag{5.1}$$

Where the resistivity C is the correction factor, t is the thickness of the sample and R is the electrical resistance. Following this, the electrical conductivity, σ, of the GDL can be found by the reciprocal of the resistivity:

$$\sigma = \frac{1}{\rho} \tag{5.2}$$

To measure the thickness of the samples, a micrometre was employed. There was variability in thickness among the GDL samples and even slight variations within individual samples at different locations. To address this, thickness measurements were taken at five evenly spaced points on each GDL sample, and an average value was calculated. For electrical resistance measurements, the GDL samples were fixed to an insulating plate, and copper electrodes measuring 10 mm × 10 mm × 5 mm were placed on the samples. Using a high-precision ohmmeter (RS Pro 804, RS Components, UK) with a resolution of 0.01 mΩ, the electrical resistance of the samples was recorded. Resistance values were then determined in accordance with Ohm's law.

5.3.3 Permeability

The permeability of the GDL samples can be approximately determined using Darcy's law. This is because the gas flow rates used in the following experimental setup were kept very low.

$$Q = \frac{kA\Delta P}{\mu L} \tag{5.3}$$

The flow rate (Q) through a porous material is calculated by taking the product of the permeability (k), cross-sectional area (A), and pressure drop (ΔP), and dividing it by the product of the viscosity (μ) of the fluid and the thickness (L) of the sample [42]. The permeability was determined experimentally using the setup shown in Figure 5-3, as utilised by Orogbemi et al. [101] .

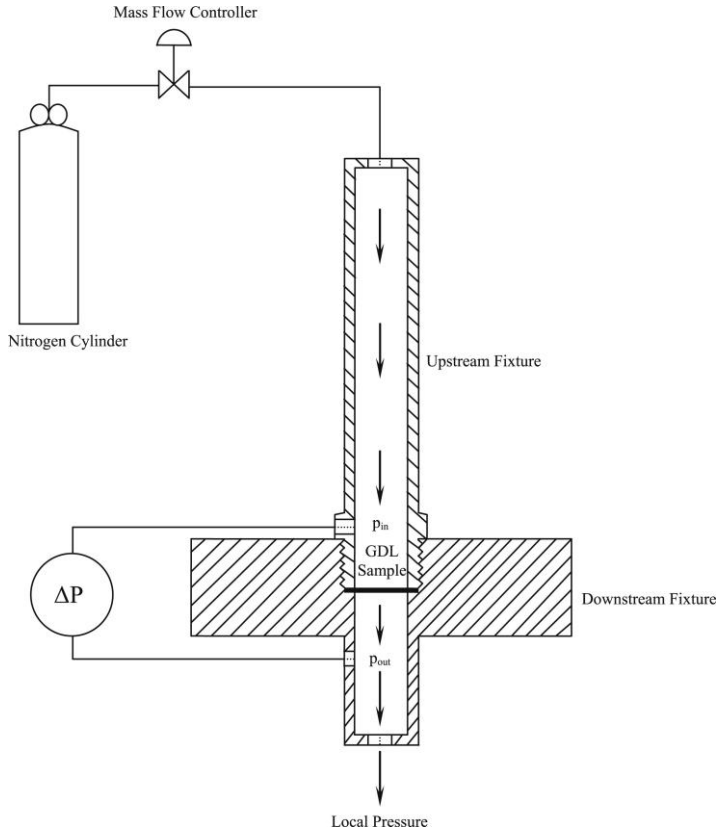

Figure 5-3 Experimental setup used to measure through-plane permeability [101].

The setup is shown in Figure 5-3 includes one fixture upstream and another downstream, allowing for a controlled flow of air through the sample while measuring the pressure drop across it. The samples are prepared with a 25.4 mm diameter punch. The circular samples are then placed between the fixtures, which exposes a 20 mm diameter area to airflow. The nitrogen gas flow rate is regulated using an HFC-202 flow controller, adjustable from 0.0-0.1 standard litres per minute (SLPM). A PX653 differential pressure sensor, with a measurement range of ±12.5 Pa, records the pressure difference across the sample. By applying Darcy's Law (Equation 5.3), the gas permeability of each sample is calculated across various flow rates, averaging the results. This procedure is repeated for all five samples in each category detailed in Table 5-1.

5.3.4 Pore Size Distribution

Mercury intrusion porosimetry (MIP) is a technique frequently used for analysing the pore size distribution of materials. In MIP, mercury is introduced to a sample of the GDL. Initially, the mercury resists penetration into the GDL pores due to its high surface tension. As pressure is incrementally increased, the mercury begins to enter the GDL's pores, initially filling the larger pores and subsequently the smaller ones [126]. The measurement of mercury intrusion pressure, which inversely correlates with pore size, allows for the determination of the pore size distribution. This method presumes pores are cylindrical and overlooks closed pores, a simplification considered reasonable for carbon paper materials [207].

Understanding the pore size distribution is vital for insights into the mass transport dynamics of gases and liquid water within the GDL's porous structure. It is also crucial for the modelling and enhancement of mass transport processes within fuel cells [126].

GDL pores are generally categorised into micropores (under 50 nm), mesopores (between 50 and 7000 nm), and macropores (over 7000 nm), with macropores being the most abundant in the GDL structure [63]. However, incorporating a microporous layer (MPL) can modify this distribution, enhancing the proportion of micropores and mesopores [79]. While macropores assist in gas diffusion, micropores are essential for the efficient removal of liquid water [[208], [210]].

5.3.5 Contact Angle

The wettability of a material is quantified by its contact angle. Angles less than 90° indicate hydrophilicity and angles over 90° show hydrophobicity [90]. To assess the contact angle on the GDL samples, the sessile drop method was utilised, involving the precise placement of water droplets on the GDL's surface. High-resolution images were taken within the initial three seconds of droplet placement to capture the dynamic contact angle accurately [208]. This procedure was repeated for ten measurements per sample to determine an average contact angle, reflecting the material's wettability characteristics accurately. Figure 5-4 shows a typical contact angle image taken from the measurements in this study.

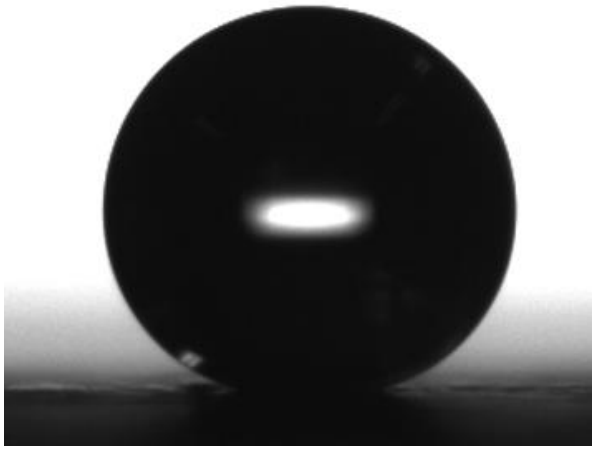

Figure 5-4 A typical water droplet on the surface of a GDL sample.

5.3.6 Morphology

Scanning Electron Microscopy (SEM) allows the GDL surface morphology, MPL and fibre structure to be examined. This level of detail can reveal how the structural characteristics of the GDL influence key functions, such as facilitating gas distribution, managing water within the cell, and providing mechanical support to the membrane and catalyst layers. The ability to closely observe these microscopic features aids in understanding how modifications to the GDL, like changes in fibre density or the addition of an MPL, can lead to improvements in overall fuel cell efficiency and durability [[203], [210], [211]].

In this analysis, GDL samples were first cut into 1 cm x 1 cm squares, then attached to SEM stubs, and placed on the specimen stage. The SEM (JEOL - Model JSM-6010LA), operating at 10 kV, was used to capture the micrographs.

5.4 Results and Discussion

The abbreviations of the samples used in this investigation are shown in Table 5-3, these will be referred to throughout this section.

Table 5-3 Abbreviations of the samples used in this investigation.

Sample Type	Abbreviation
Single sided MPL coated GDLs	
Single sided Vulcan black	SVB
Double sided MPL coated GDLs	
Double sided Vulcan black	DVB
Double sided coating containing small pore forming particles (10 μm) at 10% content	S10_10
Double sided coating containing small pore forming particles (10 μm) at 20% content	S10_20
Double sided coating containing small pore forming particles (10 μm) at 30% content	S10_30
Double sided coating containing large pore forming particles (30 μm) at 10% content	L30_10
Double sided coating containing large pore forming particles (30 μm) at 20% content	L30_20
Double sided coating containing large pore forming particles (30 μm) at 30% content	L30_30

5.4.1 In-plane Electrical Conductivity Measurements

When considering the in-plane conductivity (Figure 5-5), it is important to note that the error bars in this figure, represent the 95% confidence intervals around an average value derived from the five samples that were measured. The error bars must be taken into account when examining the data, as they suggest that some of the differences are down to statistical occurrences.

All the samples exhibit a high degree of similarity. This can be attributed to the use of the same carbon black (Vulcan black) for the MPL across all samples. A comparison between the 0.25 mg/cm^2 and 1.25 mg/cm^2 loadings reveals only a minor difference, the largest variation between the highest and lowest values being ~ 800 S/m. This observation aligns with the expectation, given that all the samples are composed of the same material. Interestingly, for the MPLs treated with pore forming agent, there is no significant difference observed for the in-plane electrical conductivity. Thus, the consistency in the results across different loadings and sample compositions underscores the uniform characteristics of the material used. Importantly, the pore forming agent treated MPL retains its electrical conductivity properties.

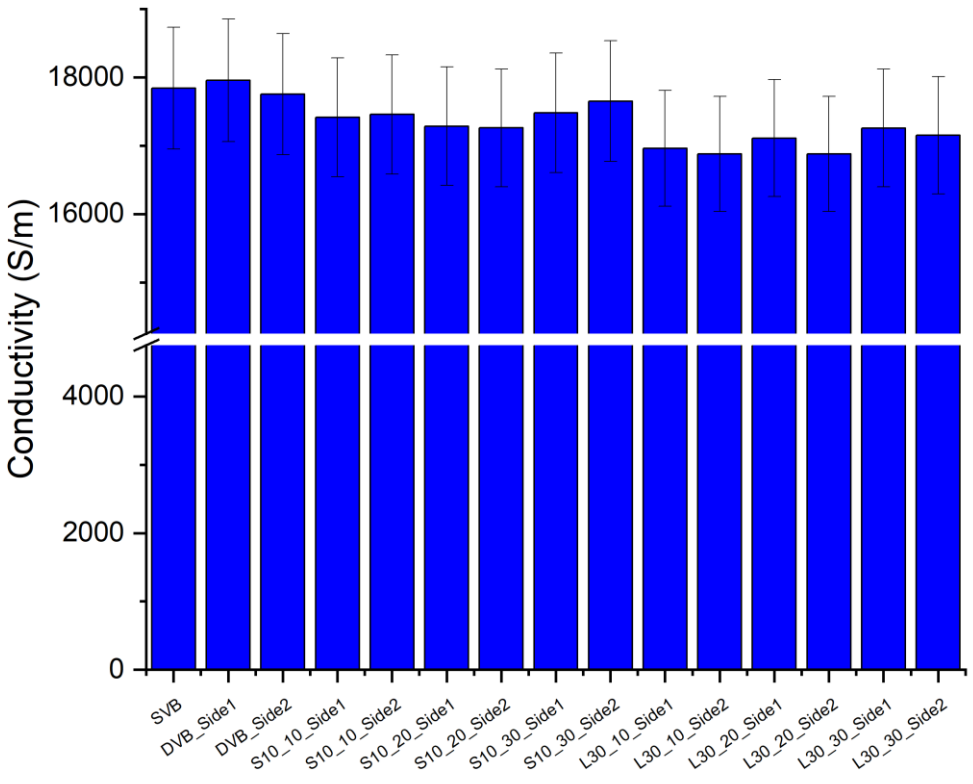

Figure 5-5 In-plane electrical conductivity of the MPL samples.

5.4.2 Permeability Measurements

The permeability of the gas diffusion layer is intimately linked to its physical structure and morphology, especially in terms of porosity and pore size distribution [89]. As depicted in Figure 5-6, the double-sided configuration demonstrates lower permeability compared to the single-sided configuration. This result is consistent with expectations, as the inclusion of an additional layer of MPL facing the BPP not only increases the thickness of the GDL but also fills in the surface pores of the GDL substrate. Specifically, the permeability decreases from 7.9×10^{-13} m^2 for the SVB to 5.9×10^{-13} m^2 for the DVB.

Upon the addition of the pore former, a noticeable increase in permeability is observed. While there is minimal difference between the pore former particle sizes of 10 µm and 30 µm, a significant difference is seen when the content of pore former is increased. As more pore forming agent is added, the samples progressively become more permeable. For instance, in the samples with the largest amount of pore forming agent (30% composition), S10_30 has a permeability of 6.9×10^{-13} m^2 and L30_30 has a permeability of 7.1×10^{-13} m^2. This is an increase in permeability compared to the DVB sample which contains no pore forming agent. When examining the error bars of the data, it can be seen that the SVB sample, containing no pore forming agents, is distinctly different to the rest of the samples. The double-sided MPL coated GDLs all have slight error bar overlaps which could mean that there are some statistical differences in the data that are not due to experimental measurements. Overall, this data suggests that the permeability can be influenced by the addition of pore former, and the more pore former added, the more permeable the sample becomes. This observation underscores the role of pore formers in modifying the permeability of the GDL.

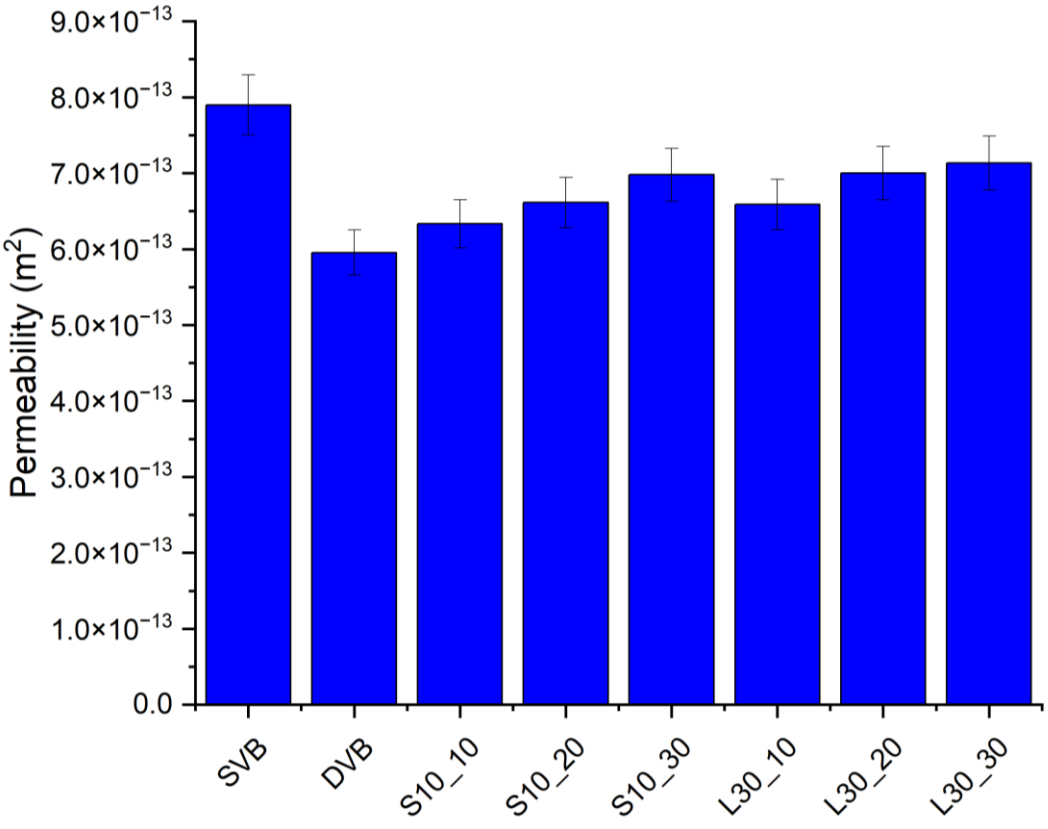

Figure 5-6 Permeability of the GDL samples.

5.4.3 Pore Size Distribution

Figure 5-7 shows the pore size distribution across different samples, showcasing a wide array of pore sizes that display the anisotropic microstructure of the GDL. This anisotropic nature accounts for the diverse pore sizes observed within the GDL [212]. To facilitate a clearer understanding, the pore sizes in Figure 5-7 are categorised into three groups: micropores (less than 50 nm), mesopores (50 to 7000 nm), and macropores (larger than 7000 nm), adhering to the classifications previously outlined.

An initial observation from the figure reveals that the incorporation of an additional MPL with the DVB sample results in a higher concentration of micropores compared to the SVB sample. Conversely, the SVB sample shows a greater volume of macropores than the DVB. This begins to shift with the introduction of pore forming agents. The introduction of these pore forming particles induces a decline in micropore content, while the volume of macropores increases. Such a trend is expected, considering that the sizes of the pore forming agents, specifically 10 µm and 30 µm, are categorised within the macropore range. This adjustment in pore size distribution underscores the significant impact that pore forming agents have on altering the microstructural composition of the GDL, effectively increasing its macropore content while reducing microporosity. Despite the reduction in micropores of the samples with pore forming agents compared to the DVB, they still have a greater amount of micropores compared to SVB. It is anticipated that this approach will preserve an optimal balance between micropores and macropores, ensuring effective mass transport while maintaining good electrical contact with the second coating of MPL facing the BPP.

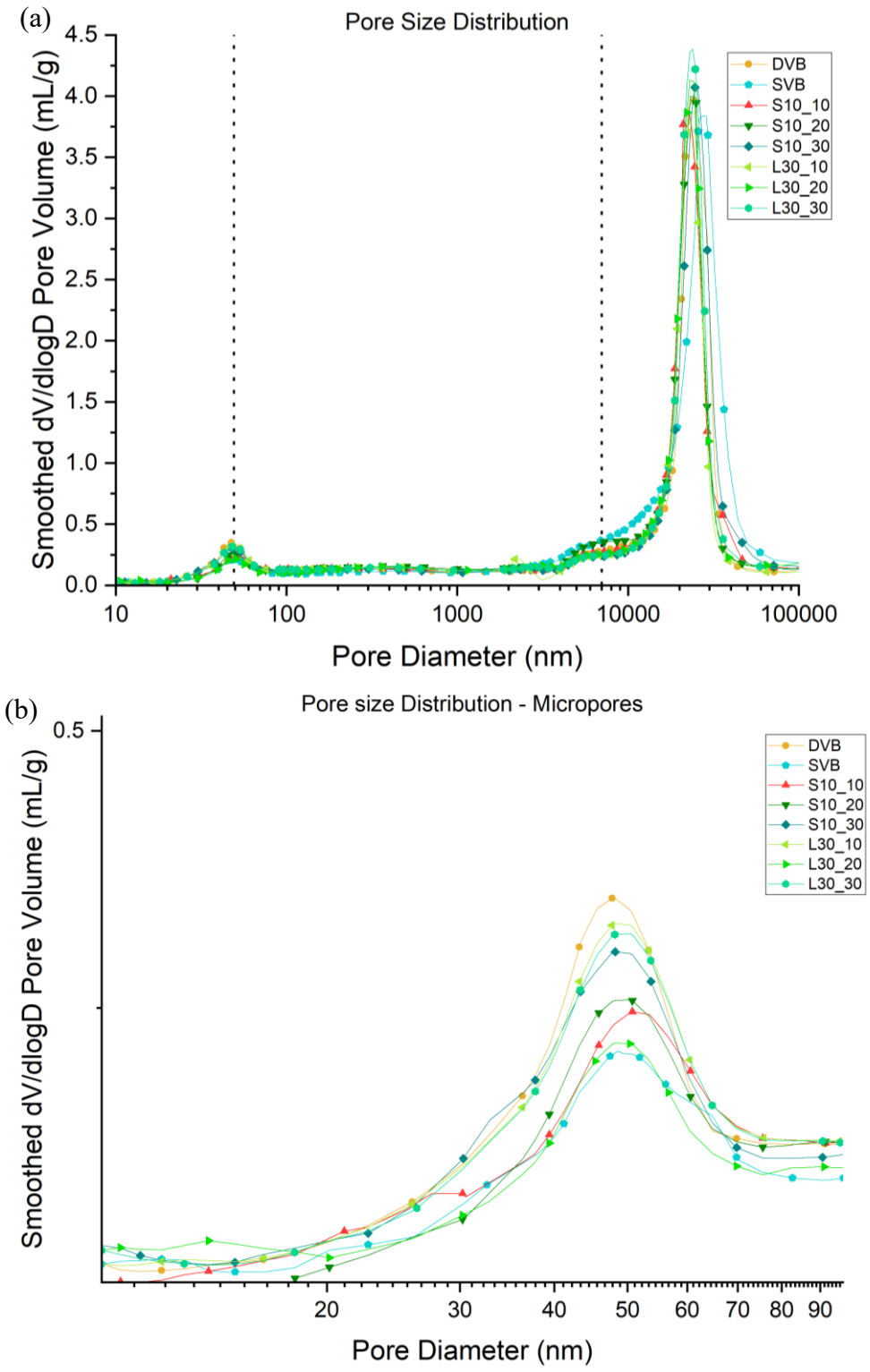

Figure 5-7 (a) Pore size distribution of the samples, (b) a more detailed look at the pore size distribution in the micropore region.

Figure 5-8 presents the porosity levels of the GDL samples, highlighting a notable variation across different samples. The sample marked as SVB emerges with the highest porosity, recorded at 75.8%. Following this, a decrease in porosity is observed with the DVB sample, which showcases the lowest porosity at 71%. This reduction is expected, considering that the DVB sample includes an additional MPL layer facing the BPP, effectively occupying more of the GDL's pore spaces. Further examination reveals a consistent trend, where porosity incrementally rises with the increase in the size of the pore forming agent; specifically, samples with 30 µm sized agents exhibit greater porosity compared to those with 10 µm particles. Additionally, a direct correlation is found between the amount of pore-forming agent added and the subsequent rise in porosity within the samples, indicating that both the size and quantity of pore forming agents play a significant role in shaping the GDL porosity.

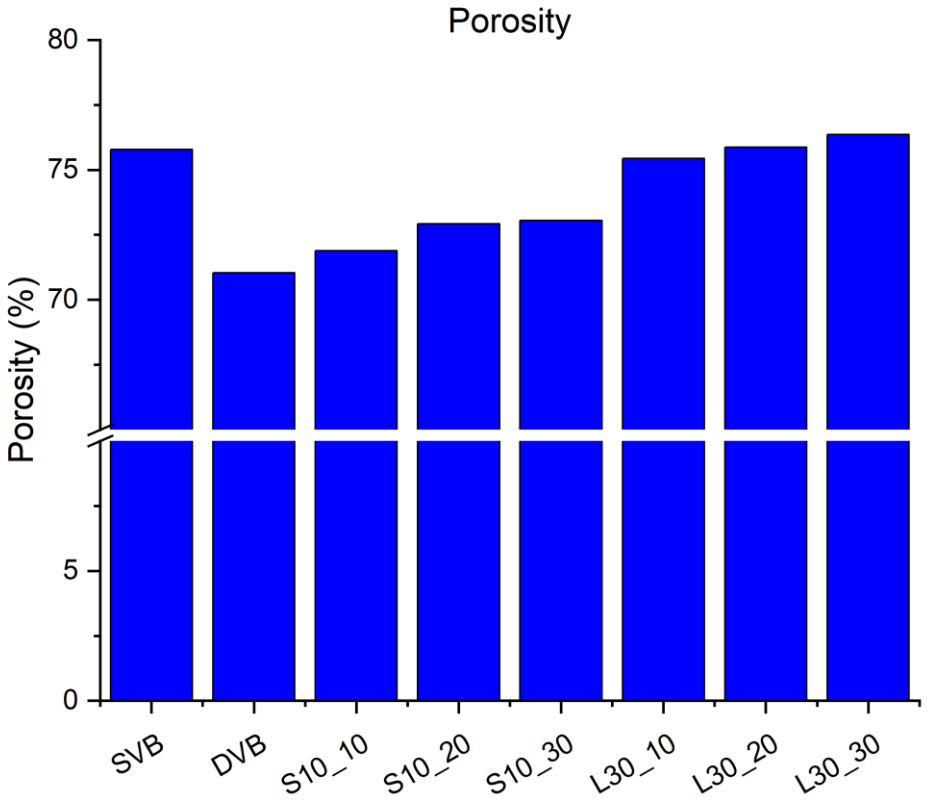

Figure 5-8 Porosity comparison of the GDL samples.

5.4.4 Contact Angle

The ability of a GDL to manage liquid water significantly impacts the performance of a PEMFC, largely due to the GDL's wettability. The wettability is influenced by the combined effects of the material's physical attributes and its surface morphology, which govern how water droplets interact with the MPL surface. Figure 5-9 displays the results from this study for the contact angle of each sample. The graph shows a uniform pattern among all tested GDL samples, all of which were hydrophobic with contact angles exceeding 140°. Even in samples that incorporated pore-forming agents, the contact angles consistently stayed above 140° without any significant variation. Between all the samples there is a maximum variation of 2°. In addition to this, there is a significant overlap of the ±5 % error bars, which would also imply little observable variation. This uniformity suggests that the wettability is primarily determined by the 20 wt. % PTFE content, with the pore-forming agents having minimal impact. Therefore, the constant presence of PTFE is identified as the key factor influencing the wettability properties of these MPLs.

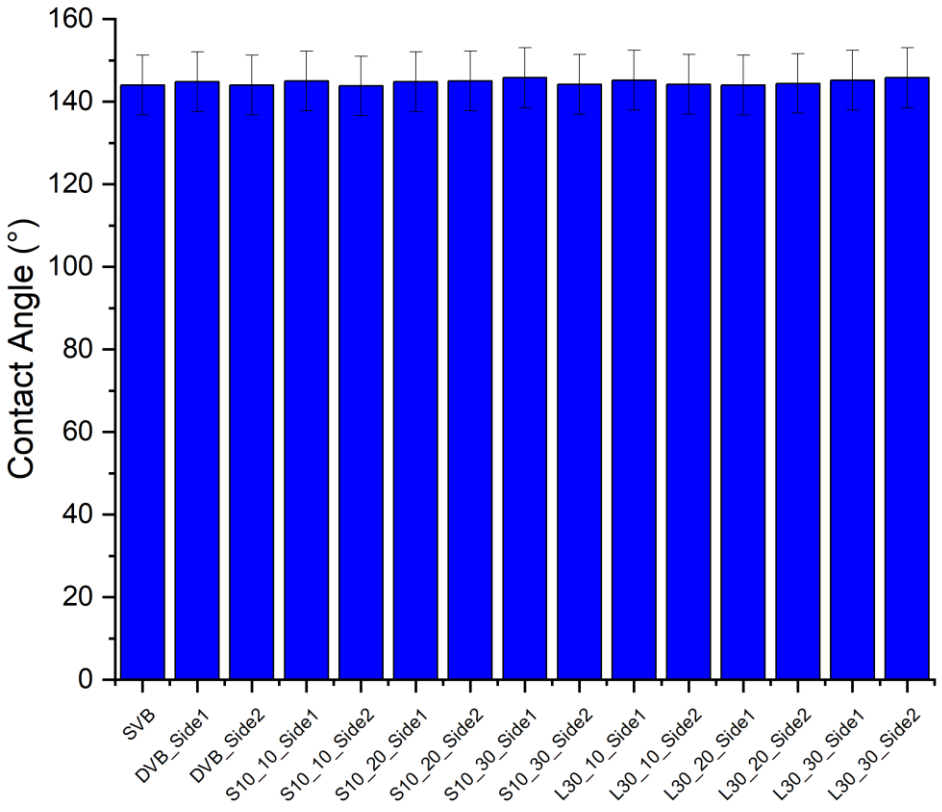

Figure 5-9 Contact angle measurements of GDL samples.

5.4.5 Morphology

Scanning Electron Microscopy (SEM) analysis was utilised to examine the surface structures and morphologies of the various MPL surfaces of the GDL. The SEM images, presented in Figure 5-10 and Figure 5-11, show the comparative surface structures between Vulcan black MPLs for double and single-sided coating and with the integration of pore forming agents.

In Figure 5-10, the SEM images for both SVB and DVB at loadings of 1.25 mg/cm^2 and 0.25 mg/cm^2 are depicted. These images reveal that the Vulcan black produces a smooth MPL surface. At the lower loading of 0.25 mg/cm^2, the smooth surface provided by Vulcan black tends to fill most of the GDL pores, yet the fibres of the GDL remain visible, and natural pore formation begins to emerge on the surface.

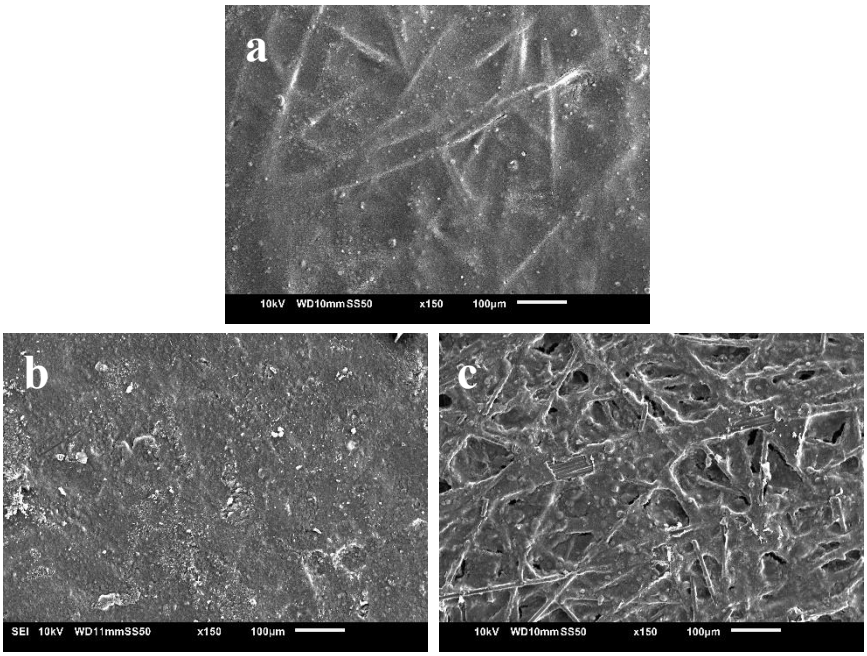

Figure 5-10 SEM images for (a) SVB 1.25 mg/cm^2 loading, (b) DVB 1.25 mg/cm^2 loading, (c) DVB 0.25 mg/cm^2 loading.

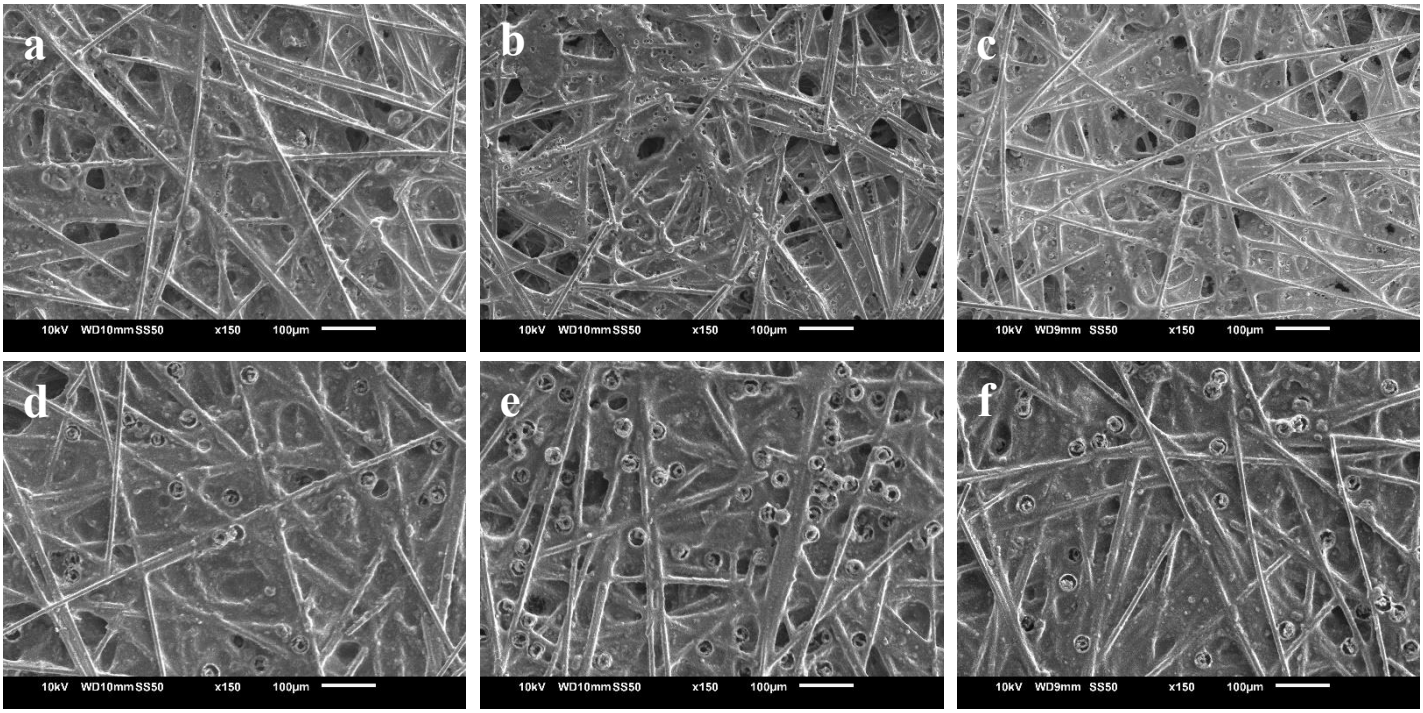

Figure 5-11 SEM images for the 0.25 mg/cm^2 samples facing the BPP for different pore forming agent sizes and compositions (a) S10_10, (b) S10_20, (c) S10_30, (d) L30_10, (e) L30_20, (f), L30_30.

Figure 5-11 examines the impact of pore forming agents on the 0.25 mg/cm^2 side facing the BPP. Images labelled A-C illustrate the effects of using 10 µm particles at varying concentrations (10%, 20%, 30%). These images highlight that the particles create distinct pores post-sintering, introducing a mix of artificial and natural pores across the MPL surface.

Furthermore, images D-F focus on the 30 µm particle additions. These larger particles are shown to create significantly bigger pores than the 10 µm. As anticipated, an increase in the concentration of these particles correlates with a rise in the quantity of artificial pores formed.

An interesting observation from the SEM analysis is that the artificial pores contribute to the enlargement of some natural pores, for both the 10 µm and 30 µm particles. It was also observed, that in the instances involving 30 µm particles, there was evidence of residual matter from the pore forming agents within the artificially created pores. Overall, it is clearly indicated that pore forming agents can play a role in modifying the MPL's surface morphology.

5.5 Conclusions and Future Work

The SEM analysis provided clear evidence that the MPL treatment using the pore forming agents, under standard sintering conditions of 350°C, successfully modified the MPL structure. A notable distinction in pore size was observed between the effects of using 10 µm and 30 µm pore forming particles. Also, these pore forming agents not only enlarged the naturally occurring pores within the MPL but also introduced larger artificial pores. However, for the 30 µm particle size, there was a slight residue left in the artificially created pores, indicating incomplete removal of the pore forming material.

Despite these structural changes, the fundamental properties such as in-plane electrical conductivity and contact angle remained unaffected by the addition of pore forming agents. This outcome is particularly beneficial as it maintains the GDL's essential electrical contact and hydrophobic characteristics, both critical for efficient water management and overall fuel cell performance.

The permeability tests further demonstrated that the MPLs treated with pore forming agents increased the GDL's permeability. The permeability was more dependent on the concentration of the pore forming agent rather than the size of the particles used. Similarly, the porosity was enhanced, showing a direct correlation with both the concentration and the size of the pore-forming agents, thus affirming the impact of MPL treated with a pore forming agent on the overall GDL structure.

Furthermore, the pore size distribution analysis indicated that when a pore forming agent was introduced to the MPL, a shift towards more macropores and a reduction in micropores was observed. This shift helped maintain a balance in the pore size distribution that is crucial for optimal fuel cell operation. Among the samples, SVB exhibited the lowest number of micropores and the DVB sample showed the highest number of micropores.

Future research should focus on in-situ fuel cell testing to thoroughly evaluate the performance of samples under various relative humidity conditions (25%, 50%, 75%, and 100%). This comprehensive testing will provide valuable insights into how the MPLs, modified with pore-forming agents, handle water management across a wide range of conditions. One key aspect of this will be to determine whether the MPLs can effectively retain humidity in low-humidity conditions, which is crucial for maintaining optimal fuel cell performance. Conversely, it will also be important to find out if these MPLs can efficiently expel liquid water in high-humidity conditions, thus preventing flooding and ensuring continuous operation.

Another topic of exploration for these MPLs is the placement of pore-forming agents. Introducing these pore forming agents on the side of the MPL facing the CL could yield different results. By examining this configuration, it could be determined which side of the double-sided MPL-coated GDL is most advantageous for the inclusion of pore formers. This could lead to enhanced water management, improved gas diffusion, and overall better performance of the fuel cell.

In summary, these studies will not only help in better understanding the impact of structural modifications on MPLs but also in optimising the design of double-sided MPL-coated GDLs. This will ultimately contribute to the development of more efficient and reliable fuel cells, capable of performing well under a variety of operational conditions. The findings of this study emphasise the delicate equilibrium required in optimising fuel cell components and open up opportunities for future research aimed at improving the efficiency and dependability of fuel cells under a wide array of operational scenarios.

Chapter 6: Conclusions and Future Work

6.1 Conclusions

The performance of a PEMFC is significantly influenced by the internal materials it consists of, especially the GDL and the MPL. The GDL is made from carbon fibres whereas the MPL is comprised of carbon black and PTFE. The MPL is conventionally applied to the side of the GDL that faces the CL. This enhances the fuel cell performance by improving electrical contact and facilitating the expulsion of excess liquid water.

The MPL is a critical component in fuel cells, despite its small size, it has a significant impact on the overall performance. Its primary functions include improving the contact resistance and managing liquid water within the fuel cell. By enhancing contact resistance, the MPL ensures effective electrical connectivity between the various layers of the fuel cell. Additionally, it helps prevent liquid water flooding, which can impede the flow of reactant gases and reduce the fuel cell's efficiency.

The main structure investigated for the MPL in this thesis was the novel double-sided MPL coated GDL, this was compared and contrasted to the conventional single-sided MPL coated GDL. The double-sided configuration involves applying MPL coatings on both sides of the GDL, with one layer facing the BPP and the other facing the CL. Research has shown that this configuration can help lower contact resistance, thus enhancing electrical conductivity. However, adding a second MPL layer increases the GDL's thickness and alters the pore size distribution. Consequently, there is a trade-off between improved electrical conductivity and the efficiency of mass transport processes. This thesis has explored this trade-off and the effects of a double-sided MPL coated GDL. Also, this innovative MPL coating highlighted the intrinsic link between the materials used in a fuel cell and its overall performance.

The main aim of this thesis is to explore the potential of the double-sided MPL coated GDL. Including the use of novel materials, and structures for the MPL, to enhance overall fuel cell performance. This involves investigating different carbon blacks for use in the MPL, the addition of graphene to the MPL and artificial pore modification of the MPL, using pore forming agents. These investigations were used to find the most effective solutions for the double-sided MPL coated GDL. By optimising the properties of the MPL, this research aims to achieve better electrical contact, improved water management, and ultimately, higher overall efficiency of the fuel cell. Through detailed analysis and experimentation, this thesis seeks to contribute to the advancement of fuel cell technology by providing new insights into the role and optimisation of the MPL.

The three research chapters in this thesis, explore and build on the knowledge of the MPLs, in relation to the double-sided MPL coating. In-depth characterisation of the MPLs was carried out, both ex-situ and in-situ. Ex-situ experiments included: in-plane electrical conductivity, permeability, wettability (contact angle), pore size distribution (using MIP) and surface morphology (using SEM). In-situ measurements consisted of single-cell measurements which produced polarisation curves, power density curves and EIS data. The key findings of each research chapter are summarised as follows.

Chapter 3 explored the novel double-sided MPL coated GDL, in comparison with the conventional single-sided MPL coated GDL. Two different carbon blacks were compared as the MPL material: Vulcan black and Ketjenblack.

- Firstly, the double-sided MPL coated GDL fabrication method was refined using the doctor blade method, enabling both sides of the GDL to be coated with an MPL, without compromising the structural integrity of either of the coatings. A loading of 1.25 mg/cm^2 was applied to the GDL side facing the CL and a 0.25 mg/cm^2 loading was applied facing the BPP.

- Results showed that the in-plane electrical conductivity of all MPL coated GDLs is slightly lower than that of the uncoated GDL, due to the higher PTFE content in the MPL. Additionally, it was found that the in-plane electrical conductivity was minimally affected by the MPL loading or carbon black type.

- Permeability measurements indicated that permeability is almost unaffected by whether the GDL is single or double-sided MPL coated, but it is more sensitive to the type of carbon black used. MIP data revealed that adding an MPL causes a favourable shift in pore size distribution, with prominent micropores in both single and double-coated MPLs. The double-sided MPL coating slightly increased the number of micropores and mesopores compared to the single-sided MPL coating.

- Contact angle measurements showed a slight increase in hydrophobicity with the addition of the MPL, with no significant differences between the carbon black types or loading levels. SEM imaging revealed that the 0.25 mg/cm² loading does not fully cover the surface of the GDL and the pores of the GDL were visible. MPL penetration into the carbon substrate was higher with Vulcan black compared to Ketjenblack.

- In-situ fuel cell testing showed that the DVB case performed exceptionally well under high humidity conditions, outperforming SKB, DKB, and SVB at 50%, 75%, and 100% relative humidity. This is attributed to the favourable balance of mesopores and micropores in the DVB case, which effectively manages excess water. At 25% relative humidity, the SVB case performed better than the DVB case, indicating its suitability for low humidity conditions due to shorter diffusion paths.

Overall, the double-sided configurations were found to perform better, with Vulcan black proving to be the superior carbon black type.

Chapter 4 then investigated making further improvements to the double-sided MPL coated GDL with the use of novel materials. Graphene was chosen for its excellent electrical properties and selected as the novel material to introduce into the double-sided MPL coated GDL structure.

The impact of double-sided MPL coated GDLs versus conventional single-sided MPL coatings was examined regarding key characteristics and fuel cell performance. Two types of carbon were used for the MPL coatings: Vulcan black and graphene. This was to evaluate the effects of introducing graphene into the double-sided MPL coating and to determine its optimal placement and ratio. Various samples with different coating permutations were investigated, with MPL loadings of 1.25 mg/cm² on the CL side and 0.25 mg/cm² on the BPP side.

- In terms of permeability, when considering the type of carbon used in the MPL, Graphene based MPLs demonstrated a higher permeability than Vulcan black MPLs. With regards to MPL coating configuration, the double-sided MPL coated samples were less permeable than single-sided ones.

- Graphene showed higher in-plane electrical conductivity than Vulcan black. Notably, a 50% mixture of graphene and Vulcan black achieved conductivity equivalent to pure graphene. Contact angle measurements showed no significant variation, suggesting that PTFE content, rather than carbon type, influences hydrophobicity.

- MIP analysis revealed that the addition of an MPL increases the number of micropores, with double-sided coatings creating more micropores than single-sided ones. Vulcan black MPLs generated more micropores than graphene-based MPLs, improving water management capabilities. This highlights the importance of micropores in effective water management and overall performance.

- SEM analysis showed differences in surface characteristics: graphene exhibited more surface cracks, while Vulcan black had a smoother surface. At a loading of 0.25 mg/cm², these differences were more pronounced due to the lower loading exposing the larger pores of the carbon substrate.

- Fuel cell performance data indicated that the pure graphene samples, both double and single-sided coatings, had the lowest performance, likely due to fewer micropores and less effective water management, despite their better electrical conductivity.

The D_VB100_G100 sample, with Vulcan black facing the CL and graphene facing the BPP, exhibited optimal pore size distribution along with improved electrical conductivity. In particular, it was found that the natural cracks and pores formed by the graphene layer facing the BPP allowed for effective water expulsion. This configuration performed the best in the overall fuel cell testing.

Chapter 5 expanded on the findings from the previous two research chapters and explored the optimisation of better electrical contact and mass transport processes. Conventional Vulcan black was used for all the MPL coatings. In addition to this, pore forming agents were used to artificially create more pores and cracks in the MPL coating facing the BPP, to imitate the structure provided by graphene.

- The SEM analysis demonstrated that the MPL treatment using pore-forming agents, under standard sintering conditions of 350°C, effectively modified the MPL structure. A clear distinction in pore size was observed between the effects of 10 µm and 30 µm pore forming particles. These pore forming agents not only enlarged the natural pores within the MPL but also introduced larger artificial pores. However, the 30 µm particles left slight residues in the artificial pores, indicating incomplete removal of the pore-forming material.

- Despite these structural changes, fundamental properties such as in-plane electrical conductivity and contact angle remained unaffected by the pore-forming agents. This is beneficial as it maintains the GDL's essential electrical contact and hydrophobic characteristics, which are critical for efficient water management and overall fuel cell performance.

- Permeability tests showed that MPLs treated with pore-forming agents increased the GDL's permeability, which was more dependent on the concentration of the pore forming agent than the particle size. Porosity also increased, correlating with both the concentration and size of the pore forming agents, confirming the significant impact of the treatment on the GDL structure.
- Pore size distribution analysis indicated a shift towards more macropores and fewer micropores, maintaining a crucial balance for optimal fuel cell operation.

Overall Conclusion

The research studies in this thesis showed that the double-sided MPL configuration was found to be the most effective at improving fuel cell performance. Particularly at relative humidities of 50%, 75%, and 100%, where it significantly outperformed other MPL configurations. Among the carbon black particles tested, Vulcan black emerged as the most suitable, providing the best overall performance. Graphene showed optimal results when applied to the side of the GDL facing the BPP.

Fundamental properties such as in-plane electrical conductivity, permeability, and contact angle were mainly influenced by the type of carbon used in the MPL, rather than if the sample was double-sided or single-sided MPL coated GDL.

Moreover, the type of carbon and whether the MPL was single or double-sided had a significant impact on the pore size distribution. Pore size distribution was shown across all of the studies to be a crucial factor for water management and a good balance of micropores and mesopores provided by the double-sided MPL structure helped to improve fuel cell performance.

The graphene layer facing the BPP excelled in balancing the electrical conductivity and permeability while maintaining effective water expulsion. Although pore forming agents were used to alter the Vulcan black MPL structure facing the BPP, it was difficult to replicate the natural structure provided by graphene.

In summary, the double-sided MPL configuration with Vulcan black facing the CL and graphene facing the BPP proved to be the most effective setup, balancing electrical conductivity, and water management

Polymer electrolyte membrane fuel cells are anticipated to see a global increase in usage, making the findings of this thesis relevant both within and outside academic circles. This work has extensively used and discussed various characterisation methodologies that assess the structural and electrochemical performance of MPL materials and structures. Important developments have been made in understanding the double-sided MPL coated GDL, with respect to characterisation and fuel cell performance. These insights are valuable additions to the existing literature and will allow for future research in both academic and industrial applications.

6.2 Recommendations for Future Work

There are numerous potential research avenues for optimising the MPL and integrating new designs into PEM fuel cells. Suggested topics for further investigation and recommendations to enhance the research impact are as follows:

- A particularly interesting avenue for further research would be to explore how different carbon substrates interact with a double-sided MPL coating. This thesis focused on investigating GDLs made from carbon paper (Toray Carbon Paper 060 PTFE 10 wt. %). This material was consistently used throughout all the experiments to ensure uniformity in the test conditions. However, this raises an intriguing question about the potential interactions and performance improvements that might be observed with different GDL substrates. This could include not only other types of carbon paper but also carbon cloth, which might offer different physical and structural properties. The variation in structure, porosity, and morphology among these materials could behave differently with the double-sided MPL coating which in turn could significantly impact the overall performance of the fuel cells.

- Another promising topic of investigation would be the testing and optimisation of novel materials used in the double-sided MPL coated GDLs. This thesis looked into two different carbon blacks and graphene for MPL fabrication. Future research could investigate the specific formulations and optimum ratios of carbon black and graphene in the samples. Novel materials usage could extend to the use of CNTs and different types of graphene particles. Each type of graphene, from single-layer to multi-layered or even graphene oxide, brings distinct properties that could be explored within the MPL. Moreover, the addition of novel materials, could alter the optimum loading for each coating of the MPL and this would need to be investigated.

- Another valuable line of research could focus on the use of different pore forming agents within the double-sided MPL coated GDLs. Different types of pore forming agents could be explored to investigate whether they behave differently or produce better results. Exploring various types of pore forming agents alongside different fabrication techniques, could have the potential to refine the porosity and, consequently, the performance of GDLs.

- The concept of a double-sided MPL coated GDL structure opens up intriguing possibilities for further modification, particularly through the incorporation of composite layers to create graded porosity. This gradation in porosity can be crucial for optimising water management within fuel cells. The implementation of a porosity gradient from the direction of the CL to the BPP could be an interesting structure to design and study with the double-sided MPL coated GDL. Similar to this, graded hydrophobicity (and even hydrophilicity) could be explored in order to improve the water management capabilities of the GDL under a wide range of humidity conditions.

- Throughout the experiments conducted in this thesis, graphite BPPs were used consistently to maintain uniformity and control within the experimental setup. Graphite, known for its good electrical conductivity and corrosion resistance, is widely used in fuel cell BPP applications. However, exploring other BPP materials, such as various metals, could open up new insights into the dynamics with a double-sided MPL coated

GDL. Metals, offering different physical and chemical properties compared to graphite, might significantly alter the behaviour of the double-sided MPL coated GDL. Investigating how these alternative materials interact with the double-sided MPL could reveal whether there is a notable change in results, possibly leading to improvements in performance or cost-effectiveness.

- An intriguing topic of research is the detailed examination of how the MPL penetrates the GDL, which is of particular interest with regard to the double-sided MPL coated GDL configuration. Understanding the penetration dynamics is crucial because it may significantly impact the overall pore size distribution and porosity of the GDL, which in turn affects the performance of the fuel cell. It would be particularly interesting to explore how the MPL's penetration into the GDL alters the GDL's properties and whether these changes are further influenced by a double-sided MPL configuration. Such insights could lead to improved designs that optimise the design. Additionally, examining how various carbon materials (both conventional and novel materials) interact differently with the GDL substrate, could provide deeper insights into material-specific behaviours and their implications on the overall GDL structure. To accurately assess the MPL penetration, utilising imaging techniques such as X-ray Computed Tomography (XCT) could be extremely beneficial. XCT offers a non-destructive way to visualise and measure the extent of MPL penetration within the GDL in three dimensions, providing a clear analysis of how the MPL integrates with the GDL structure. This method could help validate the impact of different materials and fabrication techniques on the structural properties of the GDL.

- Investigating different fabrication methods of the double-sided MPL coated GDL, such as spray coating versus doctor blade, could reveal significant differences in how these methods affect MPL surface structure and penetration into the GDL substrate. This in turn could affect the overall properties of the GDL. Each technique might offer unique advantages or pose certain challenges in terms of uniformity, thickness, and pore structure.

- Another interesting study would be to accurately quantify the contact resistance data for both double-sided and single-sided MPL coated GDLs. By conducting such research, it would be possible to compare these configurations directly, offering insights into how the MPLs affect overall fuel cell performance. However, accurately measuring contact resistance presents a significant challenge that requires specialist equipment and precise techniques, due to the intricate interfaces and materials involved. Furthermore, extending this investigation to include novel materials could provide a deeper understanding of how different substances influence the contact resistance. This data could help to optimise the design of fuel cells, as it helps identify which configurations and materials offer the best way to lower the contact resistance.

- Durability testing is an important tool when looking at new designs and materials within fuel cells. It would be particularly interesting to test the durability of the double-sided MPL coated GDL. This design is promising, but its long-term performance and stability under various operational stresses remain to be thoroughly assessed. By examining the degradation and overall robustness of this configuration, any areas that may require further improvement can be identified. Moreover, durability testing of different carbon

materials can reveal which options are the most resilient and suitable for long-term use in fuel cells.

- A techno-economic analysis could be carried out to assess the viability of manufacturing double-sided MPL coated GDLs, especially in terms of cost-effectiveness relative to the performance enhancements in fuel cells. This analysis would involve, determining whether the process of creating a double-sided MPL coated GDL can be scaled up. Scaling up manufacturing processes typically reduces unit costs through economies of scale, but this must be weighed against the complexity and initial investment required for the setup. It is also necessary to analyse the cost implications of this manufacturing process compared to the benefits gained in fuel cell performance. This includes calculating potential increases in efficiency, lifespan, and reliability of fuel cells, and how these improvements could translate into cost savings or higher revenues in practical applications. Additionally, the inclusion of novel materials like graphene, needs careful consideration. It is typically more expensive to use graphene than conventional carbon black materials. The analysis should therefore factor in whether the integration of graphene makes the process expensive, or if the performance gains justify the higher costs. A techno-economic analysis could provide valuable insights into the economic feasibility and potential of the double-sided MPL coated GDL in a manufacturing process.

References

[1] S. H. Mohr, J. Wang, G. Ellem, J. Ward, and D. Giurco, “Projection of world fossil fuels by country,” 2014, doi: 10.1016/j.fuel.2014.10.030.

[2] M. Meinshausen *et al.*, “LETTERS Greenhouse-gas emission targets for limiting global warming to 2 6C,” *Nature*, vol. 458, 2009, doi: 10.1038/nature08017.

[3] S. Chu, Y. Cui, and N. Liu, “The path towards sustainable energy Photovoltaic devices,” *Nat. Publ. Gr.*, vol. 16, 2016, doi: 10.1038/NMAT4834.

[4] P. A. Stott *et al.*, “Attribution of extreme weather and climate-related events,” *WIREs Clim Chang.*, vol. 7, pp. 23–41, 2016, doi: 10.1002/wcc.380.

[5] N. G. M. L. US Department of Commerce, “Global Monitoring Laboratory - Carbon Cycle Greenhouse Gases.”

[6] “The Climate Change Act 2008 (2050 Target Amendment) Order 2019,” 2019.

[7] “The Paris Agreement | UNFCCC,” 2015. https://unfccc.int/process-and-meetings/the-paris-agreement/the-paris-agreement (accessed Jun. 29, 2021).

[8] M. Ball, A. Basile, and T. N. Veziroglu, *Compendium of Hydrogen Energy: Hydrogen Use, Safety and the Hydrogen Economy*. Burlington: Elsevier Science, 2015.

[9] IEA, “Net Zero by 2050 - A Roadmap for the Global Energy Sector,” 2021, Accessed: Jul. 28, 2021. [Online]. Available: www.iea.org/t&c/.

[10] S. J. Davis *et al.*, “REVIEW SUMMARY Net-zero emissions energy systems,” 2018, doi: 10.1126/science.aas9793.

[11] P. Hoffmann, *Tomorrow’s Energy, Revised and Expanded Edition : Hydrogen, Fuel Cells, and the Prospects for a Cleaner Planet*. MIT Press, 2012.

[12] K. Mazloomi and C. Gomes, “Hydrogen as an energy carrier: Prospects and challenges,” *Renew. Sustain. Energy Rev.*, vol. 16, pp. 3024–3033, 2012, doi: 10.1016/j.rser.2012.02.028.

[13] Z. Abdin, A. Zafaranloo, A. Rafiee, W. Mérida, W. Lipiński, and K. R. Khalilpour, “Hydrogen as an energy vector,” *Renew. Sustain. Energy Rev.*, vol. 120, p. 109620, Mar. 2020, doi: 10.1016/J.RSER.2019.109620.

[14] T. M. Gür, “Review of electrical energy storage technologies, materials and systems: challenges and prospects for large-scale grid storage,” *Energy Environ. Sci.*, vol. 11, no. 10, pp. 2696–2767, Oct. 2018, doi: 10.1039/C8EE01419A.

[15] M. Boudellal, *Power-To-Gas : Renewable Hydrogen Economy for the Energy Transition*. Walter de Gruyter GmbH, 2018.

[16] N. Z. Muradov and T. N. Veziroğlu, “From hydrocarbon to hydrogen–carbon to hydrogen economy,” *Int. J. Hydrogen Energy*, vol. 30, no. 3, pp. 225–237, Mar. 2005, doi: 10.1016/J.IJHYDENE.2004.03.033.

[17] H. Nazir *et al.*, “Is the H 2 economy realizable in the foreseeable future? Part II: H 2 storage, transportation, and distribution,” 2020, doi: 10.1016/j.ijhydene.2020.05.241.

[18] P. T. Moseley and J. Garche, *Electrochemical Energy Storage for Renewable Sources and Grid Balancing*. Elsevier, 2015.

[19] B. Chukwudi Tashie-Lewis and S. G. Nnabuife, “Hydrogen Production, Distribution, Storage and Power Conversion in a Hydrogen Economy-A Technology Review,” *Chem. Eng. J. Adv.*, vol. 8, p. 100172, 2021, doi: 10.1016/j.ceja.2021.100172.

[20] A. M. Oliveira, R. R. Beswick, and Y. Yan, “A green hydrogen economy for a renewable energy society,” *Curr. Opin. Chem. Eng.*, vol. 33, p. 100701, Sep. 2021, doi: 10.1016/J.COCHE.2021.100701.

[21] T. Drennen and J. Rosthal, *Pathways to a Hydrogen Future*. lsevier Science & Technology, 2007.

[22] N. Z. Muradov, T. Nejat, and V. ˇlu, “‘‘‘Green”’ path from fossil-based to hydrogen economy: An overview of carbon-neutral technologies,” *Int. J. Hydrogen Energy*, vol. 33, pp. 6804–6839, 2008, doi: 10.1016/j.ijhydene.2008.08.054.

[23] F. Barbir, *PEM Fuel Cells: Theory and Practice*. Elsevier Science & Technology, 2005.

[24] D. for E. S. and N. Z. (DESNZ), “UK ENERGY IN BRIEF 2023,” 2023.

[25] N. A. Al-Mufachi and N. Shah, “The role of hydrogen and fuel cell technology in providing security for the UK energy system,” *Energy Policy*, vol. 171, p. 113286, Dec. 2022, doi: 10.1016/J.ENPOL.2022.113286.

[26] G. Correa, P. M. Muñoz, and C. R. Rodriguez, “A comparative energy and environmental analysis of a diesel, hybrid, hydrogen and electric urban bus,” *Energy*, vol. 187, p. 115906, Nov. 2019, doi: 10.1016/J.ENERGY.2019.115906.

[27] K. G. Logan, J. D. Nelson, and A. Hastings, “Electric and hydrogen buses: Shifting from conventionally fuelled cars in the UK,” 2020, doi: 10.1016/j.trd.2020.102350.

[28] “UK Hydrogen Strategy,” 2021.

[29] L. Carrette, K. A. Friedrich, and U. Stimming, “Fuel cells: Principles, types, fuels, and applications,” *Chemphyschem*, pp. 163–193, 2000.

[30] B. Sørensen, *Hydrogen and Fuel Cells: Emerging Technologies and Applications*. Elsevier Science & Technology, 2005.

[31] V. Hacker and S. Mitsushima, *Fuel Cells and Hydrogen: From Fundamentals to Applied Research,*. Elsevier, 2018.

[32] M. Spinelli, D. Di Bona, M. Gatti, E. Martelli, F. Vigan, and S. Consonni, “Assessing the potential of molten carbonate fuel cell-based schemes for carbon capture in natural gas-fired combined cycle power plants,” *J. Power Sources*, vol. 448, p. 227223, 2020, doi: 10.1016/j.jpowsour.2019.227223.

[33] J. D. Slater, T. Chronopoulos, R. S. Panesar, F. D. Fitzgerald, and M. Garcia, “Review and techno-economic assessment of fuel cell technologies with CO 2 capture ☆,” 2019, doi: 10.1016/j.ijggc.2019.102818.

[34] F. Wang *et al.*, “A comprehensive review on high-temperature fuel cells with carbon capture,” 2020, doi: 10.1016/j.apenergy.2020.115342.

[35] J.-H. Wee, “Which type of fuel cell is more competitive for portable application: Direct methanol fuel cells or direct borohydride fuel cells?,” *J. Power Sources*, vol. 161, pp. 1–10, 2006, doi: 10.1016/j.jpowsour.2006.07.032.

[36] T. Wilberforce, A. Alaswad, A. Palumbo, M. Dassisti, and A. G. Olabi, “Advances in stationary and portable fuel cell applications,” *Int. J. Hydrogen Energy*, vol. 41, no. 37, pp. 16509–16522, Oct. 2016, doi: 10.1016/J.IJHYDENE.2016.02.057.

[37] I. Staffell and R. Green, “The cost of domestic fuel cell micro-CHP systems,” 2012, doi: 10.1016/j.ijhydene.2012.10.090.

[38] H. Aki, T. Wakui, and R. Yokoyama, “Development of an energy management system for optimal operation of fuel cell based residential energy systems,” 2016, doi: 10.1016/j.ijhydene.2016.09.079.

[39] I. Staffell *et al.*, “The role of hydrogen and fuel cells in the global energy system,” *Energy Environ. Sci.*, vol. 12, no. 2, pp. 463–491, Feb. 2019, doi: 10.1039/C8EE01157E.

[40] S. Barrett, “European CHIC project under way to make hydrogen public transport a commercial reality,” *Fuel Cells Bull.*, vol. 2010, no. 11, pp. 12–15, Nov. 2010, doi: 10.1016/S1464-2859(17)30065-2.

[41] A. Lozanovski, N. Whitehouse, N. Ko, and S. Whitehouse, “Sustainability Assessment of Fuel Cell Buses in Public Transport,” 2018, doi: 10.3390/su10051480.

[42] M. Mench, *Fuel Cell Engines*. John Wiley & Sons, 2008.

[43] T. Wilberforce *et al.*, “Developments of electric cars and fuel cell hydrogen electric cars,” *Int. J. Hydrogen Energy*, vol. 42, no. 40, pp. 25695–25734, Oct. 2017, doi: 10.1016/J.IJHYDENE.2017.07.054.

[44] J. H. Hirschenhofer, D. B. Stauffer, Engleman R.R, and Klett M.G., *Fuel Cell Handbook*, vol. Fourth Edition. 1998.

[45] A. Hermann, T. Chaudhuri, and P. Spagnol, “Bipolar plates for PEM fuel cells: A review,” *Int. J. Hydrogen Energy*, vol. 30, pp. 1297–1302, 2005, doi: 10.1016/j.ijhydene.2005.04.016.

[46] S. Park, J. W. Lee, and B. N. Popov, “A review of gas diffusion layer in PEM fuel cells: Materials and designs,” *International Journal of Hydrogen Energy*, vol. 37, no. 7. Elsevier Ltd, pp. 5850–5865, Apr. 01, 2012, doi: 10.1016/j.ijhydene.2011.12.148.

[47] H. M. Chang and M. H. Chang, “Effect of gas diffusion layer with double-side microporous layer coating on polymer electrolyte membrane fuel cell performance,” *J. Fuel Cell Sci. Technol.*, vol. 10, no. 2, Apr. 2013, doi: 10.1115/1.4023841.

[48] G.-M. Huang and M.-H. Chang, “Effect of Gas Diffusion Layer With Double-Side Microporous Layer Coating on Proton Exchange Membrane Fuel Cell Performance Under Different Air Inlet Relative Humidity,” 2014. [Online]. Available: www.electrochemsci.org.

[49] J. Z. X.-Z. Yuan, C. Song, H. Wang, *Electrochemical Impedance Spectroscopy in PEM Fuel Cells: Fundamentals and Applications*. Springer London Dordrecht Heidelberg New York, 2010.

[50] X. Yuan, H. Wang, J. Colin Sun, and J. Zhang, “AC impedance technique in PEM fuel cell diagnosis—A review,” *Int. J. Hydrogen Energy*, vol. 32, no. 17, pp. 4365–4380, Dec. 2007, doi: 10.1016/J.IJHYDENE.2007.05.036.

[51] A. M. Dhirde, N. V. Dale, H. Salehfar, M. D. Mann, and T. H. Han, “Equivalent electric circuit modeling and performance analysis of a PEM fuel cell stack using impedance spectroscopy,” *IEEE Trans. Energy Convers.*, vol. 25, no. 3, pp. 778–786, Sep. 2010, doi: 10.1109/TEC.2010.2049267.

[52] S. Asghari, A. Mokmeli, and M. Samavati, “Study of PEM fuel cell performance by electrochemical impedance spectroscopy,” *Int. J. Hydrogen Energy*, vol. 35, no. 17, pp. 9283–9290, Sep. 2010, doi: 10.1016/J.IJHYDENE.2010.03.069.

[53] C. Brunetto, A. Moschetto, and G. Tina, “PEM fuel cell testing by electrochemical impedance spectroscopy,” *Electr. Power Syst. Res.*, vol. 79, no. 1, pp. 17–26, Jan. 2009, doi: 10.1016/J.EPSR.2008.05.012.

[54] G. Hoogers, *Fuel Cell Technology Handbook*. CRC Press, 2003.

[55] Z. Chen, *Non-Noble Metal Fuel Cell Catalysts*. John Wiley & Sons, 2014.

[56] P. Yi, L. Peng, T. Zhou, J. Huang, and X. Lai, “Composition optimization of multilayered chromium-nitrideecarbon film on 316L stainless steel as bipolar plates for proton exchange membrane fuel cells,” 2013, doi: 10.1016/j.jpowsour.2013.02.034.

[57] N. J. Cooper, T. Smith, A. D. Santamaria, and J. W. Park, “Experimental optimization of parallel and interdigitated PEMFC flow-field channel geometry,” 2015, doi: 10.1016/j.ijhydene.2015.11.153.

[58] J. Zhao, A. Ozden, S. Shahgaldi, I. E. Alaefour, X. Li, and F. Hamdullahpur, “Effect of Pt loading and catalyst type on the pore structure of porous electrodes in polymer electrolyte membrane (PEM) fuel cells,” 2018, doi: 10.1016/j.energy.2018.02.134.

[59] Y. Wang, *PEM Fuel Cells: Thermal and Water Management Fundamentals*. Momentum Press, 2013.

[60] R. Omrani and B. Shabani, “Gas diffusion layer modifications and treatments for improving the performance of proton exchange membrane fuel cells and electrolysers: A review,” 2017, doi: 10.1016/j.ijhydene.2017.09.132.

[61] E. Ogungbemi *et al.*, “Fuel cell membranes – Pros and cons,” *Energy*, vol. 172, pp. 155–172, Apr. 2019, doi: 10.1016/J.ENERGY.2019.01.034.

[62] A. Ozden, S. Shahgaldi, X. Li, and F. Hamdullahpur, “A review of gas diffusion layers for proton exchange membrane fuel cells-With a focus on characteristics, characterization techniques, materials and designs,” *Prog. Energy Combust. Sci.*, vol. 74, pp. 50–102, 2019, doi: 10.1016/j.pecs.2019.05.002.

[63] A. El-Kharouf, T. J. Mason, D. J. L. Brett, and B. G. Pollet, “Ex-situ characterisation of gas diffusion layers for proton exchange membrane fuel cells,” *J. Power Sources*, vol. 218, pp. 393–404, Nov. 2012, doi: 10.1016/J.JPOWSOUR.2012.06.099.

[64] A. Jayakumar, S. P. Sethu, M. Ramos, J. Robertson, and A. Al-Jumaily, “A technical review on gas diffusion, mechanism and medium of PEM fuel cell,” *Ionics 2014 211*, vol. 21, no. 1, pp. 1–18, Nov. 2014, doi: 10.1007/S11581-014-1322-X.

[65] J. T. Gostick, M. W. Fowler, M. D. Pritzker, M. A. Ioannidis, and L. M. Behra, “In-plane and through-plane gas permeability of carbon fiber electrode backing layers,” *J. Power Sources*, vol. 162, pp. 228–238, 2006, doi: 10.1016/j.jpowsour.2006.06.096.

[66] L. Cindrella *et al.*, “Gas diffusion layer for proton exchange membrane fuel cells-A review,” *J. Power Sources*, vol. 194, pp. 146–160, 2009, doi: 10.1016/j.jpowsour.2009.04.005.

[67] C. Chan, N. Zamel, X. Li, and J. Shen, “Experimental measurement of effective diffusion coefficient of gas diffusion layer/microporous layer in PEM fuel cells,” *Electrochim. Acta*, vol. 65, pp. 13–21, Mar. 2012, doi: 10.1016/J.ELECTACTA.2011.12.110.

[68] C. J. Tseng and S. K. Lo, “Effects of microstructure characteristics of gas diffusion layer and microporous layer on the performance of PEMFC,” *Energy Convers. Manag.*, vol. 51, no. 4, pp. 677–684, Apr. 2010, doi: 10.1016/J.ENCONMAN.2009.11.011.

[69] D. R. P. Morris and J. T. Gostick, “Determination of the in-plane components of the electrical conductivity tensor in PEM fuel cell gas diffusion layers,” *Electrochim. Acta*, vol. 85, pp. 665–673, Dec. 2012, doi: 10.1016/J.ELECTACTA.2012.08.083.

[70] D. Hasan Ahmed, H. Jin Sung Ã, and J. Bae, “Effect of GDL permeability on water and thermal management in PEMFCs-I. Isotropic and anisotropic permeability,” 2008, doi: 10.1016/j.ijhydene.2008.04.024.

[71] S. Li, J. Yuan, M. Andersson, G. Xie, and B. Sundén, “Influence of anisotropic gas diffusion layers on transport phenomena in a proton exchange membrane fuel cell,” *Int. J. Energy Res.*, vol. 41, no. 14, pp. 2034–2050, Nov. 2017, doi: 10.1002/ER.3763.

[72] D. Todd, S. Bennett, and W. M. Erida, “Anisotropic electrical resistance of proton exchange membrane fuel cell transport layers as a function of cyclic strain,” 2016, doi: 10.1016/j.ijhydene.2016.02.111.

[73] S. Malik, L. Smith, J. Sharman, E. M. Holt, and S. P. Rigby, “Pore Structural Characterization of Fuel Cell Layers Using Integrated Mercury Porosimetry and Computerized X-ray Tomography,” *Ind. Eng. Chem. Res.*, vol. 55, no. 41, pp. 10850–10859, Oct. 2016, doi: 10.1021/ACS.IECR.6B01617.

[74] E. A. Wargo, V. P. Schulz, S. R. Kalidindi, and E. C. Kumbur, “Electrochimica Acta Resolving macro-and micro-porous layer interaction in polymer electrolyte fuel cells using focused ion beam and X-ray computed tomography,” *Electrochim. Acta*, vol. 87, pp. 201–212, 2013, doi: 10.1016/j.electacta.2012.09.008.

[75] G. Lin *et al.*, “Effect of pore size distribution in the gas diffusion layer adjusted by composite carbon black on fuel cell performance,” *Int. J. Energy Res.*, vol. 45, no. 5, pp. 7689–7702, Apr. 2021, doi: 10.1002/ER.6350.

[76] X. Wang *et al.*, “A bi-functional micro-porous layer with composite carbon black for PEM fuel cells,” *J. Power Sources*, vol. 162, pp. 474–479, 2006, doi: 10.1016/j.jpowsour.2006.06.064.

[77] C. S. Kong, D.-Y. Kim, H.-K. Lee, Y.-G. Shul, and T.-H. Lee, “Infuence of pore-size distribution of diffusion layer on mass-transport problems of proton exchange membrane fuel cells,” 2002.

[78] J. H. Nam and M. Kaviany, “Effective diffusivity and water-saturation distribution in single- and two-layer PEMFC diffusion medium,” *Int. J. Heat Mass Transf.*, vol. 46, no. 24, pp. 4595–4611, Nov. 2003, doi: 10.1016/S0017-9310(03)00305-3.

[79] H. K. Lee, J. H. Park, D. Y. Kim, and T. H. Lee, “A study on the characteristics of the diffusion layer thickness and porosity of the PEMFC,” *J. Power Sources*, vol. 131, no. 1–2, pp. 200–206, May 2004, doi: 10.1016/J.JPOWSOUR.2003.12.039.

[80] Z. Tayarani-Yoosefabadi, D. Harvey, J. Bellerive, and E. Kjeang, “Stochastic microstructural modeling of fuel cell gas diffusion layers and numerical determination of transport properties in different liquid water saturation levels,” *J. Power Sources*, vol. 303, pp. 208–221, Jan. 2016, doi: 10.1016/J.JPOWSOUR.2015.11.005.

[81] J. H. Chun *et al.*, “Determination of the pore size distribution of micro porous layer in PEMFC using pore forming agents under various drying conditions,” *Int. J. Hydrogen Energy*, vol. 35, no. 20, pp. 11148–11153, Oct. 2010, doi: 10.1016/J.IJHYDENE.2010.07.056.

[82] J. T. Gostick, M. W. Fowler, M. A. Ioannidis, M. D. Pritzker, Y. M. Volfkovich, and A. Sakars, “Capillary pressure and hydrophilic porosity in gas diffusion layers for polymer electrolyte fuel cells,” *J. Power Sources*, vol. 156, no. 2, pp. 375–387, Jun. 2006, doi: 10.1016/J.JPOWSOUR.2005.05.086.

[83] S. Didari, A. Asadi, Y. Wang, and T. A. L. Harris, “Modeling of composite fibrous porous diffusion media,” 2014, doi: 10.1016/j.ijhydene.2014.04.011.

[84] T. Dubeshter, P. K. Sinha, A. Sakars, G. W. Fly, and J. Jorne, “Measurement of Tortuosity and Porosity of Porous Battery Electrodes,” *J. Electrochem. Soc.*, vol. 161, no. 4, pp. 599–605, 2014, doi: 10.1149/2.073404jes.

[85] M. Espinoza, M. Andersson, J. Yuan, and B. Sundén, “Compress effects on porosity, gas-phase tortuosity, and gas permeability in a simulated PEM gas diffusion layer,” *Int. J. Energy Res.*, vol. 39, no. 11, pp. 1528–1536, Sep. 2015, doi: 10.1002/ER.3348.

[86] I. V Zenyuk, D. Y. Parkinson, L. G. Connolly, and A. Z. Weber, “Gas-diffusion-layer structural properties under compression via X-ray tomography,” 2016, doi: 10.1016/j.jpowsour.2016.08.020.

[87] H. Li *et al.*, “A review of water flooding issues in the proton exchange membrane fuel cell,” *J. Power Sources*, vol. 178, no. 1, pp. 103–117, Mar. 2008, doi: 10.1016/J.JPOWSOUR.2007.12.068.

[88] G. Velayutham, J. Kaushik, N. Rajalakshmi, and K. S. Dhathathreyan, “Effect of PTFE Content in Gas Diffusion Media and Microlayer on the Performance of PEMFC Tested under Ambient Pressure,” *Fuel Cells*, vol. 7, no. 4, pp. 314–318, Aug. 2007, doi: 10.1002/FUCE.200600032.

[89] M. S. Ismail, T. Damjanovic, D. B. Ingham, M. Pourkashanian, and A. Westwood, “Effect of polytetrafluoroethylene-treatment and microporous layer-coating on the electrical conductivity of gas diffusion layers used in proton exchange membrane fuel cells,” *J. Power Sources*, vol. 195, pp. 2700–2708, 2010, doi: 10.1016/j.jpowsour.2009.11.069.

[90] W. Chen and F. Jiang, “Impact of PTFE content and distribution on liquidegas flow in PEMFC carbon paper gas distribution layer: 3D lattice Boltzmann simulations,” 2016, doi: 10.1016/j.ijhydene.2016.02.159.

[91] K. Jiao and X. Li, “Effect of surface dynamic wettability in proton exchange membrane fuel cells,” 2010, doi: 10.1016/j.ijhydene.2010.05.027.

[92] M. Mortazavi and K. Tajiri, “Effect of the PTFE content in the gas diffusion layer on water transport in polymer electrolyte fuel cells (PEFCs),” 2013, doi: 10.1016/j.jpowsour.2013.06.138.

[93] D. Bevers, R. Rogers, and M. Von Bradke, “Examination of the influence of PTFE coating on the properties of carbon paper in polymer electrolyte fuel cells,” *J. Power Sources*, vol. 63, no. 2, pp. 193–201, Dec. 1996, doi: 10.1016/S0378-7753(96)02465-2.

[94] N. Alhazmi, D. Ingham, M. Ismail, K. Hughes, L. Ma, and M. Pourkashanian, “The through-plane thermal conductivity and the contact resistance of the components of the membrane electrode assembly and gas diffusion layer in proton exchange membrane fuel cells,” 2014, doi: 10.1016/j.jpowsour.2014.07.082.

[95] T. Chen, S. Liu, J. Zhang, and M. Tang, “Study on the characteristics of GDL with different PTFE content and its effect on the performance of PEMFC,” 2018, doi: 10.1016/j.ijheatmasstransfer.2018.09.097.

[96] J. Moreira *et al.*, “Innuence of the hydrophobic material content in the gas diiusion electrodes on the performance of a PEM fuel cell,” 2003. [Online]. Available: www.sciencedirect.comwww.elsevier.com/locate/ijhydene.

[97] R. Balzarotti, S. Latorrata, M. Mariani, P. G. Stampino, and G. Dotelli, “Optimization of Perfluoropolyether-Based Gas Diffusion Media Preparation for PEM Fuel Cells,” 2020, doi: 10.3390/en13071831.

[98] D. Sianesi, G. Marchionni, and R. J. De Pasquale, “Perfluoropolyethers (PFPEs) from Perfluoroolefin Photooxidation,” *Organofluor. Chem.*, pp. 431–461, 1994, doi: 10.1007/978-1-4899-1202-2_21.

[99] P. Gallo Stampino *et al.*, “Surface treatments with perfluoropolyether derivatives for the hydrophobization of gas diffusion layers for PEM fuel cells,” *J. Power Sources*, vol. 196, pp. 7645–7648, 2011, doi: 10.1016/j.jpowsour.2011.04.039.

[100] A. Bottino, G. Capannelli, A. Comite, C. Costa, and A. L. Ong, “Microporous layers based on poly(vinylidene fluoride) and sulfonated poly(vinylidene fluoride),” *Int. J. Hydrogen Energy*, vol. 40, no. 42, pp. 14690–14698, Nov. 2015, doi: 10.1016/J.IJHYDENE.2015.08.099.

[101] O. Orogbemi, D. Ingham, M. Ismail, K. Hughes, L. Ma, and M. Pourkashanian, “Through-plane gas permeability of gas diffusion layers and microporous layer: Effects of carbon loading and sintering,” 2017, doi: 10.1016/j.joei.2016.11.008.

[102] M. S. Ismail, D. Borman, T. Damjanovic, D. B. Ingham, and M. Pourkashanian, “On the through-plane permeability of microporous layer-coated gas diffusion layers used in proton exchange membrane fuel cells,” *Int. J. Hydrogen Energy*, vol. 36, no. 16, pp. 10392–10402, Aug. 2011, doi: 10.1016/J.IJHYDENE.2010.09.012.

[103] H. Taira and H. Liu, “In-situ measurements of GDL effective permeability and under-land cross-flow in a PEM fuel cell,” 2012, doi: 10.1016/j.ijhydene.2012.03.030.

[104] M. Hossain, Z. Islam, and P. Pollard, “Investigation of species transport in a gas diffusion layer of a polymer electrolyte membrane fuel cell through two-phase modelling,” 2012, doi: 10.1016/j.renene.2012.10.008.

[105] L. Holzer *et al.*, “Microstructure-property relationships in a gas diffusion layer (GDL)

for Polymer Electrolyte Fuel Cells, Part II: pressure-induced water injection and liquid permeability," 2017, doi: 10.1016/j.electacta.2017.04.141.

[106] P. Rama *et al.*, "A Numerical Study of Structural Change and Anisotropic Permeability in Compressed Carbon Cloth Polymer Electrolyte Fuel Cell Gas Diffusion Layers," *Fuel Cells*, vol. 11, no. 2, pp. 274–285, Apr. 2011, doi: 10.1002/FUCE.201000037.

[107] F. S. Nanadegani, E. N. Lay, and B. Sunden, "Effects of an MPL on water and thermal management in a PEMFC," *Int. J. Energy Res.*, vol. 43, no. 1, pp. 274–296, Jan. 2019, doi: 10.1002/ER.4262.

[108] M. S. Ismail, D. B. Ingham, K. J. Hughes, L. Ma, and M. Pourkashanian, "Effective diffusivity of polymer electrolyte fuel cell gas diffusion layers: An overview and numerical study," 2015, doi: 10.1016/j.ijhydene.2015.06.073.

[109] Y. Gao, A. Montana, and F. Chen, "Evaluation of porosity and thickness on effective diffusivity in gas diffusion layer," 2016, doi: 10.1016/j.jpowsour.2016.12.052.

[110] P. Mangal *et al.*, "Experimental study of mass transport in PEMFCs: Through plane permeability and molecular diffusivity in GDLs," *Electrochim. Acta*, vol. 167, pp. 160–171, 2015, doi: 10.1016/j.electacta.2015.03.100.

[111] E. Sadeghi, N. Djilali, and M. Bahrami, "Effective thermal conductivity and thermal contact resistance of gas diffusion layers in proton exchange membrane fuel cells. Part 1: Effect of compressive load," *J. Power Sources*, vol. 196, pp. 246–254, 2011, doi: 10.1016/j.jpowsour.2010.06.039.

[112] G. Maggio ', V. Recupero, and C. Mantegazza, "Modelling of temperature distribution in a solid polymer electrolyte fuel cell stack," 1996.

[113] Y. Shan and S.-Y. Choe, "A high dynamic PEM fuel cell model with temperature effects," *J. Power Sources*, vol. 145, pp. 30–39, 2005, doi: 10.1016/j.jpowsour.2004.12.033.

[114] E. Nikooee, G. Karimi, and X. Li, "Determination of the effective thermal conductivity of gas diffusion layers in polymer electrolyte membrane fuel cells: A comprehensive fractal approach," *Int. J. Energy Res.*, vol. 35, no. 15, pp. 1351–1359, Dec. 2011, doi: 10.1002/ER.1896.

[115] E. Sadeghi, M. Bahrami, and N. Djilali, "Analytic determination of the effective thermal conductivity of PEM fuel cell gas diffusion layers," *J. Power Sources*, vol. 179, pp. 200–208, 2008, doi: 10.1016/j.jpowsour.2007.12.058.

[116] J. Ramousse, S. Didierjean, O. Lottin, and D. Maillet, "Estimation of the effective thermal conductivity of carbon felts used as PEMFC Gas Diffusion Layers," *Int. J. Therm. Sci.*, vol. 47, pp. 1–6, 2008, doi: 10.1016/j.ijthermalsci.2007.01.018.

[117] M. Khandelwal and M. M. Mench, "Direct measurement of through-plane thermal conductivity and contact resistance in fuel cell materials," *J. Power Sources*, vol. 161, pp. 1106–1115, 2006, doi: 10.1016/j.jpowsour.2006.06.092.

[118] G. Karimi, X. Li, and P. Teertstra, "Measurement of through-plane effective thermal conductivity and contact resistance in PEM fuel cell diffusion media," *Electrochim. Acta*, vol. 55, no. 5, pp. 1619–1625, Feb. 2010, doi: 10.1016/J.ELECTACTA.2009.10.035.

[119] H. Sadeghifar, N. Djilali, and M. Bahrami, “Effect of Polytetrafluoroethylene (PTFE) and micro porous layer (MPL) on thermal conductivity of fuel cell gas diffusion layers: Modeling and experiments,” 2013, doi: 10.1016/j.jpowsour.2013.09.136.

[120] G. Unsworth, N. Zamel, and X. Li, “Through-plane thermal conductivity of the microporous layer in a polymer electrolyte membrane fuel cell,” 2011, doi: 10.1016/j.ijhydene.2011.12.012.

[121] R. B. Ferreira, D. S. Falcão, V. B. Oliveira, and A. M. F. R. Pinto, “Experimental study on the membrane electrode assembly of a proton exchange membrane fuel cell: effects of microporous layer, membrane thickness and gas diffusion layer hydrophobic treatment,” *Electrochim. Acta*, vol. 224, pp. 337–345, Jan. 2017, doi: 10.1016/J.ELECTACTA.2016.12.074.

[122] I. Nitta, T. Hottinen, O. Himanen, and M. Mikkola, “Inhomogeneous compression of PEMFC gas diffusion layer Part I. Experimental,” *J. Power Sources*, vol. 171, pp. 26–36, 2007, doi: 10.1016/j.jpowsour.2006.10.076.

[123] Ö. Aydin, M. Zedda, and N. Zamel, “Challenges Associated with Measuring the Intrinsic Electrical Conductivity of Carbon Paper Diffusion Media,” *Fuel Cells*, vol. 15, no. 3, pp. 537–544, Jun. 2015, doi: 10.1002/FUCE.201400125.

[124] M. S. Ismail, D. B. Ingham, L. Ma, and M. Pourkashanian, “The contact resistance between gas diffusion layers and bipolar plates as they are assembled in proton exchange membrane fuel cells,” *Renew. Energy*, vol. 52, pp. 40–45, Apr. 2013, doi: 10.1016/j.renene.2012.10.025.

[125] D. Ye, E. Gauthier, J. B. Benziger, and M. Pan, “Bulk and contact resistances of gas diffusion layers in proton exchange membrane fuel cells,” 2014, doi: 10.1016/j.jpowsour.2014.01.082.

[126] A. Ozden, I. E. Alaefour, S. Shahgaldi, X. Li, C. O. Colpan, and F. Hamdullahpur, “Gas Diffusion Layers for PEM Fuel Cells: Ex- and In-Situ Characterization,” *Exergetic, Energ. Environ. Dimens.*, pp. 695–727, 2018, doi: 10.1016/B978-0-12-813734-5.00040-8.

[127] E. Antolini, “Carbon supports for low-temperature fuel cell catalysts,” *Appl. Catal. B Environ.*, vol. 88, no. 1–2, pp. 1–24, Apr. 2009, doi: 10.1016/J.APCATB.2008.09.030.

[128] J. P. Owejan, J. E. Owejan, W. Gu, T. A. Trabold, T. W. Tighe, and M. F. Mathias, “Water Transport Mechanisms in PEMFC Gas Diffusion Layers,” 2010, doi: 10.1149/1.3468615.

[129] X. Wang, Y.-T. Liu, X.-F. Zhang, H. Song, and G.-P. Wu, “Effects of the carbon black properties in gas diffusion layer on the performance of proton exchange membrane fuel cells,” 2023, doi: 10.1016/j.ijhydene.2023.04.056.

[130] E. Antolini, R. R. Passos, and E. A. Ticianelli, “Effects of the carbon powder characteristics in the cathode gas diffusion layer on the performance of polymer electrolyte fuel cells,” 2002.

[131] Z. Chen, W. Pan, L. Tang, X. Chen, and F. Wang, “Journal Pre-proof Effect of carbon material and surfactant on ink property and resulting surface cracks of fuel cell microporous layers Effect of carbon material and surfactant on ink property and resulting surface cracks of fuel cell microporous layers Article Effect of carbon

material and surfactant on ink property and resulting surface cracks of fuel cell microporous layers," *Chinese J. Chem. Eng.*, 2024, doi: 10.1016/j.cjche.2024.01.023.

[132] L. R. Jordan, A. K. Shukla, T. Behrsing, N. R. Avery, B. C. Muddle, and M. Forsyth, "Effect of diffusion-layer morphology on the performance of polymer electrolyte fuel cells operating at atmospheric pressure."

[133] L. R. Jordan, A. K. Shukla, T. Behrsing, N. R. Avery, B. C. Muddle, and M. Forsyth, "Diffusion layer parameters influencing optimal fuel cell performance," *J. Power Sources*, vol. 86, no. 1–2, pp. 250–254, Mar. 2000, doi: 10.1016/S0378-7753(99)00489-9.

[134] J. Zhang, *PEM Fuel Cell Electrocatalysts and Catalyst Layers: Fundamentals and Applications*. Springer Science & Business Media, 2008.

[135] E. Akbari and Z. Buntat, "Benefits of using carbon nanotubes in fuel cells: a review," 2016, doi: 10.1002/er.3600.

[136] Y. Gao, G. Q. Sun, S. L. Wang, and S. Zhu, "Carbon nanotubes based gas diffusion layers in direct methanol fuel cells," *Energy*, vol. 35, no. 3, pp. 1455–1459, Mar. 2010, doi: 10.1016/j.energy.2009.11.031.

[137] A. M. Kannan, P. Kanagala, and V. Veedu, "Development of carbon nanotubes based gas diffusion layers by in situ chemical vapor deposition process for proton exchange membrane fuel cells," *J. Power Sources*, vol. 192, no. 2, pp. 297–303, Jul. 2009, doi: 10.1016/J.JPOWSOUR.2009.03.022.

[138] Z. Tang, C. K. Poh, Z. Tian, J. Lin, H. Y. Ng, and D. H. C. Chua, "In situ grown carbon nanotubes on carbon paper as integrated gas diffusion and catalyst layer for proton exchange membrane fuel cells," *Electrochim. Acta*, vol. 56, no. 11, pp. 4327–4334, Apr. 2011, doi: 10.1016/J.ELECTACTA.2011.01.035.

[139] H.-Y. Du *et al.*, "High performance of catalysts supported by directly grown PTFE-free micro-porous CNT layer in a proton exchange membrane fuel cell," *J. Mater. Chem.*, vol. 21, no. 8, pp. 2512–2516, Feb. 2011, doi: 10.1039/C0JM03215H.

[140] R. Schweiss, M. Steeb, P. M. Wilde, and T. Schubert, "Enhancement of proton exchange membrane fuel cell performance by doping microporous layers of gas diffusion layers with multiwall carbon nanotubes," 2012, doi: 10.1016/j.jpowsour.2012.07.078.

[141] H. Su and Y. H. Hu, "Recent advances in graphene-based materials for fuel cell applications," *Energy Sci. Eng.*, vol. 9, no. 7, pp. 958–983, Jul. 2021, doi: 10.1002/ESE3.833.

[142] M. J. Leeuwner, D. P. Wilkinson, and E. L. Gyenge, "Novel Graphene Foam Microporous Layers for PEM Fuel Cells: Interfacial Characteristics and Comparative Performance," 2015, doi: 10.1002/fuce.201500031.

[143] A. Ozden, S. Shahgaldi, J. Zhao, X. Li, and F. Hamdullahpur, "Assessment of graphene as an alternative microporous layer material for proton exchange membrane fuel cells," 2017, doi: 10.1016/j.fuel.2017.11.109.

[144] A. Arvay *et al.*, "Characterization techniques for gas diffusion layers for proton exchange membrane fuel cells e A review," 2012, doi: 10.1016/j.jpowsour.2012.04.026.

[145] D. Spernjak *et al.*, “Enhanced Water Management of Polymer Electrolyte Fuel Cells with Additive-Containing Microporous Layers,” *ACS Appl. Energy Mater.*, vol. 1, no. 11, pp. 6006–6017, Nov. 2018, doi: 10.1021/ACSAEM.8B01059/ASSET/IMAGES/LARGE/AE-2018-010594_0008.JPEG.

[146] S. Hou *et al.*, “Enhanced low-humidity performance in a proton exchange membrane fuel cell by developing a novel hydrophilic gas diffusion layer,” *Int. J. Hydrogen Energy*, vol. 45, no. 1, pp. 937–944, Jan. 2020, doi: 10.1016/J.IJHYDENE.2019.10.160.

[147] R. Schweiss, M. Steeb, and P. M. Wilde, “Mitigation of Water Management in PEM Fuel Cell Cathodes by Hydrophilic Wicking Microporous Layers,” *Fuel Cells*, vol. 10, no. 6, pp. 1176–1180, Dec. 2010, doi: 10.1002/FUCE.201000003.

[148] R. Mukundan *et al.*, “Effect of Hydrophilic Treatment of Microporous Layer on Fuel Cell Performance,” *ECS Trans.*, vol. 33, no. 1, pp. 1109–1114, Oct. 2010, doi: 10.1149/1.3484604/XML.

[149] M. Ahn, Y. H. Cho, Y. H. Cho, J. Kim, N. Jung, and Y. E. Sung, “Influence of hydrophilicity in micro-porous layer for polymer electrolyte membrane fuel cells,” *Electrochim. Acta*, vol. 56, no. 5, pp. 2450–2457, Feb. 2011, doi: 10.1016/J.ELECTACTA.2010.11.063.

[150] C. Simon, J. Endres, B. Nefzger-Loders, F. Wilhelm, and H. A. Gasteiger, “Interaction of Pore Size and Hydrophobicity/Hydrophilicity for Improved Oxygen and Water Transport through Microporous Layers,” *J. Electrochem. Soc.*, vol. 166, no. 13, p. F1022, Sep. 2019, doi: 10.1149/2.1111913JES.

[151] T. Kitahara, H. Nakajima, and K. Mori, “Hydrophilic and hydrophobic double microporous layer coated gas diffusion layer for enhancing performance of polymer electrolyte fuel cells under no-humidification at the cathode,” *J. Power Sources*, vol. 199, pp. 29–36, Feb. 2012, doi: 10.1016/J.JPOWSOUR.2011.10.002.

[152] T. Kitahara, H. Nakajima, M. Inamoto, and M. Morishita, “Novel hydrophilic and hydrophobic double microporous layer coated gas diffusion layer to enhance performance of polymer electrolyte fuel cells under both low and high humidity,” *J. Power Sources*, vol. 234, pp. 129–138, Jul. 2013, doi: 10.1016/J.JPOWSOUR.2013.01.150.

[153] T. Kitahara, H. Nakajima, M. Inamoto, and K. Shinto, “Triple microporous layer coated gas diffusion layer for performance enhancement of polymer electrolyte fuel cells under both low and high humidity conditions,” *J. Power Sources*, vol. 248, pp. 1256–1263, Feb. 2014, doi: 10.1016/J.JPOWSOUR.2013.10.066.

[154] S. Hirakata *et al.*, “Effects of Gas Diffusion Electrodes with Hydrophilic Layer on Cold Start Behavior and Cell Performance of Polymer Membrane Fuel Cells,” 2012.

[155] S. Hirakata *et al.*, “Investigation of the effect of a hydrophilic layer in the gas diffusion layer of a polymer electrolyte membrane fuel cell on the cell performance and cold start behaviour,” *Electrochim. Acta*, vol. 120, pp. 240–247, Feb. 2014, doi: 10.1016/J.ELECTACTA.2013.12.050.

[156] J. H. Chun *et al.*, “Development of a novel hydrophobic/hydrophilic double micro porous layer for use in a cathode gas diffusion layer in PEMFC,” *Int. J. Hydrogen*

Energy, vol. 36, no. 14, pp. 8422–8428, Jul. 2011, doi: 10.1016/J.IJHYDENE.2011.04.038.

[157] F. B. Weng, C. Y. Hsu, and M. C. Su, "Experimental study of micro-porous layers for PEMFC with gradient hydrophobicity under various humidity conditions," *Int. J. Hydrogen Energy*, vol. 36, no. 21, pp. 13708–13714, Oct. 2011, doi: 10.1016/J.IJHYDENE.2011.07.141.

[158] T. Kitahara, T. Konomi, and H. Nakajima, "Microporous layer coated gas diffusion layers for enhanced performance of polymer electrolyte fuel cells," *J. Power Sources*, vol. 195, no. 8, pp. 2202–2211, Apr. 2010, doi: 10.1016/j.jpowsour.2009.10.089.

[159] P. Deevanhxay, T. Sasabe, S. Tsushima, and S. Hirai, "Effect of liquid water distribution in gas diffusion media with and without microporous layer on PEM fuel cell performance," 2013, doi: 10.1016/j.elecom.2013.07.001.

[160] E. E. Barus, A. C. Louk, S. Gauthier, S. I. Abarzhi, and K. R. Sreenivasan, "Synchrotron Investigation of Microporous Layer Thickness on Liquid Water Distribution in a PEM Fuel Cell You may also like Fabrication And Analysis Of 3d Wind Sonic Using A Dual Transduser Sensor Arrangement," doi: 10.1149/2.0221507jes.

[161] J. M. Morgan and R. Datta, "Understanding the gas diffusion layer in proton exchange membrane fuel cells. I. How its structural characteristics affect diffusion and performance," 2013, doi: 10.1016/j.jpowsour.2013.09.090.

[162] P. Antonacci, S. Chevalier, J. Lee, R. Yip, N. Ge, and A. Bazylak, "Feasibility of combining electrochemical impedance spectroscopy and synchrotron X-ray radiography for determining the influence of liquid water on polymer electrolyte membrane fuel cell performance," *Int. J. Hydrogen Energy*, vol. 40, no. 46, pp. 16494–16502, Dec. 2015, doi: 10.1016/J.IJHYDENE.2015.10.008.

[163] P. Antonacci *et al.*, "Balancing mass transport resistance and membrane resistance when tailoring microporous layer thickness for polymer electrolyte membrane fuel cells operating at high current densities," *Electrochim. Acta*, vol. 188, pp. 888–897, Jan. 2016, doi: 10.1016/J.ELECTACTA.2015.11.115.

[164] A. Z. Weber and J. Newman, "Effects of Microporous Layers in Polymer Electrolyte Fuel Cells," *J Electrochem Soc*, 2005, doi: 10.1149/1.1861194.

[165] S. Park, J. W. Lee, and B. N. Popov, "Effect of carbon loading in microporous layer on PEM fuel cell performance," *J. Power Sources*, vol. 163, no. 1, pp. 357–363, Dec. 2006, doi: 10.1016/J.JPOWSOUR.2006.09.020.

[166] U. Pasaogullari and C. Y. Wang, "Two-phase transport and the role of micro-porous layer in polymer electrolyte fuel cells," *Electrochim. Acta*, vol. 49, no. 25, pp. 4359–4369, Oct. 2004, doi: 10.1016/J.ELECTACTA.2004.04.027.

[167] D. Gerteisen, T. Heilmann, and C. Ziegler, "Enhancing liquid water transport by laser perforation of a GDL in a PEM fuel cell," *J. Power Sources*, vol. 177, pp. 348–354, 2008, doi: 10.1016/j.jpowsour.2007.11.080.

[168] M. P. Manahan, J. T. Clement, A. K. Srouji, S. W. Brown, T. Reutzel, and M. M. Mench, "Laser Modified Fuel Cell Diffusion Media: Engineering Enhanced Performance via Localized Water Redistribution," *J. Electrochem. Soc*, vol. 161, p.

1061, 2014, doi: 10.1149/2.0591410jes.

[169] Z. Lu, J. Waldecker, X. Xie, M.-C. Lai, D. S. Hussey, and D. L. Jacobson, "Investigation of Water Transport in Perforated Gas Diffusion Layer by Neutron Radiography," *ECS Trans.*, vol. 58, no. 1, p. 315, Aug. 2013, doi: 10.1149/05801.0315ECST.

[170] H. Markötter *et al.*, "Influence of cracks in the microporous layer on the water distribution in a PEM fuel cell investigated by synchrotron radiography," 2013, doi: 10.1016/j.elecom.2013.04.006.

[171] C. Simon, D. Kartouzian, D. Müller, F. Wilhelm, and H. A. Gasteiger, "Impact of Microporous Layer Pore Properties on Liquid Water Transport in PEM Fuel Cells: Carbon Black Type and Perforation," *J. Electrochem. Soc.*, vol. 164, no. 14, pp. F1697–F1711, Dec. 2017, doi: 10.1149/2.1321714JES/XML.

[172] J. H. Chun *et al.*, "Development of a porosity-graded micro porous layer using thermal expandable graphite for proton exchange membrane fuel cells," *Renew. Energy*, vol. 58, pp. 28–33, Oct. 2013, doi: 10.1016/J.RENENE.2013.02.025.

[173] H. Tang, S. Wang, M. Pan, and R. Yuan, "Porosity-graded micro-porous layers for polymer electrolyte membrane fuel cells," *J. Power Sources*, vol. 166, no. 1, pp. 41–46, Mar. 2007, doi: 10.1016/J.JPOWSOUR.2007.01.021.

[174] T. Ha *et al.*, "Experimental study on carbon corrosion of the gas diffusion layer in polymer electrolyte membrane fuel cells," 2011, doi: 10.1016/j.ijhydene.2011.06.098.

[175] T. Arlt, M. Klages, M. Messerschmidt, J. Scholta, and I. Manke, "Influence of artificially aged gas diffusion layers on the water management of polymer electrolyte membrane fuel cells analyzed with in-operando synchrotron imaging," 2016, doi: 10.1016/j.energy.2016.10.061.

[176] H. Liu *et al.*, "Accelerated Degradation of Polymer Electrolyte Membrane Fuel Cell Gas Diffusion Layers," *J. Electrochem. Soc.*, vol. 164, no. 7, p. F704, May 2017, doi: 10.1149/2.0081707JES.

[177] J. Wu *et al.*, "In situ accelerated degradation of gas diffusion layer in proton exchange membrane fuel cell Part I: Effect of elevated temperature and flow rate," *J. Power Sources*, vol. 195, pp. 1888–1894, 2010, doi: 10.1016/j.jpowsour.2009.10.022.

[178] V. Radhakrishnan and P. Haridoss, "Effect of cyclic compression on structure and properties of a Gas Diffusion Layer used in PEM fuel cells," 2010, doi: 10.1016/j.ijhydene.2010.07.009.

[179] Y. Yang, X. Zhou, B. Li, and C. Zhang, "Recent progress of the gas diffusion layer in proton exchange membrane fuel cells: Material and structure designs of microporous layer," *Int. J. Hydrogen Energy*, vol. 46, no. 5, pp. 4259–4282, Jan. 2021, doi: 10.1016/J.IJHYDENE.2020.10.185.

[180] T. Bednarek and G. Tsotridis, "Issues associated with modelling of proton exchange membrane fuel cell by computational fluid dynamics," *J. Power Sources*, vol. 343, pp. 550–563, Mar. 2017, doi: 10.1016/J.JPOWSOUR.2017.01.059.

[181] T. Swamy, E. C. Kumbur, and M. M. Mench, "Characterization of Interfacial Structure in PEFCs: Water Storage and Contact Resistance Model," *J. Electrochem. Soc.*, 2009, doi: 10.1149/1.3247585.

[182] C. J. Netwall, B. D. Gould, J. A. Rodgers, N. J. Nasello, and K. E. Swider-Lyons, "Decreasing contact resistance in proton-exchange membrane fuel cells with metal bipolar plates," *J. Power Sources*, vol. 227, pp. 137–144, Apr. 2013, doi: 10.1016/j.jpowsour.2012.11.012.

[183] W. Schmittinger and A. Vahidi, "A review of the main parameters influencing long-term performance and durability of PEM fuel cells," *Journal of Power Sources*, vol. 180, no. 1. Elsevier, pp. 1–14, May 15, 2008, doi: 10.1016/j.jpowsour.2008.01.070.

[184] F. E. Hizir, S. O. Ural, E. C. Kumbur, and M. M. Mench, "Characterization of interfacial morphology in polymer electrolyte fuel cells: Micro-porous layer and catalyst layer surfaces," *J. Power Sources*, vol. 195, no. 11, pp. 3463–3471, Jun. 2010, doi: 10.1016/J.JPOWSOUR.2009.11.032.

[185] H. Tawfik, Y. Hung, and D. Mahajan, "Metal bipolar plates for PEM fuel cell—A review," *J. Power Sources*, vol. 163, no. 2, pp. 755–767, Jan. 2007, doi: 10.1016/J.JPOWSOUR.2006.09.088.

[186] E. Alizadeh, M. Ghadimi, M. M. Barzegari, M. Momenifar, and S. H. M. Saadat, "Development of contact pressure distribution of PEM fuel cell's MEA using novel clamping mechanism," *Energy*, vol. 131, pp. 92–97, Jul. 2017, doi: 10.1016/j.energy.2017.05.036.

[187] A. S. Gago *et al.*, "Protective coatings on stainless steel bipolar plates for proton exchange membrane (PEM) electrolysers," 2016, doi: 10.1016/j.jpowsour.2015.12.071.

[188] L. Zhang, Y. Liu, H. Song, S. Wang, Y. Zhou, and S. J. Hu, "Estimation of contact resistance in proton exchange membrane fuel cells," *J. Power Sources*, vol. 162, pp. 1165–1171, 2006, doi: 10.1016/j.jpowsour.2006.07.070.

[189] X. Lai, an Liu, L. Peng, and J. Ni, "A mechanical-electrical finite element method model for predicting contact resistance between bipolar plate and gas diffusion layer in PEM fuel cells," *J. Power Sources*, vol. 182, pp. 153–159, 2008, doi: 10.1016/j.jpowsour.2008.03.069.

[190] H. Wang, M. A. Sweikart, and J. A. Turner, "Stainless steel as bipolar plate material for polymer electrolyte membrane fuel cells," 2002, doi: 10.1016/S0378-7753(03)00023-5.

[191] P. Zhou, C. W. Wu, and G. J. Ma, "Contact resistance prediction and structure optimization of bipolar plates," *J. Power Sources*, vol. 159, no. 2, pp. 1115–1122, Sep. 2006, doi: 10.1016/J.JPOWSOUR.2005.12.080.

[192] E. Sadeghi, N. Djilali, and M. Bahrami, "Effective thermal conductivity and thermal contact resistance of gas diffusion layers in proton exchange membrane fuel cells. Part 2: Hysteresis effect under cyclic compressive load," *J. Power Sources*, vol. 195, no. 24, pp. 8104–8109, Dec. 2010, doi: 10.1016/J.JPOWSOUR.2010.07.051.

[193] I. Nitta, O. Himanen, and M. Mikkola, "Contact resistance between gas diffusion layer and catalyst layer of PEM fuel cell," 2007, doi: 10.1016/j.elecom.2007.10.029.

[194] R. Makharia, M. F. Mathias, and D. R. Baker, "Measurement of Catalyst Layer Electrolyte Resistance in PEFCs Using Electrochemical Impedance Spectroscopy," *J. Electrochem. Soc.*, vol. 152, no. 5, p. A970, 2005, doi: 10.1149/1.1888367.

[195] G. R. Molaeimanesh, M. Nazemian, and M. S. Student, “Investigation of GDL compression effects on the performance of a PEM fuel cell cathode by lattice Boltzmann method,” 2017, doi: 10.1016/j.jpowsour.2017.05.078.

[196] D. Cha, J. H. Ahn, H. S. Kim, and Y. Kim, “Effects of clamping force on the water transport and performance of a PEM (proton electrolyte membrane) fuel cell with relative humidity and current density,” 2015, doi: 10.1016/j.energy.2015.10.045.

[197] J. Millichamp *et al.*, “Mechanisms and effects of mechanical compression and dimensional change in polymer electrolyte fuel cells e A review,” 2015, doi: 10.1016/j.jpowsour.2015.02.111.

[198] A. Vikram, P. R. Chowdhury, R. K. Phillips, and M. Hoorfar, “Measurement of effective bulk and contact resistance of gas diffusion layer under inhomogeneous compression e Part I: Electrical conductivity,” 2016, doi: 10.1016/j.jpowsour.2016.04.110.

[199] W. R. Chang, J. J. Hwang, F. B. Weng, and S. H. Chan, “Effect of clamping pressure on the performance of a PEM fuel cell,” *J. Power Sources*, vol. 166, pp. 149–154, 2007, doi: 10.1016/j.jpowsour.2007.01.015.

[200] C. Simon, F. Hasché, and H. A. Gasteiger, “Influence of the Gas Diffusion Layer Compression on the Oxygen Transport in PEM Fuel Cells at High Water Saturation Levels,” *J. Electrochem. Soc.*, vol. 164, no. 6, pp. F591–F599, Mar. 2017, doi: 10.1149/2.0691706JES/XML.

[201] A. Bates *et al.*, “Simulation and experimental analysis of the clamping pressure distribution in a PEM fuel cell stack,” 2013, doi: 10.1016/j.ijhydene.2013.03.049.

[202] D. Chen and H. Peng, “A Thermodynamic Model of Membrane Humidifiers for PEM Fuel Cell Humidification Control,” 2005, doi: 10.1115/1.1978910.

[203] F. Aldakheel *et al.*, “Gas permeability, wettability and morphology of gas diffusion layers before and after performing a realistic ex-situ compression test,” *Renew. Energy*, vol. 151, pp. 1082–1091, May 2020, doi: 10.1016/J.RENENE.2019.11.109.

[204] A. Z. Weber and J. Newman, “Effects of Microporous Layers in Polymer Electrolyte Fuel Cells,” 2005, doi: 10.1149/1.1861194.

[205] I. C. Okereke, M. S. Ismail, D. B. Ingham, K. Hughes, L. Ma, and M. Pourkashanian, “Single- and Double-Sided Coated Gas Diffusion Layers Used in Polymer Electrolyte Fuel Cells: A Numerical Study,” *Energies*, vol. 16, no. 11, p. 4363, Jun. 2023, doi: 10.3390/EN16114363/S1.

[206] A. Ozden, I. E. Alaefour, S. Shahgaldi, X. Li, C. O. Colpan, and F. Hamdullahpur, “Gas Diffusion Layers for PEM Fuel Cells: Ex- and In-Situ Characterization,” *Exergetic, Energ. Environ. Dimens.*, pp. 695–727, Jan. 2018, doi: 10.1016/B978-0-12-813734-5.00040-8.

[207] H. Giesche, “Mercury porosimetry: A general (practical) overview,” *Part. Part. Syst. Charact.*, vol. 23, no. 1, pp. 9–19, Jun. 2006, doi: 10.1002/PPSC.200601009.

[208] Z. Fang, A. G. Star, and T. F. Fuller, “Effect of Carbon Corrosion on Wettability of PEM Fuel Cell Electrodes,” *J. Electrochem. Soc.*, vol. 166, no. 12, pp. F709–F715, 2019, doi: 10.1149/2.0231912JES.

[209] F. M. Smits, “Measurement of Sheet Resistivities with the Four-Point Probe,” *Bell Syst. Tech. J.*, vol. 37, no. 3, pp. 711–718, 1958, doi: 10.1002/J.1538-7305.1958.TB03883.X.

[210] M. Mench and E. C. Kumbur, *Polymer Electrolyte Fuel Cell Degradation*. Academic Press, 2011.

[211] F. C. Lee *et al.*, “Alternative architectures and materials for PEMFC gas diffusion layers: A review and outlook,” *Renew. Sustain. Energy Rev.*, vol. 166, p. 112640, Sep. 2022, doi: 10.1016/J.RSER.2022.112640.

[212] S. Litster, D. Sinton, and N. Djilali, “Ex situ visualization of liquid water transport in PEM fuel cell gas diffusion layers,” *J. Power Sources*, vol. 154, no. 1, pp. 95–105, Mar. 2006, doi: 10.1016/J.JPOWSOUR.2005.03.199.

[213] R. R. Rashapov, J. Unno, and J. T. Gostick, “Characterization of PEMFC Gas Diffusion Layer Porosity,” *J. Electrochem. Soc.*, vol. 162, no. 6, pp. F603–F612, Mar. 2015, doi: 10.1149/2.0921506JES/XML.

[214] Y. Zhai, H. Zhang, J. Hu, and B. Yi, “Preparation and characterization of sulfated zirconia (SO42−/ZrO2)/Nafion composite membranes for PEMFC operation at high temperature/low humidity,” *J. Memb. Sci.*, vol. 280, no. 1–2, pp. 148–155, Sep. 2006, doi: 10.1016/J.MEMSCI.2006.01.028.

[215] G. Gnana Kumar, A. R. Kim, K. Suk Nahm, and R. Elizabeth, “Nafion membranes modified with silica sulfuric acid for the elevated temperature and lower humidity operation of PEMFC,” *Int. J. Hydrogen Energy*, vol. 34, no. 24, pp. 9788–9794, Dec. 2009, doi: 10.1016/J.IJHYDENE.2009.09.083.

[216] A. Z. Weber and J. Newman, “Effects of Microporous Layers in Polymer Electrolyte Fuel Cells,” *J. Electrochem. Soc.*, vol. 152, no. 4, p. A677, Mar. 2005, doi: 10.1149/1.1861194.

[217] J. T. Gostick, M. A. Ioannidis, M. W. Fowler, and M. D. Pritzker, “On the role of the microporous layer in PEMFC operation,” *Electrochem. commun.*, vol. 11, no. 3, pp. 576–579, Mar. 2009, doi: 10.1016/J.ELECOM.2008.12.053.

[218] H. Zamora, P. Cañizares, M. A. Rodrigo, and J. Lobato, “Improving of Micro Porous Layer based on Advanced Carbon Materials for High Temperature Proton Exchange Membrane Fuel Cell Electrodes,” doi: 10.1002/fuce.201400139.

[219] A. Ta heri Najafabadi, M. J. Leeuwner, D. P. avid Wilkinson, and dLG yenge, “Electrochemically Produced Graphene for Microporous Layers in Fuel Cells,” doi: 10.1002/cssc.201600351.

[220] A. Ozden, S. Shahgaldi, X. Li, and F. Hamdullahpur, “A graphene-based microporous layer for proton exchange membrane fuel cells: Characterization and performance comparison,” 2018, doi: 10.1016/j.renene.2018.03.065.

[221] M. Mariani, S. Latorrata, S. Patrignani, P. Gallo Stampino, and G. Dotelli, “Characterization of novel graphene-based microporous layers for Polymer Electrolyte Membrane Fuel Cells operating under low humidity and high temperature,” *Int. J. Hydrogen Energy*, vol. 45, no. 11, pp. 7046–7058, Feb. 2020, doi: 10.1016/J.IJHYDENE.2019.12.213.

[222] M. J. Leeuwner, A. Patra, D. P. Wilkinson, and E. L. Gyenge, “Graphene and reduced

graphene oxide based microporous layers for high-performance proton-exchange membrane fuel cells under varied humidity operation," *J. Power Sources*, vol. 423, pp. 192–202, May 2019, doi: 10.1016/J.JPOWSOUR.2019.03.048.

[223] F. C. Lee *et al.*, "Optimisation and characterisation of graphene-based microporous layers for polymer electrolyte membrane fuel cells," *Int. J. Hydrogen Energy*, May 2023, doi: 10.1016/J.IJHYDENE.2023.05.003.

[224] S. Park *et al.*, "Design of graphene sheets-supported Pt catalyst layer in PEM fuel cells," *Electrochem. commun.*, vol. 13, no. 3, pp. 258–261, Mar. 2011, doi: 10.1016/J.ELECOM.2010.12.028.

[225] F. Ruscillo *et al.*, "Characterisation of Novel and High Performing Double-Sided Microporous-Layers-Coated Gas Diffusion Layers for Polymer Electrolyte Membrane Fuel Cells," *Energies 2023, Vol. 16, Page 7601*, vol. 16, no. 22, p. 7601, Nov. 2023, doi: 10.3390/EN16227601.

[226] Z. Chen *et al.*, "Crack evolution during the film drying process of fuel cell microporous layer ink," *Colloids Surfaces A Physicochem. Eng. Asp.*, vol. 650, p. 129283, Oct. 2022, doi: 10.1016/J.COLSURFA.2022.129283.

[227] J. Park, H. Oh, Y. Il Lee, K. Min, E. Lee, and J. Y. Jyoung, "Effect of the pore size variation in the substrate of the gas diffusion layer on water management and fuel cell performance," *Appl. Energy*, vol. 171, pp. 200–212, Jun. 2016, doi: 10.1016/J.APENERGY.2016.02.132.

[228] C. S. Kong, D. Y. Kim, H. K. Lee, Y. G. Shul, and T. H. Lee, "Influence of pore-size distribution of diffusion layer on mass-transport problems of proton exchange membrane fuel cells," *J. Power Sources*, vol. 108, no. 1–2, pp. 185–191, Jun. 2002, doi: 10.1016/S0378-7753(02)00028-9.

[229] J. Liu, C. Yang, C. Liu, F. Wang, and Y. Song, "Design of Pore Structure in Gas Diffusion Layers for Oxygen Depolarized Cathode and Their Effect on Activity for Oxygen Reduction Reaction," 2014, doi: 10.1021/ie403975r.

[230] T. Li *et al.*, "Preparation of hierarchical-pore gas diffusion layer for fuel cell," *J. Mater. Sci.*, vol. 55, no. 11, pp. 4558–4569, Apr. 2020, doi: 10.1007/S10853-019-04323-9/FIGURES/9.

[231] T. Tanuma, M. Kawamoto, and S. Kinoshita, "Effect of Properties of Hydrophilic Microporous Layer (MPL) on PEFC Performance," *J. Electrochem. Soc.*, vol. 164, no. 6, pp. F499–F503, Mar. 2017, doi: 10.1149/2.0371706JES/XML.

Appendix

Appendix A: Presentations and Prizes

Table A-1 Oral and poster presentations.

Type of Presentation	Event	Date	Location
Oral	CDT Winter School	September 2021	University of Nottingham
Poster	1st UK-Japan Symposium on Advanced Materials for Hydrogen and Fuel Cells	December 2021	University of Sheffield
Oral	CDT Spring School	April 2022	University of Cardiff
Poster	6th RSC Energy Sector Early Career Symposium Royal Society of Chemistry	November 2022	Burlington House, London
Oral	Your Entrepreneurs Scheme 22	December 2022	University of Nottingham
Oral	CDT Spring School	May 2023	University of Sheffield
Oral	The 2nd FERIA Conference, the European Conference on Fuel and Energy Research and Its Applications	September 2023	University of Sheffield
Poster	2nd UK-Japan Symposium on Advanced Materials for Hydrogen and Fuel Cells	January 2024	University of Hull
Poster	UK Energy Storage Conference	April 2024	University of Nottingham
Poster	All-Energy and Dcarbonise	May 2024	SEC Glasgow

Awards and Prizes

6th RSC Energy Sector Early Career Symposium, November 2022 – 3rd place

Renewable Energy Hackathon at The University of Sheffield, November 2023 – 1st place

Appendix B: Resilient Decarbonised Fuel Energy Systems Centre for Doctoral Training Work Completed

This EngD is part of the Centre for Doctoral Training (CDT) in Resilient Decarbonised Fuel Energy Systems. The CDT is carried out by a collaboration of three universities: the University of Sheffield, the University of Nottingham (host) and the University of Cardiff. This particular project is funded by the Engineering & Physical Sciences Research Council (EPSRC) and the International Flame Research Federation (IFRF).

As part of the EngD, the CDT for Resilient Decarbonised Fuel Energy Systems requires the completion of 180 credited modules from the Universities at Sheffield, Nottingham and Cardiff. These modules aim to give a comprehensive understanding of decarbonising energy systems and provide professional skills. For these modules, 150 credits are compulsory, with 30 optional credits.

Table B-1 CDT modules completed.

Module Type	Course Provider	Module Title	Credits
Core	Nottingham	Power Generation and Carbon Capture and Storage	10
Core	Nottingham	Low Carbon Processes	10
Core	Nottingham	Industrial Mini Project	10
Core	Nottingham	International Visit	10
Core	Nottingham	Industrial Case Studies	10
Core	Nottingham	Energy Systems & Policy	10
Core	Nottingham	Communication and Public Engagement for Energy Researchers	10
Core	Nottingham	Research and Professional Skills	10
Core	Nottingham	Research Portfolio 1	10
Elective	Nottingham	Energy Storage	10
Elective	Nottingham	Technologies for the Hydrogen Economy	10
Core	Cardiff	Energy Systems and Policy	10
Core	Cardiff	Risk and Hazard Management in the Energy Sector	10
Core	Sheffield	Pilot Scale Facilities Training at TERC	20
Core	Sheffield	Research Portfolio 2	20
Elective	Sheffield	Machine Learning and Adaptive Intelligence	15
Elective	Sheffield	Thesis Writing Principles	5
Elective	Sheffield	Japanese Language I	15

Appendix C: Training Completed

Table C-1 shows the training undertaken at Sheffield to assist with laboratory work and other project work. Training in ethics was also required of researchers at the University of Sheffield. was required for various practical aspects.

Table C-1 Training completed for the EngD.

Training	Description
Professional Behaviour and Ethical Conduct	Ethics in the research environment.
Thesis Writing- Principles and Practice	A mixture of self-study and online class sessions to help understand the structure of a thesis.
Using Posters to Communicate Your Research	Help to prepare and deliver an academic poster.
SEM Training	To be able to use the SEM equipment.
Gas Cylinder Training	Introduction gas cylinders and how to safely use them.
MPL Ink Preparation and Fabrication	How to make MPL ink and apply it to a GDL.
GDL Permeability Testing	To measure the permeability of a GDL sample.
GDL Electrical In-plane Testing	To measure the in-plane electrical conductivity of a GDL sample.
Contact Angle Measurements	Use of the sessile drop method to determine the wettability of my samples.
Fuel Cell Test Station	Training on how to assemble and test a fuel cell in order to characterise my samples.

Appendix D: Research Collaborations

Research Collaboration Between the University of Sheffield and the University of Birmingham

Introduction

I had the opportunity to visit the University of Birmingham, specifically the Birmingham Centre for Fuel Cell and Hydrogen Research. This centre is renowned both nationally and internationally for its pioneering work in fuel cell technologies. The focus here is on the research and development, applications, and demonstrations of various fuel cell and hydrogen systems and technologies.

The overall aim of my visit was to deepen my understanding of fuel cell technology through learning new lab skills. This included learning how to set up and conduct experiments with through-plane electrical conductivity setups, making MEAs, assembling a fuel cell, and operating a fuel cell test station. Additionally, I had the chance to test my samples in the test station, applying the theoretical knowledge I've acquired in a practical setting.

Through Plane Electrical Conductivity

Through plane, conductivity was measured as a function of compression. The setup can be seen in Figure D-1.

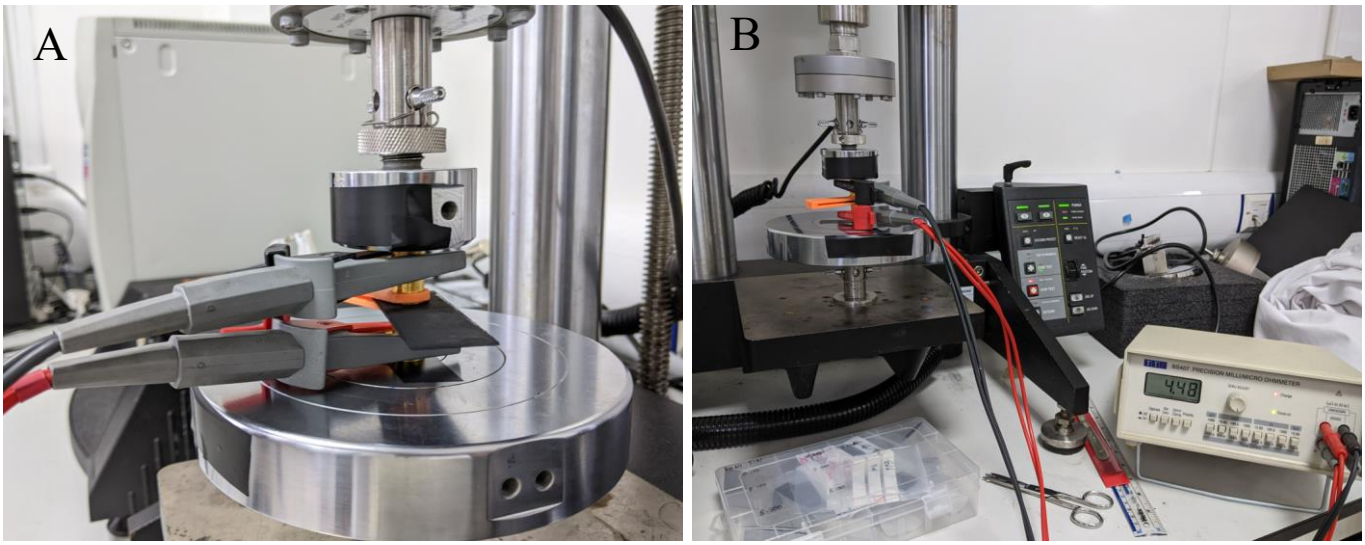

Figure D-1 Through plane electrical conductivity.

A piece of GDL sample is sandwiched between two gold-coated copper rods. The gold-coated copper rods are insulated with the press by using insulation tape to ensure that electric current does not pass into the press. Crocodile clips are then attached to the gold-coated copper rods and the resistance is measured using a four-wire Kelvin micro-ohmmeter (BS407 precision Milli/Micro-ohmmeter). Compression force is applied to the GDL using an Instron 5848 MicroTester. The following increments of compression were applied: 60 N/cm^2, 100 N/cm^2, 140 N/cm^2, 180 N/cm^2, 200 N/cm^2. Each compression force is held for 30 seconds and the reading from the ohmmeter is taken. The compression at 140 N/cm^2 is particularly significant as this is the typical compression expected within the fuel cell.

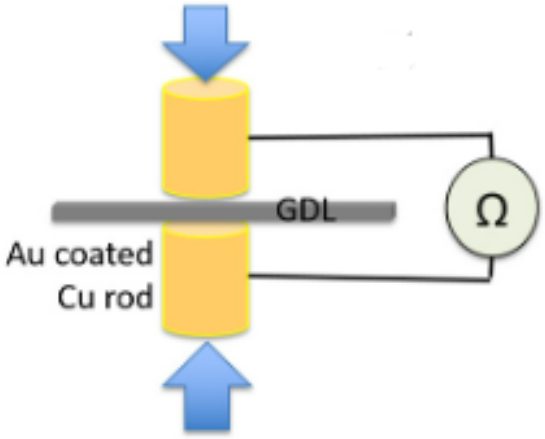

Figure D-2 Schematic of the through plane electrical conductivity.

The measured resistance (R_{Total}) across the system is shown in Figure D-2 is a combination of the following resistances:

$$R_{Total} = 2R_{Au-Cu} + 2R_{Au-\frac{Cu}{GDL}} + R_{GDL} \quad (D.1)$$

A graph can then be plotted to show compression on the X-axis and total resistance on the Y-axis. The same can be done for the contact resistance ($R_{Au-Cu/GDL}$) as R_{Au-Cu} and R_{GDL} can be found.

MEA Construction

MEA construction is important for in-situ fuel cell testing, this is because the active area will affect the outcome of the results. Therefore, the lining up of the active area must be accurate.

Firstly, the MEA must be prepared by cutting out the relevant components. In this case: GDL coated with MPL for the cathode side, Freudenberg C2 MPL coated GDL for the anode side and the catalyst coated membrane (CCM).

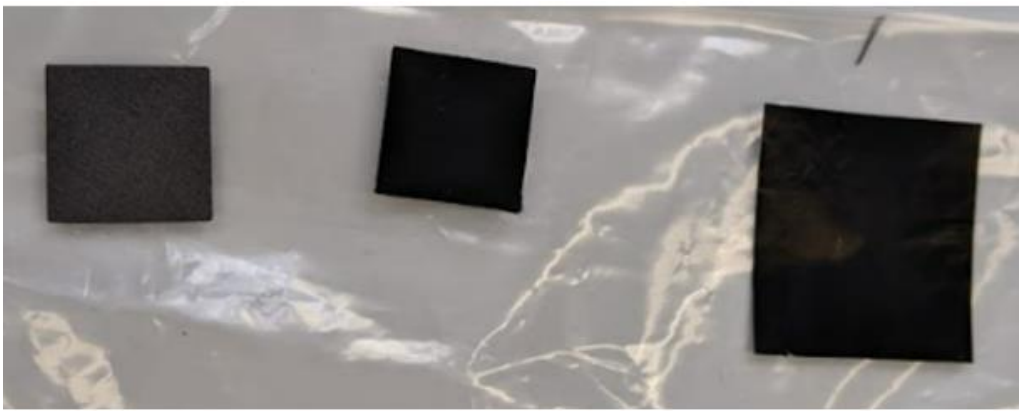

Figure D-3 GDL for cathode and anode and the CCM.

The GDL should be cut to the active area size for the fuel cell, in this case, 2.25 cm^2 x 2.25 cm^2. These samples were cut using a stencil to ensure consistency in size. The CCM is slightly larger than the active area at 4 cm^2 x 4 cm^2.

Following this, the layers must be assembled. This is done with the aid of a PTFE stencil, as pictured in Figure D-4. The stencil helps to align all the layers accurately so that the maximum

2.25 cm^2 x 2.25 cm^2 active area can be achieved. The MEA is then placed in some foil to hot press the sample and bind the layers together.

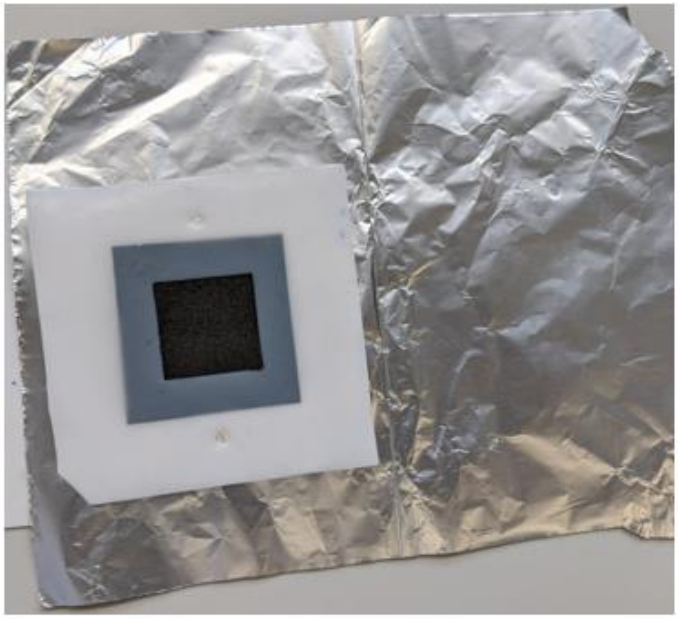

Figure D-4 Alignment of the layers for the MEA.

The MEA folded within the foil is then placed in a hot plate compression unit as shown in Figure D-5. The hot plate is set at 140°C and the MEA is placed on it to preheat for 2 minutes. A very small compression force is then applied, no more than the first setting on the compression machine. If too large a compression is applied, the MEA components, in particular, the GDL can be distorted. The MEA is then hot pressed for another 2 minutes at 140°C. Once carefully removed from the compression unit, the MEA should be bound together and ready for use in a fuel cell.

Figure D-5 Hot pressing of the MEA.

Fuel Cell Assembly and Setup

Once the MEA is assembled it can be inserted into the fuel cell and tested. The MEA can be placed on to one of the bipolar plates as shown in Figure D-6. The Fuel Cell is then sandwiched together with the MEA between both bipolar plates.

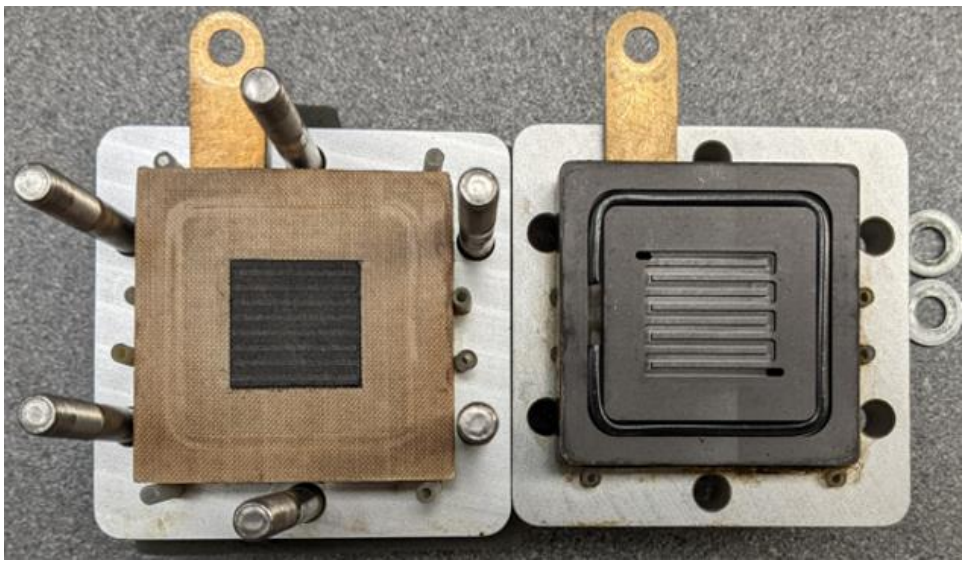

Figure D-6 MEA placed inside a fuel cell.

The bolts on the fuel cell then need to be fastened to keep everything together. A device to tighten the bolts can be used. The tightness of the bolts must be specified beforehand to ensure the optimum compression of the layers within the fuel cell for the specific experiment type. In this case, 3.5 Nm of torque was applied. When securing the bolts, it is best to do them in an alternating “X” pattern to ensure an even pressure distribution of the fuel cell, thus reducing the chances of inadvertently damaging the MEA.

Figure D-7 Securing the fuel cell.

The fuel cell and then be connected to the test station, the test station used in this experiment was a Scribner Fuel Cell Test System. The components of the fuel cell and the attachments to the test station can be seen in Figure D-9.

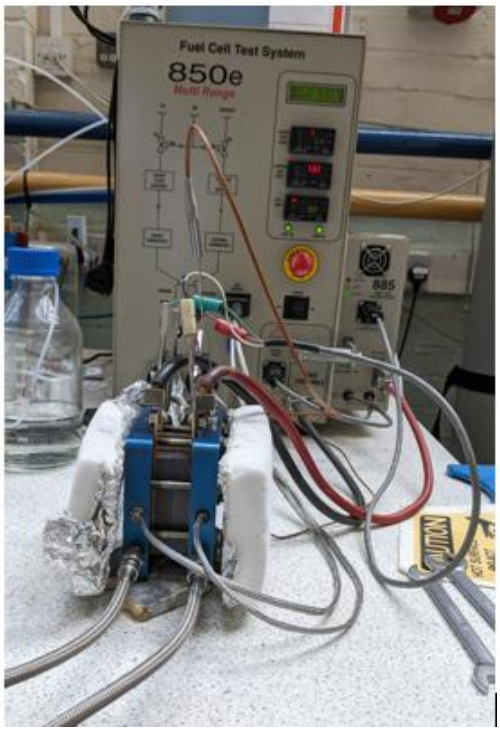

Figure D-8 Fuel cell test station.

In this case, the fuel cell is covered with some insulation to help keep it at the desired temperature. However, this is not always necessary.

Figure D-9 shows the different components that need to be connected to the fuel cell before the testing operation can be carried out. They consist of the following:

- External current collection wires
- Temperature measurement probe
- Inlet gas pipes
- Heating probes to heat the fuel cell
- Insulation
- Outlet gas pipes

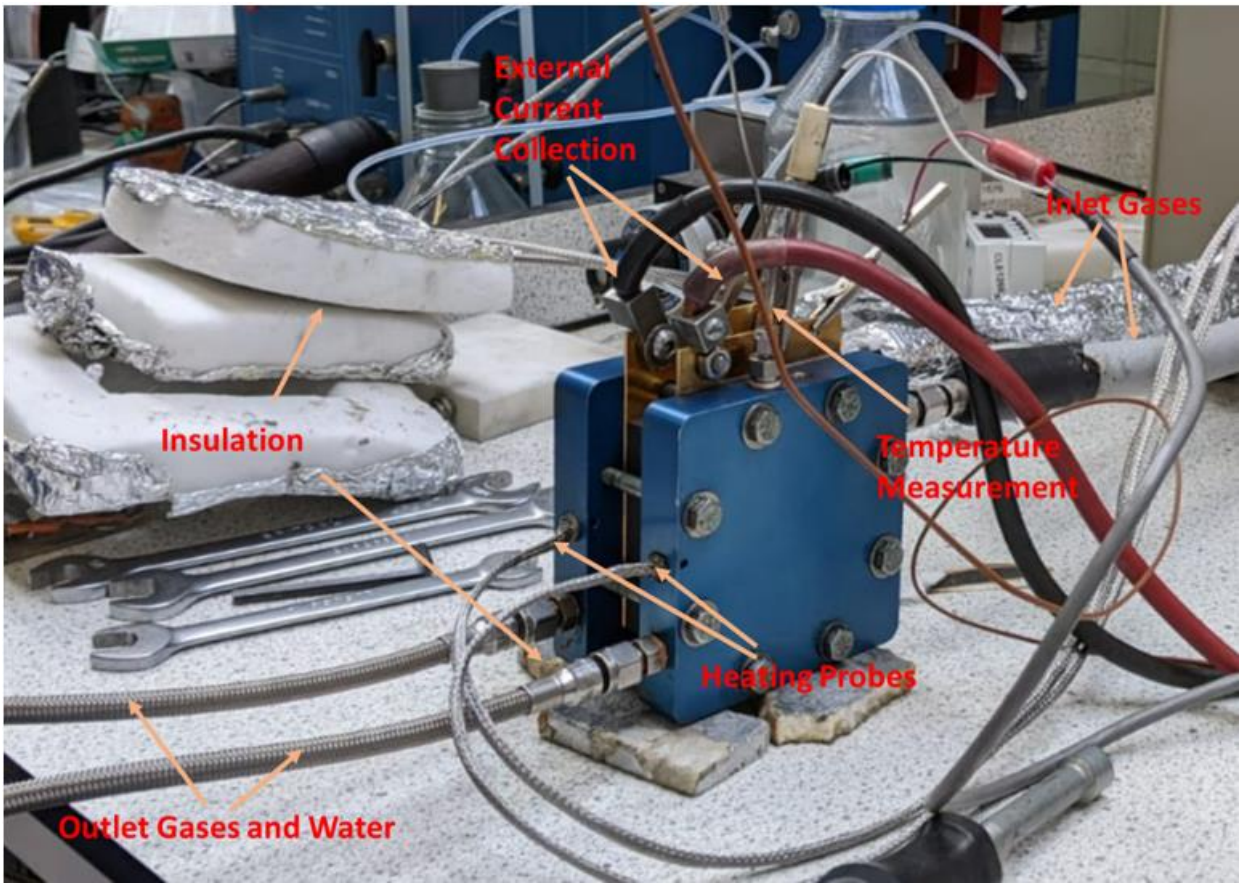

Figure D-9 Fuel cell components.

External Current Collection Wires

Used to collect the current from the operating fuel cell. The data is then sent to the computer and a polarisation curve can be plotted. The resolution of the polarisation curve can be set by the user before the test is carried out.

Temperature Measurement Probe

This is used to measure the temperature of the fuel cell. It ensures that the temperature of the fuel cell is at the correct operating temperature before data is collected. The temperature of the inlet gases is measured via the Scribner unit.

Inlet Gas Pipes

These provide the fuel cell with the reactant gases, in this case, hydrogen and air. The gas is humidified and brought to temperature via the scriber test unit. This will be displayed on the unit and controlled via the integrated computer.

Heating Probes to Heat the Fuel Cell

These are inserted into the bipolar plates and will heat the fuel cell to the desired temperature for the test.

Insulation

This ensures that the fuel cell is at a steady temperature, however as mentioned above, insulation is not always applied to a fuel cell.

Outlet Gas Pipes

These pipes allow for the waste gases and water to leave the fuel cell. A back pressure is always applied to the outlet pipes. This is to ensure the removal of liquid water and prevent flooding in the fuel cell. The backpressure will be set according to test requirements.

Once the fuel cell is successfully set up it can be used in operation. The fuel cell is first set at the desired temperature. The fuel cell in this experiment was set at a temperature of 80°C. The inlet gases (hydrogen and air) were also set at 80°C. The fuel cell was then humidified for 15 hours via the inlet gases. This is to ensure that the membrane is fully functional before polarisation data is acquired. Once this has been completed, the fuel cell can be used for the collection of data for the polarisation curves. This process is repeated for the different testing temperatures.

Concluding Remarks

During my visit to the University of Birmingham's Centre for Fuel Cell and Hydrogen Research, I gained a wealth of valuable experience and new skills. One of the highlights was gaining insights into the assembly process of fuel cells and learning firsthand how to test them. This practical knowledge was particularly enlightening and will undoubtedly enhance my future projects.

Additionally, I had the unique opportunity to observe how another hydrogen research group operates. Seeing their approaches to similar challenges, offered a new perspective and ideas for approaches to my work.

Working closely with the researchers at the University of Birmingham, we managed to build on previous collaborations, which resulted in further collaboration towards a research paper. Overall, the visit was educational and has significantly contributed to both my personal and professional development.

Research Collaboration Between the University of Sheffield and Kyushu University

Introduction

A collaboration on fuel cell research was carried out between the Energy 2050 team at the University of Sheffield and the I^2CNER group at Kyushu University. I was sent to Kyushu University from the University of Sheffield for a total of 8 weeks, from 14th May to 14th July 2023. I was based at Kyushu University's I^2CNER research facilities on the Itoshima Campus in Fukuoka, Japan. During my stay, I was hosted by Prof. Nishihara and his fuel cell research group.

The primary objective of this visit was to foster the exchange of knowledge and enhance collaboration between the two universities. My research involves the improvement of the overall fuel cell performance with the application of a double-sided microporous layer (MPL) coated gas diffusion layer (GDL). I fabricated these samples at the University of Sheffield and took them to Kyushu University for in-situ fuel cell testing. The main objectives of the visit are as follows:

- Learn how to make a catalyst coated membrane
- Created membrane electrode assemblies with my GDL samples
- Test my GDL samples in-situ
- Learn how to set up and run tests on a fuel cell
- Carry out contact angle measurements

Energy 2050

Situated within the University of Sheffield's Energy Institute, Energy 2050 constitutes a community comprising over 120 academics and over 250 doctoral candidates who specialise in progressing energy research and innovation. Energy 2050 places its focus on several specific areas. These include decarbonisation of energy sources, carbon capture, utilisation, and storage (CCUS), waste to energy and advancements in hydrogen fuel cells.

I^2CNER

I²CNER is dedicated to the progression of energy systems that mitigate CO_2 emissions and crafting a sustainable future. I^2CNER's initiatives revolve around propelling the technological progression of the hydrogen economy and refining CO_2 capture and sequestration methods. Research encompasses solid oxide fuel cells, polymer electrolyte membrane fuel cells (PEMFCs), as well as the entire spectrum of hydrogen production, storage, and utilisation.

Experimentation and Research

The following sections detail the research and experimental methods that I carried out at Kyushu University. These include CCM fabrication, fuel cell assembly, fuel cell testing and contact angle measurements.

CCM Fabrication

The catalyst ink was prepared by combining Pt/C (TEC10E50E, lot 1019-8581, 46.8 wt. Pt%, Tanaka, Japan), 5 wt. % Nafion solution (Wako, Japan), deionised water, and highly purified ethanol (99.5 vol%, Wako, Japan). This was then mixed using an Ultra Sonic Homogenizer UH-600 from SMT Corporation for 30 minutes. This was to ensure a uniform distribution of the Pt catalyst in the ink.

Figure D-10 Ink is placed into the sonic mixer for 30 minutes.

The ink was then placed into the spraying machine device (Nordson K.K., C3J). A Nafion 212 membrane was secured to a movable-hot plate via vacuum, below the spraying device. A 1 cm^2 region was then masked onto the Nafion 212 which would be the area where the catalyst ink would be deposited. The catalyst ink was subsequently sprayed directly onto the Nafion membrane until a loading of 0.3 $mgPt/cm^2$ was achieved.

Figure D-11 Spraying machine with vacuum plate in the foreground.

To ensure comprehensive integration of the membrane and the catalyst ink, the resulting CCMs were placed within a hot press (Sinto Digital Press CYPT-10) at 132 °C and 0.3 kN for 180 seconds. This final step was crucial in achieving effective bonding of the individual components.

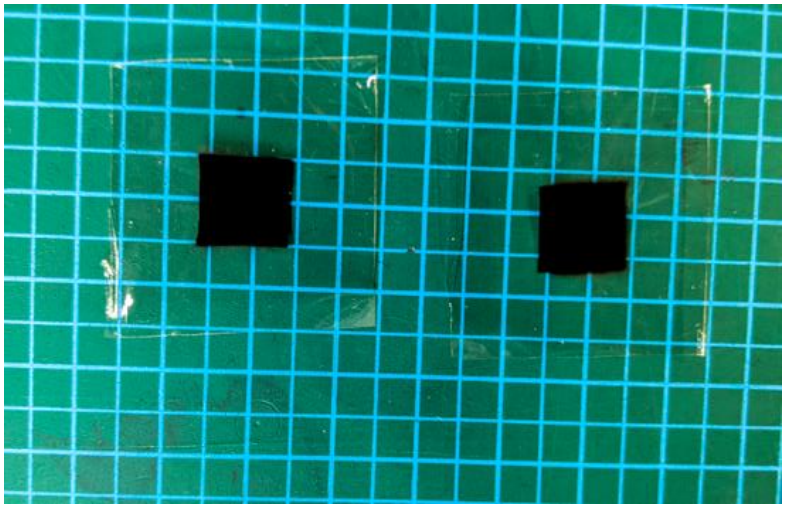

Figure D-12 Resulting CCMs after spraying and hot press.

Fuel Cell Assembly and Testing

A single cell with a 1 cm^2 active area, provided by the Japanese Automotive Research Institute (JARI), was utilised for the in-situ fuel cell testing. The fuel cell was equipped with graphite bipolar plates featuring serpentine-type flow fields, operating in counterflow mode. The fuel cell MEA was constructed using my samples at the cathode and uncoated Toray HGP 60 at the anode. The CCMs that were made using the above method were also placed in the fuel cell. The fuel cell was then placed in a constant-temperature oven and connected to the inlet and outlet gas supply lines. The constant temperature oven ensured a constant and even operating temperature of the fuel cell which was set at 80°C.

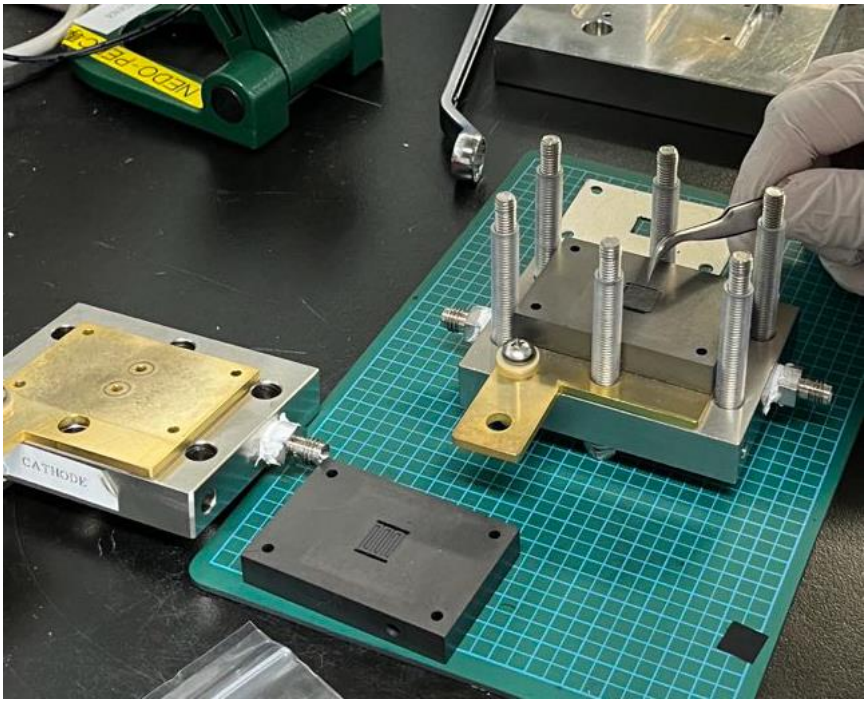

Figure D-13 Fuel cell assembly, the anode side GDL is placed onto the flow field.

The fuel cell test station (AUTOPEM-CVZ01, Toyo Corporation, Japan) was then connected to the fuel cell itself. This station facilitated the regulation of factors such as humidification, cell temperature, and gas flow throughout the testing process. The fuel cell maintained constant volumetric flow rates of 0.139 L/min for hydrogen at the anode and 0.332 L/min for air at the cathode.

Before in-situ measurements, the cell underwent a 16-hour conditioning process at a voltage of 0.6 V and relative humidity (RH) of 100%. Polarisation curves were measured using an electrochemical interface impedance analyser (Solartron SI-1287).

Operated at 80°C, the fuel cell and inlet gases (hydrogen and air) were also set to 80°C and humidified. Subsequently, polarisation, electrochemical impedance spectroscopy (EIS) and oxygen transport resistance data were collected across four RH conditions: RH 100%, RH 75%, RH 50%, and RH 25%. This extensive range of humidity conditions enabled a comprehensive evaluation of the fuel cell's performance across varying humidity levels.

Figure D-14 Fuel cell test station with the constant temperature oven at the bottom of the picture.

Contact Angle Measurements

The contact angle analysis of the samples utilised the sessile drop method. A singular water droplet was positioned on the GDL surface and high-resolution images were captured within the initial three seconds of droplet placement. Contact angle measurements were then obtained, involving ten measurements for each sample, followed by the calculation of an average value.

Effective water management is a critical concern in fuel cell operation. Hence, understanding how water behaves with materials within the fuel cell helps to optimise fuel cell design. This is done by looking at the GDL hydrophobicity through contact angle characterisation. A contact angle below 90° indicates hydrophilicity, while a contact angle exceeding 90° signifies hydrophobicity of the substance.

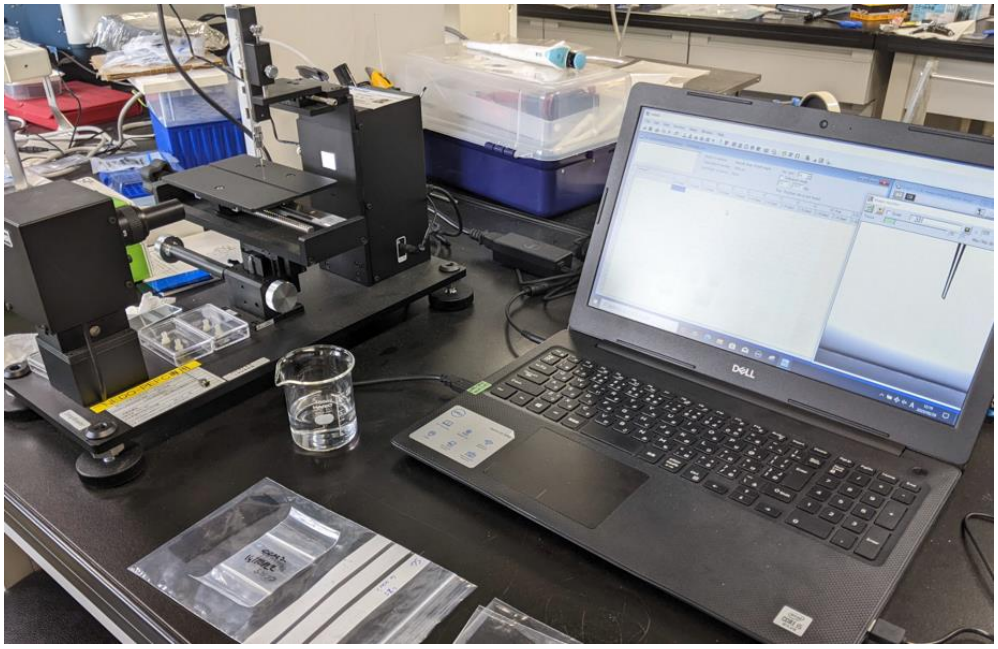

Figure D-15 Contact angle setup.

Conclusion

The collaboration between the University of Sheffield and Kyushu University provided me with a unique opportunity to engage with a different research team, foster relations between the different universities and learn new skills. The research conducted at Prof. Nishihara's research group has significantly boosted my understanding of the; operation, construction and maintenance of fuel cell systems. It has also helped to advance my PhD work on the study of gas diffusion layers.